



UNIVERSITE D'AIX-MARSEILLE

ED 62 – SCIENCES DE LA VIE ET DE LA SANTE

Laboratoire Adhésion et Inflammation -U1067-UMR 7333

Thèse présentée pour obtenir le grade universitaire de docteur

Discipline : Biologie
Spécialité : Immunologie

Xuan LUO

In vitro quantitative study of T cell adhesive haptotaxis

Soutenance le 14/06/2019 devant le jury :

Stéphanie DESCROIX	CNRS	Rapporteur
Olivier THOUMINE	CNRS	Rapporteur
Alice NICOLAS	CNRS	Examineur
Arnauld SERGE	AMU	Examineur
Oliver THEODOLY	CNRS	Directeur de thèse

To my family

谨以此作，献给我的家人

Acknowledgements

When I am writing down these words, I finally come to realize that the adventure which I embarked on almost four years ago has come to a point where I need to conclude my work by thanking everyone. It has been an incredible ride, one that would not have been possible without the help from so many to whom I will be forever grateful.

First and foremost, I would like to offer my sincere gratitude to my dear PhD supervisor Dr. Olivier Théodoly for accepting me to be his student. There is nothing more precious for me than having someone who is as exemplary in science as in life to be my advisor during this important stage of my life and this once-in-a-lifetime adventure. I will dearly miss our time together over these years both in and outside the work. Thank you for your guidance, your precious help at the bench and far beyond, your rigor, your patience, your optimism, your conviction and most importantly, thank you for letting me be myself (*and putting up with it...*)!

My sincere gratitude also goes to my beloved “Mrs. Boss” Dr. Marie-Pierre Valignat for the precious help which I have been fortunate enough to receive over all these years. Many thanks for your guidance – notably on the microscopy which has also set the bar high for everyone taking images on the “Zeiss MPV” and on the life-saving improvements of the tracking analysis – and for a lovely time together both in and outside the lab (*watch out I might come back and chase you on the trail someday!*). More importantly, thanks for showing me daily what a woman in science is capable of both on a professional and personal level – do know that I have been in awe the entire time!

This project, and probably my PhD life in general, would have been much more difficult had I not had the generous help from our talented, dedicated, highly professional and impressively organized engineer Martine Pélicot. Thank you for going above and beyond for everyone and to keep the lab in order. Thank you also for your constant kindness and sense of humor which, I am sure, have always been very therapeutic for everyone in the lab. We are lucky to have you!

I have had the pleasure to initiate a new project with my PhD using a novel technique through collaboration with a young start-up. I am grateful for all the help I got along the way and all that I have learned thanks to Dr. Vincent Studer for the interesting discussion and hosting me in Bordeaux, Dr. Pierre-Olivier Strale for helping me with my experiments in Bordeaux and the continuous discussion and support, Dr. Aurélien Duboin, Dr. Josselin Ruaudel, Dr. Louise Bonnemay, Mr. Romuald Vally and Ms. Hélène Delobel as well as the entire Alvéole team for the constant communication via different platforms and their hospitality during my visits.

My gratitude extends to all members of the jury who have kindly accepted to review and evaluate my work: to Drs. Stéphanie Descroix and Olivier Thoumine for being my reviewers and to Drs. Alice Nicolas and Arnaud Sergé for being my examiners.

I would also like to thank all other researchers and staff in the lab for all the discussion and lovely moments spent together. Special mention goes to Dr. Pierre-Henri Puech for all the drawing-related help; to Dr. Philippe Robert for the fruitful discussion regarding immunology, cars, planes, for the pool-side mojito parties and for teaching me all the good stuff that I had not learnt in my previous French lessons; to Dominique Touchard for the help on some experiments and for keeping me apprised of the latest Apple product line; to Valentine Seveau for continuing the project; to Christine Erismann and Sophie Gall for all the administrative assistance.

Many thanks to all the students and post-docs (past and present) in the lab for a memorable journey together and for the friendship we have forged. Special mentions go to: Dr. Thomas Sbarrato for initiating the first assays on the printer prototype and help me transitioning into the project upon my arrival; Dr. Laurene Aoun for the precious help on microfluidics, the company during late-night experiments and of course for all our food/selfie/photo-related assays; Dr. Yongjian (Jim) Wang for the endless office food supply and daily support; Dr. Paulin Nègre for the additional help on MatLab and on handling the very unpredictable μ Manager; Dr. Alexander Hornung for helping with Ibidi channels at the beginning of my PhD; to my fellow PhD candidates (now both doctors): Dr. Anaïs Sadoun for answering all my questions prior to my joining the lab and for all the enjoyable moments and meaningful discussions later on, Dr. Cristina Gonzalez Gutierrez for the endless energy that would light up the room and for all the memorable old-couple-style exchanges between us 😊; to the next generation: Geoffrey Delhaye, Nicolas Garcia Seyda, Farah Mustapha – thanks for your help and kindness on the daily basis – my best wishes to all of you!

One important reason for which I was attracted to the academia in the first place is the ability to teach and contribute to the future, so I would like to thank all the trainees whom I had the pleasure to directly or indirectly mentor for giving me the opportunity to do just that: Omar Ndao, Ethan Del Ghingaro, Marie Gavazzi, Quentin Fabrega. Whatever I do next, this personal mission will continue.

Another cause close to my heart is bridging the gap between science and the general public for which I would like to thank the associations “13 Minutes Jeune Chercheurs”, “13 Minutes Chercheurs”, “Tous Chercheurs”, “Pi day” and the Department of Culture and Scientific Communication at Aix-Marseille University for letting me be a part of these terrific events dedicated to scientific communication. Seeing first-hand what we have achieved together has always been one of the most satisfying moments of my PhD.

During my years in Marseille, I have had the pleasure to meet probably the most helpful, tightly-knit and caring Chinese community in France. My sincere thanks go to the Association of Chinese Students and Researchers in Marseille and to all the friends I have made here. Thank you for everything – not only for the fun and craziness that we will always remember, but also for being exemplary in representing our country abroad.

My heartfelt thanks also go to all my old friends (from primary school, junior and senior high, college and UTC) who are now in various places in the world. Although it is getting more and more difficult to meet up, I am so grateful that we have not lost touch and still have each other's back. It is so inspiring to see how wonderfully you are living your life. Thank you for your understanding, your continuous support and for constantly inspiring me to be my better self.

Finally, my eternal gratitude must go to my beloved family: we have been thousands of miles apart for many years, but your love has never been absent. Thank you for your unconditional support. Most importantly, thank you for raising me up to more than I can be – I love you endlessly and this work is for you.

Abstract

An efficient immune response relies on a rapid recruitment of leukocytes from the blood system to the inflamed or damaged tissue. As they leave the blood stream and travel to inflammation site, leukocytes are captured by the endothelium and migrate along the vessel wall to reach permissive transmigration sites. These processes are mediated by multiple external biochemical and physical cues among which the role of adhesion molecules remains unclear. Guidance of cells by molecules anchored on a substrate, known as haptotaxis, is arguably crucial in development, immunology and cancer. Adhesive haptotaxis has been described in the case of mesenchymal cells that develop strong pulling forces with their substrates and orient via a tug of war mechanism – a competition between cells' adherent pulling edges. In the case of amoeboid cells that migrate with minimal interaction with their substrate, the existence of adhesive haptotaxis has yet to be evidenced. In this project, we studied the crawling of human T lymphocytes on substrates with spatially modulated adhesion. and observed robust adhesive haptotaxis with surface concentrations of integrin ligands found on high endothelial venules. These finding, together with the *in vivo* overexpression of ICAM-1 and VCAM-1 at transmigration portals, suggest that adhesive haptotaxis could promote leukocyte recruitment. Mechanistically, we show that integrin-mediated adhesive haptotaxis of lymphocytes differs both from active chemotaxis, because no mechanotransduction was detected, and from the passive tug of war mechanism of mesenchymal cells, because different integrins support opposite phenotypes. Cells favored more adherent zones with VLA-4 and, counterintuitively, less adherent zones with LFA-1. These results reveal that integrins control differential adhesive haptotaxis behaviors without mechanotransduction. We further investigated the mechanism behind this specific haptotactic phenotype mediated by LFA-1 and find that the lamellipodial dynamics, rather than the integrin expression level, is involved. Preliminary findings with VASP deficient T cells indicate also that VASP protein may play an important role in T cell adhesive haptotaxis.

Keywords: micropatterning, haptotaxis, integrins, T lymphocytes, cell guidance

Résumé

Une réponse immunitaire efficace repose sur un recrutement rapide de leucocytes du système sanguin vers les tissus enflammés ou endommagés. Lorsqu'ils quittent la circulation sanguine et se rendent au site de l'inflammation, les leucocytes sont capturés par l'endothélium et migrent le long de la paroi du vaisseau pour atteindre les sites de transmigration. Ces processus sont médiés par de multiples signaux externes biochimiques et physiques parmi lesquels le rôle des molécules d'adhésion reste flou. Le guidage des cellules par des molécules ancrées sur un substrat, appelé haptotaxie, est sans doute crucial pour le développement, l'immunologie et le cancer. L'haptotaxie adhésive a été décrite dans le cas de cellules mésenchymateuses qui développent des forces de traction importantes avec leurs substrats et s'orientent via un mécanisme de "tir à la corde" - une compétition entre les bords adhérents des cellules. Dans le cas de cellules amiboïdes qui migrent avec une interaction minimale avec leur substrat, l'existence d'une haptotaxie adhésive reste incertaine. Dans ce projet, nous avons étudié la migration des lymphocytes T humains sur des substrats dont l'adhésion est spatialement modulée. Nous avons observé une haptotaxie adhésive robuste des lymphocytes sur les surfaces dont la concentration des ligands intégrines correspond à celle trouvées sur les veinules postcapillaires à endothélium épais. Ces constatations correspondent donc à la surexpression de ICAM-1 et de VCAM-1 observée *in vivo* aux sites de transmigration et suggèrent que l'haptotaxie adhésive pourrait favoriser le recrutement des leucocytes. D'un point de vue mécanistique, nous montrons que l'haptotaxie adhésive des lymphocytes à médiation par les intégrines diffère à la fois de la chimiotaxie active, car aucune mécanotransduction n'a été détectée, et du mécanisme de "tir à la corde" passif des cellules mésenchymateuses, car différentes intégrines supportent des phénotypes opposés. Les cellules ont préféré des zones plus adhérentes avec VLA-4 et, contre-intuitivement, des zones moins adhérentes avec LFA-1. Ces résultats révèlent que les intégrines contrôlent les comportements différentiels d'haptotaxie adhésive sans mécanotransduction. Nous avons également étudié le mécanisme à l'origine de ce phénotype haptotactique spécifique induit par LFA-1 et avons découvert que la dynamique du lamellipode, plutôt que le niveau d'expression de l'intégrine, était impliquée. Les résultats préliminaires avec des lymphocytes T déficients en VASP indiquent également que la protéine VASP pourrait jouer un rôle important dans l'haptotaxie adhésive des lymphocytes T.

Mots-clés : micropatterning, haptotaxie, intégrines, lymphocytes T, guidage cellulaire

List of abbreviations

PBMC	Peripheral Blood Mononuclear Cell
PRRs	Pattern Recognition Receptors
PAMPs	Pathogen-Associated Molecular Patterns
DAMPs	Damage Associated Molecular Patterns
APC	Antigen Presenting Cell
PSGL-1	P-Selectin Glycoprotein Ligand-1
ICAM-1	Intercellular Adhesion Molecule-1
VCAM-1	Vascular Adhesion Molecule 1
VLA-4	Very Late Antigen 4
LFA-1	Lymphocyte Function-associated Antigen-1
Mac-1	Macrophage antigen-1
GPCR	G-Protein Coupled Receptor
JAMs	Junctional Adhesion Molecules
PECAM-1	Platelet Endothelial Cell Adhesion Molecule-1
ECM	Extra-Cellular Matrix
MIDAS	Metal Ion-Dependent Adhesion Site
DC	Dendritic Cell
ROCK	Rho-associated protein kinase
HEV	High Endothelial Venule
FDC	Fibroblastic Dendritic Cell
FRC	Fibroblastic Reticular Cell
GEF	Guanine nucleotide Exchange Factor
SCS	Subcapsular Sinus
WASp	Wiskott-Aldrich Symptom protein
GAGs	Glycosaminoglycans
GRK6	G-protein-coupled Receptor Kinase 6
S1P	Sphingosine 1 Phosphate
S1PR	Sphingosine 1 Phosphate Receptor

EC	Endothelial cell
TEM	Transendothelial Migration
HSCs	Hematopoietic Stem Cells
MHC	Major Histocompatibility Complex
PDA	Polydopamine
PEG	Poly(Ethylene Glycol)
PLL-g-PEG	Polylysine-g- Poly(Ethylene Glycol)
HUVEC	Human Umbilical Vein Endothelial Cell
μCP	Micro-Contact printing
PDMS	Polydimethylsiloxane
LAPAP	Laser-Assisted Adsorption by Photobleaching
LIMAP	Light-Induced Molecular Adsorption of Proteins
IL	Interleukin
APTS	3-Aminopropyltriethoxysilane
IgG	Immunoglobulin G
VASP	Vasodilator-stimulated phosphoprotein

Table of contents

Acknowledgements.....	iv
Abstract.....	vii
Résumé.....	viii
List of abbreviations.....	ix
Table of contents.....	xi
1 Introduction.....	1
1.1 Immunity and leukocyte extravasation.....	1
1.1.1 The immune system.....	1
1.1.2 Leukocyte extravasation cascade.....	4
1.1.3 Effector T cells.....	8
1.2 Motility and guidance: from molecular components to cellular response.....	11
1.2.1 Actin cytoskeleton and actin-based motility.....	11
1.2.2 Integrins: key player in leukocyte migration.....	20
1.2.3 Leukocyte motility.....	26
1.2.4 Various guidance cues in leukocyte migration.....	33
1.3 Surface micro-patterning.....	45
1.3.1 Necessity for well-defined <i>in vitro</i> assays.....	45
1.3.2 Soluble gradient transfer with microfluidics.....	45
1.3.3 Gradient patterning with microcontact printing.....	48
1.3.4 Surface patterning with light.....	51
1.4 Open questions and project outline.....	57
2 General experimental set-up.....	59
2.1 Human primary T cell culture.....	59
2.2 Surface patterning.....	59
2.2.1 System set-up and patterning method.....	59
2.2.2 Device fabrication and surface coatings.....	60
2.3 Microscopy.....	62
2.3.1 Fluorescence microscopy and quantification.....	62
2.3.2 RICM microscopy.....	63
2.4 Cell adhesion and migration assay.....	64

2.5	Cell tracking and analysis.....	65
3	Optimization of photopatterning for immune cells	67
3.1	Additive patterning on PLL-PEG coated substrates.....	67
3.1.1	Protein A can be patterned directly onto PLL-PEG substrate	67
3.1.2	The patterning is oxygen-dependent.....	67
3.1.3	Fc-ICAM adsorption on patterned Protein A is specific but non-functional.....	68
3.1.4	Avidin/biotin sandwich strategy also yields specific but non-functional ICAM pattern	69
3.2	Additive patterning on SVA-PEG coated substrates.....	70
3.2.1	ICAM adsorption via patterned Protein A is specific and functional	70
3.2.2	Wet-SEEC microscopy allows label-free protein pattern detection and can be applied to cell migration assay	71
3.2.3	ICAM surface gradient pattern is functional but with too limited range	73
3.3	Subtractive patterning on protein coated substrates	75
3.3.1	ICAM molecules are sensitive to UV and can be used for subtractive patterning	75
3.3.2	Subtractive patterning also requires photo-initiator	75
3.3.3	Subtractive patterning is also oxygen dependent	76
3.3.4	Creating patterns with gradual amount of adhesion molecules	77
3.4	Photopatterning substrates with modulated adhesion	78
4	Probing the existence of T cell adhesive haptotaxis.....	81
4.1	Strategy to probe adhesive haptotaxis	81
4.2	Direction of migrating T cells is biased on substrates with adherent and non-adherent stripes	82
4.3	Lymphocytes display integrin-mediated haptotaxis on globally adhesive substrates	84
4.4	Integrin-mediated haptotaxis increases with adhesion contrast.....	86
4.5	VLA-4 integrins mediate a preference for high adhesion zones like mesenchymal cells	86
4.6	LFA-1 integrins mediate a unique preference for low adhesion zones	88
4.7	Mechanotransduction is not detected in integrin-mediated haptotaxis.....	88
4.8	Lymphocytes orient either with or against gradients of adhesion	89
4.9	Discussion	90
5	Adhesive haptotaxis at population level with perturbation of cell-substrate adhesion..	92
5.1	Different migratory phenotypes during adhesive haptotaxis mediated by LFA-1....	92

5.2	High-affinity LFA-1 activated by Mn ²⁺ enriches “persistent” phenotype on higher adhesion zones	94
5.2.1	LFA-1 activation by Mn ²⁺	94
5.2.2	LFA-1 activation by Mn ²⁺ with Calcium depletion.....	96
5.3	Anti-LFA-1 monoclonal antibody treatment leads to “persistent” phenotype.....	98
5.3.1	TS1/22 treatment leads to cell immobilization and subsequent “persistent” phenotype.....	99
5.3.2	Hi1/11 enriches “persistent” phenotype on areas with higher adhesion	101
5.4	“Zig-zag” phenotype remains dominant following Lovastatin treatment.....	103
5.5	Attempt to locally deplete LFA-1 enriches “persistent” phenotype favoring higher adhesion zones	105
5.6	LFA-1 staining reveals no significant difference in integrin expression between “zig-zag” and “persistent” phenotype	107
5.7	Geometrical perturbation induces orientation shift on ICAM-1 but not VCAM-1 substrates	109
5.8	Discussion	111
6	Adhesive haptotaxis at single-cell level	113
6.1	Single-cell assay confirms different phenotypes present during adhesive haptotaxis	113
6.2	Subcellular level adhesion modulation reveals lamellipodia as adhesion sensor favoring the least adhesion zone.....	114
6.3	Discussion	116
7	Adhesive haptotaxis at population level with perturbation of lamellipodial dynamic ..	118
7.1	WASP-deficient T cells exhibit unimpaired adhesive haptotaxis with dominant “zig-zag” phenotype	118
7.2	VASP knock-out cells exhibit unimpaired adhesive haptotaxis with slightly reduced “zig-zag” phenotype.....	120
7.3	Discussion	122
8	Conclusion and perspective	124
9	Bibliography	127
	Appendice.....	i
	Appendix 1 T cell culture protocol	ii
	Appendix 2 PDMS microwell preparation protocol	iv
	Appendix 3 Glass-bottom Ibidi channel preparation protocol	v
	Appendix 4 Optical protein printing protocol	vi
	Appendix 5 Cell adhesion and migration assay protocol	ix

Appendix 6 Fluorescent quantification protocol	xii
Appendix 7 ICAM beads protocol.....	xiii
Appendix 8 Calcium influx detection experimental protocol	xiv
Appendix 9 Cell fixation and integrin staining protocol.....	xv
Appendix 10 Cell tracking and analysis protocol	xvii

1 Introduction

This chapter will present both the biological and technological contexts of this work through literature review. It is divided into four sections: the first section will give a brief introduction on immunity and the leukocyte extravasation cascade. The second section will focus on cell motility and guidance in which key molecular components responsible for cell motility will be reviewed. Cellular response mediated by these molecules and external guidance cues will also be addressed. The third section will give a technological overview on surface-patterning techniques which is widely used to study cell motility. The fourth section will present the open questions that lead to this project as well as the outline of this work.

1.1 Immunity and leukocyte extravasation

1.1.1 The immune system

The immune system is a host defense system comprising many biological structures and processes within an organism that protects it against disease. To function properly, an immune system must detect a wide variety of agents, known as pathogens, from viruses to parasitic worms, and distinguish them from the organism's own healthy tissues. In many species, the immune system can be classified into subsystems: the innate immune system that is present in plants, the invertebrates and the vertebrates as well as the adaptive immune system that is only present in the vertebrates.

1.1.1.1 Leukocytes: soldiers of the immune system

Leukocytes (white blood cells) are the cells of the immune system that are involved in both innate and adaptive immune responses. All leukocytes are produced and derived from multipotent hematopoietic stem cells in the bone marrow (Figure 1-1). They can be classified into two broad categories either by structure (granulocytes or agranulocytes) or by cell lineage (myeloid cells or lymphoid cells).

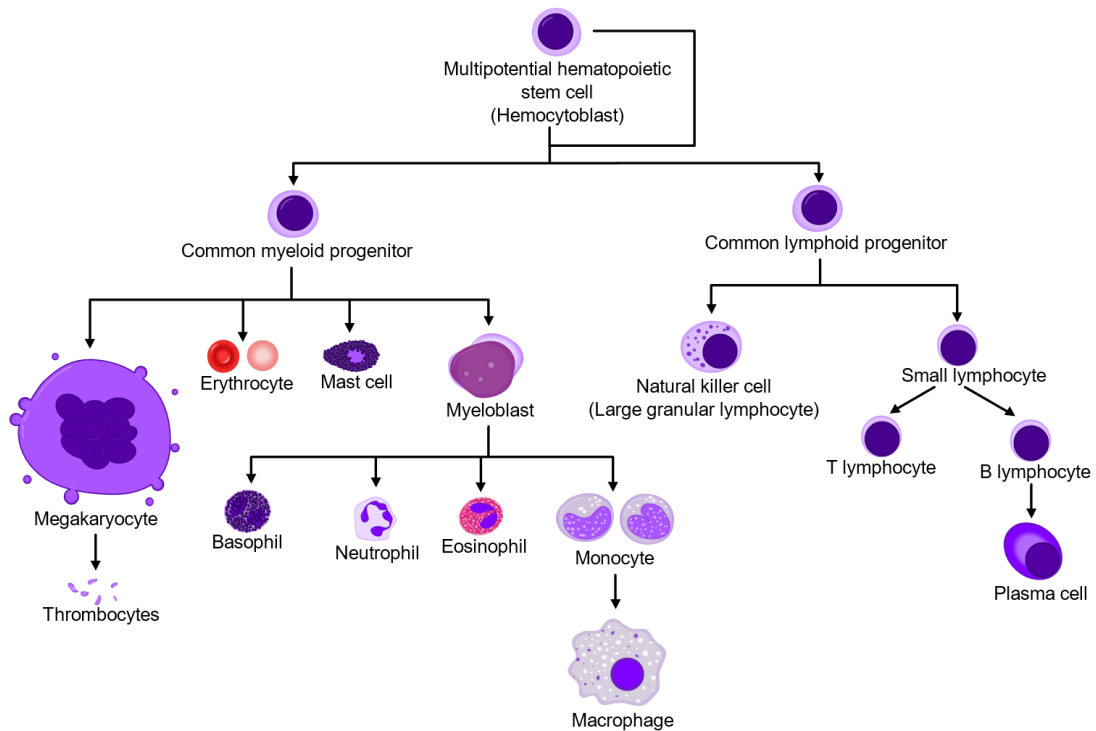


Figure 1-1 General schematics of hematopoiesis showing different subsets of leukocytes and their progenitors

These two broad categories can be further divided into five main types:

- Neutrophils: they are the most abundant leukocytes, constituting more than half of the circulating leukocytes (Alberts et al., 2002). They are the first responders of the immune system and are active in phagocytosis.
- Eosinophils: these cells account for only 1% of circulating leukocytes but they are important in responding to infections with parasites. They are also prominent in allergic reactions. They don't phagocytose but instead release chemical products which perforate cell membranes.
- Basophils: Representing also around 1% of circulating leukocytes, they are chiefly responsible for initiating inflammatory responses by releasing chemicals such as histamine and heparin and are common contributors to allergic responses.
- Lymphocytes: They are mainly involved in adaptive immune system and include B lymphocytes – which specialize in antibody production and T lymphocytes – which mediate B lymphocyte activity and destroy virus-infected cells.
- Monocytes: Around 5% of circulating leukocytes are monocytes. They share phagocytosis duty with neutrophils, but their most important function is to migrate into the tissue and differentiate into either macrophages – which will remain in the tissue and phagocytose or dendritic cells – which will present pathogen fragments to lymphocytes.

1.1.1.2 The innate immune system

During the first critical hours or days of exposure to a new pathogen, the innate immune system is activated to protect the organism. The first arm of the innate immune system is the different physical barriers such as the skin, the gastrointestinal tract, the respiratory tract, the nasopharynx, cilia, eyelashes and other body hair. Other barriers also exist such as the mucus secreted by the respiratory and gastrointestinal tract that serve to trap and entangle microorganisms (Boyton & Openshaw, 2002). When microorganisms breach these barriers, innate leukocytes are the second arm of the innate immune system (Alberts et al., 2002). They are mainly composed of phagocytes (macrophages, neutrophils and dendritic cells), which engulf and eliminate invading pathogens. Contrary to what has long been described, the innate immune system is not entirely non-specific. With Pattern Recognition Receptors (PRRs) (Akira, Uematsu, & Takeuchi, 2006) expressed by the innate leukocytes, it is capable of identifying Pathogen-Associated Molecular Patterns (PAMPs), which are associated with microbial pathogens (H. Kumar, Kawai, & Akira, 2011) and Damage Associated Molecular Patterns (DAMPs), which are associated with tissue damages. These various actors of the innate immune system construct the first line of defense against invading pathogens and provides important cues for the function of adaptive immune system.

1.1.1.3 The adaptive immune system

The innate immune system is activated directly by pathogens and defends all multicellular organisms against infection. In vertebrates, pathogens, together with the innate immune responses they activate, further stimulates adaptive immune system. The innate immune system calls adaptive immune responses into play only when it recognizes molecules characteristic of invading pathogens and can distinguish between different class of pathogens and recruit the most effective form of adaptive immune response to eliminate them.

The function of adaptive immune responses is to destroy invading pathogens and any toxic molecules they produce. Because these responses are destructive, it is crucial that they be made only in response to molecules that are foreign to the host and not to the molecules of the host itself. The ability to distinguish what is foreign from what is self is a fundamental feature of the adaptive immune system. It has evolved to provide a wide and finely-tuned repertoire of recognition for both self- and

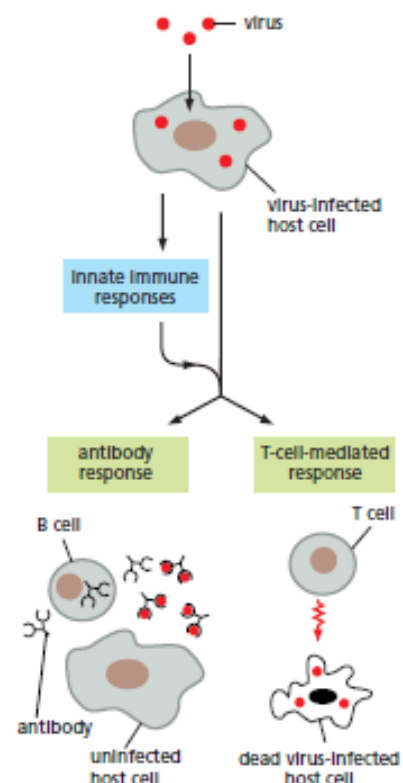


Figure 1-2 The two main classes of the adaptive immune response: the antibody and the T-cell mediated response (Alberts et al., 2002)

nonself-antigens. The adaptive responses are thus highly specific to the pathogen that induced them. In addition to the specificity, another fundamental feature is their ability to generate immunologic memory and therefore provide long-term protection.

Adaptive immune responses are carried out by a specific class of leukocytes called lymphocytes: T lymphocytes for the T cell-mediated responses and B lymphocytes for the antibody responses. In antibody responses, B lymphocytes are activated to secrete antibodies, which are proteins called immunoglobulins. They will then circulate in the bloodstream and permeate other body fluids, where they bind specifically to the foreign antigen that stimulated their production causing it to inactivate, which prevents the antigen from binding to the host (Alberts et al., 2002). In T cell-mediated responses, T lymphocytes are activated upon encounter with an Antigen Presenting Cell (APC). Activated T lymphocytes react directly against a foreign antigen that is presented to them on the surface of the host cell. The T lymphocyte, for instance, can kill a virus-infected host cell that has viral antigen presented on its surface and thus eliminate the infected cell before the virus has had a chance to replicate (Figure 1-2). In other cases, the T lymphocyte can also stimulate phagocytes or B lymphocytes to help eliminate the pathogens. Called into action by the innate immune responses, the adaptive immunity involves a tightly regulated interplay between antigens presenting cells and T and B lymphocytes, which facilitate pathogen-specific immunologic effector pathways, generation of immunologic memory, and regulation of host immune homeostasis (Bonilla & Oettgen, 2010).

1.1.2 Leukocyte extravasation cascade

The success of an immune response depends on the prompt recruitment of leukocytes from blood circulation to the afflicted site where they exert their effector function. To do so, leukocytes will first exit the blood circulation via the extravasation – a highly regulated system mobilizing different ligands and receptors present both on leukocytes and the endothelium. Under homeostatic conditions, leukocytes utilize the comprehensive circulatory system to examine the entire body for signs of infection. Upon infection, circulating leukocytes are recruited from the blood to the tissue. Their recruitment is a strictly regulated cascade of events involving different molecular mechanisms. It can be described as a sequential process having the following events: capture and rolling, arrest and adhesion strengthening, intravascular crawling and transmigration (Figure 1-3) (Ley, Laudanna, Cybulsky, & Nourshargh, 2007).

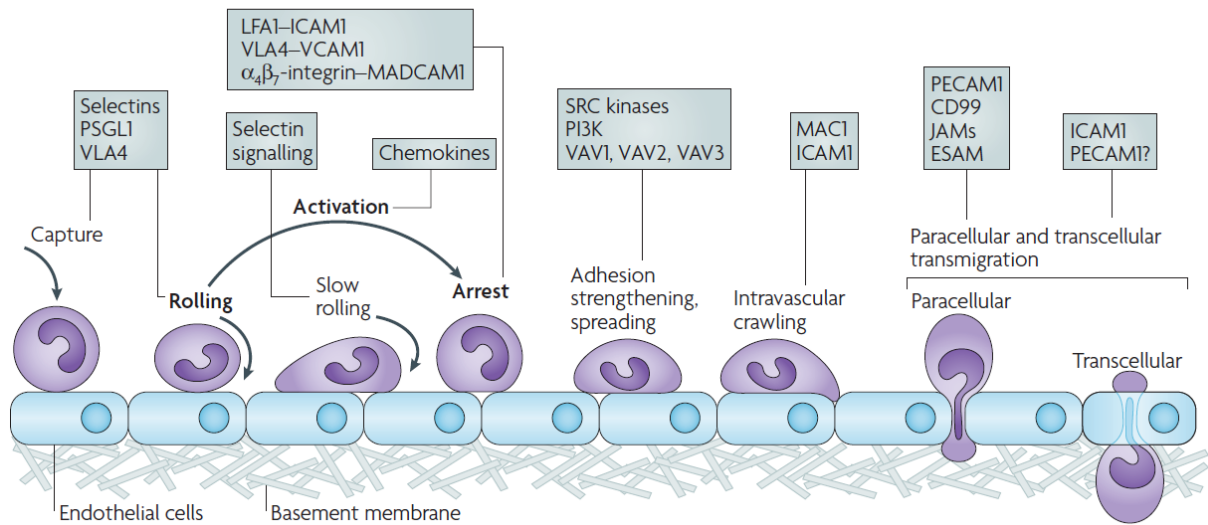


Figure 1-3 Schematic view of the events in the leukocyte recruitment cascade with proteins involved in each step (Ley, Laudanna, Cybulsky, & Nourshargh, 2007)

1.1.2.1 Capture and rolling

In order to leave the vasculature, leukocytes must become marginalized, leave the center of the blood stream, and decelerate to come into contact with the vascular endothelium. However, due to the shear force of the blood flow in the post-capillary venules, collisional contact duration between leukocytes and unstimulated endothelium is very brief (i.e. 25ms) (Simon & Goldsmith, 2002). Therefore, specific interaction between leukocytes and stimulated endothelium is required.

In fact, during inflammation, locally released stimuli (e.g. bacterial peptides, chemokines, and damage-associated molecular patterns etc.) activate endothelial cells in the nearby venules to upregulate adhesion molecules on the plasma membrane which will aid leukocytes' capture and slow rolling. Selectins are a family of long adhesion molecules extending from the plasma membrane which facilitate the capture of circulating leukocytes onto the endothelium: L-selectin is expressed by most leukocytes whereas P- and E-selectins are expressed by inflamed endothelial cells and/or activated platelets. Increased expression of P- and E-selectin on activated endothelium induced leukocytes tethering (Kunkel & Ley, 1996; Petri, Phillipson, & Kubes, 2008). Once tethered, leukocytes can rapidly release and reengage selectin ligand bonds, resulting in a slow rotational movement along the endothelium named rolling. PSGL-1 (P-selectin glycoprotein ligand-1) has a dominant role as the ligand for all three selectins (P-, E-, and L-selectin), contrary to what its name implies. Also, the binding of PSGL-1 to L-selectin on the leukocyte nucleates leukocyte-leukocyte interaction, by which adherent leukocyte facilitate secondary leukocyte tethering (Eriksson, Xie, Werr, Thoren, & Lindbom, 2001). Importantly, selectins actually require shear force to support adhesion; the rolling cells detach when flow is stopped (R. Alon, Hammer, & Springer, 1995; Finger et al., 1996; Lawrence,

Kansas, Kunkel, & Ley, 1997; Li et al., 2016; Yago et al., 2004). Although rolling is mainly mediated by selectins, some integrins also participate in rolling. Berlin et al. have shown that lymphocytes can roll on immobilized Vascular Adhesion Molecule 1 (VCAM-1) by engaging their cell-surface Very Late Antigen 4 (VLA-4, also known as $\alpha_4\beta_1$ integrin) (Berlin et al., 1995). VLA-4 dependent rolling is mainly seen for monocytes and monocyte-like cell lines (Jason R. Chan, Hyduk, & Cybulsky, 2001; Huo, Hafezi-Moghadam, & Ley, 2000), T cell-lines (Berlin et al., 1995) and T cells (Singbartl et al., 2001). Rolling along the endothelium increases the efficiency of leukocyte encounters with chemokines and other inflammatory mediators presented on the luminal endothelium and integrin-dependent leukocyte arrest.

1.1.2.2 Arrest and subsequent adhesion

During inflammation, endothelial cells are stimulated by inflammatory cytokines to express adhesion molecules and synthesize chemokines and other chemo-attractants that are presented on their luminal surface. After being activated by chemokines sequestered on the endothelium, rolling leukocytes adhere to the endothelium by rapid formation of shear-resistant binding mediated by specialized leukocyte integrins (Rose, Alon, & Ginsberg, 2007). Integrins are non-covalently associated heterodimeric cell surface adhesion molecules consisting of combinations of α and β subunits. Leukocytes express at least 10 members of the integrin family belonging to the β_1 -, β_2 - and β_7 -subfamilies (Luo, Carman, & Springer, 2007) Integrins relevant for leukocyte recruitment belong to β_1 - and β_2 -integrin families (Ley et al., 2007): LFA-1 (Lymphocyte Function-associated Antigen-1, CD11a/CD18, $\alpha_L\beta_2$) for all the effector leukocytes; Mac-1 (Macrophage antigen-1, CD11b/CD18, $\alpha_M\beta_2$) for neutrophils and monocytes and VLA-4 for (Very Late Antigen-4, CD49d/CD29, $\alpha_4\beta_1$) monocytes, eosinophils and various effector lymphocytes (Nourshargh & Alon, 2014).

Most circulating leukocytes express integrins in a low affinity state (Carman & Springer, 2003). Upon binding of chemokines to G-protein-coupled receptors (GPCRs) expressed on leukocytes, a complex intracellular signaling network is triggered within milliseconds (Ronen Alon & Feigelson, 2009; Dixit & Simon, 2012; Ley et al., 2007; Shamri et al., 2005). This induces integrins to undergo an almost instantaneous change in conformation (Shamri et al., 2005), which is necessary for binding to its ligand expressed on stimulated endothelial cells (Ley et al., 2007). Different subsets of leukocytes bind with different ligands via integrins expressed on their cell surface. Neutrophils mainly adhere through LFA-1 to ICAM-1 (Intercellular Adhesion Molecule-1) expressed by endothelial cells, which mediates neutrophils adhesion to the vascular wall under shear flow (Ley et al., 2007; Petri et al., 2008). During lymphocyte recruitment into the tissue, LFA-1 is the dominant integrin involved in adhesion (Dustin & Springer, 1988; Shamri et al., 2005) by binding to its ligand ICAM-1 (Shamri et al., 2005). As described above, LFA-1 prevails in a low affinity state on most circulating lymphocytes. Stimulation of lymphocyte-GPCRs by the chemokines rapidly shifts LFA-1 integrin to high affinity state (Carman & Springer, 2003). For T lymphocytes, they are not only recruited to

tissue but also home to lymph nodes. *In vitro* study of T-lymphocyte adhesion to the specialized lymph node endothelium (high endothelial venule, HEV) demonstrated that besides LFA-1, VLA-4 is also involved in T-cell adhesion and the effects of VLA-4 and LFA-1 are overlapping and additive (Faveeuw, Mauro, E, Price, & Ager, 2000). In contrast to neutrophils and lymphocytes, β_2 -integrins seem to play a moderate role in monocyte adhesion. Instead, β_1 -integrins seem to play a more substantial role in monocyte adhesion to endothelium by VLA-4 binding to VCAM-1 (Vascular Cell Adhesion Molecule-1) (Ley et al., 2007; Nourshargh & Alon, 2014).

1.1.2.3 Intravascular crawling

Post arrest, leukocytes rapidly protrude and use their integrins to translocate (crawl) on the apical aspects of the endothelium to search for exit cues (Figure 1-3) (Nourshargh & Alon, 2014). Different subsets of leukocyte have been observed to crawl on the vessel wall. Adherent neutrophils and monocytes were observed to crawl significant distances within the vessel (Auffray et al., 2007; Phillipson et al., 2009; R. Sumagin, Prizant, Lomakina, Waugh, & Sarelius, 2010). Adherent T-lymphocytes have been seen crawl over the luminal surface of the endothelium (Shulman et al., 2009). Intravascular crawling of neutrophils is dependent on leukocyte β_2 -integrin Mac-1 and its ligand ICAM-1 expressed on endothelial cells (R. Sumagin et al., 2010). For monocytes and T lymphocytes, they were also shown to crawl long distance on the endothelium in a LFA-1 dependent manner (Auffray et al., 2007; Shulman et al., 2009; R. Sumagin et al., 2010). In most inflammatory settings, leukocytes crawling is both chemokine-GPCR stimulated and integrin-dependent and is tightly regulated by actomyosin machineries serially triggered by GPCR-activated small GTPase and integrin occupancy events (Nourshargh & Alon, 2014). Multiple guidance cues such as intravascular chemokines and shear stress generated by blood flow are involved in leukocyte crawling. During intravascular crawling, leukocytes also rearrange their cytoskeleton to migrate via interaction between their surface-expressed integrins and the corresponding endothelial ligands. Understanding the guiding mechanism involved in leukocyte planar migration is at the center of our study. Upcoming sections will present more detailed information regarding important molecular components involved in leukocyte planar migration as well as the motility characteristics.

1.1.2.4 Transmigration

The last step of the cascade is the leukocyte transmigration outside the vasculature and into the tissue. Multiple molecular and cellular events enable crawling leukocytes to initiate breaching out the endothelium and start transmigration. This process requires accurately timed adhesive interactions with the luminal aspect of the endothelium and the morphological change in leukocyte to go through tight endothelial junctions and pores. Leukocyte transmigration can occur via migration through junctions between adjacent endothelial cells (paracellular transmigration) or through the body of the endothelial cells

(transcellular transmigration). Paracellular transmigration remains the primary route accounting for ~70% ~90% transmigration events (Ley et al., 2007).

Both modes of transmigration are supported by leukocyte-driven molecular changes in the endothelium to facilitate leukocyte passage. Integrin-mediated leukocyte adhesion can trigger clustering of endothelial ICAM-1 and VCAM-1 that provide stable platform for leukocyte firm adhesion and transmigration (Carman & Springer, 2004). Ligation of ICAM-1 and VCAM-1, together with their partner proteins can also elicit multiple signaling events that induce endothelial cells to reduce their barrier properties (Nourshargh & Alon, 2014). Moreover, ICAM-1 ligation can also result in tyrosine phosphorylation of key endothelial cell junction molecules whose response can lead to activation of endothelial intracellular myosin (Carman & Springer, 2008). The contraction of the adjacent endothelial cells can help further opening the junction to allow leukocyte to pass through. Once leukocytes have engaged with endothelial junctions, breaching of endothelium is regulated by adhesion molecule expressed selectively, or at high density at the border of endothelial cells, such as VE-Cadherin, JAMs (Junctional Adhesion Molecules), PECAM-1 (Platelet Endothelial Cell Adhesion Molecule-1). Leukocyte transmigration itself can affect the cell surface redistribution and internalization of key cell border structures, the recycling of intercellular pools of these molecules and their enzymatic cleavage. This will allow the continuous removal of intercellular cadherin bonds that will open the junction, the increase of local concentration of adhesion molecules that may ligate to leukocyte and thus actively induce the whole transmigration process. Once outside the endothelium, the leukocytes will further breach the basal membrane and the embedded pericytes to reach the tissue where they will further migrate to join the inflamed site.

Interestingly, leukocyte transmigration seems to occur at predefined places ('transmigration hotspot') and some locations even favor successive transmigration of multiple leukocytes (Schimmel, Heemskerk, & Van Buul, 2017) suggesting that different cues may guide leukocyte to the site of transmigration. Once in the tissue, leukocytes are also guided by external cues to reach the afflicted site (Weber et al., 2013). In the following sections, we will also cover the different guidance cues for leukocyte transmigration into the tissue.

1.1.3 Effector T cells

In this study, human effector T cells are chosen as our cellular model. Here, we will give a general presentation on their maturation, activation and the expression of different surface molecules during these processes.

T lymphocytes are derived from the multipotent hematopoietic stem cells (HSCs) that are found in the bone marrow. Their progenitor cells (lymphoid progenitor cells) migrate from the bone marrow via blood circulation to the thymus, where they mature into functional T cell

and develop their surface markers. This is the reason for the name thymus-dependent (T) lymphocytes, also known as T cells. T-cell precursors arriving in the thymus from the bone marrow spend up to a week differentiating there before they enter a phase of intense proliferation. In a young adult mouse, the thymus contains about $1-2 \times 10^8$ thymocytes. About 5×10^7 new cells are generated each day; however, only about $1-2 \times 10^6$ (roughly 2–4%) of these leave the thymus each day as mature T cells (Janeway et al., 2016). About 98% of the thymocytes that develop in the thymus also die in the thymus by apoptosis. This apparently profligate waste of thymocyte is a crucial part of T-cell development because it reflects the intensive screening and rigorous testing period to make sure that each thymocyte can recognize self-peptide - self MHC complexes and capable of self-tolerance before being exported to the periphery. At this point of their maturation, these single positive (CD4+ or CD8+) T cells are known as naïve T cells.

The naïve T cells are known to be “naïve” because they have not yet been activated even though they already reached maturation. For this, they will need to encounter their specific and fitting antigen presented by antigen presenting cells (APCs). To meet their APCs, naïve T cells exit the thymus, circulate in the blood stream, transit in the tissue and finally reach the secondary lymphoid organs such as the lymph nodes, which are the meeting points between naïve T cells and APCs. Once they reach these organs, they enter the lymph node through high endothelial venule (HEV), a specialized vessel for T cell entrance. HEV secretes chemokines and adhesion molecules that allow naïve T cells to further transmigrate into the lymph node to the paracortex via the extravasation cascade. If no infection occurs, naïve T cells re-enter the circulation for another round of scanning in another lymph node until they meet APCs. If there is an infection, APCs such as tissue-resident

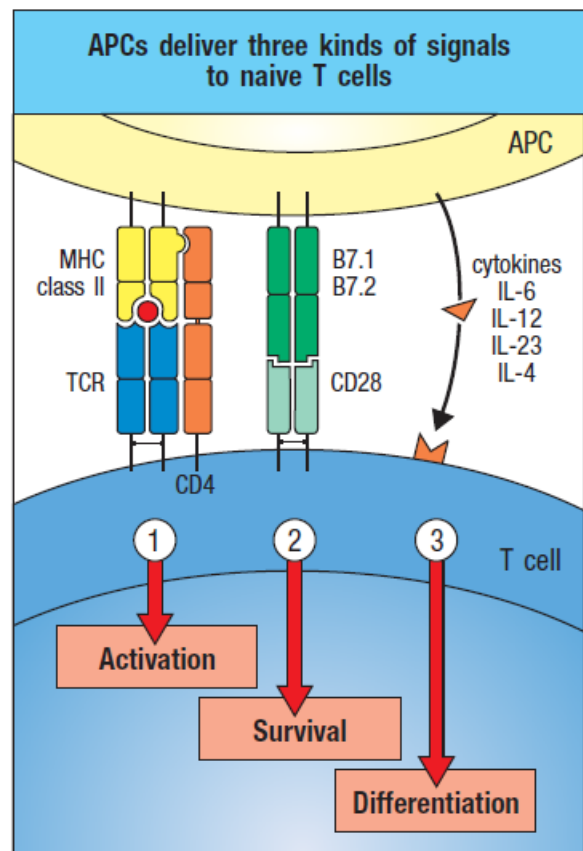


Figure 1-4 Three types of signals involved in activation of naïve T cells by APCs (Janeway et al. 2016)

DCs will mature, undergo phenotypic change to become highly mobile and upregulate their antigen presenting function. Upon antigen capture, mature DCs will transit through the tissue to reach the lymph node and enter through afferent lymphatic vessel to meet naïve T cells. T cell activation upon encounter with APCs is mediated by three types of signals (Figure 1-4): the first signal is provided by binding of the T cell receptor to its cognate peptide presented on MHC on an APC. The second signal comes from co-stimulation, in which surface receptors

on the APC are induced by a relatively small number of stimuli, usually products of pathogens, but sometimes breakdown products of cells, such as necrotic-bodies or heat shock proteins. The second signal licenses the T cell to respond to an antigen and promotes the survival and expansion of the T cells. Without it, the T cell becomes anergic, and it becomes more difficult for it to be activated in the future. This mechanism prevents inappropriate responses to self, as self-peptides will not usually be presented with suitable co-stimulation. The third type of signal comes from cytokines that direct T cell differentiation into one of the subsets of effector T cells. Upon activation by APCs, T cells undergo rapid cell division and then differentiate into effector T cells that acquire the ability to synthesize molecules required for the specialized helper (CD4+) or cytotoxic (CD8+) functions when they re-encounter their specific antigen.

Upon T cell activation, changes also occur in the different molecules expressed on the surface of naïve and effector T cells (with the example of a CD4+ T cell). Resting naïve T cells express L-selectin, through which they enter lymph node but also express at relatively low levels of other adhesion molecules such as CD2 and CD44. Upon activation, expression of L-selectin ceases and expression of ligands of P- and E-selectin are induced (eg. PSGL-1), which allows the activated T cells to roll on P- and E-selectins expressed on endothelium at the site of inflammation. Increased amounts of LFA-1 integrins are also produced, which is activated to binds its ligands ICAM-1 and ICAM-2 expressed on the inflamed endothelium and allow T cell to firmly adhere and crawl on the endothelium. VLA-4 integrin, which is not expressed on naïve T cells, is induced on activated T cells to ensure that they enter peripheral tissues at sites where they are likely to encounter infection. Activated T cells also have on their surface an increased amount of adhesion molecule CD2, ligand of LFA-3 integrin (Makgoba, Sanders, & Shaw, 1989), increasing the avidity of their interaction with potential target cells, as well as the amount of the adhesion molecule CD44. Moreover, a change occurs in the isoform of CD45 molecule expressed, activated T cell express CD45RO isoform, which associates with the T cell receptor and CD4. This change makes T cell more sensitive to stimulation of low concentration of peptide. Finally, the sphingosine-1-phosphate receptor 1 (S1PR1) is expressed by naïve T cells, allowing the egress from lymphoid tissues of non-activated cells. This receptor is downregulated several days after activation to prevent T cells from exiting during the proliferation and differentiation. After several days, it is expressed again, allowing effector T cells to exit from lymphoid tissues.


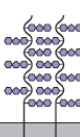




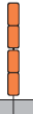



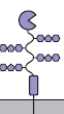
		Cell-surface molecules										
												
CD4 T cell		L-selectin	PSGL-1	S1PR1	CD45RA	CD45RO	VLA-4	CD4	T-cell receptor	LFA-1	CD2	CD44
Resting		++	-	+	+	-	-	+	+	+	+	+
Activated		-	+	-	-	+	+	+	+	++	++	++

Figure 1-5 Expression of key CD4+ T cell surface molecules before and after activation (Janeway et al., 2016)

1.2 Motility and guidance: from molecular components to cellular response

1.2.1 Actin cytoskeleton and actin-based motility

Organisms from all domains of life have a cytoskeleton which they depend on to maintain structure and to support movements. The actin cytoskeleton, a collection of actin filaments with their regulatory proteins, is the primary force-generating machinery in the cell. It can produce protrusive force through polymerization of actin filaments as well as contractile force through sliding actin filaments along bipolar filaments of myosin II. Both forces types are important in defining and changing cell shape and for cell migration. In this section, we will discuss the composition of actin cytoskeleton as well as actin-based protrusion and contraction which are involved in cell motility.

1.2.1.1 Composition of actin cytoskeleton

The actin cytoskeleton is composed of two types of actin proteins depending on their state of polymerization: the globular monomer (G-actin) and the filamentous polymer (F-actin). If a critical concentration of ATP-bound G-actin is reached, the polarization of a double-helix-shaped filament starts and thus generates F-actin. Integration of G-actin into the filament will result in hydrolysis of ATP to ADP which will allow access to the F-actin filament by depolymerization proteins, thereby participating in the equilibrium of polymerization/depolymerization of F-actin (Figure 1-6). The polarity of the actin strand is characterized by a barbed end (+), which is more dynamic than the counterpart, the pointed end (-) polymerizing ten times more slowly. Different actin-binding proteins participate in the control of filament dynamics. These proteins include monomer binding proteins (e.g. profilin), actin polymerases (e.g. formin), capping proteins, severing proteins (e.g. cofilin), cross-linking proteins (e.g. fascin) and branching proteins (e.g. Arp2/3). Collectively, these proteins maintain a large pool of actin monomers available for polymerization, nucleate assembly of new actin filaments, promote elongation or terminate elongation by capping barbed or pointed ends, sever filaments and cross filaments. Actin structure regulated by monomer polymerization and its

associated proteins is responsible for the formation of different membrane protrusions such as lamellipodia and filopodia at leading edge that generate force necessary for cell migration. The upcoming paragraphs will explain how actin cytoskeleton generate protrusive forces in these two typical structures and the role of different regulatory proteins will also be covered.

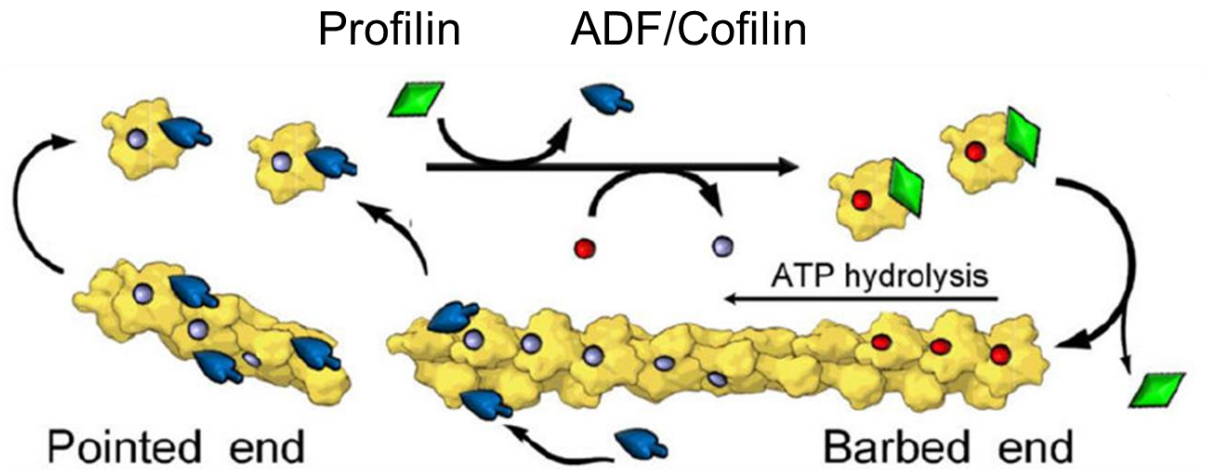


Figure 1-6 The dynamics of actin filament assembly. Polymerization of the actin filament preferentially occurs at the barbed end from ATP-actin-profilin complexes; after incorporation of an actin monomer into the filament, profilin dissociates. Polymerization-triggered ATP hydrolysis and subsequent release of inorganic phosphate from actin subunits make filaments more susceptible to depolymerization and increase their affinity for actin-depolymerizing factor (ADF)/cofilin. ADF/cofilin severs filaments, promoting their depolymerization. Released actin subunits bind to profilin, which competes off ADF/cofilin and promotes nucleotide exchange in the actin monomer, thus producing new ATP-actin-profilin complexes. (adapted from [T. Svitkina, 2018])

1.2.1.2 Actin cytoskeleton in membrane protrusion

To generate a protrusive force, cells use energy of actin polymerization (Pollard, 2016). The directionality of the protrusive force produced by actin polymerization originates from the structural polarity of actin filaments where one end (barbed end or plus end) polymerizes faster than the other (pointed end or minus end) (Woodrum, 1975). In cells, polymerizing actin filaments are oriented uniformly with their barbed end towards the plasma membrane. Whereas elongating barbed ends push on the membrane, disassembly by severing and depolymerization occurs closer to the pointed ends to release actin monomers for recycling. Polymerization of individual actin filaments produces piconewton forces (Kovar & Pollard, 2004). To produce larger forces to propel the cell forward, filaments are organized into parallel bundles in filopodia or branched network in lamellipodia.

1.2.1.2.1 Filopodia

Filopodia are slender, finger-like protrusion formed at the leading edge of migrating cells such as fibroblasts, or cells extending long processes, such as neurons. In filopodia,

individual actin filaments span the entire length of the filopodium and are uniformly oriented with their barbed ends towards the filopodium tip (Small, Isenberg, & Celis, 1978). During protrusion, actin monomers are added at the filopodium tip, move away from the tip as a part of the filament lattice, and are released at the rear of the filopodium (Mallavarapu & Mitchison, 1999; Y. L. Wang, 1985). Formation of long actin filaments in filopodia, in the cytoplasm of motile cells is challenging due to the abundant presence of capping proteins capable of binding barbed ends and terminating filament elongation. Accordingly, Ena/VASP proteins and some formins are enriched at the tip of filopodium to protect barbed ends from capping proteins (T. M. Svitkina et al., 2003; C. Yang et al., 2007). While Ena/VASP proteins are particularly important for formation of filopodia in neuronal growth cones (Lebrand et al., 2004), they share functions with formins in other cell types (Homem & Peifer, 2009). Another challenge for elongation of actin filaments in filopodia is the delivery of actin monomers and other proteins from the pools in the cell to the filopodial tip, where the polymerization takes place. Unconventional myosin X has been found to promote filopodium elongation. The myosin X dimers are thought to walk towards the barbed ends of actin filaments and deliver key actin regulatory proteins (e.g. VASP) to filopodial tip by using its motor activity (Kerber & Cheney, 2011). Fast elongation of actin filaments at filopodial tips allows for membrane protrusion, but the force produced by elongation can buckle actin filaments (Kovar & Pollard, 2004), therefore limiting their pushing ability. Cells overcome this problem by cross-linking filopodial filaments along their length to increase their collective stiffness (Vignjevic et al., 2006). The major cross-linking protein at the leading edge is fascin, a bivalent monomeric protein that makes tight cross-links between filaments. The small number of actin filaments in filopodia means that there are few pointed ends to release actin subunits. The presence of severing proteins such as ADF/cofilin (Breitsprecher et al., 2011) and myosin II (Medeiros, Burnette, & Forscher, 2006) can accelerate the actin turnover. The actin filament bundle with a filopodium functions as a scaffold to maintain the highly asymmetric shape of the filopodium. Lateral binding of actin filaments to the plasma membrane contributes to the stiffness of the filopodium and is likely mediated by proteins of the ezrin-radixin-moesin (ERM) family (Niggli & Rossey, 2008). Other membrane proteins such as IRSp53 through its I-BAR (inverted Bin/Amphiphysin/Rvs) domain stabilizes the tubular shape of the plasma membrane in leading edge filopodia. Because of their elongated shape, filopodia are believed to function as "fingers" to reach, sense, and grab a target. It can guide cell guide cell locomotion during normal morphogenesis or cancer metastasis, or form cell-cell junctions in epithelia and neurons. Filopodia can also capture pathogens for subsequent internalization (Romero et al., 2011). Consistent with these functions, tips of leading edge filopodia are enriched with adhesion and signaling proteins that could initiate adhesions when contacting adhesive surfaces and trigger cellular responses.

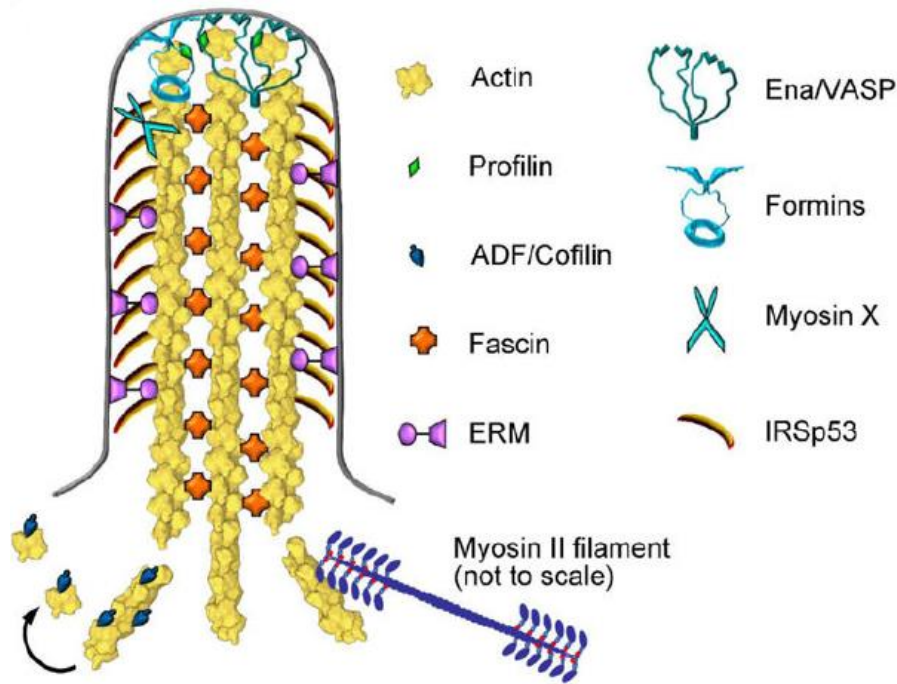


Figure 1-7 Molecular organization of filopodia: actin filament and regulatory proteins (T. Svitkina, 2018)

1.2.1.2.2 Lamellipodia

Lamellipodia are flat cellular protrusions at the leading edge of mobile cells such as migrating leukocytes. They contain a branched actin filament network formed by attachment of the pointed end of one filament to the side of another filament, with the formation of an angle of around 70° between the barbed ends of two filaments. The actin turnover in lamellipodia includes continuous nucleation of new daughter filaments at the side of preexisting mother filaments. Daughter filaments elongate and push on the membrane. Then, their barbed end is capped, and elongation is thus terminated. The disassembly of the network functions through debranching and severing of actin filaments, followed by the depolymerization of filament fragments. The molecular machinery controlling the lamellipodia formation includes many regulatory proteins besides actin itself. Among these, Arp2/3 complex is one of the essential proteins in controlling the branched network. It nucleates a daughter filament from the side of a mother filament, links the mother and daughter filament at the angle of around 70° and caps the pointed end of the daughter filament (Mullins, Heuser, & Pollard, 1998). The function of Arp 2/3 complex requires activation by a nucleation-promoting factor and binding to a mother filament to nucleate a new branch. The most important nucleation promoting-factors belong to the Wiskott-Aldrich Syndrome protein family including mainly WASp, N-WASp, WAVE1-WAVE3 in mammals. The WAVE regulatory complex typically activates the Arp2/3 complex in lamellipodia. The nucleation-promoting factors are recruited at the plasma membrane by signaling events as well as guidance cues to nucleate branched actin filament that generate protrusive force on the plasma membrane when it's needed.

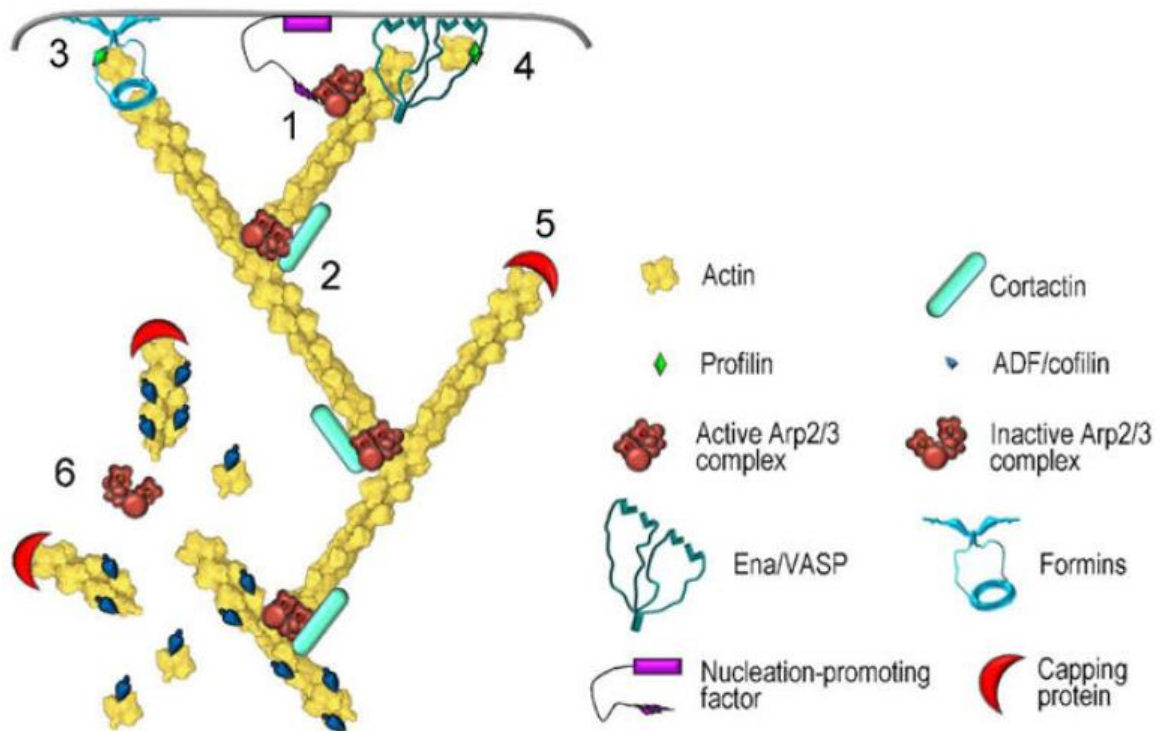


Figure 1-8 Organization of branched actin network: The Arp2/3 complex is cooperatively activated by a membrane-targeted nucleation-promoting factor and a preexisting “mother” actin filament (1). Upon activation, the Arp2/3 complex nucleates a new “daughter” actin filament at the side of the mother filament and remains associated with the branchpoint which are further stabilized by cortactin (2). The nascent filament elongates with its barbed end oriented toward the membrane. Its elongation is promoted by formins (3) and/or Ena/VASP proteins (4); After a period of elongation, the barbed end is capped by capping protein (5). Disassembly at the rear of the lamellipodial network occurs through dissociation of branches and ADF/cofilin-mediated severing (6). (Adapted from [T. Svitkina, 2018])

Constant production of new filaments by Arp2/3 requires concurrent termination of the growth of the barbed ends to prevent exponential expansion of the lamellipodial network and overconsumption of actin monomers. This task is accomplished mainly by heterodimeric capping proteins that tightly bind the barbed ends of the actin filament barbed ends. Disassembly of branched actin networks in the lamellipodia depends on severing by ADF/cofilin. The severing can also help the cell to start a new lamellipodium by creating new uncapped barbed ends (Ghosh et al., 2004). Moreover, dissociation of a daughter filament from the mother filament also contributes to the disassembly of the branched actin network. ADF/cofilin promotes the debranching by change the conformation of the mother filament and reducing the affinity for the Arp2/3 complex (C. Chan, Beltzner, & Pollard, 2009). In contrast, some other proteins stabilize the branched network: cortactin stabilizes the branches probably by forming an additional link between the Arp2/3 complex and the actin filament (Weaver et al., 2001); Formins (C. Yang et al., 2007) and Ena/VASP (Bear et al., 2002) produce long and unbranched filaments with in the branched network by enhancing filament elongation and counter-balancing the effect of capping proteins; Actin cross-linkers are also present in the lamellipodia to consolidate the entire network.

The protrusive mechanism with lamellipodia has several advantages compared with filopodia in force generation. First, short, stiff filaments are more efficient and less prone to buckling. Also, daughter filaments anchored to the mother filament can efficiently transform the energy of actin polymerization into useful work. Moreover, repetitive branching allows the network to easily expand or reorient itself by simply adjusting the rates and sites of the nucleation and capping. With these advantages, lamellipodia can generate much greater protrusive forces than filopodia and serve as the major cellular engine to propel the leading edge forward. Lamellipodia also function as navigation devices for guiding a cell around obstacles, sensing soluble guidance cues, and probing the chemical and mechanical properties of the substrates. Although lamellipodia have mostly been studied using cells cultured on a flat solid surface, cells migrating in more physiological conditions, such as a three-dimensional matrix with physiological stiffness, also use lamellipodia for protrusion.

1.2.1.3 Actomyosin-based contraction

The actin cytoskeleton generates contractile forces through mutual sliding of actin and myosin filaments. The contractile forces generated by cells are used for many purposes including migration, cell-shape change, organization of extra-cellular matrix etc. Cells exert contractile forces through various arrays of actin and myosin filaments varying from actomyosin bundles to mixed networks.

1.2.1.3.1 Myosins

Myosins are a large family of motor proteins best known for their roles in muscle contraction as well as in a wide range of other motility processes where contractile forces are necessary, such as cell migration, cytokinesis, cell-shape changes and formation of cell-cell and cell-matrix junctions in eukaryotes (Heissler & Manstein, 2013). Myosins use the energy of ATP hydrolysis to move along actin filaments (Sweeney & Holzbaur, 2018). Class II myosin are specifically designed for contraction (Figure 1-9). Its amino-terminal motor domain of the heavy chain ("head") has the ATPase and actin-binding function, whereas the "tail" mediates parallel dimerization of heavy chains. Each heavy chain binds to two different light chains-essential and regulatory-at the region between the head and the tail. Myosin II polymerizes into bipolar filaments through interaction of the tails, so the motor domains are located at the end of the filament. These bipolar filaments pull actin filaments, which are stabilized by tropomyosins, together, causing contraction. In addition to smooth muscle, cardiac and skeletal myosin II, there are three isoforms of non-muscle myosin II: myosin IIA (MIIA), myosin IIB (MIIB) and myosin IIC (MIIC). Both MIIA and MIIB are typically seen in most mammalian cells (Clark, Langeslag, Figdor, & van Leeuwen, 2007; Vicente-Manzanares, Ma, Adelstein, & Horwitz, 2009). They fulfil different but overlapping functions in cell migration. MIIA is situated all through the cell and plays a crucial role in retracting cell edges and adhesion maturation at the leading edge (Even-Ram et al., 2007; Vicente-Manzanares, Zareno, Whitmore, Choi, &

Horwitz, 2007) . MIIB localizes in the central and rear regions, but not in protrusions (Vicente-Manzanares, Koach, Whitmore, Lamers, & Horwitz, 2008). It helps to determine the overall morphology of the cell as well as facilitate adhesion maturation.

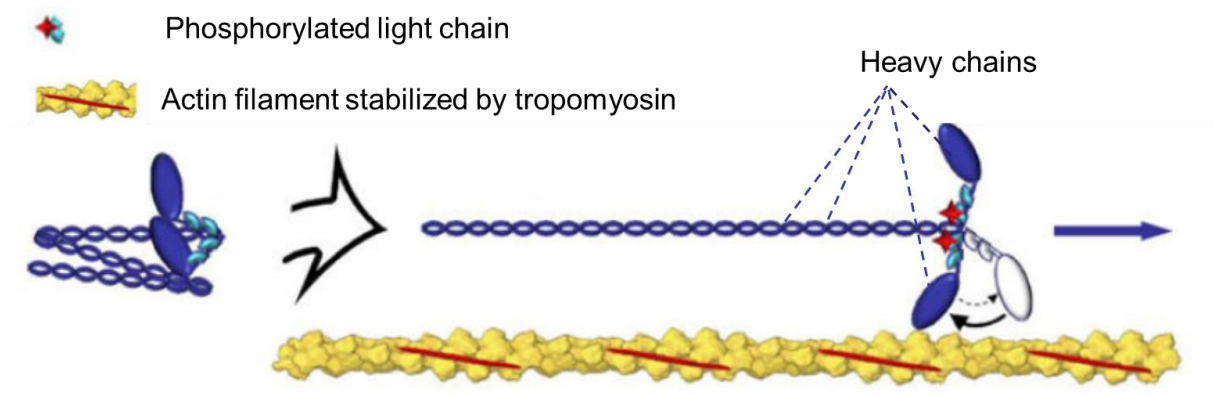


Figure 1-9 A non-muscle myosin II molecule has a folded conformation in an inactive state (left). Phosphorylation of the myosin regulatory light chain causes unfolding of the myosin II molecule and restoration of motor activity; this activated myosin II can move toward the barbed end of the actin filament by swinging its motor domain in an ATP-dependent manner (right) (T. Svitkina, 2018).

1.2.1.3.2 Contractile actin-myosin bundle

Cells can exert contractile force through a mixed bundle of actin and biopolar myosin II filaments where myosin filaments move along oppositely oriented actin filaments (Figure 1-11). In cells such as fibroblasts, this structure is known as “stress fibers”, where myosin II forms bipolar filaments aligned in the fiber axis (Figure 1-10). In these stress fibers, actin filaments have mixed polarity and variable lengths, so that oppositely oriented filaments often overlap and allow generation of larger forces. Proteins promoting barbed ends elongation - VASP and formins - participate in the assembly of actin filaments in stress fibers. VASP is present in stress fibers in a punctuate pattern (Reinhard, Jouvenal, Tripier, & Walter, 1995) and becomes particularly enriched in regions where stress fibers ruptured, where it promotes actin filament elongation to repair the damage (M. A. Smith et al., 2010).

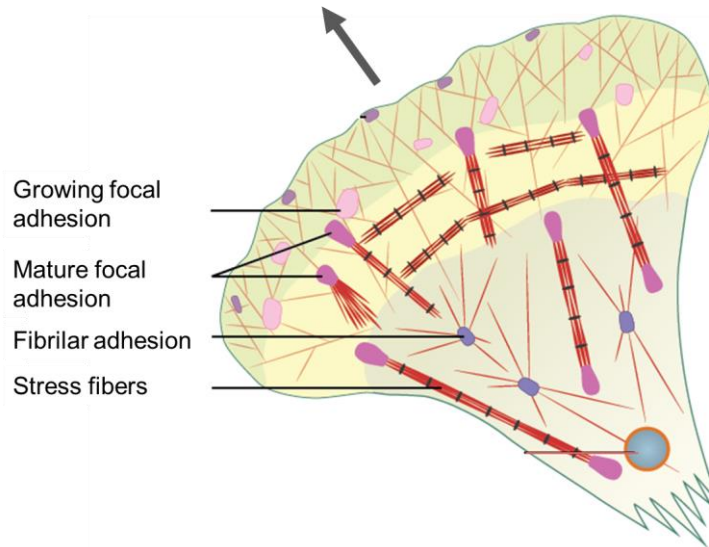


Figure 1-10 Illustration of a migrating fibroblast-like cell with focal adhesion and stress fibers

Stress fibers are attached to their ends of adhesion complex called focal adhesion (Figure 1-10). This transmembrane linkage involves members of the integrin family (P. Hu & Luo, 2013). Integrins bind directly the extracellular matrix and use adaptor proteins to bind actin filaments inside the cell (Wehrle-Haller, 2012). These adaptor proteins, such as talin and vinculin, are highly enriched in focal adhesions. In migrating cells such as fibroblasts, contractile forces generated by stress fibers are typically applied to focal adhesions. These forces can rupture the adhesion and induce local retraction of cell edge. Alternatively, they can also strengthen the adhesion, which serve as a launchpad for a new round of protrusion (Wolfenson, Bershadsky, Henis, & Geiger, 2011).

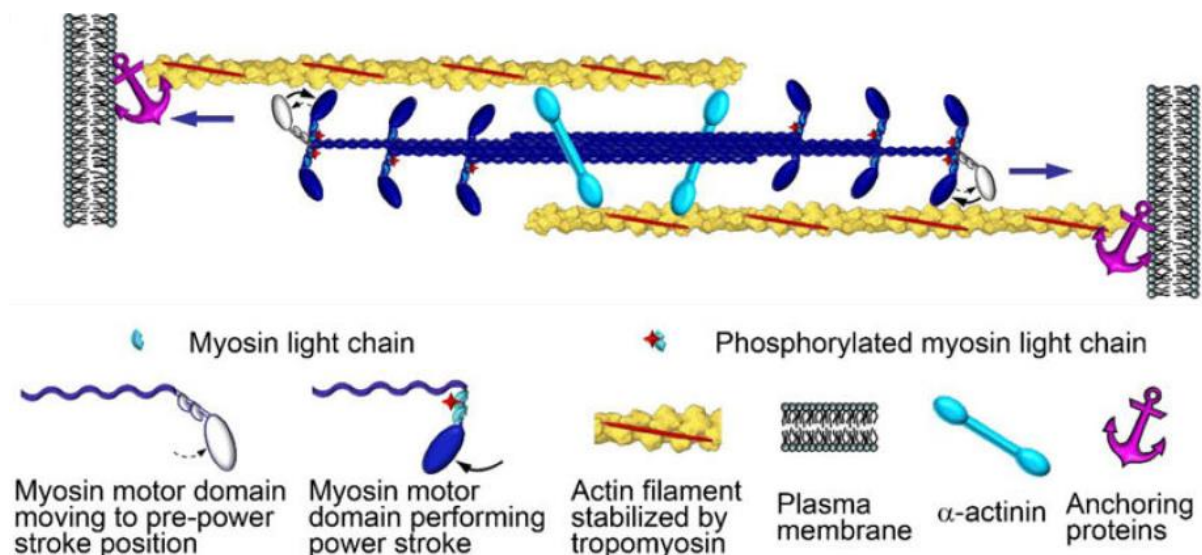


Figure 1-11 Contraction of actin-myosin II bundle mediated by bipolar filaments of myosin II that move along oppositely oriented actin filaments anchored at their barbed ends to the cell plasma membrane. (T. Svitkina, 2018).

1.2.1.3.3 Contractile actin-myosin network

To mediate contraction, actin and myosin II filaments can also be arranged into a network in which individual filaments are oriented at a range of angles. A characteristic pattern of the actomyosin network is the “cell cortex”, an actomyosin layer coating the plasma membrane in many cells. The molecular connections between the plasma membrane and the actin-myosin II network are not yet well understood and may depend on additional transmembrane and adaptor proteins. ERM-family proteins are candidates (Niggli & Rossy, 2008) as their depletion decreases membrane-to-cortex attachments (Diz-Muñoz et al., 2010). Many other proteins that can bind to both actin and the membrane, such as formins, Ena/VASP, may also contribute to this linkage. The contraction also leads to changes in cell shape and remodels tissues in processes such as tissue morphogenesis. Moreover, the cortical actin-myosin II network underlying the plasma membrane defines the mechanical properties of the cell surface, generate surface tension that allows cell to resist external forces and produces internal pressures (Salbreux, Charras, & Paluch, 2012). Local damage of the cortex or detachment from the plasma membrane leads to the formation of the bleb, a bubble-like cellular protrusion initially lacking structure-building actin or other components. Once the generation of the bleb equilibrates the hydrostatic pressure pulse, F-actin is recruited into the new protrusion through the contraction of the cortical actin-myosin II network (Ridley, 2011). Blebs often form during apoptosis and are common during cytokinesis, in which they help to release excessive intracellular pressure in daughter cells.

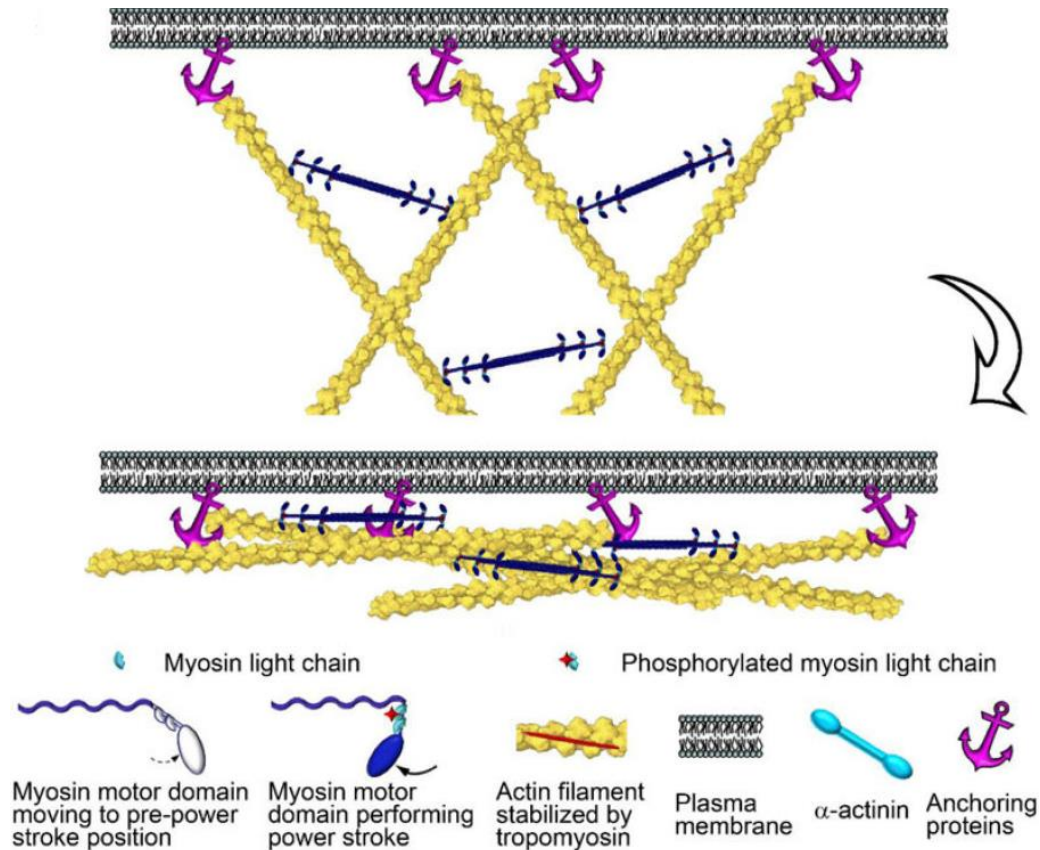


Figure 1-12 Contraction of actin-myosin II network mediated by bipolar filaments of myosin II that move along non-aligned actin filaments anchored at their barbed ends to the cell plasma membrane. (T. Svitkina, 2018)

1.2.2 Integrins: key player in leukocyte migration

While actomyosin network generates either protrusive or contractile force necessary for cell migration, these forces need to be transduced to achieve cell locomotion. A key component in this process is the integrin – the major family of adhesion molecules that mediates cell adhesion and migration. Integrins function much more than simple adhesion molecules. They can link to both cytoskeleton and extra-cellular matrix (ECM) or the surface of other cells. Through this association, integrins transmit both chemical and mechanical information. In this section, we will first introduce the structure of the integrin and their corresponding ligands. Then, we will present the crucial step of integrin activation through “inside-out” and “outside-in” signaling as well as the role of mechanical forces.

1.2.2.1 Structure

Integrins are heterodimeric transmembrane proteins of non-covalently associated α and β subunits. In vertebrates, there are 18 α and 8 β subunits that can assembly into 24 different integrins (Figure 1-13). The leukocytes express at least 10 members of the integrin family belonging to the β_1 -, β_2 -, β_7 subfamilies (Luo et al., 2007). The β_2 and β_7 integrins are

exclusively expressed on leukocytes, whereas the β_1 integrins are expressed on a wide variety of cells throughout the body (Luo et al., 2007).

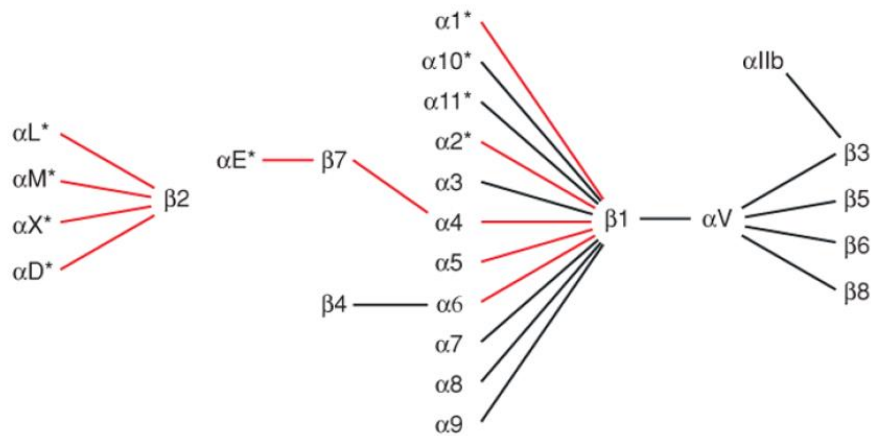


Figure 1-13 Integrin subunits combination: red lines indicate integrins expressed in leukocytes while Asterisk indicate the presence of I-domain on α subunit (Luo et al., 2007)

The α and β subunits are constructed from several domains with flexible linkers between them (Figure 1-14). Each subunit has a large extracellular domain and one transmembrane domain and a short cytoplasmic tail (except β_4 integrins), which indirectly associate with the actomyosin network. The α chain consists of five extracellular domains: a seven-bladed β -propeller, a thigh, and two calf domains and a Genus domain in between. In addition, nine of the 18 integrin α chains express an α -I domain (including most of the leukocyte integrins), inserted between blades 2 and 3 of the β -propeller. The β chain has seven domains with flexible and complex interactions. A β -I domain, which is the homologue of the α -I domain, is inserted in a hybrid domain, which is in turn inserted in a plexin-semaphorin-integrin (PSI) domain. Those are followed by four epidermal growth factor (EGF) domain. In integrins in which it is present, the α -I domain is the major ligand-binding site. Moreover, divalent cations are universally required for ligand binding in all integrins. In α -I domains the metal coordinating residues, and the residues surrounding the metal-binding site, are important for ligand binding. Therefore, this site has been designated the metal ion-dependent adhesion site (MIDAS) and physiologically binds Mg^{2+} . Like the α -I domain, the β -I domain contains a MIDAS for binding negatively charged residues, which physiologically binds Mg^{2+} (Xiao, Takagi, Coller, Wang, & Springer, 2004). Additionally, there are two adjacent metal ion-binding sites, which physiologically bind Ca^{2+} (Xiao et al., 2004), share some coordinating residues in common with the MIDAS, and are known as the LIMBS (ligand-induced metal ion-binding site) and ADMIDAS (adjacent to metal ion dependent adhesion site) (Xiong et al., 2001, p. 3).

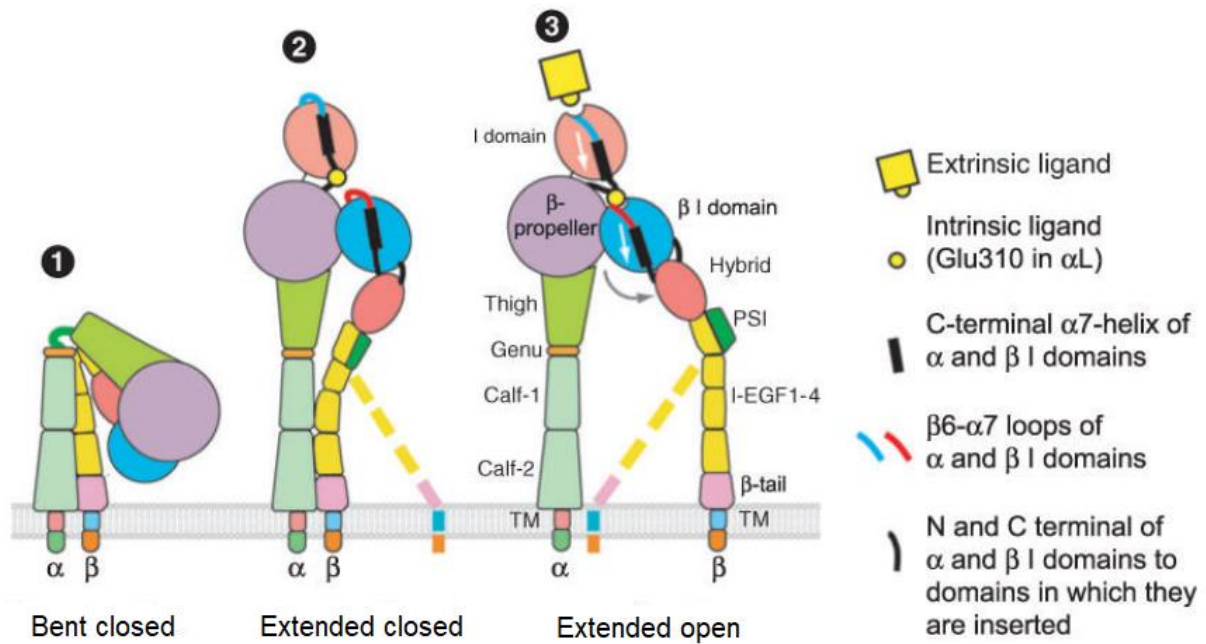


Figure 1-14 Schematics showing the structure of integrin containing α -I domain and different conformations. The β subunit lower legs are flexible and are therefore shown in what may be the predominant (solid representation) and less predominant (dashed lines) orientations. (from[Luo et al., 2007])

Integrins adopt distinct conformations that have different ligand-binding affinities (Figure 1-14). In the bent closed and extended closed conformations, the lower leg pieces and transmembrane regions of α and β subunits remain associated and the ligand-binding site is closed (Luo et al., 2007). In the extended open conformation, the swing-away of the hybrid domain from the α subunit and unclasp of the lower leg pieces and transmembrane regions correlate with a rearrangement of the ligand-binding MIDAS, a piston like movement of an α -helix away from the ligand binding pocket resulting in complete opening of ligand binding site (Luo et al., 2007). The bent closed conformation results in low affinity of ligand binding. In the case of $\alpha_L\beta_2$ integrin (also known as LFA-1), which is predominately expressed by leukocytes, conformational change from bent close to extended open resulted in a 9000 times increase in affinity, strongly supporting that conformational change regulates affinity (Shimaoka et al., 2003). The change from bent close to extended close conformation also resulted in a 500 times increase in affinity, showing an intermediated binding-affinity (Shimaoka et al., 2003). The shift from the bent closed/extended bent conformation to extend open conformation is termed "integrin activation", which will be discussed in 1.2.2.3.

1.2.2.2 Ligands

A characteristic feature of most integrin receptors is their ability to bind a wide variety of ligands. Conversely, many extracellular matrix and cell surface adhesion proteins bind to multiple integrin receptors. Integrin-ligand combination can be clustered into four main classes, based on the nature of the molecular interaction (Campbell & Humphries, 2011). All

five α_v integrins, two β_1 integrins (α_5 , α_v) and $\alpha_{II}\beta_3$ recognize ligands containing an RGD tripeptide active site. $\alpha_4\beta_1$, $\alpha_4\beta_7$ and $\alpha_9\beta_1$, the four members of the β_2 subfamily, bind to an acidic motif, named "LDV", that is functionally related to the RGD. Fibronectin contains this sequence and other ligands such as VCAM-1 and MAdCAM-1 employ also these sequences. Four α subunits containing α -I-domain combine with β_1 and form a distinct laminin/collagen-binding subfamily. Integrins expressed on leukocytes and their corresponding major ligands are summarized down below (Luo et al., 2007). In this study, we mainly focused on two major leukocyte integrins - $\alpha_L\beta_2$ (LFA-1) and $\alpha_4\beta_1$ (VLA-4). These two integrins play crucial roles in leukocyte adhesion and migration both inside the vessel and in the tissue. Moreover, they are also tightly involved in the guidance of leukocyte migration. Respectively, we mainly concentrated on the ICAM-1 (principal ligand of LFA-1) and VCAM-1 (principal ligand of VLA-4) that not only enable linkage to integrins, but also may be involved in leukocyte guiding. This part of the project will be detailed in the following chapters.

Integrin	Distribution	Major ligand(s)
$\alpha_L\beta_2$, LFA-1, CD11a/CD18	Lymphocytes , NK cells, monocytes, macrophages, dendritic cells, neutrophils	ICAM-1 , -2, -3, -5
$\alpha_M\beta_2$, Mac-1, CR3, CD11b/CD18	Monocytes, macrophages, neutrophils, NK cells	iC3b, fibrinogen, heparin, many others
$\alpha_X\beta_2$, p150,95, CR4, CD11c/CD18	Monocytes, macrophages, NK cells, dendritic cells	iC3b, fibrinogen, heparin, many others
$\alpha_D\beta_2$	Monocytes, macrophages, eosinophils, neutrophils	ICAM-3, VCAM-1
$\alpha_4\beta_1$, VLA-4, CD49d/CD29	Lymphocytes , monocytes, eosinophils	VCAM-1 , fibronectin
$\alpha_4\beta_7$, LPAM-1	Lymphocytes, monocytes, NK cells	MAdCAM-1, fibronectin
$\alpha_E\beta_7$, HML-1	Intra-epithelial T lymphocytes	E-cadherin
$\alpha_1\beta_1$, VLA-1, CD49a/CD29	Long-term activated T lymphocytes, B lymphocytes, monocytes	Collagen
$\alpha_2\beta_1$, VLA-2, GPIa, CD49b/CD29	long-term activated T lymphocytes, B lymphocytes, monocytes	Collagen
$\alpha_5\beta_1$, VLA-5, CD49e/CD29	T lymphocytes, monocytes	Fibronectin
$\alpha_6\beta_1$, VLA-6, GPIc, CD49f/CD29	T lymphocytes, monocytes	Laminin

Table 1-1 Table summarizing integrins expressed on leukocytes and their major ligands (proteins and cells involved in this study are in bold) (from[Luo et al., 2007])

1.2.2.3 Activation

In 1.2.2.1, we discussed different conformations of the integrin which also tightly regulate its ligand-binding affinity. The transition from low-affinity conformation to high-affinity conformation is termed "integrin activation". One important characteristics of the

integrin is their bidirectionality, which means that the same activation can be induced by intracellular (“inside-out”) and extracellular (“outside-in”) signals (Figure 1-15).

1.2.2.3.1 Inside-out signaling

Two integrin bind proteins are indispensable for the integrin inside-out activation: talin and kindlin. Talin comprises an amino-terminal FERM (erzin, radixin, and moesin) domain followed by a short, flexible linker and a large carboxy-terminal rod domain. The FERM domain binds to the NPXT motif of β integrin cytoplasmic tails. The talin domain harbors multiple actin-binding domains and vinculin-binding sites, many of which are mechanosensitive and only become exposed under tensile forces. Although N-terminal FERM domain is sufficient for integrin-binding (Ye et al., 2010), the actin-binding rod domain is required for cell adhesion and spreading, suggesting that actomyosin-force mediate the latter process (Theodosiou et al., 2016; X. Zhang et al., 2008). Kindlins are also FERM-domain containing proteins consisting of three members (kindlin 1-3) (X. Zhang et al., 2008). Kindlin-2 is expressed ubiquitously outside the hematopoietic system, whereas kindlin-1 is mainly expressed in epithelial cells and kindlin -3 is restricted to the hematopoietic system (Rognoni, Ruppert, & Fässler, 2016). Kindlin binds to the distal NxxY motif of integrin tails. Kindlin functions as a protein-protein interaction hub by recruiting the integrin-linked protein complex, paxillin and the Arp2/3 complex to integrins (Böttcher et al., 2017; Fukuda et al., 2014; Theodosiou et al., 2016).

In leukocytes, resting cells mostly express integrins in the low-affinity conformation; in case of inflammation, circulation leukocytes must be rapidly recruited to the endothelium, where integrin ligands ICAM-1 and VCAM-1, as well as membrane associated chemokines are strongly induced. In this case, agonist-induced chemokine signaling converges on Rap1 GTPase and its effector Rap1-GTP-interacting adapter molecule (RIAM), which binds to and activates copious amount of talin (Lagarrigue, Kim, & Ginsberg, 2016). Activated talin binds to the cytoplasmic tail of β integrin. This interaction causes the separation of transmembrane and the extracellular domain. Kindlin which also contains a FERM domain interacts with the β subunit to further stabilize the high-affinity conformation and allows ligand-binding. This agonist-induced talin activation is a unique property of hematopoietic cells to ensure that integrins induced into high affinity conformation are instantly linked to its ligands and the actomyosin network so that the binding can be quickly stabilized by the mechanical forces (Hogg, Patzak, & Willenbrock, 2011) to achieve efficient adhesion under high-shear blood flow.

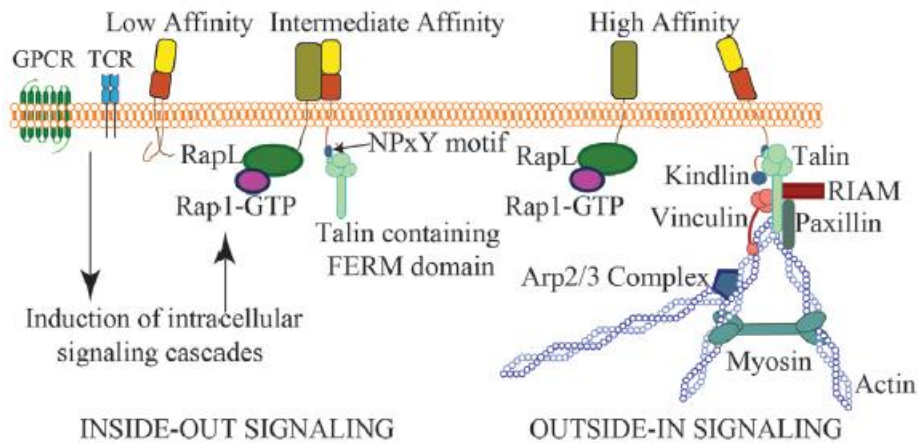


Figure 1-15 Schematics of integrin “inside-out” and “outside-in” signaling (from [Walling & Kim, 2018])

1.2.2.3.2 Outside-in signaling and the role of mechanical forces

Both the presence of immobilized ECM ligands and the presence of membrane anchored integrin counter-receptors are prerequisites to form a stable extended-open conformation, which is otherwise unstable. As integrin is a mechanosensitive protein, the force generated from ligand binding can also further enhance the stabilization of high-affinity integrins and induce downstream signaling involving the actomyosin regulation. This process is referred to as “outside-in signaling”. The signaling cascade activated upon ligand binding enhances the connection between the actomyosin system and integrin by recruiting talin, increases force transduction and eventually strengthens the bond between integrin and its ligand, which is the characteristic of a “catch bond”. Ligand-binding force can further strength the bonds between $\alpha_L\beta_2$ (LFA-1), $\alpha_M\beta_2$ (Mac-1) integrins and ICAM-1, as well as between $\alpha_5\beta_1$ integrin and fibronectin via catch-bond formation (Sun, Costell, & Fässler, 2019). Blood shear flow also acts as a facilitator of leukocytes arrest on the endothelium by stabilizing high affinity conformation (Ronen Alon & Dustin, 2007). In addition, the lateral force generated by actin flow also participate in stabilization of the high affinity conformation: in LFA-1, the key leukocyte integrin, binding to ICAM-1 and actin result in tension along the β_2 unit and stabilizes the high affinity conformation (Nordenfelt et al., 2017). Downstream signals are induced by the lateral actin force via outside-in signaling, which may result in altered actin dynamic through Rac, Rho signaling. Meanwhile, one should note that the dependence of the integrin high affinity conformation on forces may differ among integrins as they presumably display differential talin-binding and/or kindlin-binding affinities and different energy landscapes in the presence of distinct ligands (Sun et al., 2019). An additional mechanism to stabilize integrin-mediated adhesion is integrin clustering, which concentrates multiple binding affinities at a defined point to greatly increase the local adhesion strength. Avidity also allows integrins that are detached from the ligand by high mechanical forces to swiftly rebound to the ligand and substantially extend the adhesion lifetime (Sun, Guo, & Fässler, 2016) under the condition that the switch from extended open to the more stable bended close conformation

occurs more slowly than the rebinding event. Finally, integrin clustering stabilizes downstream mechanical linkages by laterally distributing high-tensile loads, thereby contributing to adhesion lifetime extension (Schoen, Pruitt, & Vogel, 2013).

1.2.2.3 Effects of Ca^{2+} and Mn^{2+}

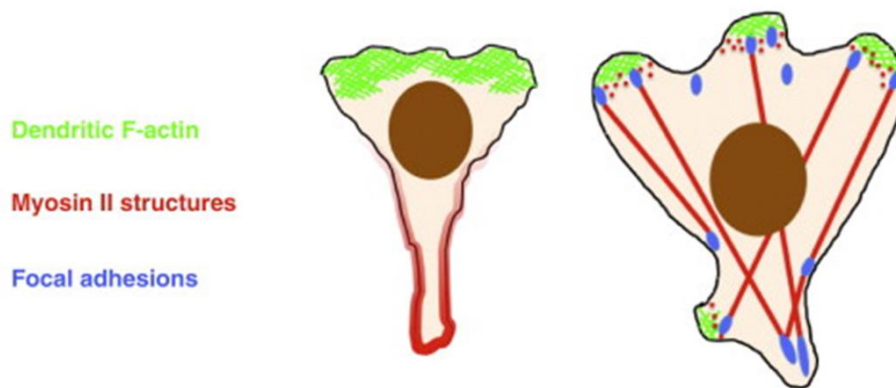
Divalent cations are universally required for integrin ligand binding and their concentrations can influence integrin binding affinity. Addition of Mn^{2+} or removal of Ca^{2+} increases ligand-binding affinity and adhesiveness of almost all integrins, which can be explained by the binding of metal ions to the LIMBS (ligand-induced metal ion-binding site) and ADMIDAS (adjacent to metal ion dependent adhesion site) (Chen, Salas, & Springer, 2003; Mould, Barton, Askari, Craig, & Humphries, 2003). Mutational studies show that the LIMBS functions as a positive regulatory site, and the ADMIDAS functions as a negative regulatory site (Chen et al., 2003; Mould et al., 2003). For most integrins, Ca^{2+} has both positive and negative regulatory effects. High concentrations of Ca^{2+} inhibit adhesion, whereas low concentrations of Ca^{2+} synergize with suboptimal Mg^{2+} concentrations to support adhesion. The LIMBS mediates the synergistic effects of low Ca^{2+} concentrations (Chen et al., 2003; Mould et al., 2003), whereas the ADMIDAS mediates the negative regulatory effects of higher Ca^{2+} concentrations, which are competed by Mn^{2+} (Chen et al., 2003). Given the positive regulatory effect of Mn^{2+} on integrin affinity, it is used in this study to induce and stabilize the high affinity conformation of the LFA-1 integrin.

1.2.3 Leukocyte motility

The ability of cells to migrate as a whole is essential for all multicellular organisms. For immune cells, their fast motility allows them to survey tissues, find and destroy pathogens, and initiate immune response. Cell motility relies on the remodeling of cell shape, a process that is highly controlled both in space and in time to allow cell polarization and coordination of movements (Ridley et al., 2003). As detailed in the previous section, this process is ensured by the actin cytoskeleton through rapid and dynamic remodeling that provides the physical basis of diverse types of protrusion to allow complex cell motility. In most migrating cells on 2D substrates, the leading edge is made of a thin and planar lamellipodium composed of branched actin network. Filopodia are also present at the leading edge, either embedded in the lamellipodium or emitted independently. Behind the leading edge, the shape of the cell body is maintained by actin cortex. Importantly, different cell types are endowed with different motility characteristics. In this context, leukocytes are classified as cells exhibiting amoeboid motility as compared to cells such as fibroblasts or smooth muscle cells classified as cells exhibiting mesenchymal motility. Amoeboid and mesenchymal motility are two modes of cell migration that lie at the opposite extremes of cell migration. In this section, we will focus on the motility of leukocytes. After a brief comparison between mesenchymal and amoeboid motility, we will review the leukocyte motility both in 2D and 3D environment.

1.2.3.1 Mesenchymal vs amoeboid motility

Amoeboid and mesenchymal motility reflect the coordinated functions of the respective cell type (Figure 1-16). Amoeboid motility, reminiscent of the amoeba *Dictyostelium discoideum*, is characterized by rapid locomotion (cell speed varies between 5-20 $\mu\text{m}/\text{min}$) (Friedl & Weigelin, 2008). This migratory property is attributed to the strong cell polarization leading to a well-defined cell front and rear. This strong change in shape allows cells to efficiently protrude at the front via lamellipodium on 2D surfaces. The rear of the cell has a cylindrical shape named "uropod" that is enriched in actomyosin bundles mediating contractility and propelling cell forward. Amoeboid cells undergo cyclic actin polymerization at cell front and actomyosin contraction at rear to move forward. Amoeboid motility reflects the role of leukocytes as "professional migrators" that must rapidly crawl out of blood circulation and then over great distance in the tissues to mediate innate and adaptive immune response. On the contrary, mesenchymal cells move much more slowly (cell speed is less than 1 $\mu\text{m}/\text{min}$) (Friedl & Weigelin, 2008). They typically exhibit multiple and competing protrusions (lamellipodia and filopodia) (Petrie, Doyle, & Yamada, 2009). Another characteristic feature of mesenchymal motility is strong, integrin-mediated adhesion complex to the extracellular matrix (known as the focal adhesion) to which attached actomyosin fibers are formed into thick stress fibers. The mesenchymal cells migrate through traction along the extracellular matrix with matrix degradation, through expression of matrix metalloproteinases. The motility mode reflects the intimate relation between mesenchymal cells and the extracellular matrix in general, exemplified by the role of fibroblast in secretion and mechanochemical remodeling of extracellular matrix through wound healing.



	Amoeboid	Mesenchymal
Migration speed	Fast, 5-20 $\mu\text{m}/\text{min}$	Slow, <1 $\mu\text{m}/\text{min}$
Polarity	Well defined front and rear	Multiple and competing lamellipodia
Adhesion	Weak adhesion	Strong adhesion to ECM with integrin-mediated focal adhesion complexes
Actin cytoskeleton	Branched actin network at cell front; from mid-body to cell rear, cortical actomyosin mediates contractility	Branched actin network at leading edge, actin-myosin bundles mediate contractility behind the leading edge and form thick stress forms attached to focal adhesion

Figure 1-16 Amoeboid vs Mesenchymal motility. The illustration (from [Bear & Haugh, 2014]) and table comparing the structural and dynamic features of both amoeboid and mesenchymal migration

1.2.3.2 Leukocyte migration in 2D and 3D environments

As already mentioned above, leukocytes use the amoeboid mode of migration to rapidly scan the environment and initiate immune response. Leukocyte can migrate along or through most tissues of the body. Both 2D surfaces such as the inner vessel wall, the peritoneum and pleura and 3D environment composed of cellular (lymph node) and fibrillar ECM components can serve as substrates of leukocyte migration.

1.2.3.2.1 Leukocyte migration on 2D surfaces

For migration in 2D environment, leukocytes must polarize into the typical “hand-mirror” shape with the well-defined leading edge, the mid-body and the cell rear. Rho GTPases act as molecular switches and cycle between active (GTP-bound) and inactive (GDP-bound) states, which are regulated by various guanine nucleotide exchange factors (GEFs), GTPase-activating proteins (GAPs), and guanine nucleotide dissociation inhibitors (GDIs) (Tybulewicz & Henderson, 2009). Rho GTPases intracellular segregation gives rise to cell polarization: Rac, Cdc42 mainly locate at cell front where Rac mediates actin polymerization and Cdc42 mediates the persistence of the leading edge; RhoA mediates cortical rigidity and contractility at cell rear (Weninger, Biro, & Jain, 2014). Leukocytes generate protrusive forces at the

leading edge through actin polymerization that pushes out lamellipodia while using actomyosin contractile force to retract the uropod. These intracellular forces can deform cell body but still need to be transmitted to the environment to drive locomotion. Migration across 2D substrates requires integrin-mediated adhesion to anchor cells to the surface, notably through binding of integrin $\alpha_4\beta_1$ (VLA-4, Very Late Antigen-4) and $\alpha_L\beta_2$ (LFA-1, Lymphocyte Function-associated Antigen-1) to counterpart ligands VCAM-1 and ICAM-1 on endothelial cells (Ley et al., 2007). Although the adhesion of amoeboid cells is generally weaker compared to mesenchymal cells without mature focal adhesion (Dupré, Houmadi, Tang, & Rey-Barroso, 2015), it is enough to anchor cells in presence of blood circulation, exemplified by the intravascularly crawling neutrophils resisting the shear force of the blood stream (Phillipson et al., 2006). Surface adhesion is a prerequisite for migration in 2D under physiological condition, but the actual locomotion requires membrane-parallel traction forces against the direction of the cell movement (also known as the retrograde forces). When leukocytes move with actin-based protrusions, actin filaments push themselves backwards while protruding the membrane by polymerizing and expanding against the mechanical resistance of the plasma membrane. Contractility in cell rear supports this retrograde movement of the actin cortex, enhancing the retrograde force that can be transmitted to the substrate via transmembrane receptors. One important side-effect of substrate adhesion is the disassembly of adhesion at the rear of the cell. Myosin-II dependent contraction at the uropod also supports de-adhesion and retraction. Accordingly, inhibition of myosin-II lead to elongated phenotype of migrating neutrophils (Eddy, Pierini, Matsumura, & Maxfield, 2000) and lymphocytes (Morin et al., 2008; A. Smith, Bracke, Leitinger, Porter, & Hogg, 2003) owing to impaired tail retraction. To summarize, leukocytes migrate on 2D surfaces through forces generated by actin polymerization combined with actomyosin contraction. Transducing of these forces require adhesion to the substrates via integrins. Upon adhesion to the surface, the retrograde forces generated by actin protrusion and supported by actomyosin contraction together enable cell locomotion.

1.2.3.2.2 Leukocyte migration in 3D environments

Leukocytes, once recruited from blood circulating, crawl on 2D vessel linings before transmigrating through the endothelium into the tissue, where they will continue migrating in a 3D environment to carry out their effector functions. Leukocytes such as neutrophils and monocytes directly migrate to the site of infection or damage to provide a rapid response, while tissue-resident dendritic cells (DCs) that detect danger at the periphery tissue migrate to lymph node to present antigen to T lymphocytes, which in turn interact with B lymphocytes to fully activate the adaptive immune response. Unlike migration in 2D on the vessel wall, which requires adhesion to the substrate via integrin receptors, leukocyte migration in 3D can occur without integrin-mediated adhesion and largely depends on cytoskeletal deformability (Lämmermann & Sixt, 2009).

- 3D Migration in defined *in vitro* systems

Multiple *in vitro* reductionist systems are developed to study leukocytes migration in 3D collagen gel and in confinement. Collagen gel forms a porous 3D fibrillar network allowing leukocyte nonproteolytic migration (Wolf, Müller, Borgmann, Bröcker, & Friedl, 2003). When embedded in such 3D network and fully surrounded by this scaffold, leukocytes can migrate in an integrin-independent mode as shown by randomly migrating T cells upon blockade of integrin (Friedl, Entschladen, Conrad, Niggemann, & Zänker, 1998) or by integrin-depleted dendritic cells, neutrophils and B cells in a chemotactic gradient (Lämmermann et al., 2008). Leukocyte migration in such loose collagen mesh is driven by actin polymerization (Lämmermann et al., 2008). Moreover, when facing narrower pores in denser collagen gel, migration of leukocytes becomes dependent on RhoA activation, Rho-associated protein kinase (ROCK) and myosin II-dependent contraction (Lämmermann et al., 2008). Upon chemical blockade of ROCK or myosin II, the rigid nucleus of dendritic cells becomes stuck. With a trailing rear and an advancing front, DCs become elongated (Lämmermann et al., 2008). One should also note that the restriction pore size varies among different cell types and depends on the cell diameter, nuclear size and rigidity (Le Berre, Aubertin, & Piel, 2012; Wolf et al., 2013). Unlike in 2D where leukocytes crawl with flat adhesive lamellipodia, they form different protrusions including pseudopodia, filopodia or blebs that can extend through matrix pores and fibers of the 3D collagen gel. The complexity of the 3D environment requires tight coordination of different frontal protrusions for efficient locomotion. For example, dendritic cells lacking such coordination due to depletion of Rho family GTPase Cdc42 (Lämmermann et al., 2009) or its effector DOCK8 (Harada et al., 2012) get entangled in 3D collagen gel. Moreover, for the same cell type, changing the 3D matrix geometry can also reveal distinct migration modes, which can be exemplified by macrophage. Unlike other leukocyte subsets, macrophage exhibit adhesion- and protease-dependent mesenchymal migration mode in non-porous dense collagen gel but switch to non-proteolytic, contraction-dependent amoeboid dependent migration mode once they are embedded in porous matrix of fibrillar collagen (Goethem, Poincloux, Gauffre, Maridonneau-Parini, & Cabec, 2010).

Like migration in 3D fibrillar matrix, leukocytes do not require integrin-adhesive force to migrate in highly-confined environments. In a classical study by Malawista et al. (Malawista & Chevance, 1997), human neutrophils performed “chimneying” when squeezed between two surfaces. Several other experiments using microfluidic channels have also shown that leukocytes migration in confinement is integrin-independent but required myosin-II based contraction for optimal motility, even though blockade of myosin II still allows residual movement with reduced speed. Myosin II deficient DCs migrate in confined microchannels at only half of the median speed compared to control cells (Heuzé et al., 2013). Activated T cells migrate in micro-channels independent of channel coatings (with either integrin or non-integrin ligands), but upon myosin II inhibition, they dropped their migration speed by half

(Jacobelli et al., 2010). Recent studies further show that actomyosin network tightly controls the migration pattern of DCs in confinements related to their function. Immature DCs, whose primary function is tissue patrolling, migrate in confined microchannels with alternative slow and fast motility phases (Vargas et al., 2016). Each velocity phase is associated with a distinctive organization of the actin cytoskeleton. The slow phases rely on Arp2/3-induced branched actin nucleation at the front of the cell; this antagonizes cell movement and promotes antigen internalization (Chabaud et al., 2015). In contrast, fast sequences depend on formin mDia1 that generates bundled actin at the rear of the cell (Vargas et al., 2016). Each stage is accompanied by the redistribution of myosin II, which behaves as a limiting factor and maintains a balance between antigen capture and cell motility (Chabaud et al., 2015; Lavi, Piel, Lennon-Duménil, Voituriez, & Gov, 2016; Solanes et al., 2015). Arp2/3 and mDia1 rearrangements appear to be in a delicate equilibrium. Chemical or genetic inhibition of Arp2/3 results in an increase in immature dendritic cell speed and persistence, in the absence of cell activation. Immature DCs subsequently adopt a needle-like shape that depends on F-actin nucleation by formins (Leithner et al., 2016; Vargas et al., 2016). This indicates that immature DCs do not require the Arp2/3 complex for cell motility in confinement. However, disruption of the lamellipodia by genetic inhibition of the WAVE complex (an Arp2/3 activator) abolishes immature DCs' ability to turn in collagen gels and reduces their migration in CCL3 chemokine gradients (Leithner et al., 2016). Upon maturation, activated DCs are mainly responsible for antigen transport to the lymph node and therefore increase their speed and persistence and therefore their ability to reach the target quickly (Vargas et al., 2016). Regarding the cytoskeleton, the Cdc42-Arp2/3 axis is deactivated in mature DCs leading to loss of actin and lamellipodium at cell front. Therefore, activated DCs predominantly display actin bundles (nucleated by mDia1) at their rear (Vargas et al., 2016).

- *In vivo* 3D migration

Studies using *in vitro* system have provided us with precious information on the plasticity of leukocytes and their capacity to adapt when migrating in defined 3D environment. However, one should note that *in vivo* interstitial organs are highly heterogenous and dynamically changing. Non-lymphoid organs mainly consist of fibrillar connective tissues while lymphoid organs such as lymph node are packed with cells. Understanding leukocytes migration in 3D *in vivo* is thus of great importance. With the help of *in vivo* imaging technique such as intravital imaging, studies have been made regarding the leukocyte migration in fibrillar (most non-lymphoid organs) and cell-rich (lymphoid organs such as lymph nodes) environment. In non-lymphoid organs where connective tissues form a 3D tissue maze of confinement, leukocytes appear to navigate in a nonproteolytic and low-adhesive manner (Friedl & Weigelin, 2008). Neutrophils recruited from blood circulation need to flexibly reorient themselves in the tissue and migrate at high speed to reach the site of insults. Talin-deficient neutrophils lacking high-affinity integrin migrate have similar speed and

directionality as wild-type neutrophils to site of sterile injury in the ear skin dermis (Lämmermann et al., 2013). In agreement with previous work in collagen gel (Lämmermann et al., 2008) and integrin blocking study in mouse skin (Hyun et al., 2012), the interstitial geometry of the dermis appears to be sufficient for adhesion-independent neutrophil migration based only on force generated by actomyosin cytoskeleton (Lämmermann et al., 2013). Unlike neutrophils that are recruited to the tissue from the blood stream, many dendritic cells are already tissue-resident and serve currently as the best studied model for interstitial migration. As mentioned above, immature DCs carry out tissue patrolling function in adhesion-independent manner and upon maturation, they move in a highly directed manner to the nearest lymphatic vessel. DC crawling into lymphatics and lymph node doesn't require integrin receptors (Lämmermann et al., 2008), but is guided by tissue-immobilized gradients of the CCR7 ligand CCL21 (Weber et al., 2013). Migration of matured DCs is dependent on the forces of actin polymerization (Lämmermann et al., 2008). Accordingly, DCs depleted in actin regulators such as Rac (Benvenuti et al., 2004), WASp and mDia1 (Bouma, Burns, & Thrasher, 2009; Noronha et al., 2005; Snapper et al., 2005; Tanizaki et al., 2010) show impaired migration towards lymph node. When passing through narrow pores in the tissue, actomyosin contraction helps DCs enter terminal lymphatics. Moreover, in agreement with an essential role for coordinating the cytoskeleton during physiological interstitial migration, DC migration becomes heavily perturbed when cells cannot maintain spatial and temporal asymmetries, which is regulated by the axis DOCK8-Cdc42-WASp. DCs deficient in DOCK8 (Harada et al., 2012), Cdc42 (Lämmermann et al., 2008; Luckashenak, Wähe, Breit, Brakebusch, & Brouck, 2013) and WASp (Bouma et al., 2009; Noronha et al., 2005; Snapper et al., 2005) all showed impaired interstitial migration even though their migration on 2D surfaces remained unimpaired. In contrast to fibrillar environment in connective tissues, other tissues are mainly composed of cellular networks where leukocytes need to navigate through a more elastic interstitium in contact with other cell types. Most of *in vivo* studies of leukocyte interstitial migration in cell-rich environment were conducted in the lymph node, the major anatomical site for the adaptive immune response, regarding dendritic cells migration into lymph node and the intranodal trafficking of T lymphocytes.

Lymph nodes contain two entries for leukocytes: the afferent lymphatics that guide leukocytes, particularly DCs, from periphery tissue through the subcapsular sinus into the functional region of lymph node and the high endothelial venule that enable lymphocytes to directly enter the lymph node. The lymph node parenchyma is functionally compartmentalized into B cell follicles containing a fibroblastic dendritic cell (FDC) network and a T cell zone (paracortex) supported by fibroblastic reticular cells (FRCs), which produce a 3D network of reticular fibers supporting the paracortex. *In vivo* imaging showed that T cell tracks were along the FRC networks (Bajénoff et al., 2006). Since FRCs also express integrin ligands ICAM-1, ICAM-2 and VCAM-1 as well as CCR7 ligands, CCL19 and CCL21, the latter of which binds onto the FRCs (Lämmermann & Germain, 2014), it was initially thought that T cell

intranodal migration could be integrin-dependent. However, integrin perturbation only resulted in minimal change in T cells motility (10-30% reduction) (Boscacci et al., 2010; Park et al., 2010; Reichardt et al., 2013; Schumann et al., 2010; Woolf et al., 2007), likely due to the absence of out-side signaling to induce high-affinity integrins without shear flow (Woolf et al., 2007). Studies later show that the basal T cell intranodal trafficking is integrin-independent, but LFA-1 engagement promotes a faster motility mode along two superimposed ICAM-1 and CCL21 decorated cellular networks (DCs and FRCs) (Reichardt et al., 2013). A more recently study argues the complementary role of LFA-1 and CCL21 in T cell intranodal migration without surface adhesion, where LFA-1 mediates the substrate friction and CCL21 mediates the cortical actin flow (Hons et al., 2018). The basal non-adhesive migration mode of T cells argues for the role of cytoskeletal forces promoting their intranodal motility in a cell-rich environment. Rather than being required to squeeze cells through anatomical constrictions in a fibrillar environment, myosin II is thought to provide contractile force to detach T cells from other cells in a “confined” cell-dense environment (Jacobelli et al., 2010; Soriano et al., 2011). Maintaining a protrusive actin network is essential for T cell intranodal migration. Interference with key actin polymerization regulators such as Rac1 (Faroudi et al., 2010), DOCK2 (a key Rac-GEF for T cells) (Nombela-Arrieta et al., 2007) resulted in severely impaired intranodal motility. As for dendritic cells, activated DCs enter the lymph node through afferent lymphatics ending in the subcapsular sinus (SCS), which is a cell-rich environment. DCs migration through the SCS appears to be integrin-independent as adhesion-deficient and integrin-null DCs migrate with similar speed through SDS and interfollicular regions (Lämmermann et al., 2008). On the other hand, DOCK8 or WASp deficient DCs seemed to migrate poorly, suggesting the role of cytoskeletal coordination for transit into deep regions of the lymph node (Bouma et al., 2009; Harada et al., 2012).

To summarize, actomyosin network plays an essential role in leukocyte motility both in 2D and 3D. Both *in vitro* and *in vivo* study have shown that integrin-mediated adhesion is required for leukocyte migration on 2D surface, where adhesion and actomyosin contraction need to be coordinated to achieve efficient migration. However, in 3D environment, either fibrillar or cell-rich, leukocytes do not need integrin to migrate and their motility depends on the coordination of actomyosin network controlled by various regulator proteins. Moreover, leukocytes migrating both in 2D and 3D encounter different guidance cues that direct them to reach the site of inflammation or damage rapidly to execute their functions. In the following section, we will present the effect of different guidance cues on leukocyte migration.

1.2.4 Various guidance cues in leukocyte migration

An efficient immune reaction requires leukocytes to be at the right place at the right time. To do so, leukocyte sometimes need guidance to navigate in the complex microenvironment. Guidance cues include chemical cues such as either soluble or surface bound chemokines or other molecules, as well as mechanical cues such as blood flow and

substrate rigidity. In this section, we will present different guidance cues involved in leukocyte migration and their discovery through *in vitro* assays and *in vivo* experiments.

1.2.4.1 Chemotaxis

Among all the guidance cues, the chemical guidance is probably the best studied. Guidance by soluble chemical cues is termed chemotaxis. It is defined as the directional migration of cells in response to a gradient of concentration of a diffusible molecule (Davies, 2013a). The phenomenon of chemotaxis was first described in bracken fern spermatozoa by Pfeffer in 1884 (Wilkinson, 1998). Shortly afterwards (1888) Leber described a similar phenomenon in mammalian leukocytes responding to a focus of injury (Wilkinson, 1998). Since then, chemotaxis has been accepted as an important mechanism for mobilizing phagocytic and immune cells at sites of infection, tissue injury, and immune reactions. Over the years, a great number of molecules of chemo-attractants have been identified including the family of chemokines and molecules from other categories such as lipid chemoattractants, N-formylated peptides and complement anaphylotoxins. A list of leukocytes' major chemoattractants and their principle receptors, which have been widely studied, are listed down below (Table 1-2). Meanwhile, one should take note of another important notion related to the chemotaxis: chemokinesis, which refers to the increase of migration speed in presence of the chemoattractant without directional preference.

Ligand	Receptor	Leukocytes receptor expression
CCL21; CCL19	CCR7	Dendritic cells, T cells, B cells
CXCL12 (SDF-1 α/β)	CXCR4	T cell, Neutrophils, B cells, dendritic cells,
CXCL13	CXCR5	B cells, T cells
CXCL8 (IL8)	CXCR1, CXCR2	Neutrophils, mast cells, macrophages
CXCL2 (MIP-2)	CXCR2	Neutrophils, monocytes, macrophages
fMLP	FPR-1,-2,-3	Leukocytes
S1P	S1PR1-5	Leukocytes

Table 1-2 Partial list of major leukocyte chemoattractants, their ligands and cellular expression (from [Koelink et al., 2012])

The chemotaxis activates intracellular signaling pathways through G-protein coupled receptor (GPCR) and results in the remodeling of the actomyosin skeleton to steer the cell migration (Figure 1-17). Some important downstream effectors upon binding of chemoattractants include the family of Rho GTPase which in turn activate numerous regulator proteins of the actomyosin network to induce cell polarity, front protrusion and rear retraction. For instance, Cdc42 determines the putative front of the polarize cell before protrusion formation (H. W. Yang, Collins, & Meyer, 2016). It activates downstream Wiskott-Aldrich Symptom protein (WASp (Rohatgi et al., 1999)) and formin mDia (Peng, Wallar, Flanders,

Swiatek, & Alberts, 2003) and form protrusion. In future protruding areas, Cdc42 inhibits the Rho GTPase RhoA, thereby confining the basal activity of RhoA activity to the trailing edge of the cell where it induces myosin II phosphorylation by Rho dependent protein kinase (ROCK) leading to actomyosin contraction. Following Cdc42 or RhoA activation, Ras activity increases in a polarized manner (H. W. Yang et al., 2016). Ras GTPases activate a plethora of signaling cascades including phosphoinositide 3-kinase (PI3K) pathways. PI3K phosphorylates the membrane lipid phosphatidylinositol (4,5)-biphosphate (PIP2) forming the second messenger lipid phosphatidylinositol (3,4,5)-triphosphate (PIP3). Inhibited by PI3K in the front of the polarized cell, phosphatase and tensin homolog (PTEN) dephosphorylates PIP3 in the retracting back of the cell promoting a steep PIP3 gradient within the cell (Sasaki, Chun, Takeda, & Firtel, 2004). This steep intracellular gradient is mandatory for induction and maintenance of cell polarity, however dispensable for chemotactic gradient sensing (Andrew & Insall, 2007). An important downstream target of PI3K is the small GTPase Rac1 which peaks in activity with its upstream activator Ras in leukocytes (H. W. Yang et al., 2016) and with Cdc42 in fibroblasts (Machacek et al., 2009), which further activate WAVE complex to activate the Arp2/3 complex to generate branched actin network.

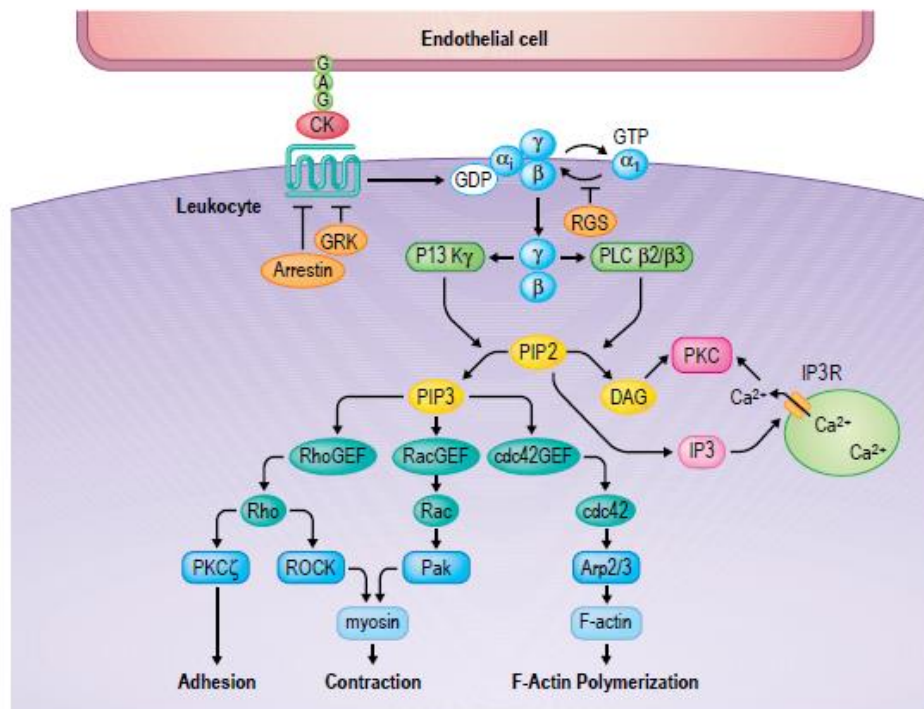


Figure 1-17 Chemokine-induced signaling transduction in chemotaxis where the PI3K pathway is particularly important for cell migration (Murphy, 2008).

Initially, the discovery of chemoattractants and the study of chemotaxis were mainly carried out through *in vitro* chemotaxis assays such as membrane assay, agarose assay and boyden chamber (Wilkinson, 1998). For example, the boyden chamber consists of a large lower chamber containing the chemoattractant solution and a smaller upper chamber with

media (Figure 1-18). Cells were seeded on the porous membrane on bottom of the upper chamber. Chemo-attractants will diffuse through the membrane and cells may transmigrate to the lower well. The principle of this method is to measure the distribution of a cell population at a fixed time point after exposure to an attractant in a concentration gradient. Although such method has provided us with valuable input regarding the leukocyte chemotaxis and is still of use today, these assays only give indirect measures of the chemotaxis and it is difficult to distinguish chemotaxis and chemokinesis since it is impossible to control the gradient profile. Moreover, these above-mentioned assays also do not provide any information on migration parameters such as migration speed and its directionality since they only measure a given time point.

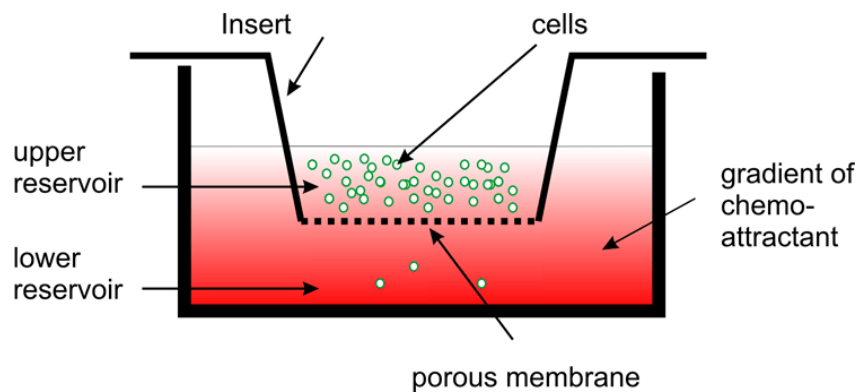


Figure 1-18 Schematic of the boyden chamber assay

The development of the microfluidics at the beginning of 20th century opened a new era of the *in vitro* chemotaxis assay. It allows generation of gradients of biomolecules with spatial and temporal control and has been used to investigate in a quantitative and reproducible fashion many biological questions including leukocyte chemotaxis (S. Kim, Kim, & Jeon, 2010). Thanks to well-controlled soluble gradients, researchers were able to gain insight regarding neutrophil decision making and steering when taxing towards the most typical neutrophil chemotactic gradients such as fMLP and IL8 (Ambravaneswaran, Wong, Aranyosi, Toner, & Irimia, 2010; Irimia, Balázs, Agrawal, & Toner, 2009; Irimia, Charras, Agrawal, Mitchison, & Toner, 2007; Saadi et al., 2007). Moreover, they were also able to develop *in vitro* microfluidic assays for diagnostic purposes and to characterize patients with immune disorders. For example, Bultler et al. established a reference set regarding neutrophils chemotaxis towards fMLP from healthy donors, compared it to those from burn injury patients and found reduced neutrophil directional migration speed (Butler et al., 2010). Berthier et al. developed a high throughput microfluidic gradient array that enables the characterization of neutrophils chemotaxis towards fMLP from patients with immunodeficiencies, which could be used for diagnostic purposes and screening (Berthier, Surfus, Verbsky, Huttenlocher, & Beebe, 2010). Lin et al. developed a microfluidic devices to generate single and competing gradients of CCL19 and CXCL12 (SDF-1) and were able to demonstrate robust T cell chemotaxis in presence of single CCL9 and CXCL12 (Lin & Butcher,

2006). They were also able to generate competing CCL19 and CXCL12 gradients using the same device and demonstrated that T cells chemotaxed towards CCL19 in the competing chemokine gradients (Lin & Butcher, 2006). This study thus demonstrated for the first time *in vitro* that T cell chemotaxis towards two chemoattractants in presence of controlled gradient generation with quantitative analysis.

Dendritic cells (DC) are the most potent and versatile antigen presenting cells in the tissue. While immature DCs patrol the tissue and express numerous chemokine receptors, mature DC downregulate most of these receptors upon activation and upregulate chemokine receptor CCR7 in order to reach the secondary lymphoid organs in a directional manner regulated by CCR7 ligands CCL21 and CCL19 (Randolph, Angeli, & Swartz, 2005). Both are secreted by stromal cells in the lymph node paracortex to properly position DCs with CCR7+ naïve T cells for their activation. CCL21, but not CCL19, is also expressed by the endothelium of lymphatic vessels in the periphery and by the high endothelial venule (Randolph et al., 2005). Thus, CCR7-mediated chemotaxis is critical for DC homing to, and positioning within, lymph nodes and for T cell activation there (Förster, Davalos-Misslitz, & Rot, 2008, p. 7). It is thus of great importance to understand the DC chemotaxis using well-defined assays. Microfluidic devices were again used to generate soluble chemokine gradient to investigate dendritic cell chemotaxis in 3D environment. Haessler et al. developed an agarose-based microfluidic assay to generate a soluble CCL19 gradient and demonstrated that dendritic cells migrated towards this gradient (Haessler, Kalinin, Swartz, & Wu, 2009). Later, the authors used the same device to investigate DCs chemotaxis under defined gradients of both CCL21 and CCL19 and demonstrated that CCL21 was a more potent chemoattractant for DC migration in 3D than CCL19 (Haessler, Pisano, Wu, & Swartz, 2011).

With the help of different microfluidic assay, it is now relatively easy to generate soluble gradient spreading over distance from a local source. Studies using such assays have provided valuable insights as to how leukocytes respond to one or several chemoattractant gradients with quantification of both gradients themselves (steepness and concentration) and cell migration parameters (speed and directionality). They have also allowed us to further mimic the *in vivo* environment by multiple soluble gradients. However, the *in vivo* environment is quite different. There, secreted chemokines are thought to be rapidly immobilized on cells or extracellular matrix surfaces by interacting with glycosaminoglycans (GAGs) (Bajénoff et al., 2007). Taking the example of two key chemokines CCL21 and CCL19 in T cell and dendritic cell homing, while both chemokines share the same receptor, they differ in their ability to mediate GAG binding. This difference is because of a highly charged 40 amino acid extension at the C terminus of CCL21 that is lacking in CCL19. It has been shown that this region immobilizes CCL21 while CCL19 is largely soluble (Schumann et al., 2010). DCs are also able to truncate CCL21 binding domain, resulting in a CCL19-like soluble CCL21. *In vivo*, only CCL21 is detectable through immunohistochemical staining, suggesting that the soluble chemokine pools were likely lost during experimental processing and only surface-bound

protein was retained (Bromley, Mempel, & Luster, 2008). Directional migration in presence of a surface-bound gradient is termed haptotaxis. Similarly, haptokinesis is defined as increased undirectional locomotion in presence of a surface-bound cue.

1.2.4.2 Haptotaxis

In this section, we will present leukocytes haptotaxis studies via both *in vivo* and *in vitro* experiments. The first part of the section will pick up where 1.2.4.1 left off and present studies reported in the literature on chemokine-induced haptotaxis mainly focused during DC homing as well T lymphocyte homing and trafficking. The second part of the section will discuss adhesiveness-induced haptotaxis, which is better studied in mesenchymal cells and remains largely unknown for leukocytes.

- Chemokine-induced haptotaxis

While it is now well established that the CCL21 and CCL19 are crucial to mature DC homing to the secondary lymphoid organs such as the lymph node, where CCL21 may form a surface-bound gradient to guide mature DC migration towards the lymphatic vessels with the help from soluble CCL19 (Schumann et al., 2010), the concept initially lacked *in vivo* experimental confirmation. Conventional immunohistochemical staining certainly can measure the distribution of surface bound chemokines in tissue, but it does not allow dynamic imaging of leukocytes migration and therefore correlate chemokine tissue distribution to migration. The recent development of live cell imaging technique has markedly improved our understanding of the leukocytes and interaction with external cues. Weber et al. demonstrated for the first time in 2013 a haptotactic CCL21 gradient within mouse skin and showed that they guide dendritic cells towards lymphatic vessels (Weber et al., 2013). Quantitative imaging revealed depots of CCL21 within the lymphatic endothelial cells and steeply decaying gradient within the perilymphatic interstitium and these gradient matched the migration patterns of the DCs, which migrated directionally towards the lymphatic vessels (Weber et al., 2013). To better understand the mechanism behind the haptotactic migration of DC along a surface-bound CCL21 gradient, Schwarz et al. later developed an *in vitro* assay with immobilized CCL21 gradient in confined migration chamber to mimic DC interstitial haptotaxis (Schwarz & Sixt, 2016). By reconstitution of immobilized CCL21 gradient *in vitro*, Schwarz et al. found that the haptotactic gradient sensing depends on the absolute CCL21 concentration in combination with the local steepness of the gradient (Schwarz et al., 2017). They also found the influence of CCR7 signal termination on DC haptotaxis and that CCR7 desensitization by G-protein-coupled receptor kinase 6 (GRK6) is crucial for maintenance of haptotactic CCL21 sensing (Schwarz et al., 2017). Moreover, in the context of the organism, immobilized haptotactic guidance cues often coincide and compete with soluble chemotactic guidance cues. A well-studied example for the significance of immobilized vs. soluble chemokine gradients remains the trafficking of dendritic cells. Having captured antigen in non-

lymphoid tissues, DCs migrate along immobilized gradients of CCL21 towards lymphatic vessels, from where they are flushed into the sinus of lymph nodes. Once in the lymph node, the cells experience the soluble chemokine CCL19, which interacts with the same receptor CCR7. It has been shown *in vitro* that the directionality of DCs migrating on homogeneously immobilized CCL21 can be biased by gradients of soluble CCL19 (Schumann et al., 2010). Additionally, exposed to competing soluble gradients of CCL19 and CCL21, DCs displayed higher sensitivity towards CCL19 (Ricart, John, Lee, Hunter, & Hammer, 2011). In contrast, if CCL21 diffusion was influenced by unspecific binding to charged extracellular matrix components, CCL21 induced directionality prevailed when opposed by a soluble CCL19 gradient (Haessler et al., 2011).

Activated effector T lymphocytes may also need surface-bound cues to reach the target tissue. A recent *in vivo* study revealed that migrating influenza specific CD8+ T cells were guided by the trail containing CXCL12 deposited by migrating neutrophils, which demonstrated for the first time a cooperative guiding between innate and adaptive immune cells in T cell recruitment into infected mice airway (Lim et al., 2015).

Another situation where chemokine-induced haptotaxis may be involved is lymphocytes homing to lymph nodes and their intranodal trafficking. The chemokine receptor CCR7, which binds to CCL21 and CCL19, is the most important chemokine system for T cells entry into secondary lymphoid organs as well as intranodal positioning, whereas the chemokine receptor CXCR5 and its ligand CXCL13 are the most important for B cells. (Okada et al., 2002). The role of these key chemokines in promoting leukocyte firm adhesion and subsequent extravasation is well known. However, open questions remain regarding the existence of any haptotactic effect and underlying mechanisms in these processes. Robust *in vitro* assays, in combination with advanced *in vivo* imaging, would be necessary to answer these questions.

- Adhesive haptotaxis

Chemokine-induced haptotaxis mediates leukocytes migration through binding to GPCR and initiating a global signaling network. Besides, there is another form of haptotaxis that is defined as the guidance by means of a gradient of adhesion. Adhesive haptotaxis was first discovered and termed long time ago. In 1965, Carter observed murine fibroblasts migration on substrates offering different adhesiveness (S. Carter, 1965). On plain, cell repellent cellulose acetate, cells were not able to adhere and accordingly not able to migrate. However, palladium vaporized cellulose acetate restored spreading and migration. When Carter shadowed parts of the cellulose acetate during palladium vacuum coating, thereby creating a gradient of adhesion sites, cells started to migrate in direction of higher adhesiveness. Carter termed this phenomenon haptotaxis and then generalized his observations and claimed that cell adhesion and migration are “interrelated”, meaning the

movement of a cell is “controlled by the relative strength of its peripheral adhesions”. Indeed, adhesive haptotaxis has been widely observed for mesenchymal cells such as cancer cells, fibroblasts, endothelial cells and neurons through different *in vitro* culture systems (Aznavoorian, Stracke, Krutzsch, Schiffmann, & Liotta, 1990; Brandley & Schnaar, 1989; S. Carter, 1965; S. B. Carter, 1967; Klominek, Robert, & Sundqvist, 1993; Mccarthy & Furcht, 1984; O’Connor, Duerr, & Bentley, 1990a; J. T. Smith et al., 2004; Thibault, Hoemann, & Buschmann, 2007), where these mesenchymal cells all migrated towards the gradient of higher adhesion. For mesenchymal cells to achieve efficient migration, substrate adhesion needs to be firm, but tightly controlled to create new, force generating nascent adhesion and disassemble matured anchoring focal adhesions (Beningo, Dembo, Kaverina, Small, & Wang, 2001). Among cells whose adhesion is mediated by integrins, the formation of nascent adhesion is influenced by the availability of the integrin ligands on the substrate. The more integrin ligands are available, the stronger the cells can adhere. In migratory cells, the leading edge does not just face forwards – the edges of the lamellipodia explore the environment to the sides of the cell and filopodia can extend great distances to the side. In this way, cells can sample the environment for guidance cues. Since cells cannot advance simultaneously towards the left-most parts and the right-most parts, an element of competition arises inevitably. Anything that tips the balance of this competition will therefore steer the cell. Inhomogeneity of integrin ligand distribution can disturb this balance: the parts of cell lamellipodium that are on the area with more integrin ligands advance more because the leading edge has something against which to push and the contractile mechanism has something against which to pull. In the “tug-of-war” between rival parts of lamellipodia, parts on more adhesive area will win and steer the cell (Figure 1-19). In this case, integrin act as the anchoring sites biasing cell migration and lamellipodia are required for haptotaxis. Additionally, integrin activation during adhesion activates intracellular signaling pathways required for lamellipodia formation and leads to local protrusion (King et al., 2016).



Figure 1-19 The tug-of-war of lamellipodium in adhesiveness-induced mesenchymal haptotaxis

In contrast to mesenchymal migration which is characterized by strong cell/substrate adhesion mediated by mature focal adhesion and strong traction forces transmitted to the substrate by contractile stress fibers, amoeboid cells migrate at high speed with low adhesion and low traction forces transferred to the substrate (Lämmermann & Sixt, 2009). On the inner

walls of blood vessels, leukocytes crawl distances of several tens or hundreds of micrometers, proposedly in search for optimal diapedesis sites (Massena & Phillipso, 2012; R. Sumagin et al., 2010; Ronen Sumagin & Sarelius, 2010). Diapedesis seems indeed to occur at specialized area of the endothelium, called “Cuplike” transmigratory structures (Carman & Springer, 2004) or “portals” (Ronen Sumagin & Sarelius, 2010). These structures are composed of vertical microvilli-like projections that are enriched in intercellular adhesion molecule-1 (ICAM-1) and vascular cell adhesion molecule-1 (VCAM-1) and surround transmigrating leukocytes (Carman & Springer, 2004). ICAM-1 was found particularly important to favor transmigration in nearby portals (Ronen Sumagin & Sarelius, 2010). Studies have also shown that surface density and distribution of endothelial ICAM-1 induced a transition from paracellular to transcellular routes, while intermediate level favored paracellular route (Abadier et al., 2015; L. Yang et al., 2005). These studies suggest that integrin ligands expressed on the endothelium may provide directional guidance to leukocytes to reach extravasation sites.

Nevertheless, to this date, adhesive haptotaxis has not been evidenced for leukocytes. The first question thus arises as to the existence of such haptotaxis among leukocytes. If so, since leukocyte adhesion is mediated by integrins and they are much more than simple adhesion molecules, another question would be their potential role in this process: do they play an active role via mechanotransduction or serve as anchoring sites to mediate tug-of-war of leading edges, as widely seen in mesenchymal cells? The discovery of adhesiveness-mediated haptotaxis for leukocyte migration will be the center of this PhD project.

1.2.4.3 Mechanotaxis

While much work has been focused on how cells react to biochemical cues, fewer efforts have been made to evaluate the impact of mechanical cues on leukocytes migration and guidance. This is particularly important for leukocytes since they are highly mobile and must encounter various mechanical cues when migrating under hemodynamic flow, and cross different tissue with different mechanical properties such as different substrate rigidity. In this section, we will present how leukocytes respond to mechanical cues and their roles in guiding leukocyte motility.

1.2.4.3.1 Flow mechanotaxis

The remarkable ability of leukocytes to leave the blood circulation, cross the endothelium and enter tissues is crucial for both innate and adaptive immunity. Leukocytes extravasation is a multistep process that involves selectin, integrins, chemokines and their corresponding ligands, whose quantity and spatial distribution are thought to provide biochemical guidance in leukocyte migration. Additionally, during the leukocyte extravasation, shear stress from the blood flow plays an important role in several processes, such as leukocyte integrin activation, pseudopod formation and transmigration (Ronen Alon & Dustin, 2007; Cinamon, Shinder, & Alon, 2001; Coughlin & Schmid-Schönbein, 2004; Moazzam,

DeLano, Zweifach, & Schmid-Schönbein, 1997; Zhu et al., 2008). More specifically, shear stress can strengthen chemokine-triggered integrin adhesion of naïve T lymphocytes. It can also lead to more efficient transmigration with increased filopodia formation when naïve T lymphocytes transmigrate across the cellular endothelium *in vitro* (Cinamon et al., 2001; Schreiber, Shinder, Cain, Alon, & Sackstein, 2007; Woolf et al., 2007). *In vivo* studies of neutrophils showed that these leukocytes migrate preferentially in the direction of blood flow (Phillipson et al., 2009; R. Sumagin et al., 2010). In the *in vitro* studies, neutrophils migrated randomly under static conditions and with a bias in the direction of flow in a shear-stress-dependent fashion that was consistent with previous *in vivo* observations (Rainger, Buckley, Simmons, & Nash, 1999; L. A. Smith, Aranda-Espinoza, Haun, & Hammer, 2007). Conversely, intravital imaging of rat CD4⁺ effector T lymphocytes bound to specialized cerebral structures, the leptomeningeal vessels, an experimental autoimmune encephalitis model revealed that the lymphocyte migration was oriented preferentially against the direction of blood flow before transmigration (Bartholomäus et al., 2009). Furthermore, when mouse CD4⁺ effector lymphocytes were observed migrating on cultured mouse brain microvascular endothelial cells or on immobilized ICAM-1 or ICAM-2 ligand, the cells migrated randomly under static conditions and slightly against the direction of flow when shear stress was applied (Steiner et al., 2010).

These examples of T lymphocyte migration suggest that different leukocyte subtypes might respond differently to shear stress compared with neutrophils or monocytes. However, these previous studies on T lymphocytes were limited to observations in the pathological context of autoimmune encephalitis in mice and only under low shear stress (1.5 dyn.cm⁻²). Leukocyte extravasation predominantly takes place in the postcapillary venules. Moreover, naïve and central memory T cells enter lymph nodes by migrating across the high endothelial venule. Studies that focused on the microvasculature have given consistent order of magnitude of the dimension of the vessels as well as the local shear stresses. The diameters of the capillary venules range between 15 and 30 µm (Koutsiaris et al., 2007; Lipowsky, Kovalcheck, & Zweifach, 1978), and local shear stresses span between 3 dyn.cm⁻² (Granger & Kubes, 1994; Koutsiaris et al., 2007) and 10 dyn.cm⁻² (Xu et al., 2004), with maximal shear stresses reaching 25-30 dyn.cm⁻² (Perry & Granger, 1991; Xu et al., 2004). Using the physiological range of shear stress, Valignat et al. investigated the migration of different subtypes of leukocytes under flow and found that both naïve and effector T cells migrate against the flow whereas neutrophils migrate, in sharp contrast, with the direction of the flow (M. P. Valignat, Theodoly, Gucciardi, Hogg, & Lellouch, 2013). It was later found that T lymphocytes migrated against the flow on ICAM-1 substrates via LFA-1 integrin and with the flow on VCAM-1 substrates via VLA-4 integrin (Dominguez, Anderson, & Hammer, 2015). This mechanotaxis phenomenon has later been observed in human hematopoietic stem and progenitor cells (Buffone, Anderson, & Hammer, 2018). The variety of flow mechanotactic responses from different leukocyte subsets and integrin-ligands show that integrins are

involved, but a precise mechanism of flow mechanotaxis controlled by integrins is still lacking. An “active” mechanism has been proposed: flow detection involved integrin outside-in signaling in response to flow shear and integrins at adhesion sites mediate mechanotransduction (del Rio et al., 2009; Hoffman, Grashoff, & Schwartz, 2011; Sawada et al., 2006; Urbich et al., 2002; Zaidel-Bar, Kam, & Geiger, 2005). Evidences of integrin-based signaling during migration under flow have been reported for endothelial cells (Urbich et al., 2002; Zaidel-Bar et al., 2005) and neutrophils (Dixit & Simon, 2012). However, Valignat et al. revealed that the T lymphocytes can, counterintuitively, steer themselves against the flow with a passive mechanism where the uropod acts as microscopic windvane without additional mechano-transduced signaling (M.-P. Valignat et al., 2014). These findings show that integrins play a more sophisticated role that cannot be simply covered by mechanotransduction. Horung et al. are the first to propose a comprehensive mechanism that explains T cell LFA-1 mediated upstream crawling, VLA-4 dominant downstream migration as well the existence of a bistable state (Alexander Hornung et al., 2018). This model reveals the crucial role of integrins where the spatial polarization of their affinity and a feedback of their activation have resulted in cell adhesion by the tip on ICAM-1 and by the rear on VCAM-1 and oriented them against or with the flow, respectively in absence of active mechano-transduction (Alexander Hornung et al., 2018).

1.2.4.3.2 Durotaxis

Another physical property that varies greatly between different tissues and that can be sensed by leukocytes is substrate rigidity or stiffness (Discher, Janmey, & Wang, 2005). Mechanosensing of global and local stiffness of the substrate during migration implicates actomyosin contraction and integrin-dependent adhesion (Pasapera et al., 2015). Generally, cells tend to migrate toward stiffer environments, a phenomenon termed as durotaxis, which is associated to increased actomyosin contractility (Trichet et al., 2012). Upon adhesion to the vascular wall, leukocytes spread and crawl on endothelial cells (EC) to find sites that permit transendothelial migration. As shown for human neutrophils, leukocytes show increased spreading and migrate slowly but more persistently on stiffer substrates (Oakes et al., 2009; Stroka & Aranda-Espinoza, 2009). Consequently, they migrate greater distances on stiffer substrates, which may facilitate their search for sites that permit transmigration. Leukocytes probe the surface of the substrate and sense local endothelium stiffness through ventral filopodia or invadosome-like protrusions and actomyosin-based contraction to respond to substrate stiffness, which is mediated by mechanosensitive transmembrane integrin receptors (Carman et al., 2007; Schaefer et al., 2014; Shulman et al., 2009). Leukocytes require an optimal substrate stiffness for maximal motility, which negatively correlates with the concentration of ECM proteins, such as fibronectin (Stroka & Aranda-Espinoza, 2009). This suggests that leukocyte durotaxis is important for leukocyte transmigration. Leukocytes respond to the stiffness of the underlying monolayer of endothelial cells, which in turn

respond to the increased stiffness of its underlying matrix through enhanced integrin-mediated mechanotransduction. The endothelial monolayer thus forms a highly heterogeneous surface for circulating leukocytes. Even a single endothelial cell within the monolayer shows a remarkable surface heterogeneity: studies showed that a single cell in a monolayer of bovine endothelial cells was stiffer at cell periphery compared to the cell center and the nucleus, forming a local stiffness gradient from periphery towards the center of the cell (Sato, Nagayama, Kataoka, Sasaki, & Hane, 2000; Schaefer et al., 2014; Stroka & Aranda-Espinoza, 2011). Schaefer et al. have proposed that leukocytes sense endothelial stiffness and crawl in a durotactic fashion towards the periphery of a single EC (transmigration “hot-spot”), possibly also with the help of the heterogeneous distribution of adhesion molecules like ICAM-1 (Nourshargh & Alon, 2014). They have identified that endothelial ICAM-1 forms mechanosensitive, functionally distinct complexes with α -actinin-4 that control, in an adaptor-specific manner, the neutrophil search for sites that permit TEM (Schaefer et al., 2014). Here, α -actinin-4 functions as a force-transmitting element that promotes maturation of the ICAM1 complex, like the role it has in integrin complexes (Roca-Cusachs et al., 2013). At the cell junction of the “hot-spot”, leukocytes are thought to be guided by the low-to-high EC stiffness gradient that exists within an individual EC towards the EC periphery. Upon their durotactic guidance towards the periphery of a single EC and, thus, prior to actual extravasation, crawling leukocytes round up, which might be linked to a local reduction in the stiffness at junctional regions and protrude their leading edge towards the abluminal side of the endothelium before breaching the endothelium through either paracellular or transcellular routes (Schaefer et al., 2014). Durotaxis is thought to be important for leukocyte intravascular crawling and transmigration. Integrins and their functions in mechanotransduction are important for durotactic response. Nevertheless, one should note that in the *in vivo* environments, where multiple cues are present, it would be difficult to decorrelate substrate rigidity gradient and adhesion gradient to assess durotaxis.

1.3 Surface micro-patterning

1.3.1 Necessity for well-defined *in vitro* assays

Scientific endeavors to understand leukocyte motility date back for decades. Enormous advances have been made in understanding different aspects of leukocyte migration in complex environment since then. More recently, the study of directed cell migration (taxi) has become of great interest. Guidance by chemical cues remains the best studied and it is widely accepted now that many chemical cues are surface-bound and could provide cells with haptotactic cues. However, many questions remain to be answered regarding the haptotaxis of different cells and underlying mechanisms. One of the obstacles that prevents us from fully understanding haptotaxis is the lack of well-adapted tools. Even though recent development in *in vivo* imaging technique and genetic modification tools have greatly advanced our ability to measure live cell migration, these experiments remain delicate to handle and difficult to control given the highly complex *in vivo* environment and heterogeneity in animal subjects. Therefore, the development of well-defined *in vitro* systems becomes crucial in that these tools will allow us to create well-controlled environment, to test individual cue quantitatively before combining multiple cues together. Such systems, which might seem incomplete and less physiological compared to animal models, find their strength in their unique ability to support well-controlled quantitative assays and to improve experimental reproducibility. In turn, these tools can be combined with *in vivo* experiment to provide a more comprehensive and in-depth understanding of haptotaxis. Development of microtechnology and its successful application to cell biology have greatly improved our ability to locally modify substrate with guidance cues to allow cell adhesion and migration. This technique is now commonly known as micropatterning. In this section, we will give a technological overview of some well-established surface patterning techniques and their applications in haptotaxis study.

1.3.2 Soluble gradient transfer with microfluidics

Microfluidics allows the manipulation of small volume of reagents. Under the microfluidic condition, the flow is laminar where the mixing occurs only by diffusion (Whitesides, 2006). In 2000, Jeon et al. created the iconic microfluidic mixer (Figure 1-20-A). Solutions containing different chemicals were introduced from the inlets and allowed to flow through the network. The fluid streams were repeatedly combined, mixed, and split to yield distinct mixtures with distinct compositions in each of the branch channel. When all the branches were recombined, a concentration gradient was established across the outlet channel (Jeon et al., 2000). The width of this channel and the total number of the branches determined the width of the gradient and the resolution of the steps making up the gradient. Based on this technique, an assortment of microfluidic systems has been used to generate diffusible gradients to study chemotaxis in bacteria, fibroblasts, stem cells and immune cells

(Wu et al., 2012). More complex systems have also been created: for instance, a shear-free device that allows the soluble gradient generated by the microfluidic system to diffuse through a membrane on the neuron (Figure 1-20-B) (Morel et al., 2012). Another example is a tunable microfluidic system that creates diffusible gradient in the collagen embedded chemotaxis chamber (Figure 1-20-C) (Aizel et al., 2017).

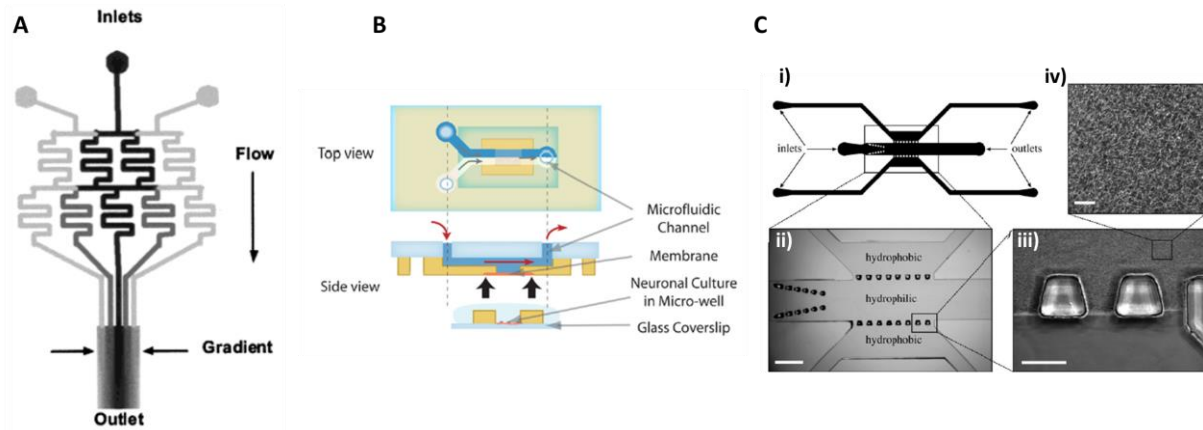


Figure 1-20 Examples of microfluidic soluble gradient: A) Microfluidic gradient mixer by Jeon et al., 2012; B) Shear-free soluble gradient achieved by combining microfluidic channels and a porous membrane by Morel et al., 2014; C) Diffusion-based soluble gradient inside the chemotaxis chamber embedded with collagen matrix: i) Whole device design. ii) Image of a PDMS replica of the chemotaxis device showing hydrophilic and hydrophobic areas. (scale bar=1 mm). iii) Epifluorescence image of a collagen network embedded in the device (scale bar=200 μm). iv) Brightfield image showing a detailed view of the junction zone of the chemotaxis chamber filled with collagen (scale bar=20 μm).

These techniques can in turn be used to create surface bound gradient by transferring the volume gradient onto the surface by adsorption. Jeon et al. used the same microfluidic mixer to generate a gradient of etching solution HF and transferred it onto the SiO_2 coated wafer and therefore created a topological gradient on the surface (Jeon et al., 2000). This flow-based gradient transfer technique has since then been used in different applications. Substrate-bound gradient of extra-cellular matrix protein laminin were generated on pre-coated poly-L-lysine substrates. These have been used to investigate the response of rat hippocampal neurons to monotonic gradient of laminin (Dertinger, Chiu, Jeon, & Whitesides, 2001). Jiang et al. utilized a microfluidic mixing network that generates a gradient of avidin in solution and immobilizes this protein on the surface of glass or poly(dimethylsiloxane) by physical adsorption (Jiang et al., 2005). The immobilized gradient of avidin was then translated into gradients of biotinylated ligands (e.g., small molecules, oligomers of DNA, polysaccharides) using the specific interaction between biotin and avidin (Jiang et al., 2005). Shi et al. used a microfluidic mixer device to generate a covalently conjugated gradient of polydopamine (PDA), which changed the wettability and the surface energy of the substrate (Figure 1-21-A) (Shi et al., 2014). The gradient was subsequently used to enable the spatial deposition of adhesive proteins on the surface to investigate human mesenchymal stem cells adhesion and spreading. Using a flow-free device, Millet et al. has generated surface-bound laminin gradient. It was

achieved by adsorbing a volume gradient diffused across microfluidic channels on to the substrates and was used to study guiding in neuron development (Millet, Stewart, Nuzzo, & Gillette, 2010). Wu et al. also used a flow-free microfluidic device to create surface-bound fibronectin gradient to study haptotactic migration for fibroblasts (Figure 1-21-B) (Wu et al., 2012). Liu et al. utilized the gradient mixer to pattern cellular adhesive Arg-Gly-Asp (RGD) peptide gradient on poly(ethylene glycol) (PEG) hydrogel and observed the response of mesenchymal stem cell to this adhesive gradient (Liu et al., 2012). With a diffusion-based device, Cho et al. created a microfluidic chamber that creates both soluble and surface-bound amyloid- β (A β) and studied the progressive microglial accumulation (Figure 1-21-C) (Cho et al., 2013).

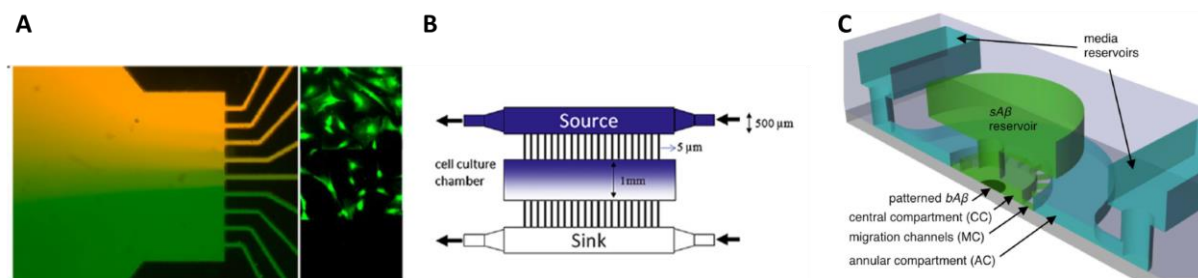


Figure 1-21 Examples of microfluidic generated surface-bound gradient: A) Covalently conjugated gradient of polydopamine (PDA) that subsequently allows binds of adhesion molecules of human mesenchymal stem cells (Shi et al, 2014); B) Surface-bond fibronectin gradient was created in the cell culture chamber by diffusion (C.Wu et al., 2012); C) Diffusion-based device that created soluble amyloid- β (A β) gradient in the migration channels as well as surface-bound A β in the central area (Cho et al., 2013).

Attempts have also been made to create multiple protein gradients. However, much fewer applications have been reported compared to single protein pattern. Wang et al. used the classic gradient mixer combined with a complex valve system to create a shear-free non-monotonic (N-shape) surface-bound laminin gradient in presence of a soluble brain-derived neurotrophic factor (BDNF) gradient and they studied the response of *Xenopus* spinal neurons (Figure 1-22) (C. J. Wang et al., 2008). Zhang et al. created two component protein gradient by perfusing chemically modified fibronectin and de novo designed vascular endothelial growth factor mimetic peptide (QK) (D'Andrea et al., 2005) through the gradient mixer onto chemically modified glass substrates to study human umbilical vein endothelial cells (HUVECs) adhesion (K. Zhang, Sugawara, & Tirrell, 2009). These attempts either require complex multi-layer microfluidic network embedded with pressurized valves or specific protein modification and peptide synthesis to allow specific bindings. They remain technically complicated and are difficult to become routinely used in the biology laboratories.

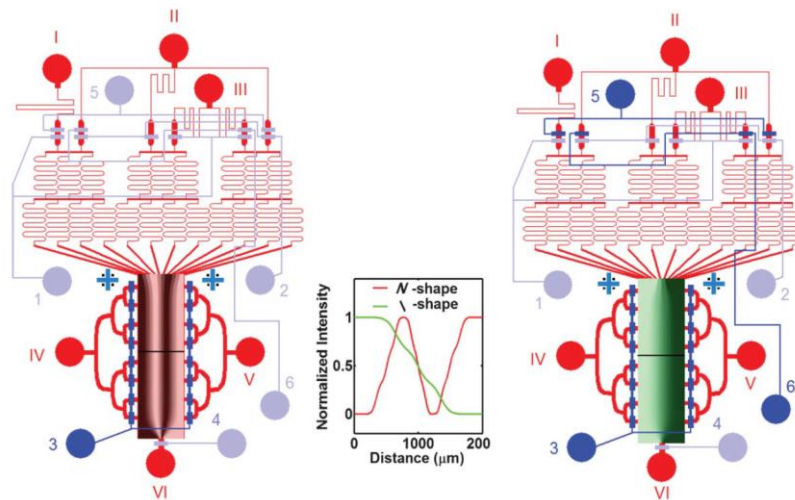


Figure 1-22 Gradient mixer-based device with multilayer configuration and embedded valves: Left: fluidic and valves configuration that created an N-shaped surface-bound laminin gradient through transfer; Right: fluidic and valves configuration that created an \-shaped soluble BDNF gradient; Middle: intensity profile of both surface-bound and soluble (Wang et al., 2008)

Since its invention in the early 21st century, microfluidics has become a powerful tool to create diffusible gradient. It can be in turn used to create surface-bound protein gradient by adsorbing soluble gradient onto the surface through either flow-based or diffusion-based microfluidic devices. Despite major advances in the development of the technique, there are some limitations: from a more technical point of view, the use of microfluidics system requires knowledge of microfluidic flow and microfabrication as well as access to clean room facilities that may be costly and not routinely available. Operation of microfluidic devices can be compromised by the presence of obstructions such as air bubbles that disturb flow, disrupt gradient profile, denature the coated-surface and disrupt gradient transfer. Different surface modifications and surface chemistry are required and not all proteins may be able to adsorb correctly on the surface. The concentration profile doesn't represent the profile of adsorbed gradient and the transfer remains difficult to control and quantify. The surface can also become saturated or multilayer of proteins may form (Squires, Messinger, & Manalis, 2008). Though there have been many applications regarding single-protein gradients, multi-protein surface patterning is difficult and not routinely available.

1.3.3 Gradient patterning with microcontact printing

Another well-established way to pattern surface-bound protein is the technique of micro-contact printing (μ CP). It is an accessible lithography technique first introduced by the Whiteside group in 1994 (A. Kumar, Biebuyck, & Whitesides, 1994). The principle of the technique relies on a stamp made of an elastomeric material that is usually polydimethylsiloxane (PDMS) cast on a master mold (usually silicon) (Figure 1-23-A, R Lagraff et al., 2011). The unmold stamps is incubated with a protein solution (ink) and let to dry (Figure 1-23-B, R Lagraff et al., 2011). Finally, the ink is transferred onto a surface by contact (Figure

1-23-C, -D, R Lagraff et al., 2011). The contact is said to be conformational as the stamp elastic properties allow it to make conformal contact even on rough surfaces.

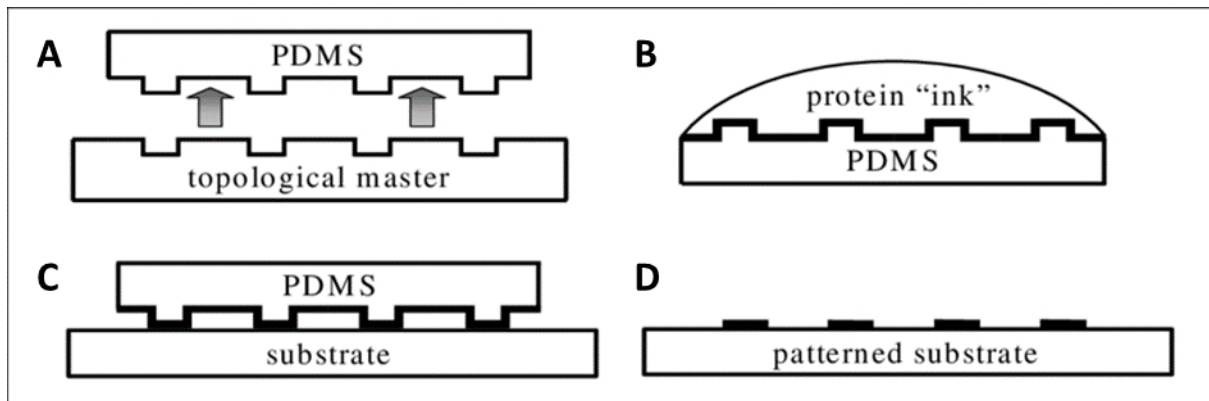


Figure 1-23 The principle of microcontact printing (Lagraff et al., 2011)

The μ CP is often presented as an accessible tool for cell patterning to create biomimic environment *in vitro*. Since the first publication revealing cells attached to the surface patterned by the μ CP (Mrksich & Whitesides, 1996), the μ CP has become a widely-used tool to create surface pattern to control cell geometry and cell shape for numerous biological applications. Mcbeath et al. used microcontact printing to produce fibronectin patterns of varying size to demonstrate that the shape and spreading area of human mesenchymal stem cells in to specific lineages (McBeath, Pirone, Nelson, Bhadriraju, & Chen, 2004). Kilian et al. used the same technique to create different geometrical fibronectin patterns and have shown that patterns that induce the increase of intracellular actomyosin tension regulate the differentiation behavior of mesenchymal stem cells (MSCs) (Kilian, Bugarija, Lahn, & Mrksich, 2010). Microcontact-printed fibronectin is also a simple way to regulate cell shape and influence cell division axis. Théry et al. have found that the spatial distribution of extracellular matrix (ECM) can determine cortical actin dynamic which in turn regulate the axis of HeLa cell division (Théry, Jiménez-Dalmaroni, Racine, Bornens, & Jülicher, 2007; Théry et al., 2005) (Figure 1-24). Hu et al. used μ CP to create covalent and non-covalent bound ECM protein patterns and demonstrated the important role of protein-substrate adhesion in determining vascular smooth muscle cell behavior (S. Hu, Chen, Zhao, Wang, & Lam, 2018). Lee et al. created adhesive polydopamine patterns on to a thermal-expandable hydrogel that facilitated the formation of spatially controlled micro-tissue of human dermal fibroblasts (HDFBs) (Lee et al., 2017). Sadoun used the μ CP to create antibody patterns to study T cell activation (Sadoun, 2018). Scientists have also attempted to use the μ CP to create multiprotein patterns: Hou et al. patterned chicken and rabbit IgGs that are perpendicular to each other on modified glass substrates. The patterns were then revealed by corresponding antibodies (Hou, Feng, Wang, & Chan, 2007). Eichinger et al. developed multi-protein patterning technique with μ CP. The precision of their technique was down to micrometer after live pattern alignment with an inverted microscope. Patterns of laminin and aggrecan were generated to investigate

astrocyte alignment (Eichinger, Hsiao, & Hlady, 2012). The use of master mold can be very expensive in case of high-resolution stamps. In an effort to make nano-scale patterning more cost-effective, Ricoult et al. created surface-bound netrin-1 digital nanodot gradient based on cost-effective replica stamps made of NOA and investigated C2C12 myoblast migration (Ricoult et al., 2013).

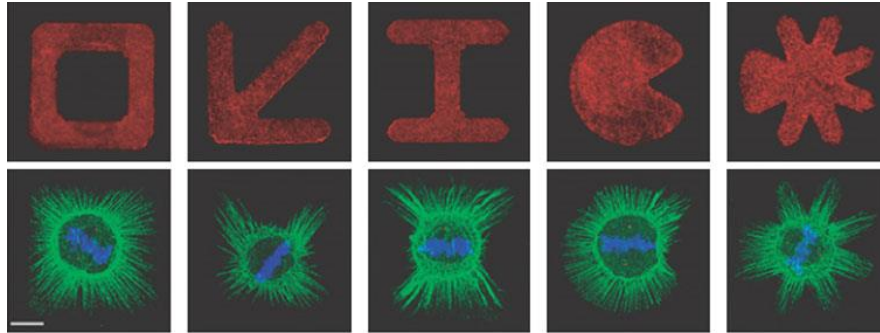


Figure 1-24 Example of different patterns generated by μ CP to investigate the role of cell geometry in regulation HeLa cell division: first row: fluorescent labeled fibronectin pattern; second row: Retraction fibres (green, second row), spindle poles (red) and the chromosomes (blue) were labelled. Scale bar=10 μ m.; (from Théry et al., 2007).

Although the μ CP has become a very popular tool to create continuous patterns where the density of grafted molecule is constant, it has also been used to create surface-bound protein gradients. These gradients are formed by patterning proteins as discrete surface-bound patches and thus a discontinuous gradient can be created by vary the surface coverage density of the patches. Fewer applications have been made in comparison to the homogenous protein patterning: Von Philipsborn et al. created discontinuous ephrin gradients made of submicron level stripes or dots of different sizes to investigate the ability of the growth cone of chick temporal retinal axons to integrate these discontinuous gradual cues (Figure 1-25) (Von Philipsborn et al., 2006). They later integrated these discontinuous gradients into a microfluidic network (Lang, von Philipsborn, Bernard, Bonhoeffer, & Bastmeyer, 2008; Von Philipsborn, Lang, Jiang, Bonhoeffer, & Bastmeyer, 2007).

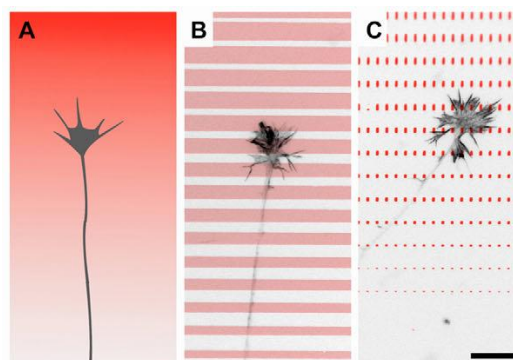


Figure 1-25 Substrate-bound gradients fabricated by microcontact printing.: A) Schematic of a growth cone in a continuous gradient; B,C) Growth cones in different discontinuous gradients fabricated by microcontact printing: B) a steep gradient built by an array of stripes and C) a shallow gradient built by dots. Antibody-stained ephrin is shown in red; phalloidin-stained actin in black. Scale bar=15 μ m (from Von Philipsborn et al., 2006).

The microcontact printing remains today one of the most popular surface patterning techniques for biological applications. Nevertheless, this widely used technique also has its shortcomings. From a technical point of view, the fabrication of master mold requires knowledge and access to lithography facility, which may be costly and not readily available for biological labs. In terms of the patterning outcome, the ink protein could be denatured during the drying process and lead to unfunctional pattern. Moreover, both the amount and the homogeneity of transferred molecule are difficult to control. For multiple protein patterning, the alignment process is experimentally complicated despite the efforts to improve its precision and efficiency. Also, the lengthy alignment procedure is also unfriendly to sensitive protein samples and may alter their functionality. The technique is the most limited in surface gradient patterning. Due to the characteristics of the technique, continuous surface gradient is not possible to be created by μ CP but only discontinuous ones with un-patterned spacings (up to millimeters) between locally patterned proteins patches. Overall, the patterning (continuous or gradual) remains un-quantitative in the sense that one cannot control the exact quantity of patterned protein on the surface after each transfer, nor the actual gradient profile transferred onto the substrate. Given the complexity of the alignment in multiprotein patterning, multiple surface-bound gradients are very difficult to achieve.

1.3.4 Surface patterning with light

1.3.4.1 Photolithography

Another surface patterning option is to pattern with light. An early technique is photolithography that applies wavelengths in the region of deep UV to obtain patterns. It requires a predesigned photomask sensitive to those wavelengths. The UV light will be projected through the photomask to expose specific areas on the surface. The material used in a photomask is normally natural quartz, synthetic quartz or fused silica (Azioune, Carpi, Tseng, Th, & Piel, 2010), but this technology has also been used for glass (Carpi, Piel, Azioune, & Fink, 2011) and for PDMS substrates (Carpi, Piel, Azioune, Cuvelier, & Fink, 2011). Azioune et al. used the photolithography to active PLL-g-PEG passivated glass substrate and subsequently patterned fibronectin/fibrinogen–Alexa 488 on UV exposed area (Figure 1-26) (Azioune, Storch, Bornens, Théry, & Piel, 2009). The RPE-1 cells were then immobilized on the fibronectin/fibrinogen pattern. This method provides a means to pattern very large surfaces in one step, but it is difficult to create gradient patterns with different profiles. However, this method typically requires a costly clean-room environment. Also, cumbersome mask alignment procedures (Théry, 2010) under biomolecule friendly wet environments usually impair the ability to generate multiprotein patterns.

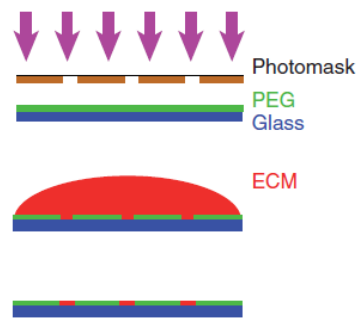


Figure 1-26 The principle of photolithography (from Théry et al.,2010)

1.3.4.2 Laser-based photopatterning

1.3.4.2.1 Laser-assisted adsorption by photobleaching

Most of the abovementioned techniques require clean room access to fabricate master wafer and photomask. Multiprotein patterning is difficult as it requires either complex microfluidic network manipulation or cumbersome alignment procedures. Laser-based photopatterning technique has now become a promising alternative to achieve maskless patterning. Bélisle et al. developed laser-assisted adsorption by photobleaching (Figure 1-27) (LAPAP) (Bélisle, Correia, Wiseman, Kennedy, & Costantino, 2008): LAPAP uses photochemical immobilization by means of photobleaching. A fluorescently tagged ligand is incubated on a protein-coated surface (typically BSA). Upon UV irradiation, the fluorophore (biotin-4-fluorecein, B4F) is photobleached and binds to the protein and thereby immobilizes the target protein via streptavidin layer. Using this method, Bélisle et al. were able to generate single protein continuous and gradient patterns by changing the laser intensity and the velocity of the focal spot displacement. The authors patterned, as a proof of concept, the laminin peptide gradient and showed the growth cone of DRG neuron was guided. In 2017, Schwarz et al. used the LAPAP technique to immobilize CCL21 chemokine gradient to study dendritic cell haptotaxis (Schwarz et al., 2017).

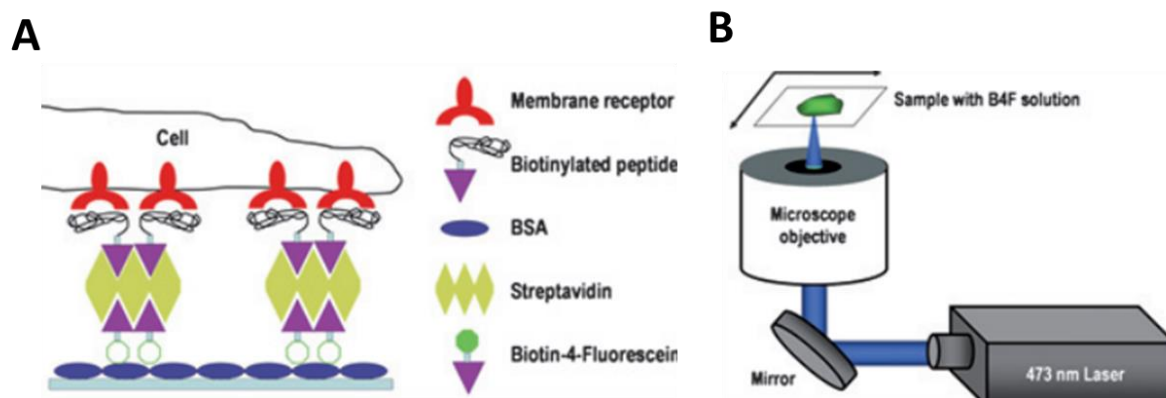


Figure 1-27 The principle of LAPAP: A) the schematics of the surface chemistry B) the optical set-up for laser writing (from B elisle et al. 2008).

The main advantage of LAPAP compared to conventional photolithographic techniques is that the use of photomask is unnecessary. Also, the fluorophore can be chosen from a wide selection of available dyes, so that the process can be carried out at wavelengths that are not harmful to proteins. However, as a serial writing process, LAPAP suffers from long processing times for larger substrate areas. Therefore, the authors later used widefield illumination via a light-emitting diode (LED) array through a spatial light modulator (SLM) for the generation of light intensity patterns (B elisle, Kunik, & Costantino, 2009). With the improved LAPAP, the authors were able to generate two continuous antibody patterns by varying the wavelengths of the laser. Compared to laser writing LAPAP, the time required for the generation of a pattern could thus be decreased from 80 to ~5 min. While this represents a significant increase in processing speed, the method is still too slow to be used to generate sets of different patterns in a cm² scale area. Scott et al. further improved the LAPAP by screening a various range of PEG monolayers surface chemistries and found that the long chain acrylated PEG can resist non-specific protein binding while permitting efficient B4F binding to PEG layer (instead of BSA layer in the original LAPAP) upon exposure to femtosecond laser pulses (Scott, Wissner-Gross, & Yanik, 2012). The authors have largely improved the scanning speed (1000000 $\mu\text{m}/\text{s}$ compared to the 10 $\mu\text{m}/\text{s}$ in the original LAPAP) and patterned single protein patterns to study direct the polarization of hippocampal neurons. However, multi-protein patterning was not available with the version of LAPAP.

Walbaur et al. later presented another improvement of the LAPAP by using a Digital Mirror Device (DMD) (Waldbaur, Waterkotte, Schmitz, & Rapp, 2012). These devices, commonly found in video projectors, comprise thousands of individually addressable micro mirrors which can be tilted to an on- or off- state (Figure 1-28). Rapid changes between these states lead to "gray values" of intermediate light intensity. By setting individual micromirror pixels to different gray values, light patterns can be created.

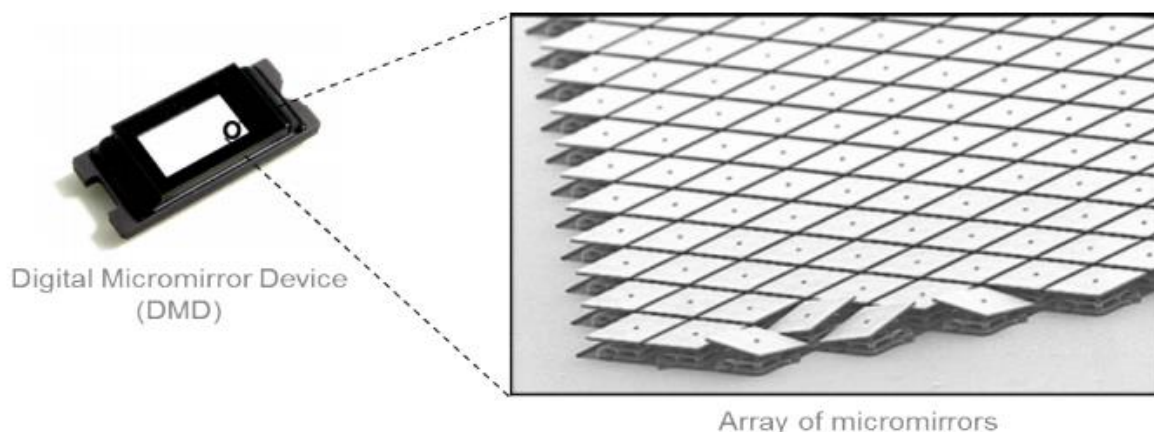


Figure 1-28 An example of DMD with the close-up of the micromirror array (from Texas Instrument website)

In their work, Walbaur et al. have combined DMD-based optical set-up with the photobleaching-based grafting chemistry and have achieved single-protein continuous and gradient pattern as well as multi-image arrays by wide-field illumination (1 min per image). The significant improvement in the illumination time is achieved with this version of LAPAP. Unfortunately, multiprotein patterns (continuous or gradient) have not been achieved with this version of DMD-based LAPAP.

1.3.4.2.2 Light-Induced Molecular Adsorption of Proteins

Recent improvements of the LAPAP technique has significantly reduced the illumination time by introducing widefield set-up with DMD, allowing patterning large area in short time. The maskless projection photopatterning method is thus a promising alternative to make fast multi-protein patterning with several challenges: such system requires a well-collimated light source to achieve micrometer resolution in the entire field of view; light sensitive grafting photochemistry is required since only a few mW/mm^2 UV power is available with current illumination sources; sequential multiple protein printing requires an efficient antifouling coating that should be compatible with several steps of illumination and rinsing.

In 2016, Strale et al. proposed a novel maskless protein patterning technique using Light-Induced Molecular Adsorption of Proteins (LIMAP) (P. O. Strale et al., 2015) to address the above-stated challenges. It has significantly improved the capacity of the current photopatterning technique: it is able to perform multiprotein patterning at sub-micrometer resolution level with different shape of gradient with very short insolation time. Moreover, the post-insolation protein incubation time is also largely shortened compared to other photopatterning techniques. LIMAP implements a UV laser ($\lambda=375\text{nm}$), an optical system based on DMD (Figure 1-29) to achieve wide-field UV projection and uses a water-soluble photo-initiator.

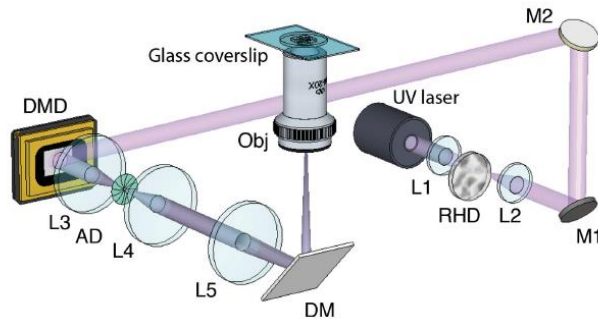


Figure 1-29 Optical set-up for LIMAP technology (from [Strale et al.,2015])

Its working principle is the following (Figure 1-30): 1) the substrate is first coated with an antifouling PEG layer; 2) the soluble photo-initiator is added onto the substrate; 3) pre-designed pattern is sent to the DMD through corresponding software and is illuminated with UV light; 4) after rinsing, the protein of interest is incubated onto the substrate; 5) if necessary, a second protein can be patterned in the same way.

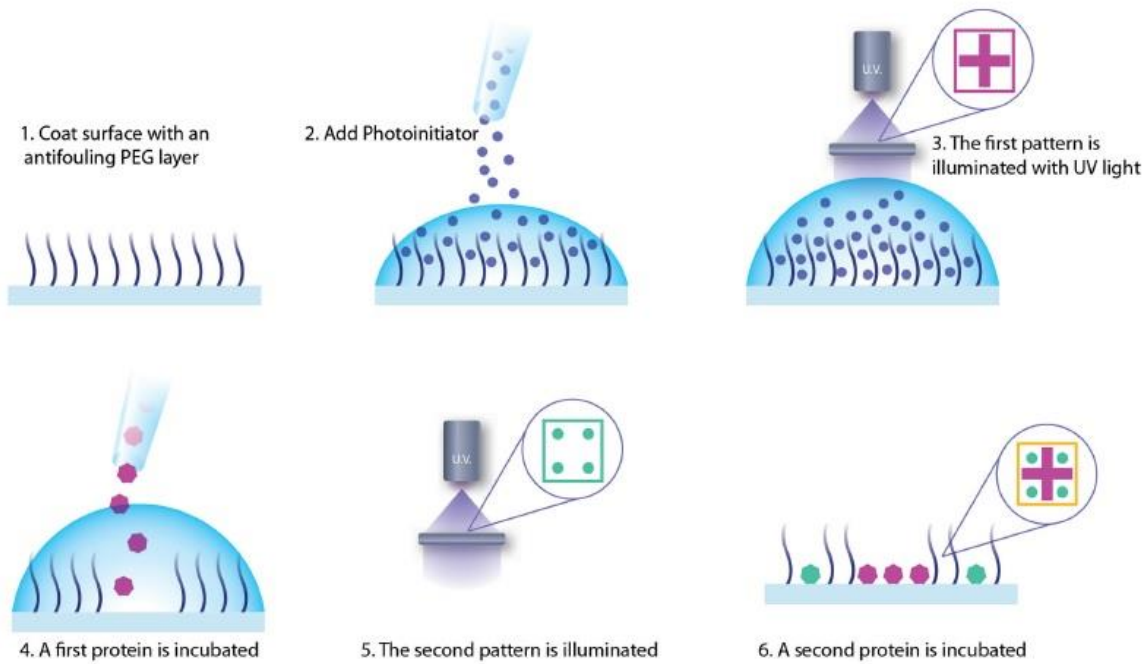


Figure 1-30 The working principle of LIMAP (from [Strale et al.,2015])

Strale et al. have demonstrated in their paper a variety of protein patterning, including single protein gradient with different profiles (logarithmic, linear and exponential) (Figure 1-31-A), double protein gradients with opposite profiles (Figure 1-31-B) as well as double sequential printing of fibronectin allowing specific cell binding of two different adherent cell types: S180 cells and mouse embryonic fibroblasts (MEFs) (Figure 1-31-C), proving that LIMAP is a powerful and versatile tool of quantifiable protein patterning with unprecedented spatial and temporal control. Moreover, patterning with LIMAP has not only reduced UV illumination

time (around 20s for each pattern) but also post-patterning incubation time (around 3 min compared to 30 min with previous LAPAP technique).

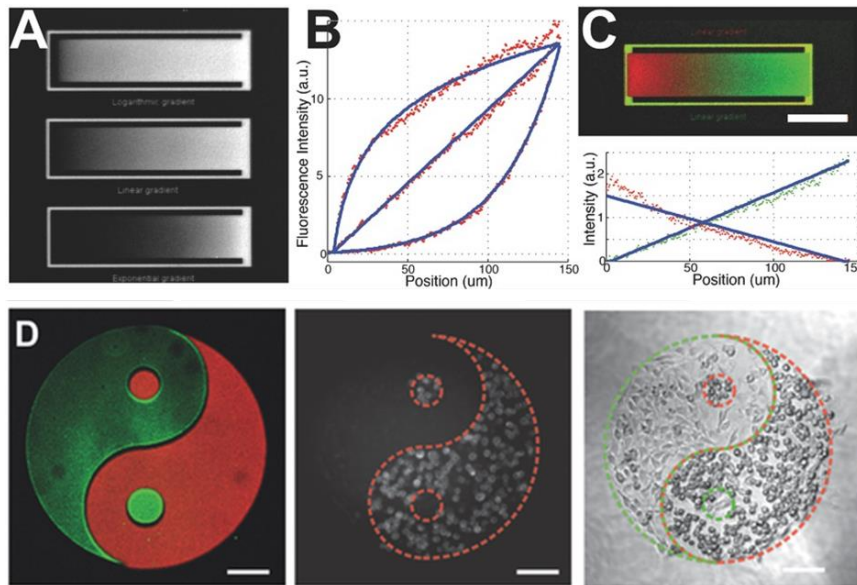


Figure 1-31 Wide-field Maskless UV patterning with LIMAP: A) Epifluorescence microscopy image of a logarithmic (top), linear (middle), and exponential (bottom) printed gradients of GFP; B) Fluorescence intensity profile (red squares) of each patterned gradient of A). The theoretical expected profile is plotted in blue. C) Top: Two-color fluorescence microscopy image of a pattern combining two opposite linear gradients of proteins: GFP in green and mCherry in red. Scale bar = 50 μm . Bottom: Fluorescence intensity profile of each linear gradient pattern. D) Left: Two-color epifluorescence microscopy image of a two-protein Yin Yang pattern composed of Cy3-labeled Fibronectin (red) and Alexa - 488 - labeled streptavidin (green). Middle: the first population of S180 cells expressing E-Cadherin GFP was first seeded. After incubation with biotinylated FN, MEF were allowed to adhere. Middle panel: Epifluorescence microscopy image showing S180 cells stably expressing E-cadherin GFP adhering only to the fibronectin "Yin" pattern. Right panel: Phase contrast images showing S180 cells and MEF adhering to the FN-coated Yin and biotinylated FN-coated Yang, respectively. Scale bar = 100 μm (from Strale et al., 2015).

Later, the LIMAP technique was commercialized into the Primo™ micropatterning system together with the photo-initiator PLPP by Alvéole (Paris, France). The applications of the technique have also been expanded besides the protein patterning on 2D substrates: Stoecklin et al. have been using the LIMAP technique to create artificial 3D microniches (Stoecklin et al., 2018); Decock et al have patterned hydrogel membrane inside a microfluidic channel (Decock, Schlenk, & Salmon, 2018). Pasturel et al. have used LIMAP to structure and pattern hydrogels in 3D (Pasturel, Strale, & Studer, 2018).

This thesis started during the beta-testing phase with the prototype of the Primo. A major difficulty of protein patterning is to achieve specific binding with low background noise and to retain the functionality of the immobilized protein. Since LIMAP is a new technique, no one had used it to study T cell migration and pattern relevant molecules. Also, the exact chemical mechanism of LIMAP remains only partially understood. Therefore, the first major challenge of this project was to test the optical system and optimize the surface chemistry of

substrates. The main objective of this optimization phase was to obtain specific and functional patterns of integrin ligands for immune cells. Results of this part of the work will be presented in Chapter 3.

1.4 Open questions and project outline

As extensively detailed in the previous sections, leukocyte migration is mediated by multiple guidance cues such as blood flow, soluble and surface-bound chemokines. However, contrary to what has been widely observed in mesenchymal cells, adhesive haptotaxis has never been evidence for leukocytes. Previous literature has shown that leukocyte transmigration seems to occur at specific locations on the endothelium where there is enrichment in adhesion molecules, notably integrin ligands ICAM-1 and VCAM-1 (Carman & Springer, 2004; Ronen Sumagin & Sarelius, 2010), which suggests that the integrin ligands expressed on the endothelium may provide directional guidance for leukocytes to reach their transmigration sites. Based on these findings, the first question therefore is: does adhesive haptotaxis really exist for leukocytes via their respective integrin-ligands?

Leukocyte migration on 2D surface requires integrin-mediated adhesion. Integrins can serve as anchoring site for cell adhesion and migration. In this case, adhesive haptotaxis can be achieved via the passive "tug-of-war" mechanism which is essentially a competition between cell edges (Davies, 2013b). This type of haptotaxis has been widely observed in mesenchymal cells where they all migrate towards areas with higher adhesion (see 1.2.4.2). However, integrins are also well-known mechanotransducers that can activate downstream signaling cascades. Another type of "active" adhesiveness-induced haptotaxis could also exist. If adhesive haptotaxis does exist for leukocytes, the second question will be: what is the underlying mechanisms of such haptotaxis? Is it achieved via the "tug-of-war" of cell edges? Or is it achieved via mechanotransduction mediated by integrins? Or is it achieved via other mechanisms?

To answer these open questions, we chose human effector T cells as our cellular model and we took advantage of recent technological advances in surface patterning method LIMAP (P.-O. Strale et al., 2016) to create an *in vitro* assay to probe the adhesive haptotaxis. The framework of the project is the following:

Firstly, we used the novel contactless and maskless optical patterning system to create micropatterns of integrin ligands ICAM-1 and VCAM-1. To obtain biofunctional patterns, we first undertook extensive technical optimization to adapt the optical patterning technique to our cells and molecules of interest. Different substrates and surface constructions have been tested and characterized until the biofunctionalization was successful: on one hand, fluorescent labeled proteins were used to visualize the pattern. In turn, patterned proteins were stained by fluorescent antibodies to quantify their surface density. On the other hand,

the functionality of the patterned substrates was tested by directly seeding human effector T cell, cellular model chosen in this work, and quantifying their adhesion and migration.

Secondly, once the biofunctionalization of patterned substrate was complete, we created substrates with different integrin ligand density (therefore yielding different adhesiveness for T cells) and with patterns of various profile. These patterns were used to assess the existence of adhesive haptotaxis for T cells. Ligand density was quantified by fluorescent antibodies; Cell adhesion was quantified by assessing cell adhesion on different substrates under flow; Cell migration was quantified by analyzing the image sequences of migrating cells with our cell tracking programs, which allowed us to obtain various migration parameters.

In the last part of the project, which is still ongoing, we set out to decipher the underlying mechanism involved in the adhesive T cell haptotaxis. We aim to understand whether integrin plays an active role in inducing mechano-transduction during T cell adhesive haptotaxis and whether it is related to its affinity state and spatial distribution. Moreover, lamellipodia has been known to be essential in mesenchymal cell haptotaxis (King et al., 2016). Therefore, we also attempt to see if the lamellipodial dynamics is responsible for the T cell adhesive haptotaxis.

In the following sections of the thesis, we will present the above-mentioned work. Chapter 2 will first present the basic experimental set-up employed in this project, accompanied by detailed experimental protocols. Chapter 3 will present the optimization of photopatterning for immune cells. Chapter 4 will present our attempt to reveal the existence of T cell adhesive haptotaxis. Chapter 5, 6 and 7 will present our ongoing effort to decipher the underlying mechanism. Chapter 8 will conclude and present future perspectives of the project.

2 General experimental set-up

This chapter will present the general experimental set-up employed in this thesis including cell culture, surface coating and patterning, microscopy as well as cell tracking analysis. More specific experimental methods will be included in the respective results sections. Please note that detailed protocols are available in the appendices.

2.1 Human primary T cell culture

Whole blood from healthy adult donors was obtained from the Etablissement Français du Sang. Peripheral Blood Mononuclear Cells (PBMC) were recovered from the interface of a Ficoll gradient (Eurobio, Evry, France). T cells were isolated with Pan T cell isolation Kit (Miltenyi Biotec, Bergisch Gladbach, Germany), then activated with antiCD3/antiCD28 Dynabeads (Gibco by Thermo Fischer Scientific, Waltham, MA) for two days according to the manufacturer's instructions. Cells were subsequently cultivated in Roswell Park Memorial Institute Medium (RPMI; Gibco by Thermo Fischer Scientific, Waltham, MA) 1640 supplemented with 25 mM GlutaMax (Gibco by Thermo Fischer Scientific, Waltham, MA), 10% fetal calf serum (FCS; Gibco by Thermo Fischer Scientific, Waltham, MA) at 37°C, 5% CO₂ in presence of Interleukin 2 (IL-2, 50 ng/ml; Miltenyi Biotec, Bergisch Gladbach, Germany) and used 7 days after activation. At the beginning of the week, the cells were split into two batch and each was subcultured every day to maintain a cell concentration of around 1.5 million/mL. At the time of use, the cells were >99% positive for pan-T lymphocyte marker CD3 and assessed for activation and proliferation with CD25, CD45RO, CD45RA and CD69 makers as judged by flow cytometry.

2.2 Surface patterning

2.2.1 System set-up and patterning method

In this project, an inverted microscope is (TI Eclipse, Nikon, France) coupled to a UV laser source ($\lambda=375$ nm) and a Digital Micromirror Device (Primo™, ALVEOLE, Paris, France) to form the photopatterning system (Figure 2-1-A). Greyscale patterns of different size and shape (8-bit images ranging from 0-255 pixels) were designed using Inkscape (Figure 2-1-B). Designed pattern was sent to the DMD. Then, the UV laser, after going through a series of mirrors and lenses, projected the pattern onto the treated glass coverslip to locally activate the surface in presence of a water-soluble photo-initiator (PLPP™, ALVEOLE, Paris, France). Samples were then rinsed with PBS solution and passivated with 4% (w/v) BSA (Sigma-Aldrich, St.Louis, MI) for 15min at room temperature. Different printing substrates were tested, and different proteins were incubated onto the surface afterwards. Patterning optimization results will be detailed in Chapter 3.

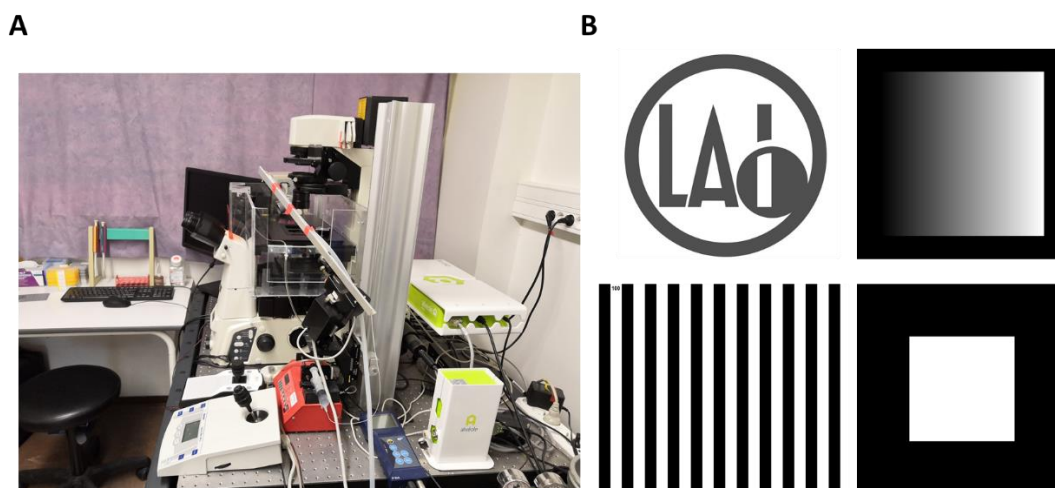


Figure 2-1 A) The experimental set-up of the protein patterning system; B) Different grey-scale pattern designs

2.2.2 Device fabrication and surface coatings

During this project, glass cover-slips (NEXTERION cover-slip, #1.5H Glass D263, SCHOTT Technical Glass Solutions, Jena, Germany) of different sizes were used as substrates that were further coated with different molecules. Both Poly(dimethylsiloxane) (PDMS) sticker and sticky-Slide VI^{0.4} (Ibidi GmbH, Martinsried, Germany) have been mounted on these coverslips to create different devices for future patterning and assays.

2.2.2.1 Glass bottom PDMS microwell

The PDMS sticker with four 3 mm × 3 mm square microwells were fabricated by cutting into a 250 μm thick silicone film (BISCO HT-6240, Rogers Corporation Carol Stream, IL, USA) with a Craft Robo Pro vinyl cutter (Graphtec, Irvine, CA, USA). A piece of 22mm x 22mm glass coverslip was activated with air plasma (Harrick Plasma, Ithaca, NY, USA) for 5 min. The PDMS sticker was then mounted on the activated coverslip. The coverslip was then treated with 3-Aminopropyltriethoxysilane (APTS, Sigma-Aldrich, St.Louis, MI, USA) for 1h at room temperature and heated at 95°C for 15 min. Afterwards, the coverslip was coated either with PLL(20)-g[3.5]-PEG(5), (SuSoS AG, Dübendorf, Switzerland) or mPolyEthylene Glycol-Succinimidyl Valerate (mPEG-SVA, Interchim, France) or adhesion molecules Fc-ICAM-1 and Fc-VCAM-1 (Intercellular Adhesion Molecule 1 and Vascular Cell Adhesion Molecule 1; R&D system, Minneapolis, MN, USA). Figure 2-2 shows a photo of the finished device containing 4 microwells.

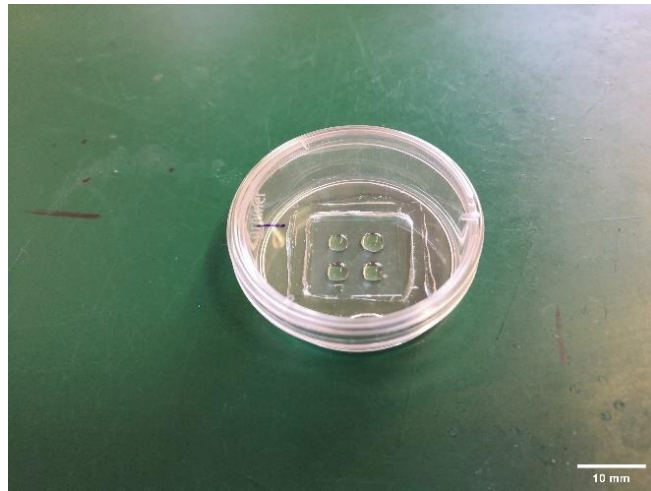


Figure 2-2 Finished glass-bottom PDMS microwell device containing four 3 mm x 3 mm microwells

2.2.2.2 Glass bottom flow chamber

The glass bottom flow chamber was fabricated using the Ibidi sticky-Slide VI^{0.4}. A piece of 25mm x 75mm coverslip was activated with air plasma. The coverslip was then treated with APTS for 1h at room temperature and heated at 95°C for 15 min. The flow chamber was then mounted by pressing firmly the sticky-slide onto the treated coverslip. Afterwards, the coverslip was coated either with mPolyEthylene Glycol-Succinimidyl Valerate (mPEG-SVA, Interchim, France) or adhesion molecules Fc-ICAM and Fc-VCAM (Intercellular Adhesion Molecule 1 and Vascular Cell Adhesion Molecule 1; R&D system, Minneapolis, MN, USA). Figure 2-3 shows a photo of the finished flow chamber with 6 channels (L x W x H = 17mm x 3.8 mm x 0.4 mm).



Figure 2-3 Finished glass-bottom flow chamber device containing six 17mm x 3.8 mm x 0.4 mm channels

2.2.2.3 Surface coatings

For antifouling PEG coatings, PLL-g-PEG was dissolved into Phosphate Buffer Saline (PBS, Gibco by Thermo Fischer Scientific, Waltham, MA) at 100µg/mL and incubated onto the

plasma-activate glass coverslip for 1h at room temperature. mPEG-SVA was dissolved into 10mM Sodium Bicarbonate buffer (Sigma-Aldrich, St.Louis, MI, USA) at 0.2 g/mL and was incubated for 1h at room temperature. The surface was rinsed with copious amount of Phosphate Buffered Saline (PBS; Gibco by Thermo Fischer Scientific, Waltham, MA, USA) and ready for use.

For continuous adhesion molecules coating, Protein A Alexa Fluor™ 647 conjugate (Thermo Fischer Scientific, Waltham, MA, USA) solution at 50µg/mL was first incubated for 1h at room temperature. Then, the coverslip was extensively rinsed with PBS and passivated with 4% (w/v) Bovine Serum Albumin (BSA; Sigma-Aldrich, St.Louis, MI) solution for 15 min at room temperature. After extensive rinsing, the surface was incubated with either Fc-ICAM or Fc-VCAM (Intercellular Adhesion Molecule 1; Vascular Cell Adhesion Molecule 1, R&D system, Minneapolis, MN) at 10 µg/mL overnight at 4°C. The surfaces are ready to use after the rinsing Fc-ICAM or Fc-VCAM in the end.

2.3 Microscopy

2.3.1 Fluorescence microscopy and quantification

Fluorescence microscopy observations and measurements were carried out on a Zeiss Z1 automated microscope (Carl Zeiss, Jena, Germany) equipped with a Snap HQ CCD camera (Photometrics, Tucson, AZ), pE-300 white LED microscope illuminator (CoolLED, Andover, UK), 20X objective (Zeiss PlanApo 20/0.8 DICII, Carl Zeiss, Jena, Germany) and piloted by µManager (Edelstein, Amodaj, Hoover, Vale, & Stuurman, 2010). PE-labeled Anti-Human CD54 (ICAM-1) or Anti-Human CD106 (VCAM-1) antibodies (eBioScience by Thermo Fischer Scientific, Waltham, MA, USA) were used for adhesion molecules quantification. First, we set up a bulk calibration curve by measuring the fluorescence intensity of 48 µm thick channels filled with antibody solutions at concentrations of 1.5, 3, 5 and 7 µg/mL (Figure 2-4). Channels were pre-treated with 1% Pluronic F127 (Sigma-Aldrich, St Louis, MO) to limit adsorption of antibodies on channel surface. In the end, channels were rinsed extensively with PBS. Residual fluorescent intensity due to adsorbed antibodies was measured and then subtracted from the previous measurements. The calibration in Figure 2-4 showed a linear relation between the fluorescent intensity and the bulk concentration.

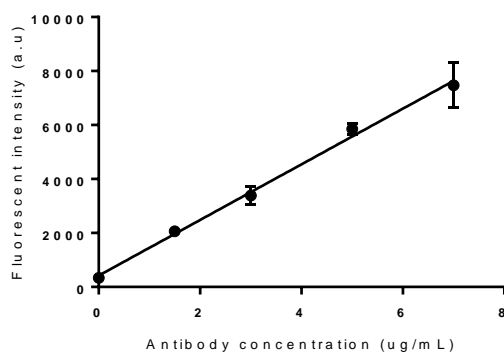


Figure 2-4 Calibration curve showing the linear relation between the fluorescent intensity of PE-labelled antiICAM and its concentration (Calibration curve from obtained with x20 objective, 48 μm in height microfluidic channel and 50 ms exposure time).

We assume that the signal is given by the total number of molecules in the thin channel, then the volume concentration can be converted to a surface concentration for a channel of 48 μm in height. This surface concentration can in turn be converted to a molecular density using the molecular weight of the antibody (150 kDa). The sample surface of the flow chamber coated with ICAM-1 or VCAM-1 was then stained with corresponding antibody at 10 $\mu\text{g}/\text{mL}$ and incubated overnight at 4°C. Images were taken the next day with the Zeiss Z1 microscope set-up. The fluorescent intensity was analyzed with ImageJ software (U. S. National Institutes of Health, Bethesda, USA) at 5 different positions. The average intensity from these 5 positions was converted into surface density of the adhesion molecules according the calibration data.

2.3.2 RICM microscopy

Reflection Interference Contrast Microscopy (RICM) was used in the project to confirm cell adhesion and observe lamellipodia dynamics on the substrates. It is a microscopic method for examination of thin layers, but it is also very useful in analyzing cell adhesion because it can be used in liquid environment and doesn't require any additional labelling. The basic principle is the following (Limozin & Sengupta, 2009; O. Theodoly, Huang, & Valignat, 2010): to form an image of the attached cell, monochromatic light is passed through a polarizer. This linear polarized light is reflected by a beam splitter towards the objective with a $\lambda/4$ plate, which focuses the light on the specimen. There are two surfaces that can reflect the polarized light: the glass surface that is emerged in the liquid medium and the surface of the cell – therefore two reflective surfaces separated by a thin film. There the final signal is resulted from the interference of these two reflections. When the cell is far from the glass surface, the signal intensity is maximal because the thickness of liquid film is infinite. When the cell is firmly adherent on the surface, the final intensity is minimal because the thickness of liquid film is null. Between these two extremes, the final signal varies according to the distance between the cell and the surface. The father is this distance, the brighter is the final signal. The reflected light will travel back to the beam splitter and pass through a second polarizer (analyzer), which

eliminates scattered light, before reaching the detector (usually a CCD camera) in order to form the final picture.

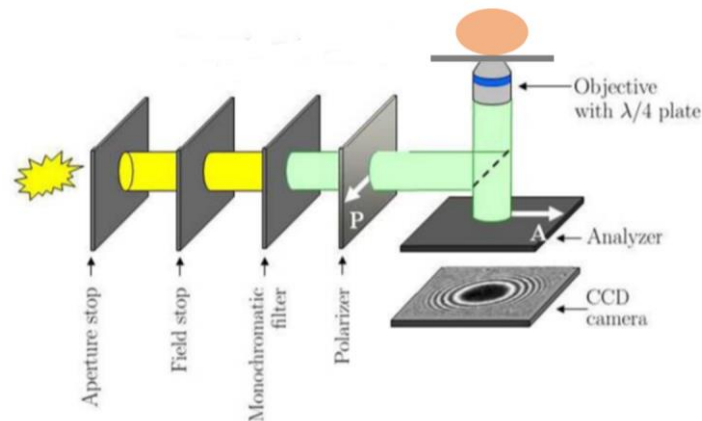


Figure 2-5 Optical set-up of RICM microscopy (adapted from [Huerre, Jullien, Theodoly, & Valignat, 2016])

In this project, the RICM set-up is mounted with a Zeiss Z1 automated microscope (Carl Zeiss, Jena, Germany) equipped with a Snap HQ CCD camera (Photometrics, Tucson, AZ), pE-300 white LED microscope illuminator (CoolLED, Andover, UK), 63X oil immersion objective (Zeiss Neofluar 63/1.25 antireflex, Carl Zeiss, Jena, Germany) and piloted by μ Manager (Edelstein et al., 2010).

2.4 Cell adhesion and migration assay

Cells were seeded into the flow chamber at the concentration of approximately 1.5 million cells/mL and incubated for 10 min at 37°C. Flow of prewarmed and CO₂ equilibrated culture media through the flow chamber was controlled using an Ibidi pump system (Ibidi GmbH, Martinsreid, Germany).

For cell adhesion assay, upon cell seeding and incubation, the flow chamber was rinsed with culture media at 1 dyn.cm⁻² to remove non-adherent cells. After rinsing, 100 bright-field images (Plan-Neofluar 10x/0.3 objective) were collected every 10 s without flow then under a shear stress at 8 dyn.cm⁻². Fluorescent images for each pattern were collected at the end of the experiment with the same objective at recorded position. The cell adhesion was quantified as the ratio between the number of adherent cells under 8 dyn.cm⁻² and that without flow after rinsing, which is then termed adhesion rate (Figure 2-6).

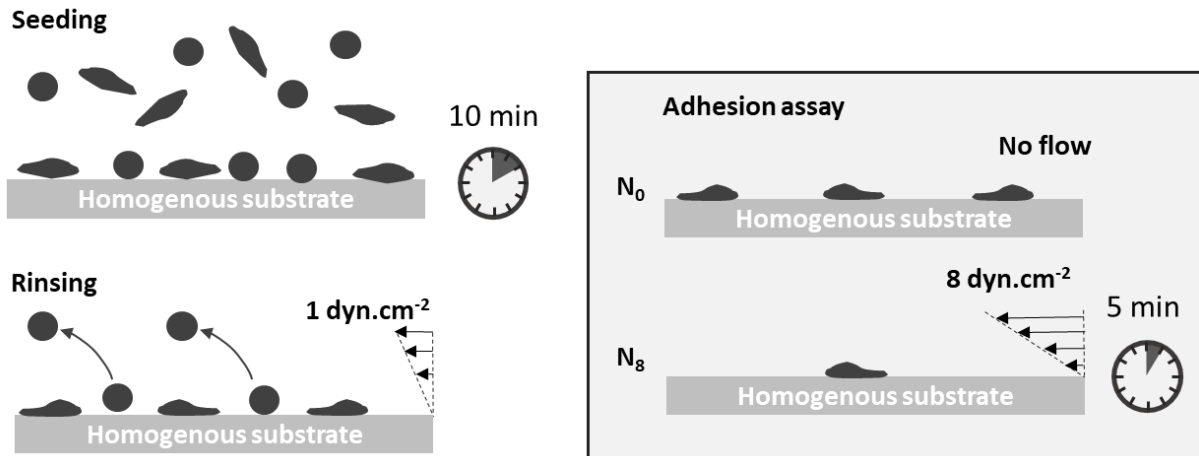


Figure 2-6 Illustration of the cell adhesion assay

For cell migration assays, 20 bright-field images (Plan-Neofluar 10x/0.3 objective) were first collected every 10s without flow to verify the state of the cells. Then, the flow chamber was rinsed with culture media at 1 dyn.cm^{-2} to remove non-adherent cells. After rinsing, 100 bright-field images (Plan-Neofluar 10x/0.3 objective) were collected every 10s. Fluorescent images for each pattern were collected at the end of the experiment with the same objective and at the same position. Additionally, bright-field and RICM images (Neofluar 63x/1.25 antiflex) were collected every 5s for each pattern to reveal cell adhesion fingerprint, and fluorescent images were collected at the end of the experiment to localize the protein patterns.

For the observation of the lamellipodial dynamics of individual cells, phase-contrast and RICM images (Neofluar 63x/1.25 antiflex) were collected every second for each pattern to reveal both the adhesion fingerprint and the lamellipodial protrusion, and fluorescent images were collected at the end of each acquisition to record the protein pattern.

2.5 Cell tracking and analysis

Home-made program developed with MATLAB software (The MathWorks, Natick, MA, USA) was used to track migrating cells as previously described in (M. P. Valignat et al., 2013). The general principle of the tracking program is the following (Figure 2-7):

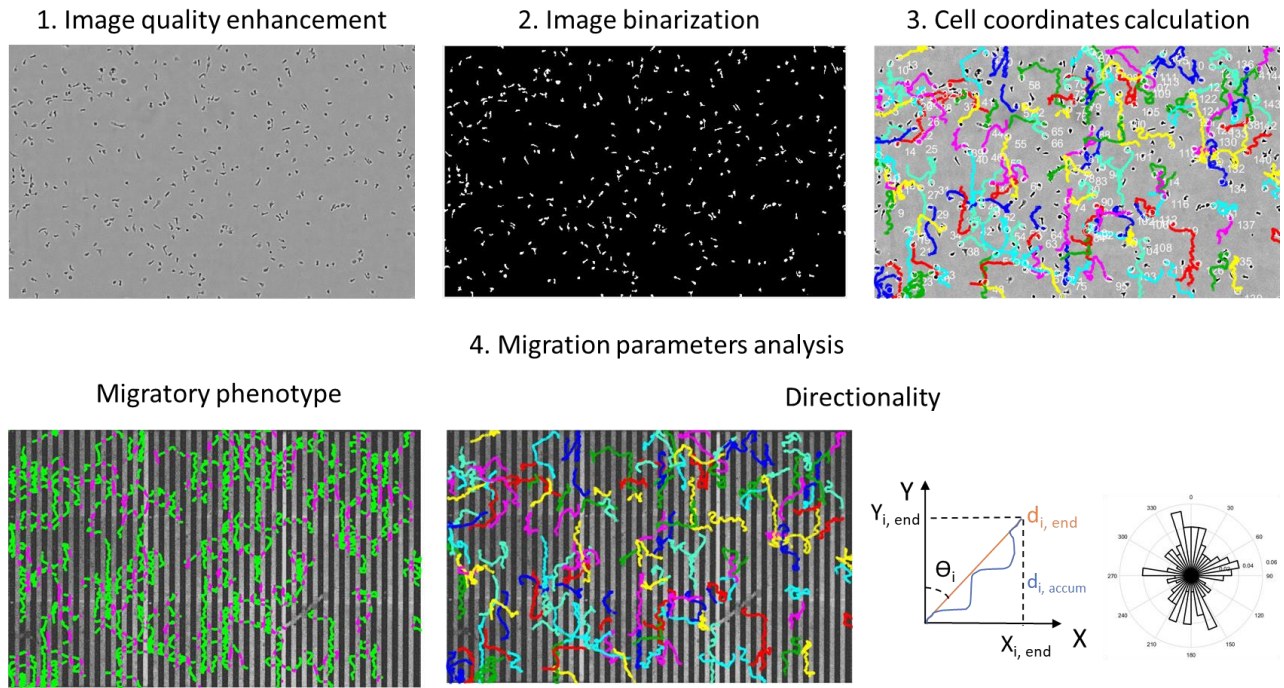


Figure 2-7 Principal steps of cell tracking analysis

1. The program performs image quality enhancement using background division and intensity normalization;
2. It binarizes the images using a user-chosen threshold to distinguish cells from the background;
3. It detects and numbers cells in the first frame and tracks them in the following frames and saves the coordinates and time points for each identified cell;
4. The program then analyzes different migration parameters. Only cells migrating for at least 30 μm are considered. In this study, to quantify cell adhesion, the program counts the number of adherent cells at 0 dyn.cm^{-2} (after rinsing) and 8 dyn.cm^{-2} to determine the adhesion rate of patterned substrates. The adhesion contrast of one substrate is calculated as the difference in adhesion rates normalized over the maximal adhesion rate. To determine the cell directionality on patterned surface, the migration angle is defined as the one between the patterned stripes and the total cell trajectory. The program calculates the fraction of cells with a migration angle $\theta < 45^\circ$ and $\theta > 45^\circ$. The anisotropy index is defined as the difference between these two fractions. To further characterize the cell migratory phenotypes and preferences on patterned surface, the program uses a binarized image of the fluorescent pattern as a mask to identify the position of each cell on the pattern. It then displays color-coded cell trajectories and calculates the percentage of cells that are on patterns with higher or lower adhesion during their entire migration.

3 Optimization of photopatterning for immune cells

This chapter will focus on the first part of the project that was dedicated to the technical optimization of protein printing LIMAP protocols to create functional adhesive substrates adapted to study T cell migration and haptotaxis through numerous empirical testing and different characterization methods.

3.1 Additive patterning on PLL-PEG coated substrates

3.1.1 Protein A can be patterned directly onto PLL-PEG substrate

Our first attempt was to create Protein A pattern by following the original LIMAP patterning protocol. The glass coverslip was pre-coated with PLL-PEG to achieve anti-fouling surface property (Figure 3-1-A). Then, pre-designed greyscale pattern was projected by UV at the wavelength of 375 nm (UV dose=800 mJ/mm²) in the presence of a soluble photoinitiator (PLPP™, ALVEOLE, Paris, France) (Figure 3-1-B). After rinsing, fluorescent labelled Protein A was incubated for 5 min at room temperature. Figure 3-1-C shows the successful pattern of the fluorescent Protein A with a low background adsorption (7% of patterned fluorescent intensity).

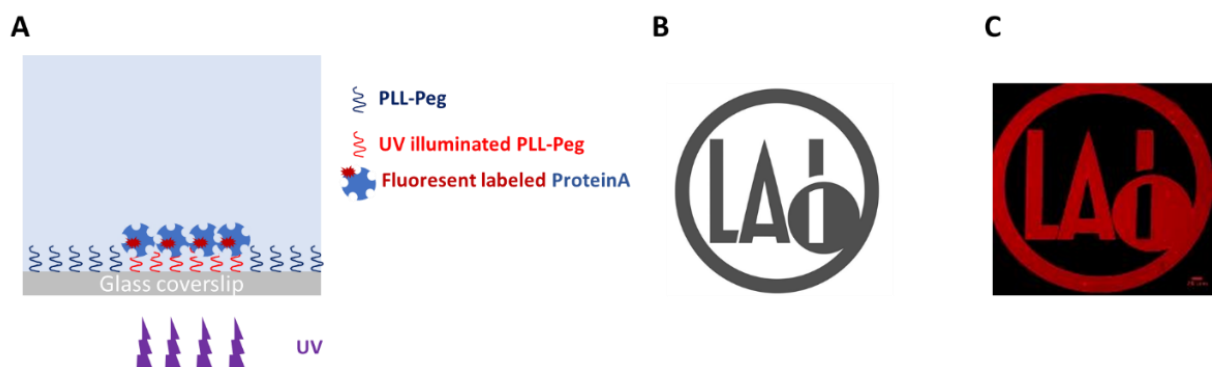


Figure 3-1 Protein A patterning on PLL-PEG: (A) Schematic showing the surface construction and patterning strategy; (B) Grey-scale pattern sent to the DMD; (C) Fluorescent Protein A pattern after incubation. Scale bar = 50 μ m

3.1.2 The patterning is oxygen-dependent

During our attempt to pattern the protein A, it has become evident that the photopatterning is oxygen-dependent, especially with large patterns that occupy the entire area of DMD. Figure 3-2 shows the large fluorescent Protein A pattern, which represents the full size of the DMD on Primo around 600 μ m x 400 μ m without (Figure 3-2-A) and with oxygen (Figure 3-2-B). In absence of oxygen during patterning, the fluorescent intensity of adsorbed protein was higher towards the inside of the pattern (area indicated by the white arrow) than the borders of the pattern thus leading to an inhomogeneous pattern. When the pattern was created in presence of oxygen, the protein adsorption became homogenous over the entire

patterned area. Although the exact chemical mechanism is still unclear, our working theory is the following: the photo-initiator creates free radicals upon UV illumination to activate the surface and the oxygen can inhibit the production of the free radicals. During the patterning, there is a local depletion of oxygen that results in the accumulation of free radicals (especially towards the inside of a large pattern). Therefore, the area having suffered from the oxygen depletion will become more activated than the rest, resulting in higher protein adsorption. The presence of oxygen can neutralize the free radical accumulation and thus ensure homogenous activation over the entire pattern. This effect has prompted us to oxygenate systematically during patterning by perfusing a mix of oxygen of carbon dioxide over the top of the microwell (Figure 3-2-C).

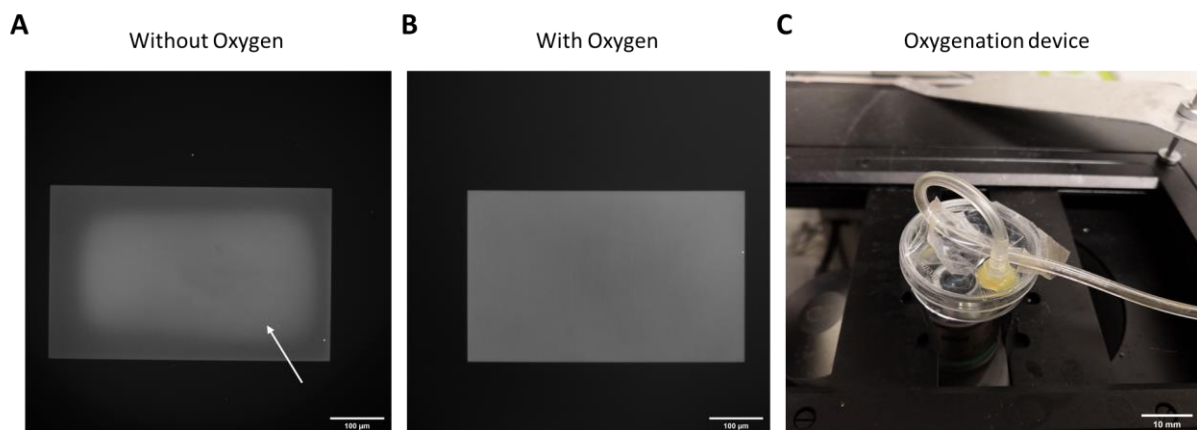


Figure 3-2 The effect of oxygen on patterning: (A) Fluorescent Protein A pattern in absence of oxygen (the white arrow indicated the area affected by oxygen depletion); (B) Fluorescent Protein A pattern in presence of oxygen; Scale bar=100 μm (C) Picture of the oxygenation device for patterning in microwells. Scale bar =10 mm

3.1.3 Fc-ICAM adsorption on patterned Protein A is specific but non-functional

The objective of this part of the work is to create functional adhesion molecule pattern to study T cell migration and haptotaxis. The successful patterning of Protein A was a first step forward because this will allow us to use it as an intermediate layer as Protein A binds to Fc fragment on Fc-ICAM with high affinity. Also, using a fluorescent-labelled Protein will also allow us to verify the quality of the pattern in real-time. So, our second attempt was to pattern the Protein A as described above and incubate Fc-ICAM solution on patterned Protein A after passivating with 4% BSA solution (Figure 3-3-A). Human primary effector T cells were then incubated on the ICAM surface for 10 min at 37°C to test its functionality. However, after rinsing, no cells remained adherent neither on the pattern nor on the rest of surface (Figure 3-3-C). This further confirmed the antifouling property of the PLL-PEG coating but also indicated the following possibilities: 1) there were not any ICAM molecules patterned on the surface; 2) ICAM molecules were patterned on the surface but were not correctly oriented; 3) ICAM molecules were patterned but denatured. To test these hypotheses, the surface was then rinsed and stained with the PE-labelled ICAM antibody. The staining revealed that the

patterning was highly specific (Figure 3-3-B) with a surface density around 1000 ICAM molecules/ μm^2 on the pattern, which corresponds to the maximal surface density of ICAM obtained by simple adsorption on a homogenous surface (Alexander Hornung et al., 2018) and a negligible background (around 10 molecules). The quantification confirmed that the ICAM adsorption on pre-patterned Protein A was highly specific and the ligand density should be enough to allow cell adhesion, but the adsorbed molecules were apparently no longer functional for cells.

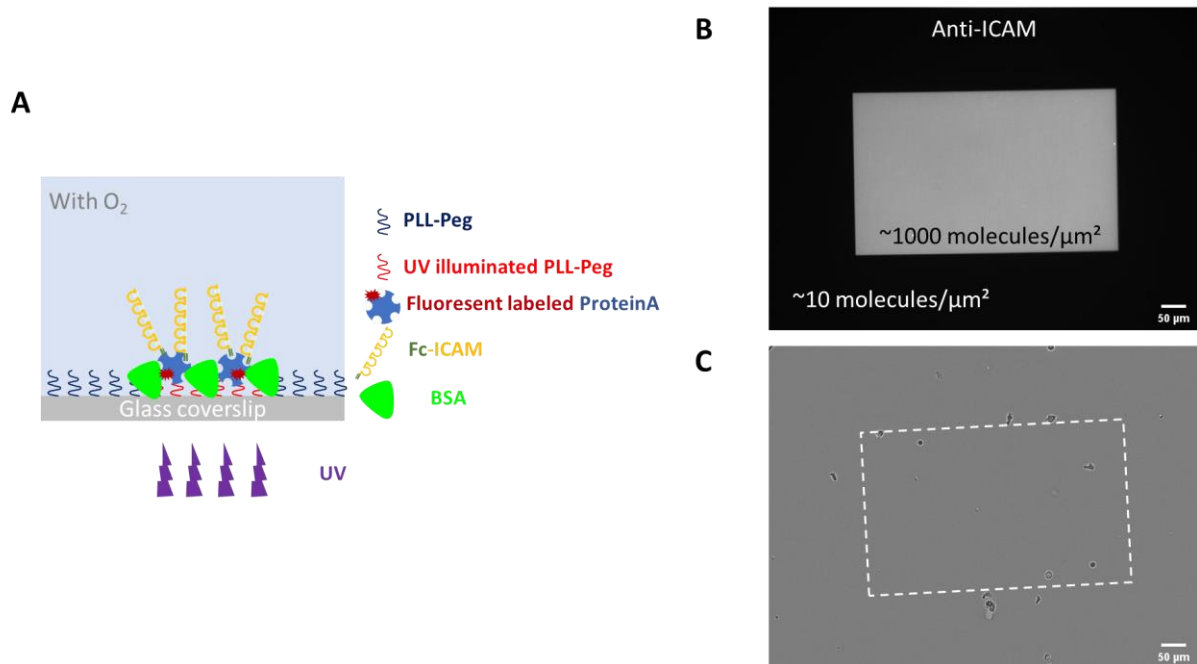


Figure 3-3 Adsorption of Fc-ICAM after Protein A patterning on PLL-PEG: (A) Schematics showing the surface construction; (B) anti-ICAM staining reveals the specificity of the adsorption as well as the ICAM surface density on the pattern and in the background; (C) Photo showing the absence of human T cell adhesion on the ICAM pattern (indicated by the white rectangle). Scale bars=50 μm

3.1.4 Avidin/biotin sandwich strategy also yields specific but non-functional ICAM pattern

Our efforts were then focused on functionalizing patterned ICAM molecules while maintaining specific binding. The hypothesis was that the strong positive charge of the polylysine (PLL) may have denatured the adsorbed ICAM molecules. One possible solution was to create a “sandwich” between the ICAM molecules and the PLL-PEG layer so ICAM molecules would be far away from the PLL and could remain functional upon adsorption. Therefore, the surface construction was slightly modified (Figure 3-4-A): instead of fluorescent labelled Protein A, biotinylated Protein A (50 $\mu\text{g}/\text{mL}$, ThermoFischer Scientific) was first patterned onto the PLL-PEG antifouling layer. Then, neutravidin (50 $\mu\text{g}/\text{mL}$, ThermoFischer Scientific) was incubated onto the patterned Protein A. After rinsing, biotinylated Protein A was again incubated. In the end, Fc-ICAM was incubated after passivation with 4% BSA. However, Figure

3-4-C showed once again the absence of functional cell and migration. Meanwhile, antibody staining confirmed specific binding with the maximal surface density (~ 1000 molecules/ μm^2) on the pattern with almost no background (Figure 3-4-B). These findings have strengthened our hypothesis that ICAM molecules may no longer be functional upon patterning on PLL-PEG substrates.

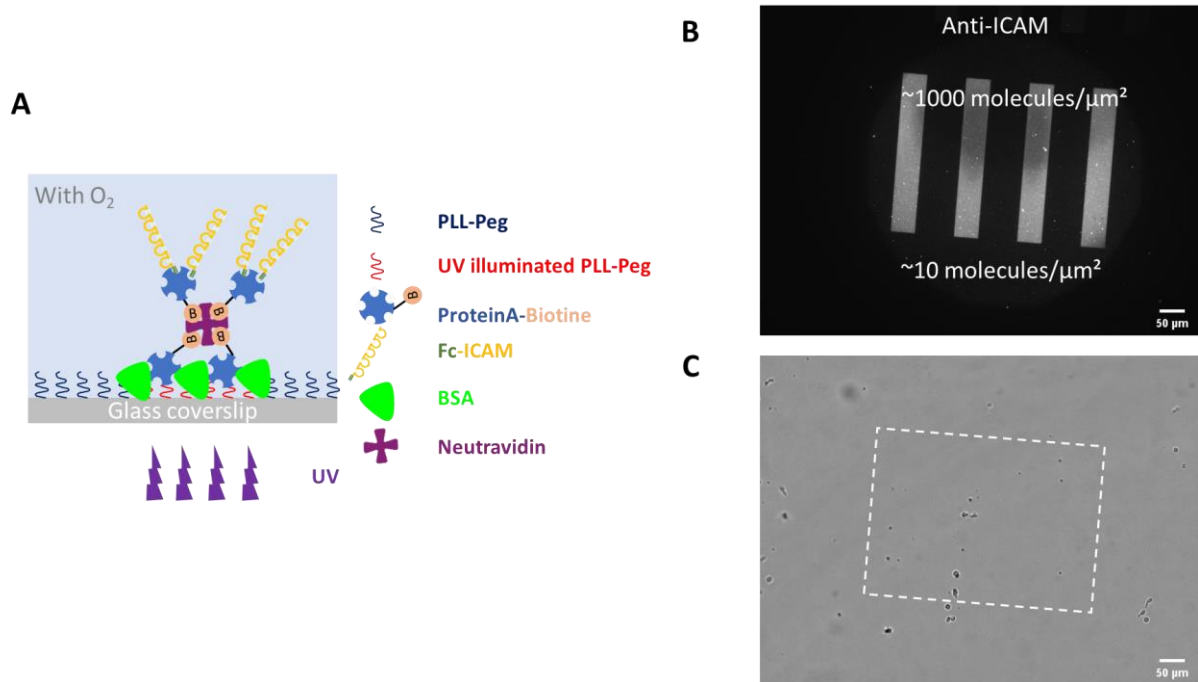


Figure 3-4 Adsorption of Fc-ICAM on PLL-PEG via biotin/avidin sandwich: (A) Schematics showing the surface construction; (B) anti-ICAM staining reveals the specificity of the adsorption as well as the ICAM surface density on the pattern and in the background; (C) Photo showing the absence of human T cell adhesion on the ICAM pattern (indicated by the white rectangle). Scale bar=50 μm

3.2 Additive patterning on SVA-PEG coated substrates

The challenge remained that the ICAM molecules lost their functionality upon adsorption onto the PLL-PEG. It has become necessary to find another anti-fouling coating for the substrate that can ensure specific binding while retaining the functionality of the ICAM molecules. The PLL-PEG coating was replaced by another polymer: mPolyEthylene Glycol-Succinimidyl Valerate (mPEG-SVA). The mPEG-SVA was grafted on APTES coated glass to create an antifouling layer on the glass substrate.

3.2.1 ICAM adsorption via patterned Protein A is specific and functional

The Protein A was first patterned onto the mPEG-SVA substrate upon UV illumination. After BSA passivation, Fc-ICAM was incubated (Figure 3-5-A). Then, cells were incubated on the surface to check its surface functionality. After rinsing, contrary to what has been observed before, cells adhered (Figure 3-5-C) and migrated specifically on the pattern as revealed by cell tracking analysis at an average speed of $17\mu\text{m}/\text{min}$ (Figure 3-5-D, see also Movie 1). These

findings supported our initial hypothesis that PLL may be the reason for ICAM denaturation. Subsequent antibody staining quantified the ICAM surface density on and off the pattern: the patterning remained highly specific with around 900 molecules/ μm^2 , which approaches saturation density determined by adsorption on continuous surface (Alexander Hornung et al., 2018) and the background adsorption was almost non-existent (Figure 3-5-B). This surface construction was used hereafter for ICAM patterning. One potential drawback could be the temporal evolution of the surface: the post-migration staining revealed that the pattern became less homogenous after experiment with cells for about 1h (Figure 3-5-B). This indicates that grafted ICAM molecules can be detached by migrating cells and therefore the surface density will decrease over time. This could be problematic for experiments that run longer as cells will detach once the surface density decreases below the adhesion threshold (around 200 molecules/ μm^2) (Alexander Hornung, 2016).

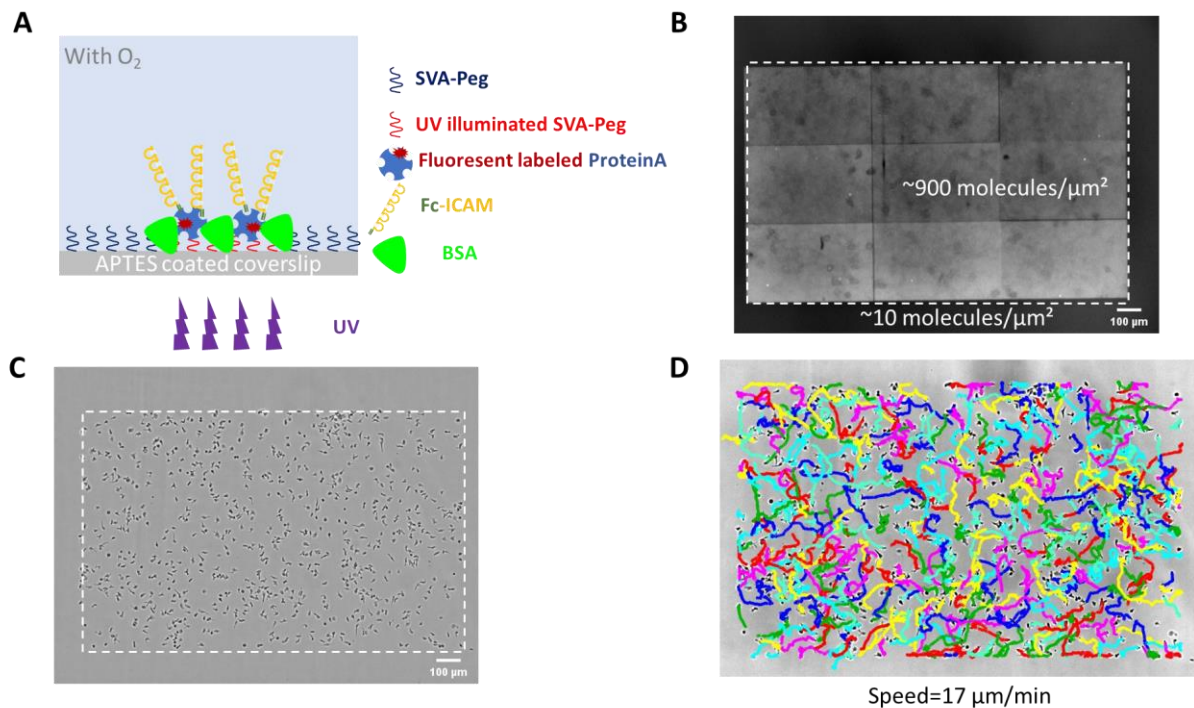


Figure 3-5 Adsorption of Fc-ICAM after Protein A patterning on mPEG-SVA: (A) Schematics showing the surface construction; (B) anti-ICAM staining reveals the specificity of the adsorption as well as the ICAM surface density on the pattern and in the background; (C) Photo showing the specific adhesion of human T cells on the ICAM pattern (indicated by the white rectangle) (D) Cell tracking analysis showing trajectories of migrating cells and the average speed. Scale bar=100 μm

3.2.2 Wet-SEEC microscopy allows label-free protein pattern detection and can be applied to cell migration assay

All our previous endeavors include the use of fluorescence microscopy: either a conjugated intermediate protein layer that can be used for direct visualization, or a conjugated antibody allowing both visualization and quantification. Nevertheless,

fluorescence microscopy has its own drawbacks: the fluorophores are sensitive to photobleaching and the fluorescent labelling is not always possible. Even when it is possible, it may alter the biochemical property and the functionality of the sample. In 2012, Ducret et al. developed a unique technique called Wet-Surface Enhanced Ellipsometry Contrast (Wet-SEEC) (Ducret, Valignat, Mouhamar, Mignot, & Theodoly, 2012). This novel optical technique allows label-free detection of inorganic and organic sample with nanometric thickness at solid/liquid interface. Theodoly et al. further demonstrated how this technique can be a powerful tool to characterize polymers and protein adsorption kinetics in combination with microfluidic systems (Olivier Theodoly et al., 2018). The successful optimization of LIMAP has presented a unique opportunity to combine these two techniques: label-free protein patterns can be generated in a fast and controlled manner with LIMAP and then be characterized with SEEC in presence of living cell.

Wet-SEEC slides are composed of a microscope coverslip bearing a layer of MgF_2 of thickness 52 nm and a layer of SiO_2 of thickness 40 nm. They were optimized to achieve anti-reflective conditions in RICM mode described above (Olivier Theodoly et al., 2018). Microscopy images were acquired with a Zeiss Z1 inverted microscope (Carl Zeiss, Jena, Germany) equipped with 63X oil immersion objective (Zeiss Neofluar 63/1.25 antilex) for imaging experiments. The microscope is equipped with a motorized aperture diaphragm to control the illumination cone projected into the objective. We used a CCD camera (Coolsnap HQ2; Photometrics) with chromatic filters for Wet-SEEC measurements. Samples were illuminated with a fiber-coupled illuminator source (PE-300, CoolLED Ltd., Andover, UK) with narrow bandpass filters (Chroma, Bellows Falls, VT, USA) piloted by a filter wheel changer (Lambda 10-3, Sutter Instrument, Novato, CA, USA). Unlabeled Protein A was first patterned onto mPEG-SVA substrate with the shape of 50 μm -wide stripes. Firstly, stripes designed with different greyscale levels (indicated on top of Figure 3-6-B) were patterned (note that the most transparency stripe receives the highest UV dose 800mJ/mm²). Human IgG was incubated on patterned Protein A after BSA passivation (Figure 3-6-A). With the Wet-SEEC mode, patterns were clearly revealed in absence of any fluorescent label (Figure 3-6-B top) and the contrast of the stripes increased with the UV dose (Figure 3-6-B bottom). Secondly, ICAM patterns (20 μm in width) were generated by incubation Fc-ICAM solution onto pre-patterned Protein A after BSA passivation. Human primary T cells were then incubated onto the surface. After rinsing, with the SEEC-mode, both patterned stripes (brighter zones in Figure 3-6-C) and adhesion zones (darker zones in Figure 3-6-C) were visible in absence of fluorescent label. Cells migrated on patterned ICAM with adhesion zones appeared exclusively on ICAM stripes (Figure 3-6-C and see also Movie 2). This type of experiment has confirmed that Wet-SEEC technique can be a label-free and non-invasive tool for living cell imaging and to decipher the link between living cells and their surrounding micro-environment. In the main project of this thesis, all living cell imagings were still performed with the transmission light mode (x10 or x63 magnification) with the help of a fluorescent-labeled protein to locate the

patterns because Wet-SEEC slides are difficult to obtain and the conventional fluorescence microscopy was enough for our imaging need.

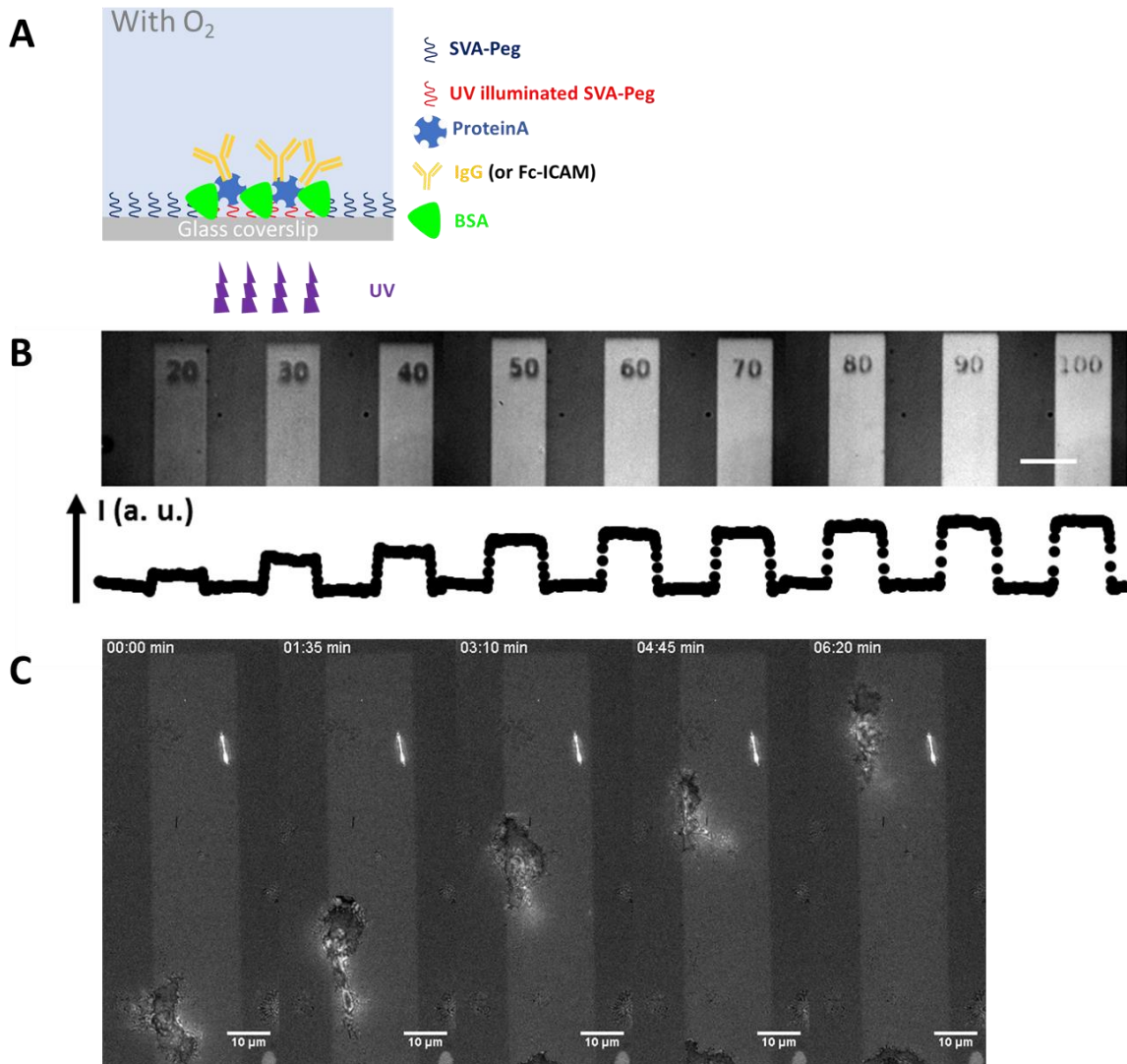


Figure 3-6 Characterization of protein patterning with Wet-SEEC microscopy: (A) Schematics of surface construction; (B) Wet-SEEC image at $\lambda = 546$ nm and $INA = 0.7$ and magnification $\times 63$ of protein layers obtained for different doses by protein patterning (top). Wet-SEEC intensity profile reveals an increase of protein adsorbed amounts versus the printing activation dose (right-bottom). Scale bar=50 μm ; (C) Wet-SEEC reveals the selective adhesion and migration of human primary T cells on ICAM adhesion molecules stripes printed by the LIMA technique and appearing in bright in the images. Non-patterned surface appears in light grey and adhesion zone of cells in black. Scale bar =10 μm

3.2.3 ICAM surface gradient pattern is functional but with too limited range

After the successful creation of continuous ICAM pattern, the next challenge was to create a surface-bound ICAM gradient to subsequently probe T cell haptotaxis. A grey-scale linear gradient pattern was sent to the DMD (Figure 3-7-B) and Protein A was patterned onto mPEG-SVA substrate. Fc-ICAM was adsorbed on patterned Protein A following passivation (Figure 3-7-A). Subsequent cell incubation revealed specific adhesion on patterned gradient and cell

migrated in a specific manner (Figure 3-7-C and Movie 3). However, Figure 3-7-B shows that cells adhered only on the second half of the gradient pattern (indicated by the white rectangle). The fluorescent quantification shows that the cells adhered on a gradient whose surface density ranges from 600-900 molecules/ μm^2 over only 200 μm (indicated by the horizontal white arrow in Figure 3-7-C and Figure 3-7-D) and the surface density remained at saturation until the end of the pattern. Our previous study has shown that cells remain adherent on a surface whose ICAM density varies between 200-1000 molecules/ μm^2 (Alexander Hornung, 2016). Therefore, cells should be able to adhere and migrate over this range, which was not the case here. These results show the limit of the patterned gradient: its functional range is too narrow to be useful in studying adhesive haptotaxis. Moreover, cells that were initially adherent cells detached when they migrated over the area with fewer than 600 molecules/ μm^2 (Figure 3-7-C, see also Movie 3). As a result, they were lost during imaging. It is therefore crucial to find another patterning strategy to create an adhesion gradient over a globally adhesive substrate.

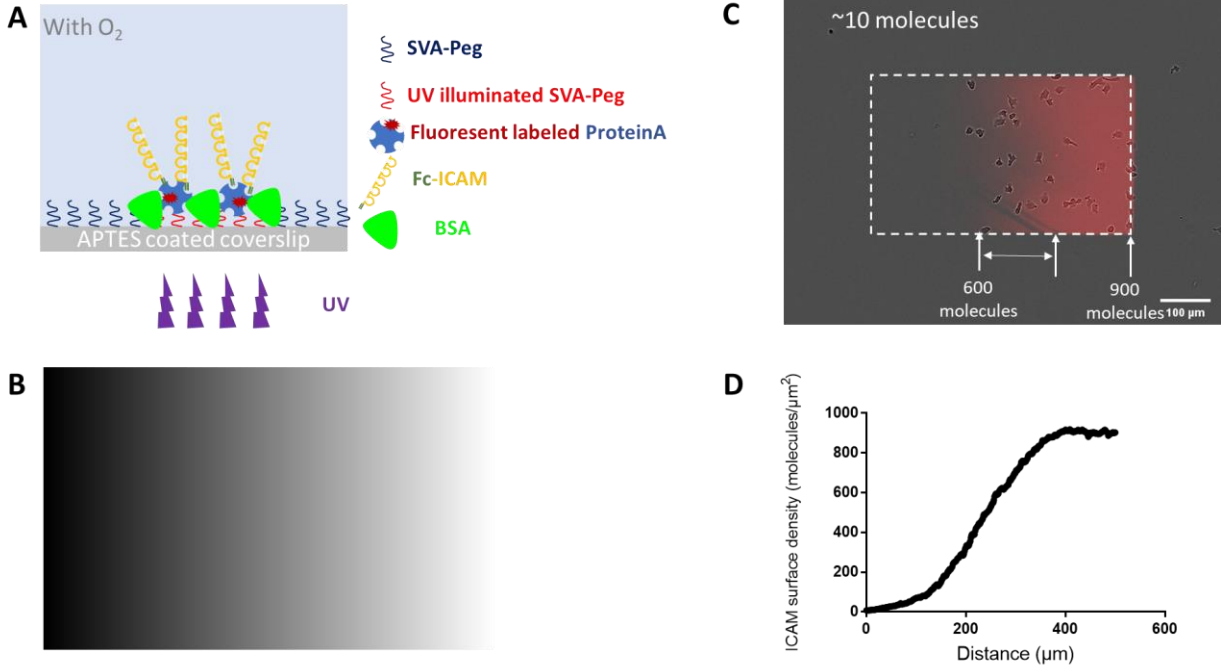


Figure 3-7 Creating ICAM surface gradient: (A) Schematics of the surface construction; (B) Grey-scale linear gradient pattern sent to the DMD; (C) Merged image showing the cells adhering only on the second half of patterned ICAM surface gradient. ICAM surface density was indicated for different areas of the surface. The entire patterned area was indicated by the white rectangle. In red: fluorescence Protein A; grey: adherent cells. (D) ICAM surface density profile over the entire patterned area shows that the ICAM surface density first increased over the pattern and then saturated at 900 molecules/ μm^2). Scale bar=100 μm

3.3 Subtractive patterning on protein coated substrates

3.3.1 ICAM molecules are sensitive to UV and can be used for subtractive patterning

Having discovered that the functional range of the patterned ICAM gradient was too narrow, we focused on efforts on finding another strategy to construct a surface gradient with a wider range (variable adhesion on surface ranging between 200-1000 ICAM molecules per μm^2). The surface construction that is routinely used in the lab consists of adsorbing Fc-ICAM molecules via intermediate Protein A layer after BSA passivation on APTES coated substrates. This surface construction was then combined with LIMAP technique: the surface was directly illuminated by UV (Figure 3-8-A). After rinsing and another BSA passivation, cells were incubated on the pattern. Figure 3-8-B shows the astonishing patterning effect: cells adhered and migrated over the entire coated surface except for the illuminated area (see also Movie 4). These results show that ICAM molecules are sensitive to UV. While this may be a limit if one wants to pattern a second protein (e.g chemokines or another type of adhesion molecule) on top of the first one, this UV-sensitivity allows us the modulate the adhesion of an already functional substrate by denaturing pre-adsorbed protein in a controlled and quantifiable manner. This method is called hereafter “subtractive patterning”.

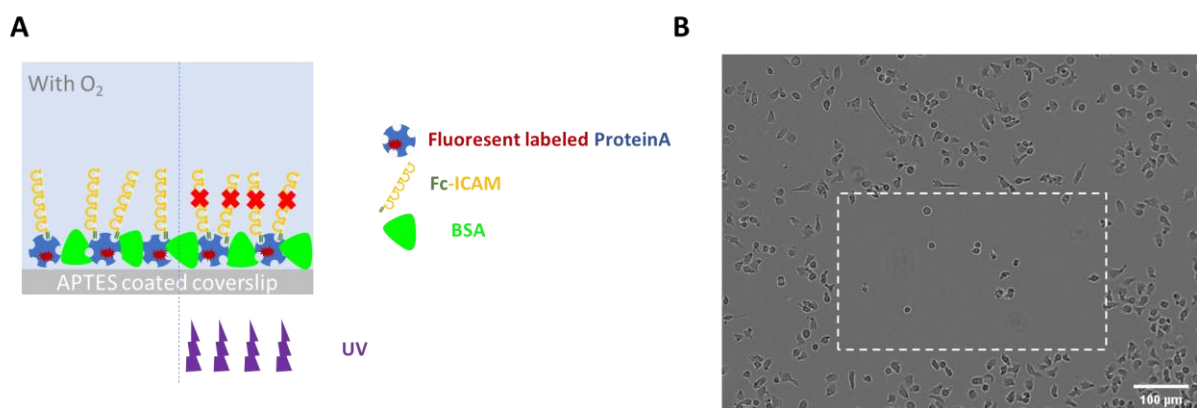


Figure 3-8 UV sensitive ICAM molecules can be used for subtractive patterning: (A) Schematics of the surface construction; (B) Photo of cells adhering on the surface except for the UV-illuminated area (indicated by the white rectangle). Scale bar = 100 μm

3.3.2 Subtractive patterning also requires photo-initiator

In the paragraphs above, the patterning was carried out in presence of the photo-initiator. Since the surface is no longer coated with PEG polymer, it is intriguing to find out whether the photo-initiator is still necessary. So, two surfaces were patterned using the surface construction in Figure 3-8-A in absence and presence of the photo-initiator. The patterning outcome was revealed with the help of fluorescent labeled Protein A. Figure 3-9 shows a drastic difference: the surface remained intact in absence of photo-initiator apart from slight

photo-bleaching (Figure 3-9-A) but was denatured in its presence and the pattern was inversely created (Figure 3-9-B). These results confirm that even in absence of PEG-coated substrates, the photo-initiator is required. Additionally, these tests also confirmed that the Protein A is also UV-sensitive. Therefore, one can use the fluorescent labeled Protein A to visualize the patterning outcome live and use cells as a final read-out to assess the functionality of the substrate. Subsequent staining can also be performed to quantify the ICAM surface molecule density.

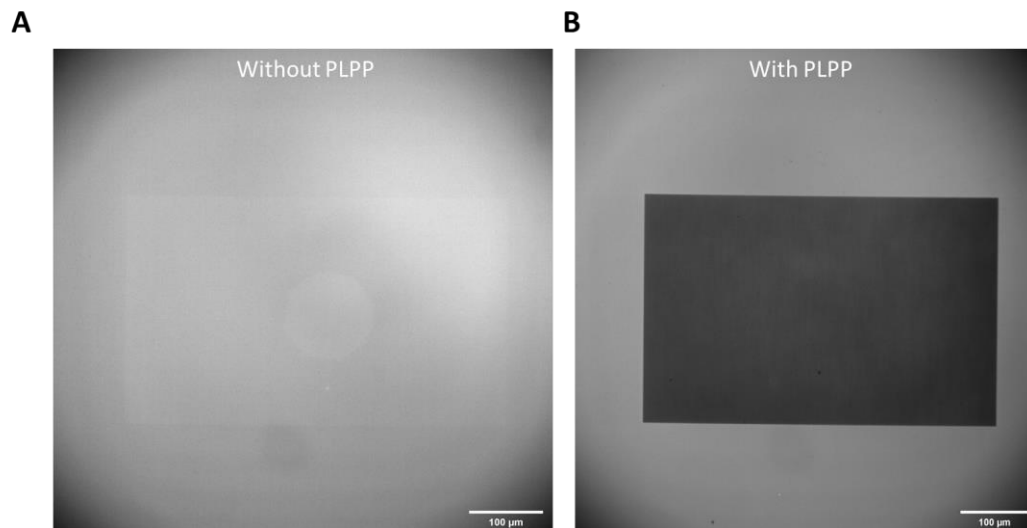


Figure 3-9 Subtractive patterning also requires photo-initiator: Fluorescent Protein A shows that the surface remains intact upon UV illumination in absence of the photo-initiator (A) and became denatured in its presence (B). Scale bar=100 µm

3.3.3 Subtractive patterning is also oxygen dependent

After confirming the role of photo-initiator, we continued to assess the role of oxygen as 3.1 demonstrated the effect of oxygen depletion on patterning with PLL-PEG substrates. The surface was first illuminated with UV without oxygen and Figure 3-10-A shows that the oxygen depletion effect was again present (affected area indicated by the white arrow) but inverted (the fluorescence was weaker on the affected area than the rest). In an endeavor to further quantify cell adhesion under flow, the previous microwell device (Figure 2-2) was replaced by glass-bottom flow chamber (Figure 2-3) with the glass-bottom coated with ICAM. Direct oxygen perfusion, which was used for patterning in open microwell to neutralize depletion, was not applicable with closed channels. A new protocol was designed to neutralize the depletion effects. We set up a simple mixing device with a syringe and an outlet that can generate a constant flow in the channel and thus continuously mix the solution (Figure 3-10-A). In case of prolonged patterning, this manual device can be automated by plugging the tubes onto a microfluidic pump. The surface was then illuminated with continuous mixing and Figure 3-10-B shows that there was no more depletion effect and the pattern became homogenous. These findings confirmed our working theory on accumulation of free radicals:

regardless of the substrates used in patterning (PEG layer or protein layer), the photo-initiator creates free-radicals upon UV illumination; local oxygen depletion causes free-radical accumulation that leads to over-activation of the substrates; more protein will be adsorbed, which leads to higher fluorescence in case of additive patterning on PEG surface and more will be denatured, which leads to lower fluorescence, in case of subtractive patterning protein coated surface.

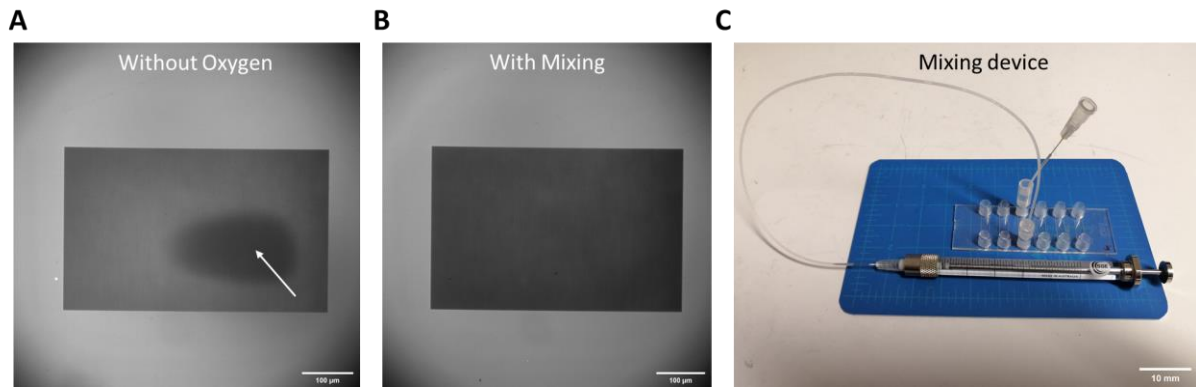


Figure 3-10 Negative patterning is also oxygen dependent: (A) Fluorescent Protein A reveals the effect of oxygen depletion (the affected area appears darker and is indicated by the white arrow); (B) The oxygen effect was neutralized with mixing; Scale bar= 100 μm (C) Photo of the fluidic mixing device for the closed flow chamber. Scale bar= 10 mm

3.3.4 Creating patterns with gradual amount of adhesion molecules

Finally, the substrate construction chosen for the rest of the project was the one that adsorb adhesion molecules through fluorescent Protein A on APTES treated glass in presence of photo-initiator and fluidic mixing (Figure 3-11-A). LIMAP was used to denature the pre-coated protein in a controlled manner and with pre-defined shapes. The intensity of the patterning was achieved by varying the greyscale of the designed pattern (the surface illuminated with the white pattern received the highest dose=800 mJ/mm² and the area between two adjacent stripes were black and therefore not illuminated) (Figure 3-11-C). Stripes with different various ICAM surface density were created with this method and the subsequent staining revealed decreasing fluorescence with increasing UV dose over the entire patterned surface (Figure 3-11-B). The intensity profile confirmed this visualization and provided quantitative information on ICAM surface density: the surface density varied from 200 to 900 molecules/μm² on patterned stripes and remained constant at 900 molecules/μm² between the stripes (Figure 3-11-D). This confirmed the robustness and the specificity of the method and the next step is to create separate substrates with modulated adhesion and quantify effective cell adhesion with flow.

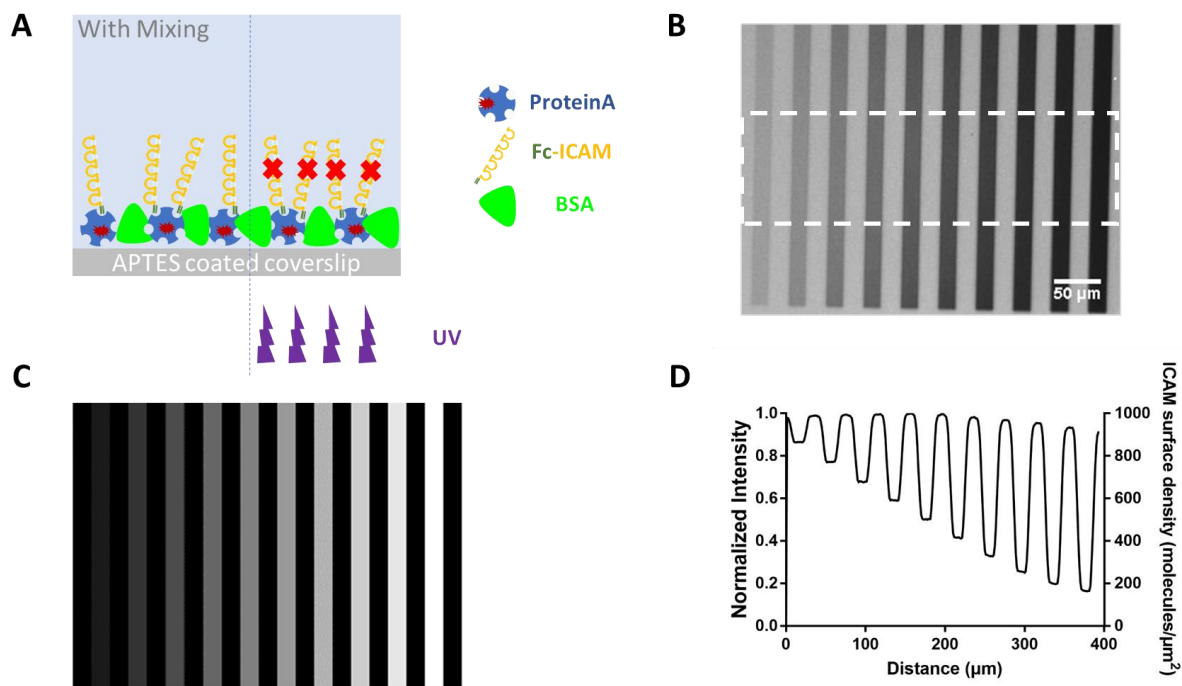


Figure 3-11 Stripe like patterns with gradual amount of ICAM molecules: (A) Schematics showing the surface construction; (B) anti-ICAM staining reveals the patterned stripes with the most illuminated stripe in black; Scale bar=50 μm ; (C) grey-scale pattern projected to the DMD with the most illuminated stripe in white and unilluminated stripe in black (D) Intensity profile with both normalized fluorescence and ICAM surface density varying from 200 molecules/ μm^2 to 900 molecules/ μm^2 .

3.4 Photopatterning substrates with modulated adhesion

In this section, continuous patterns with various amount of adhesion molecules were created. Besides ICAM-1, Fc-VCAM-1 was also successfully patterned with the same method. Cells were incubated for 10 minutes onto the patterned surfaces. After an initial rinsing with a gentle flow at 1 dyn/cm^2 to remove non-adherent cells and imaging in absence of the flow, cells were submitted to a flow at 8 dyn/cm^2 and imaged over 15 min. The adhesion rate was defined as the ratio between the number of adherent cells at 8 dyn/cm^2 and that of initially adherent cells after rinsing. Figure 3-12-A shows different cell adhesion on patterned ICAM-1 substrates with different surface density under a shear flow of 8 dyn/cm^2 . Figure 3-12-B shows the relation between the cell adhesion rate and the surface density of ICAM-1 and VCAM-1: the adhesion is null when the surface density is lower than 200 molecules/ μm^2 , increases and finally saturates around 1200 molecules/ μm^2 . These results provide quantitative proof that cell adhesion is controlled by the surface density of its corresponding integrin ligands (ICAM-1 for LFA-1 and VCAM-1 for VLA-4). Furthermore, they also show that the optimized method has successfully expanded the functional range of the patterned ICAM-1 surface: cells were adherent over the range of 200-1200 molecules/ μm^2 compared to the ICAM-1 patterned on PEG substrates on which cells only started to adhere when ICAM-1 density was above 600 molecules/ μm^2 .

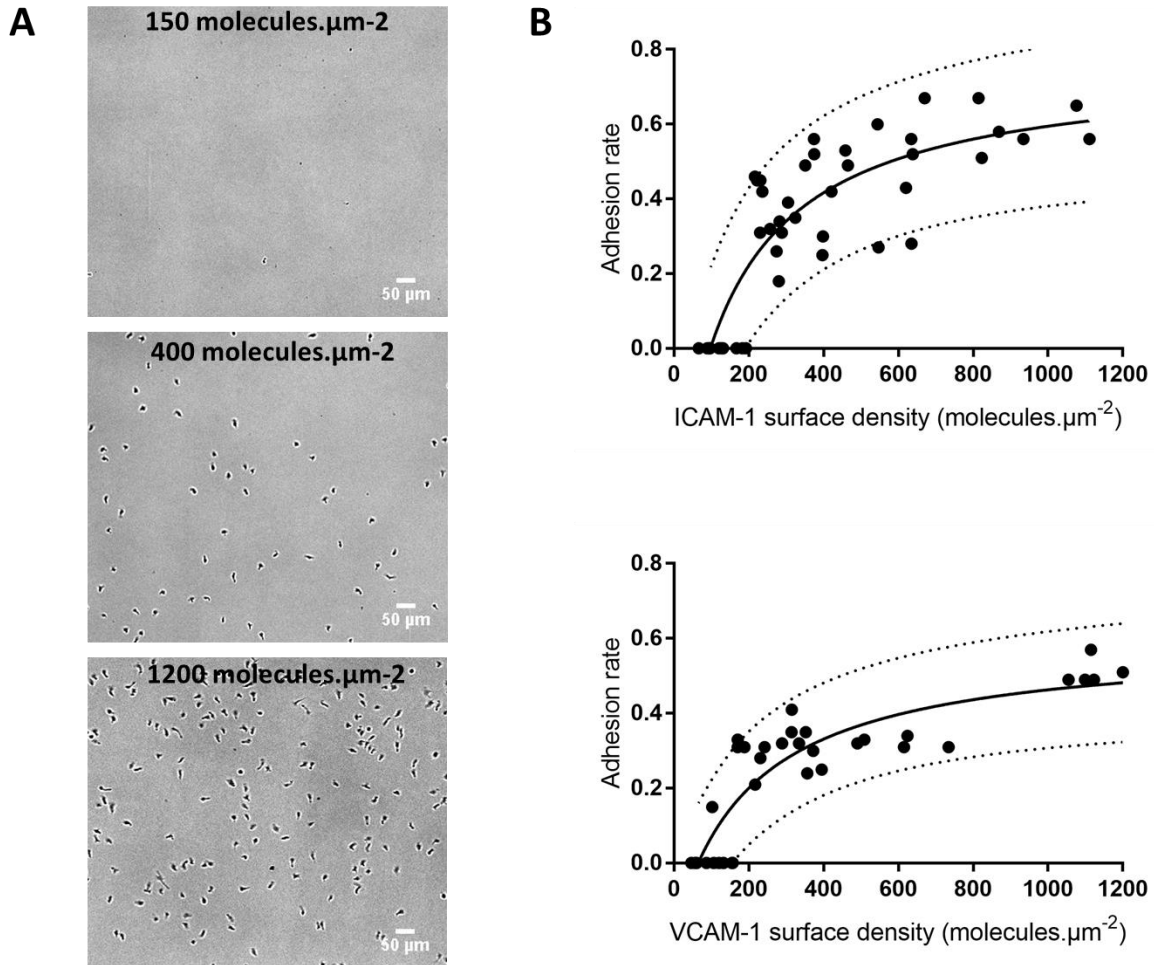


Figure 3-12: Photopatterning yields substrates with modulated adhesion (A) Images showing adhered T cells in presence of a shear flow of 8 dyn/cm² on ICAM-1 substrates with different surface density. (B) Adhesion rate versus ICAM-1 (top) and VCAM-1 (bottom) surface density. A Langmuir fit was used as a guide for the eye with a confidence interval of 90% indicated by black dashed curves. Scale bar=50 µm

Meanwhile, we also analyzed the average T cell migration speed on these substrates with modulated adhesion. Figure 3-13 shows that cell globally migrated two times faster on ICAM-1 than on VCAM-1 but the migration speed did not vary with the surface density of both adhesion molecules. These results are also consistent with our previous finding where cell speed did not vary when migrating on un-patterned homogenous surfaces with various ligand density (Alexander Hornung, 2016).

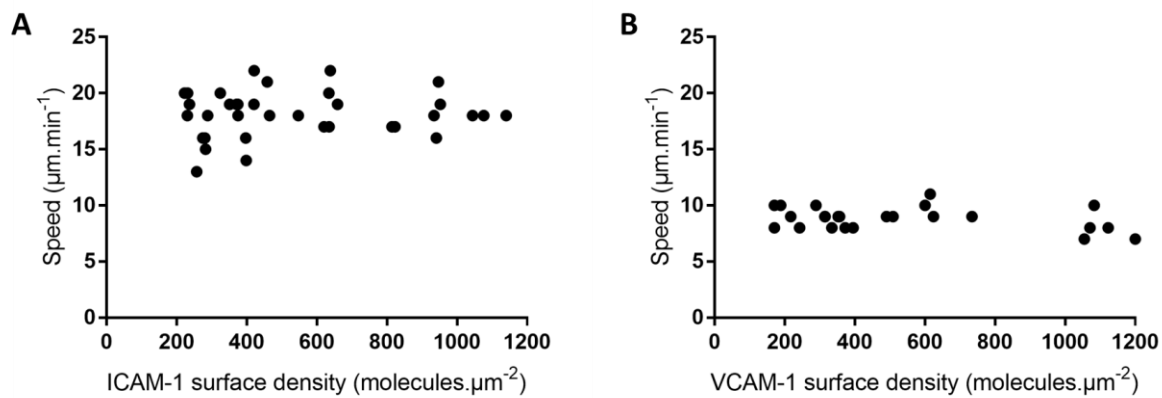


Figure 3-13 Average migration speed vs surface density of ICAM-1 (A) and VCAM-1 (B)

Now that the surface patterning was optimized and quantified, the next step will be to address the main objective of this project which is to probe T cell haptotaxis with adhesion molecules, which will be presented in the following chapter.

4 Probing the existence of T cell adhesive haptotaxis

4.1 Strategy to probe adhesive haptotaxis

The original idea to study T cell adhesive haptotaxis was to create a surface-bound CAM gradient and to monitor the T cell migratory responses (Figure 4-1-A). However, the directly patterned gradient has a too small functional range, possibly due to the partial functionality loss after patterning despite extensive optimization (Figure 3-7). Moreover, a complete characterization of T lymphocyte adhesive haptotaxis requires a screening of cell guiding phenotype versus two parameters: the concentration range and the steepness of concentration gradient (Figure 4-1-B). Such a complete screening would be too complex given the technical limitation. It would also be unwise to launch a complex screening while the very existence of the adhesive haptotaxis for T cells remains unclear.

Since an effective gradient requires first and foremost cells to sense a difference between the front and the back, we decided to simplify the screening to a single-parameter assay: the steepness of the gradient will be fixed at infinite and only the concentration range will be varied. Instead of a traditional gradient, this single-parameter approach will thus create step-like patterns made of alternated stripes of different adhesion rates. Cells travelling across adjacent stripes will experience a gradient of infinite steepness, which is the optimal condition for cells to detect the gradient. This approach is also more feasible technically as we have demonstrated that ICAM-1 and VCAM-1 molecules are UV sensitive and can therefore be degraded in a controlled manner by what we named "subtractive patterning". Cell adhesion has also been quantified on substrates with modulated ICAM-1 and VCAM-1 density. Therefore, this has enabled us to create alternated stripes with modulated adhesion on a globally functional substrate simply by varying the grey-scale of the pattern. To identify the concentration range where integrins may mediate haptotaxis, we then varied the contrast of adhesion between stripes. The width of stripes was chosen at 20 μm , slightly larger than the average diameter of adherent cells of $15 \pm 2 \mu\text{m}$, which maximizes the occurrence of simultaneous cell contacts with two adjacent stripes (Figure 4-1-C, -D).

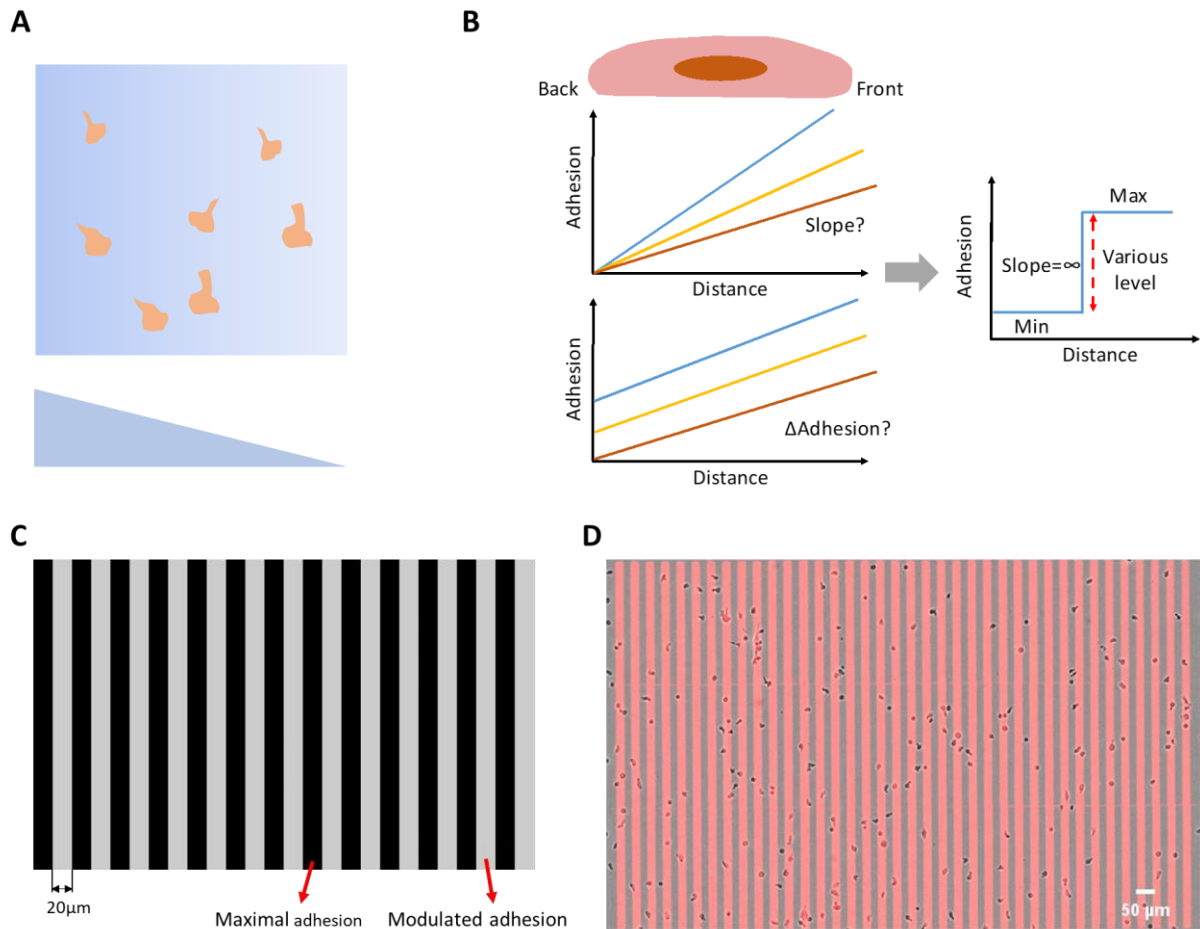


Figure 4-1 (A) Schematic illustrating the conventional strategy to create surface-bound gradient for cell haptotaxis; (B) Schematic illustrating the transition from two-parameter screening to single-parameter assay; (C) the 8-bit grayscale pattern to be sent to the DMD to create alternated stripes (20 μm in width) with maximal adhesion and modulated adhesion; (D) Merged photo showing T cells adhering on alternated stripes. In red: fluorescent Protein A pattern; In grey: adherent cells. Scale bar = 50 μm

4.2 Direction of migrating T cells is biased on substrates with adherent and non-adherent stripes

The search for the existence of haptotaxis was undertaken here with a single parameter assay by using step-like profiles made of alternated stripes of different adhesion rates. Alternated stripes of different adhesion were prepared with a maximum adhesion rate of 0.6 for half of the stripes, and at variable adhesion rates between 0 and 0.6 for the other half. We defined the “adhesion contrast” as the difference in percent between the adhesion rates on alternated stripes normalized over the maximal adhesion rate. An adhesion contrast of 0% corresponds therefore to a non-patterned homogeneous substrate (with the maximal adhesion rate of 0.6), whereas the adhesion contrast of 100% corresponds to alternated stripes of maximum and null adhesion rates. Cells trajectories were tracked for 15 min and the orientation of each individual cell was assessed from the orientation between first and final positions. Distribution of orientations were displayed on rose wind plots, and to assess

directional bias of migrating cells, we further calculated an Anisotropy Index as the difference between the cell fraction in vertical quadrants (orientation bias parallel to stripes) and in horizontal quadrants (orientation bias perpendicular to stripes). In control experiments with homogeneous substrates of maximum adhesion rate 0.6 (Figure 4-2-A and left panel of Movie 5 and 6), cells had a random motility, with anisotropy index equal to 0.0. On alternated stripes of adhesion contrast 100% (Figure 4-2-B and middle panel of Movie 5 and 6), cells travelled both on and across adherent and non-adherent stripes. T lymphocytes are indeed able to crawl on adhesive substrates and swim on anti-adhesive substrates (Aoun et al., 2019). However, portions of path with lengths of tens of micrometers appeared with a steady orientation in the direction of stripes (Figure 4-2-B), and orientation bias appears clearly on rose plots in the direction of stripes, with an anisotropy index of 0.5 for both ICAM-1 and VCAM-1 substrates. Although T cell can crawl and swim on adhesive and non-adhesive substrates, cells follow preferentially adhesive stripes, which suggest that crawling is more efficient than swimming. These results show that non-adherent zone can bias crawling orientation, but they are not a proof of existence of adhesive haptotaxis.

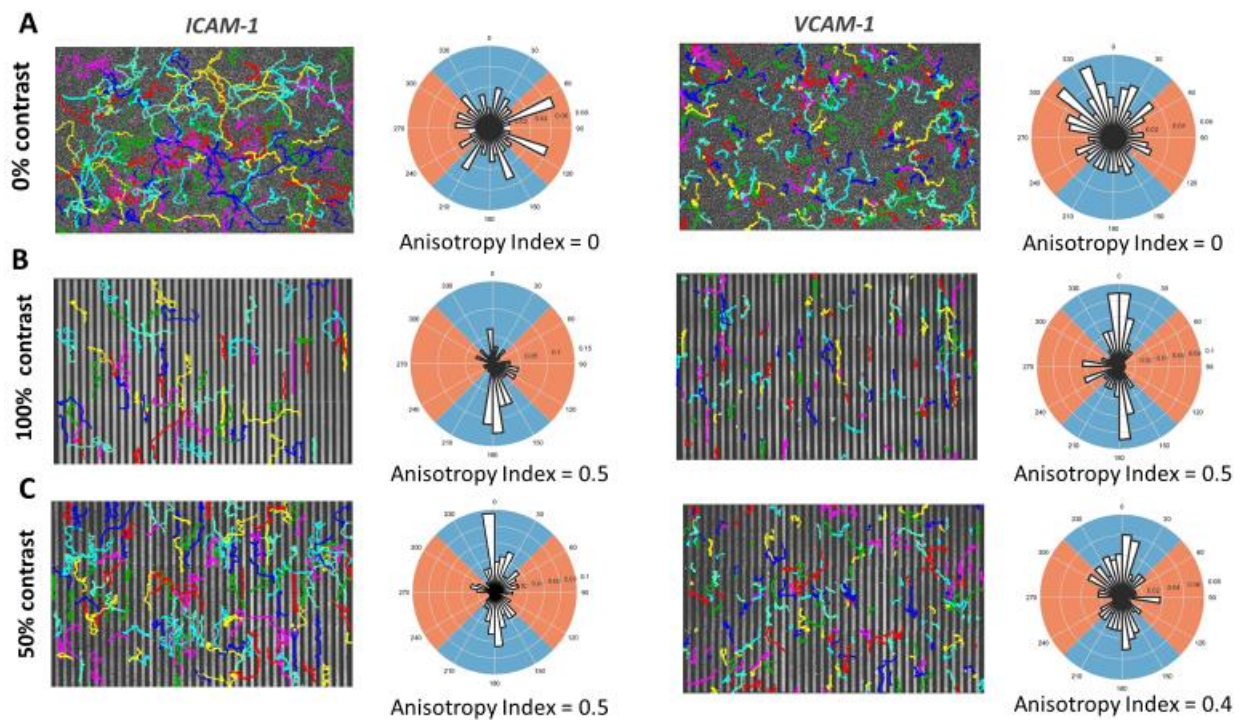
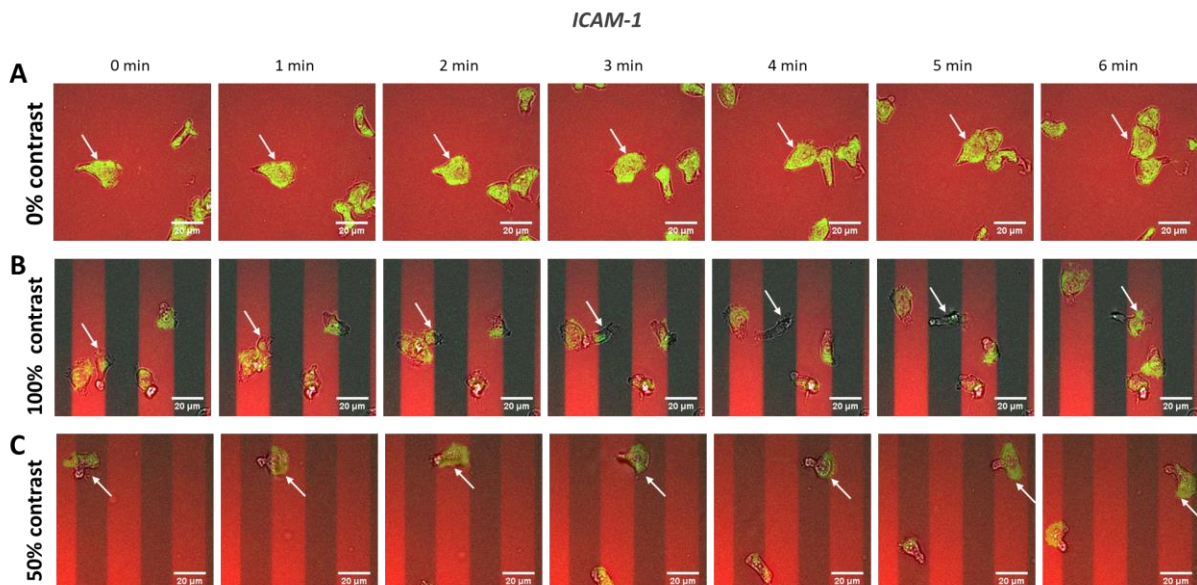


Figure 4-2 Substrates with modulated adhesion induce T cell haptotaxis. Cell tracking results on ICAM-1 (left panel) and VCAM-1 (right panel) substrates with modulated adhesion. (A) Negative control on substrates with 0% adhesion contrast where cells migrated in random directions. Cell trajectories and rose windplot were displayed for one representative experiment by tracking 195 and 343 cells for ICAM-1 and VCAM-1 substrates, respectively. (B) Positive control substrates with 100% adhesion contrast where cells exhibited biased migration in the vertical quadrants (blue). Cell trajectories and rose windplot were displayed for one representative experiment by tracking 100 and 253 cells for ICAM-1 and VCAM-1 substrates, respectively. (C) Substrates with 50% adhesion contrast where cells haptotaxed in the vertical quadrants (blue). Cell trajectories and rose windplot were

displayed for one representative experiment by tracking 189 and 313 cells for ICAM-1 and VCAM-1 substrates, respectively.

4.3 Lymphocytes display integrin-mediated haptotaxis on globally adhesive substrates

Swimming is irrelevant for leukocyte recruitment from blood because firm adhesion on vessel walls is a prerequisite of transmigration to resist blood flow. We therefore investigated here cell orientation versus modulations of adhesion rate using stripes with different and non-null adhesion rates. Figure 4-2-C corresponds to alternated stripes of adhesion rates 0.6 and 0.3. To assess the effective adhesion of cells on each stripe type, the adhesion footprint was imaged by reflection interference contrast microscopy (RICM). Figure 4-3-A to F superimpose transmission images that localize cell body (grey), fluorescence microscopy images that reveal stripes of integrin ligands (red) and RICM microscopy showing the adhesion footprint (green). On homogeneously adherent substrates (Figure 4-3-A,D, see also Movie 7 and 8), RICM signal (green) confirmed uniform cell adhesion. On substrates with adherent and non-adherent stripes (Figure 4-3-B, E and see also Movie 7 and 8), adhesion (green) signal was bright on stripes with integrin-ligand stripes (bright red) and extinct on anti-adhesive stripes (light red), which confirms that cells crawled on adherent stripes and swim over non-adherent stripes. For substrates with contrasted and non-null adhesion rates (Figure 4-3-C,F and see also Movie 7 and 8), RICM imaging confirms that cells adhered on both stripe types. These results confirm that cells were globally adhering on the substrates with stripes of modulated adhesion. The rose plots reveal nevertheless a clear preferential orientation in the direction of stripes with an anisotropy index of 0.5 and 0.4 on respectively ICAM-1 and VCAM-1 substrate. These data demonstrate unambiguously that lymphocytes are sensitive to modulations of substrate adhesion and that they orient their migration direction accordingly. Integrin-mediated adhesive haptotaxis therefore exists for crawling human T lymphocytes.



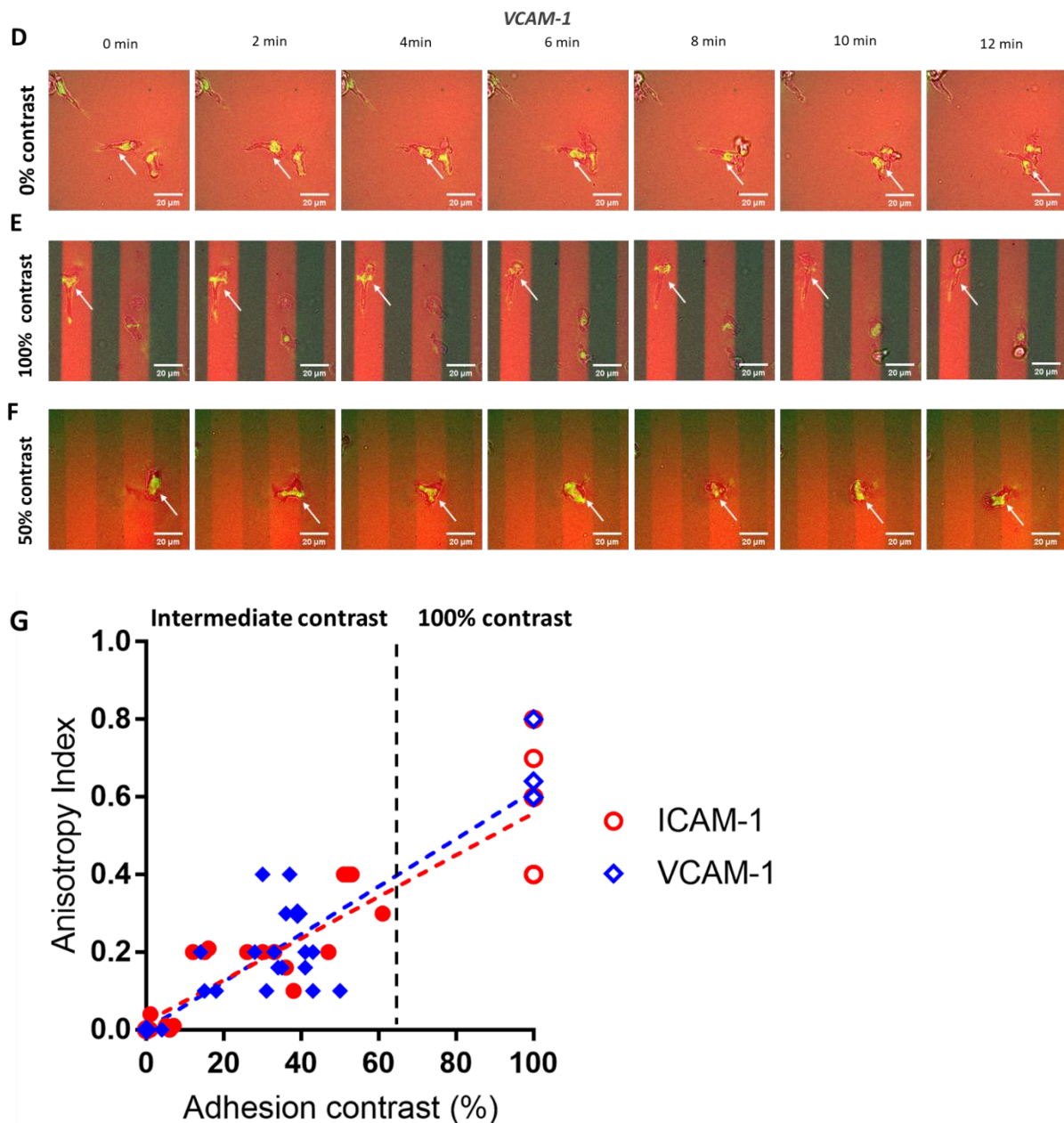


Figure 4-3 Integrin-mediated haptotaxis increases with adhesion contrast with adhesion confirmation by RICM microscopy. (A) Negative ICAM-1 control substrate with 0% contrast shows cells migrating with uniform adhesion on control substrates. (B) Positive ICAM-1 control substrate with 100% contrast shows cells migrating either in or along adherent stripes or swimming across the non-adherent stripes. One can note the absence of RICM signal in between two adherent stripes showing the absence of cell adhesion. (C) ICAM-1 substrate with 50% contrast (for which both types stripes are adherent) shows cell migrating across stripes with modulated adhesion. RICM signal confirms adhesion between stripes. (D) Negative VCAM-1 control substrate with 0% contrast shows cells migrating with uniform adhesion on control substrates. (E) Positive VCAM-1 control substrate with 100% contrast shows cells adhering and migrating on adhesive stripe. (F) Substrate with intermediate contrast (for which both types of stripes are adherent) shows cell migrating across stripes with modulated adhesion. RICM signal confirms adhesion between two stripes. In red: fluorescent signal corresponding to integrin ligand concentration; In grey: bright-field image; In green: RICM adhesion footprint imaging. Scale bar = 20 μm (G) Anisotropy index versus adhesion contrast of ICAM-1 (red) and VCAM-1 (blue) substrates. A linear fit was used as a guide for the eye indicated by dashed lines.

4.4 Integrin-mediated haptotaxis increases with adhesion contrast

To assess the range of molecular coatings allowing stimulation of integrin-mediated haptotaxis, we then varied the adhesion contrast of stripe-patterned substrates (Figure 4-3-G). For globally adhesive substrates (adhesion contrast 0-60%), the anisotropy index increased steadily with the adhesion contrast from zero to 0.46 ± 0.2 at adhesion contrast around 55%. For higher adhesion contrast, stripes with low molecular coatings are not adhesive and guiding is more a bias of crawling by non-adherent zones than a haptotaxis phenotype, as previously argued. Nevertheless, it is interesting to note that this directional bias when the adhesion contrast is at 100% appears as an extrapolation of haptotaxis assay in terms of the impact on anisotropy index. This observation suggests that haptotaxis on globally adherent substrates and orientation bias by stripes of null adhesion may result from a similar mechanism of mechanical bias of cell direction, simply due to a preference of cells to migrate on more adherent zones.

4.5 VLA-4 integrins mediate a preference for high adhesion zones like mesenchymal cells

To quantify the preference of cells for more or less adherent zones, we distinguished on Figure 4-4-A and -B the portions of cells pathway on more adhesive stripes (magenta) and less adhesive stripes (green). The preference of cells for higher adhesion zones (PHA) was then calculated for a given image as percentage of cells on stripes with higher adhesion. The preference for higher adhesion, PHA, for the adhesion contrast of 40% of Figure 4-4-A and Figure 4-4-B appears relatively stable versus time. More interestingly, cells seem to prefer higher adhesion zones on patterned VCAM-1 substrates, as usually observed with other mesenchymal cells, but lower adhesion zones on patterned ICAM-1 substrates. This tendency is confirmed by computed PHA values for many assays at different adhesion rates (Figure 4-4-C). At adhesion contrast of 0, PHA was equal to 50 % because the difference between stripes vanishes. For cells on VCAM-1 substrates, PHA increased monotonously from 50 % to 80 % versus the adhesion contrast. A similar behavior is expected with mesenchymal cell, as a tug of war mechanism favors an increase of guiding versus the adhesion contrast experienced by cell edges. At an adhesion contrast of 100%, PHA of mesenchymal cells would reach 100% because mesenchymal cells are excluded from non-adherent zones. Lymphocytes reach a maximum PHA of 80% because they can swim over non-adherent stripes. Apart from this slight difference, the common preference for high adhesion zones of mesenchymal and lymphocytes on VCAM-1 substrates and their monotonous increase of PHA with adhesion contrast suggests at this point a common mechanism of passive tug of war.

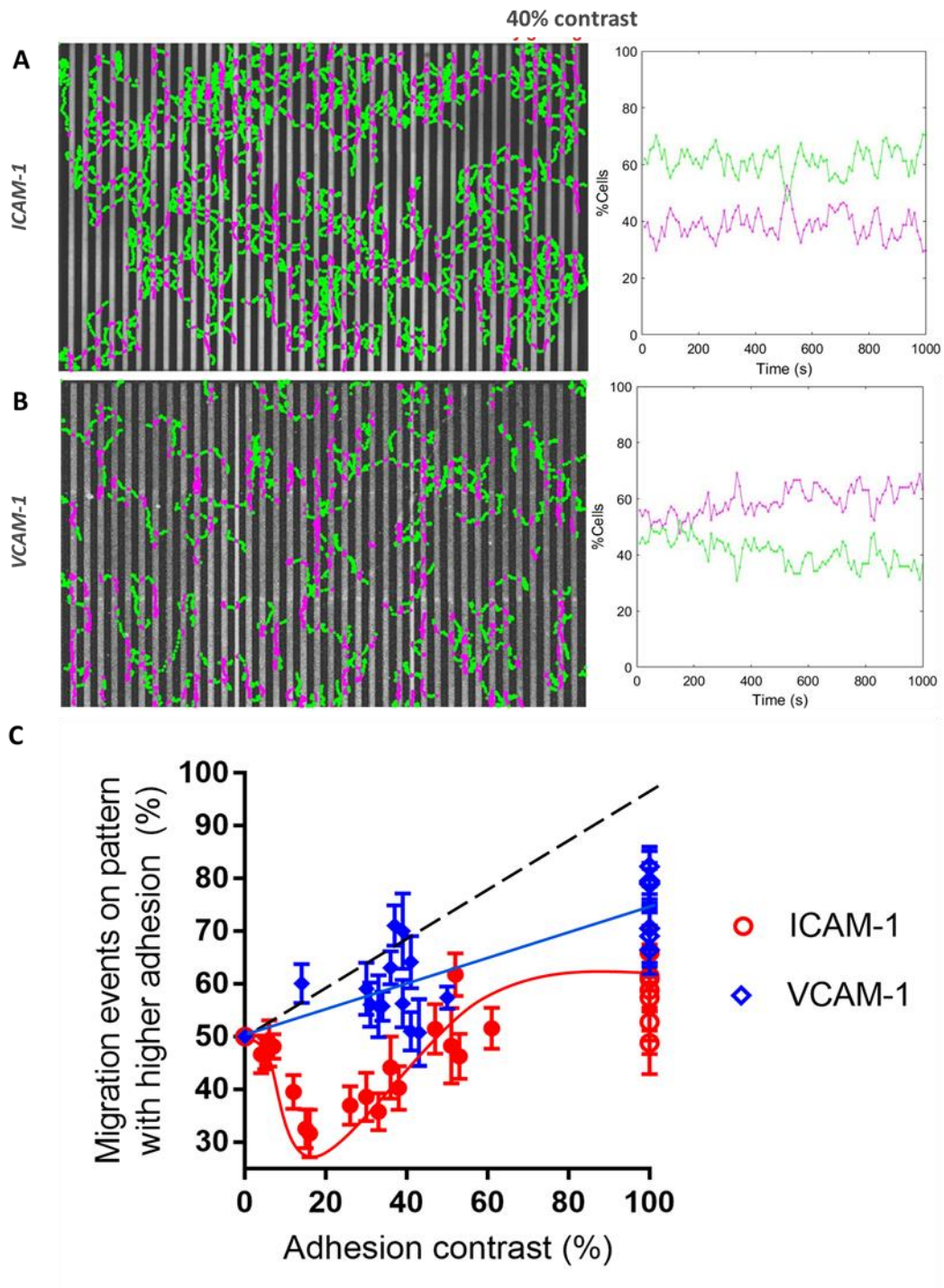


Figure 4-4 Integrin mediated haptotaxis prefers lower adhesion zone with ICAM-1 and higher adhesion zone with VCAM-1. (A, B) Characteristic cell trajectories on more adhesive (magenta) and less adhesive (green) ICAM-1 and VCAM-1 stripes with an intermediate adhesion contrast at 40%. The percentage of cells on more adhesive stripes was plotted versus time for both ICAM-1 and VCAM-1. (C) Average percentage of cells on patterns with higher adhesion versus adhesion contrast of ICAM-1 (red) and VCAM-1 (blue). Solid lines are guides for the eye for experimental data whereas black dotted line is the trend line curve for mesenchymal cells.

4.6 LFA-1 integrins mediate a unique preference for low adhesion zones

The case of patterned ICAM-1 substrates is highly singular. PHA started at 50% for a contrast of 0% and then decreased versus adhesion contrast. A minimal value of 35% was reached for an adhesion contrast around 20%. These results reveal a marked preference of lymphocytes for less adherent zones on ICAM-1 coated substrates (Figure 4-4-C). This counterintuitive behavior is highly sensitive because it concerns low adhesion contrasts. The preference for low adhesion zones observed on ICAM-1 substrates is clearly not compatible with a tug of war mechanism. LFA-1 integrins clearly mediate adhesive haptotaxis with a unique and original mechanism. However, the fact that two different integrins mediate different haptotaxis phenotypes shows that the mechanisms underlying integrin-mediated haptotaxis imply properties of integrins beyond their adhesion function. Considering the results with ICAM-1, the conclusion that guiding on VCAM-1 substrate may be simply an adhesive bias deserves further consideration. Beyond adhesion affinity, the spatio-temporal regulation of integrins or their competence to perform mechanotransduction should be considered to explain this atypical haptotaxis with LFA-1.

4.7 Mechanotransduction is not detected in integrin-mediated haptotaxis

To shed light on integrins mechanotransduction during haptotaxis, we monitored intracellular calcium activity on stripe-patterns. Figure 4-5 shows that calcium activity for cells crossing stripes of various adhesion remained negligible both on ICAM-1 and VCAM-1 coated substrates, whereas control assays with ionomycin showed an instant and intense signal. Since calcium signaling is shared by many intracellular signaling pathways, these data support that mechanotransduction is not involved in integrin-mediated haptotaxis.

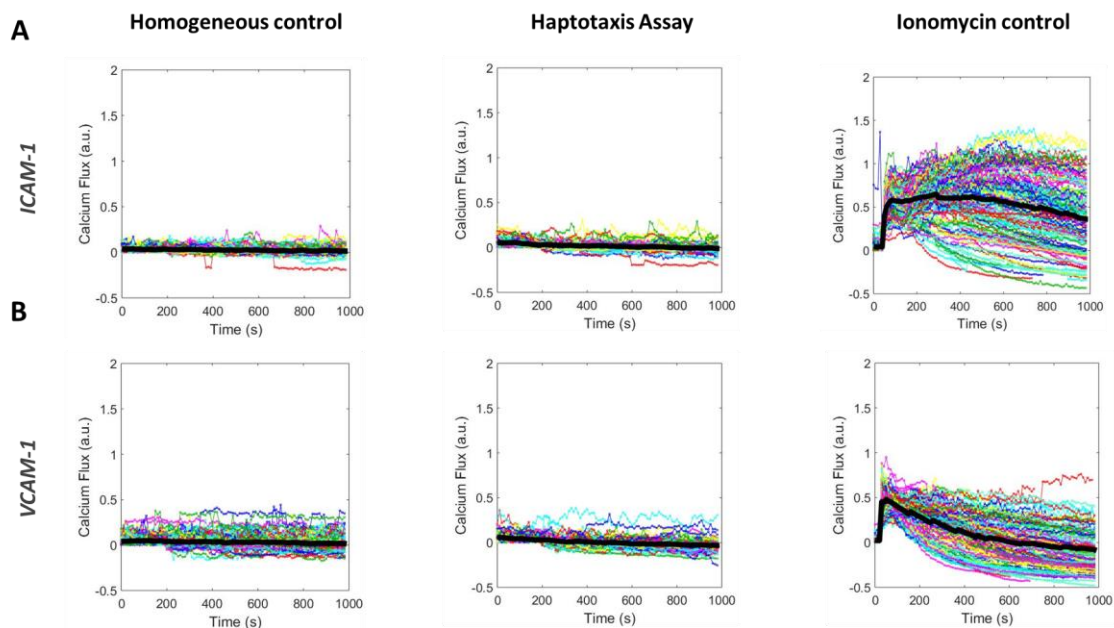


Figure 4-5 Intercellular Calcium flux detection reveals no mechanotransduction in integrin-mediated haptotaxis. The Calcium intensity was plotted as a function of time. Each colored line represents one migrating cell and the average intensity fluctuation was calculated and plotted with the thick black line. Calcium flux versus time on cells migrating on ICAM-1 (A) and VCAM-1 (B) substrates. On both homogenous surface (left) and surfaces patterned with stripes for with an intermediate adhesion contrast for haptotaxis assay (middle), no intercellular Calcium flux was detected. The control experiment with ionomycin (right) revealed an instant strong signal.

4.8 Lymphocytes orient either with or against gradients of adhesion

In order to illustrate that cells are sensitive to adhesive gradient and not only step-like adhesion profiles corresponding to stripe pattern, we prepared substrates with repeated adhesion gradients of finite steepness (left panels of Figure 4-6-A, -B). The range of adhesion rate yielding adhesion is comprised between 0.3 and 0.6. We therefore repeated positive and negative gradients between these two extreme values over distances of 40 μm . Each “gradient zone” was separated by an “accumulation zone” of constant adhesion rate, so that cells following decreasing gradients or increasing gradients should be guided to accumulation zones of respectively lower or higher adhesion rate (middle panels of Figure 4-6-A, -B). Determination of a haptotaxis index is indeed difficult because the spatial extension of gradient zones is limited. Persistent paths will therefore necessarily be short and cells escaping their preferred accumulation zone and entering the adjacent gradient zones will eventually make a U-turn by haptotaxis. A strong haptotaxis will trigger a fast U-turn and a short persistence in the gradient zone. An efficient way to assess cell haptotaxis on a large number of cells and of guiding events consists therefore of comparing cell numbers in the accumulation zones of higher and lower adhesion. Cells on VCAM-1 accumulated more in high adhesion zones, which means that cell follow increasing gradients of VCAM-1, whereas they accumulated more on low adhesion zones on ICAM-1 which means that they follow decreasing gradients of ICAM-1 (middle panels of Figure 4-6-A, -B). These assays on gradients profiles

confirm the deduction obtained on step-like profiles that lymphocytes orient with or against gradients of adhesion with respectively VCAM-1 or ICAM-1.

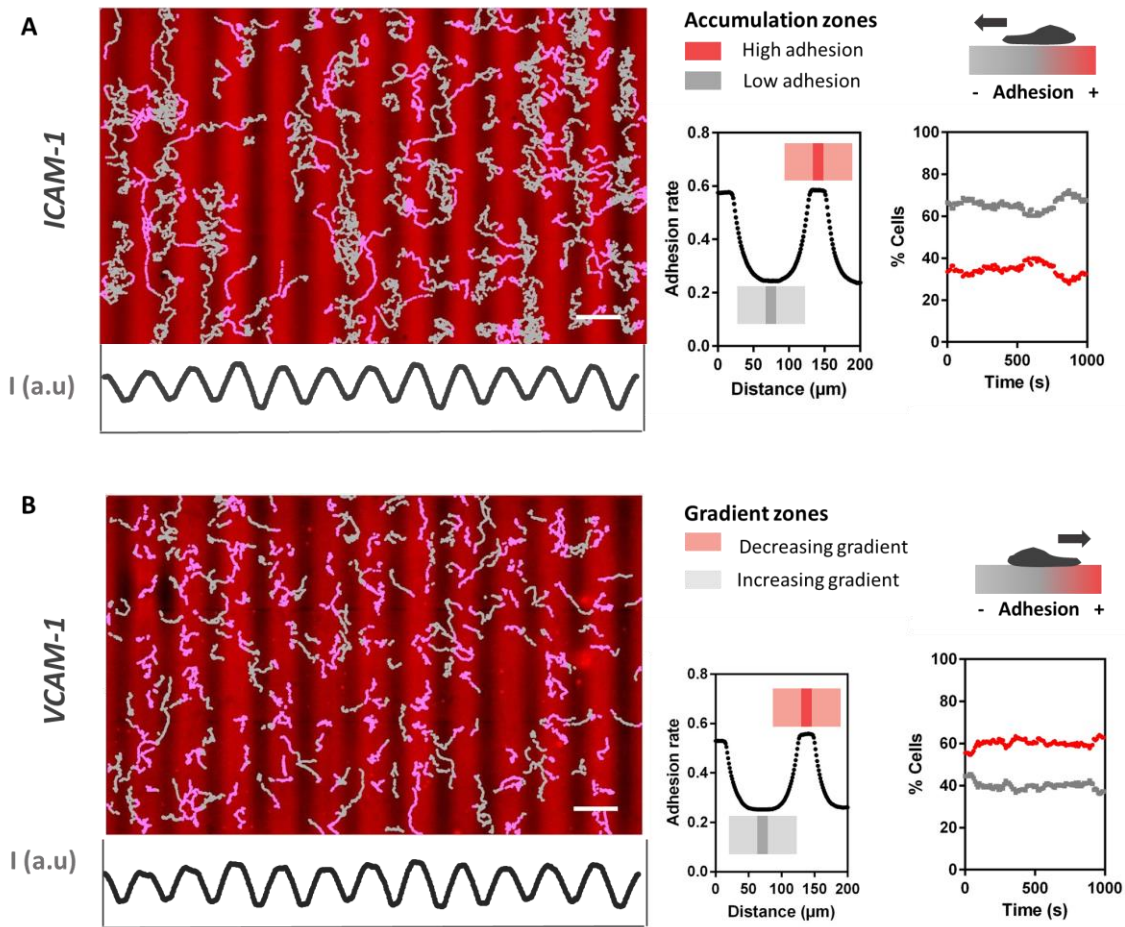


Figure 4-6 Lymphocytes orient either with gradients of adhesion on VCAM-1 and against on ICAM-1. Cell trajectories on ICAM-1 (A) and VCAM-1 (B) surface patterned with repetitive ascending and descending gradients as shown by the global profile (left panel). Rose and grey trajectories indicate cell tracks over high and low adhesion areas, respectively. A zoomed profile of the gradient was plotted versus the distance and shows the adhesion range of the gradient zones and the accumulation zones (middle panel). The percentage of cells on patterns with high (red) and low adhesion zones (grey) was plotted versus time for both ICAM-1 and VCAM-1 substrates (right panel). The tracking results were presented for one representative experiment with 178 and 217 cells for ICAM-1 and VCAM-1, respectively. Scale bar = 200 μm

4.9 Discussion

In this part of the work, we studied T lymphocytes adhesive haptotaxis at cell population level with single-parameter gradient assay created by optical patterning. T cells were subject to different patterned ICAM-1 and VCAM-1 substrates: the ones with modulated adhesion (gradient of infinite steepness) as well as repetitive gradients with finite steepness but fixed adhesion range. Our work confirmed that T lymphocyte migration is indeed sensitive to modulations of integrin-ligands concentration anchored on a matrix and exhibits adhesive haptotaxis on both ICAM-1 and VCAM-1 substrates. Our work shows also that adhesive

haptotaxis differs strongly between lymphocytes, mesenchymal cells or neuronal cells. Mesenchymal cells like fibroblasts are totally excluded from non-adhesive zones and forced to follow by default the direction of adhesive stripes (Doyle, Wang, Matsumoto, & Yamada, 2009). Similarly, growth cones of neuronal cells avoid crossing from a more adhesive to a less adhesive substrate (O'Connor, Duerr, & Bentley, 1990b). In contrast, leukocytes can travel across adhesive and non-adhesive stripes with either ICAM-1 or VCAM-1. This capability implies that a tug of war effect in the integrin-ligand zone is not always efficient and that leukocytes may have had to develop alternative mechanisms to perform adhesive haptotaxis. On VCAM-1 substrates, lymphocytes prefer high adhesion zones, so that guidance across adhering and swimming zones may appear as an extrapolation of guidance on substrates with adhesion modulations. Such properties could be explained by a tug of war effect. In contrast, a tug of war mechanism is irrelevant for lymphocyte haptotaxis on ICAM-1 substrates, because cells show a predilection for lower adhesion zones. These effects have again been confirmed when cells were subject to repetitive adhesion gradients of both ICAM-1 and VCAM-1. Cells accumulated largely on low adhesion areas on ICAM-1 substrate but on high adhesion areas on VCAM-1 substrates.

These results reveal a novel guidance of amoeboid cells mediated by integrins, and a novel haptotaxis mechanism mediated LFA-1 towards low adhesion zones. Given the fact that integrins can function both as adhesion molecule and signal transducer. An hypothetical mechanism could be that LFA-1-mediated haptotaxis may function like chemokine mediated haptotaxis (Schwarz et al., 2016; Woolf et al., 2007), in which the mechanotransduction by integrins would work in place of the chemotransduction by chemokine receptors. However, evidence of signal transduction stimulated by modulations of integrin ligand density was not detected in our work, which suggests that adhesive haptotaxis of lymphocytes may be independent of integrin mechanotransduction. Interestingly, we recently revealed that crawling lymphocytes can orient versus shear stress without integrin mechanotransduction (Alexander Hornung et al., 2018). Robust decisions on a given substrate are taken by cells to orient either with or against a flow by a mechanism involving integrin crosstalk and spatiotemporal regulation affinity but no mechanotransduction. LFA-1 and VLA-4 have their affinity activated respectively towards the front and the rear of cells, and their activation trigger crosstalk that is respectively inhibiting and activating their activity. These intricate properties may also play determinant role in the differential sensing of ligands densities by LFA-1 and VLA-4. A molecular investigation of integrins affinity level between cell front and rear on gradients of adhesion may therefore be instrumental to shed light on the mechanism of lymphocytes adhesive haptotaxis.

5 Adhesive haptotaxis at population level with perturbation of cell-substrate adhesion

5.1 Different migratory phenotypes during adhesive haptotaxis mediated by LFA-1

During LFA-1 mediated adhesive haptotaxis, cell tracks reveal different migration phenotypes. The predominant phenotype is the one that largely favors the low adhesion zone and displays zig-zag between two high adhesion zones, as shown by the green trajectories in Figure 4-4-A. Figure 5-1 (see also Movie 9) gives an example of the typical trajectory. Hereafter, this phenotype is named the “zig-zag” phenotype.

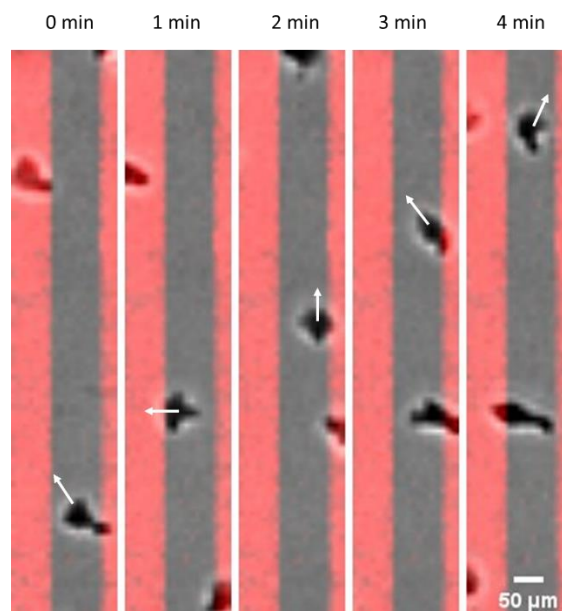


Figure 5-1 An example of a migration T cell zigzagging on low adhesion zone. White arrows indicate the direction of the cell at each time point. Scale bar = 50 μm

Another phenotype is the one that favors high adhesion zones with shorter but more persistent trajectories, as shown by magenta trajectories in Figure 4-4-A. Figure 5-2 gives an example of the trajectory (see also Movie 10). Hereafter, this phenotype is named “persistent” phenotype.

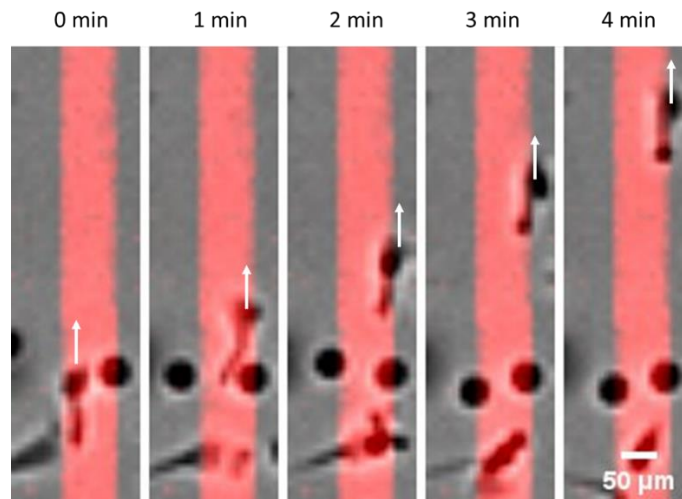


Figure 5-2 An example of a migration T cell with migrating straight on high adhesion zone. White arrows indicate the direction of the cell at each time point. Scale bar = 50 μm

Meanwhile, some cells can also cross adjacent stripes with different adhesion despite the overall directional bias in the direction of the stripes during adhesive haptotaxis, as shown by nearly horizontal cell tracks with both magenta and green trajectories in Figure 4-4-A. Figure 5-3 gives an example of this trajectory (see also Movie 11).

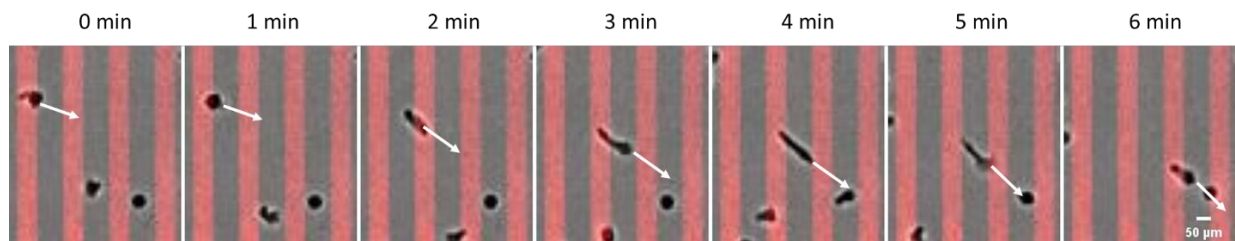


Figure 5-3 An example of a migration T cell crossing different adhesion zones. White arrows indicate the direction of the cell at each time point. Scale bar = 50 μm

In this chapter, we aim at deciphering the parameters that control the existence of these distinct phenotypes during LFA-1 mediated adhesive haptotaxis. We will mainly focus on the two prevalent phenotypes with directional bias in the orientation of the stripes – “zig-zag” and “persistent”. To better understand what may induce the predominant “zig-zag” phenotype, we will carry out different perturbation experiments at cell population level targeting the LFA-1 integrins as well as the pattern geometry to try to modulate these two phenotypes during adhesive haptotaxis.

5.2 High-affinity LFA-1 activated by Mn^{2+} enriches “persistent” phenotype on higher adhesion zones

5.2.1 LFA-1 activation by Mn^{2+}

Mn^{2+} is a potent LFA-1 activator and was used in this part of the work to stabilize the LFA-1 integrin in the high-affinity conformation. Mn^{2+} was directly added into RPMI culture media at 3mM. Cells were incubated for 10 min at 37°C in media containing Mn^{2+} and the flow chamber was then mounted to the Ibidi pump system for cell adhesion and migration assay. The presence of Mn^{2+} induced firstly visible change in cell morphology, as one can observe on bright-field image of adherent cells. Compared to control cells (Figure 5-4-A-top), cells exposed to Mn^{2+} had more elongated uropod on high adhesion zones (Figure 5-4-B-top). The cell tracking revealed 40% more adherent cells in presence of Mn^{2+} after gentle rinsing at 1 dyn.cm^{-2} following integrin activation (Table 5-1). The percentage of tracked cells was 7% lower in presence of Mn^{2+} than control cells, indicating slightly reduced cell motility upon LFA-1 activation by Mn^{2+} . The average speed of migrating cells remained stable from both control and treated cells (Table 5-1). The anisotropy index confirmed that the adhesive haptotaxis was still present (Table 5-1). However, contrary to what can be observed with control cells, where over 60% of migration cells preferred patterns with lower adhesion (Figure 5-4-A-bottom) with “zig-zag” phenotype, cells treated with Mn^{2+} favor zones with higher adhesion where cells exhibit more persistent trajectories on patterned stripes (Figure 5-4-B-bottom and Table 5-1). Figure 5-4-C shows the “close-up” of one cell with persistent phenotype migrating on high adhesion zone with attached uropod (see also Movie 12). These results indicate that the shift of predominant phenotype from “zig-zag” to “persistent” after LFA-1 activation by Mn^{2+} may come from cells migrating with attached rear on more adherent stripes.

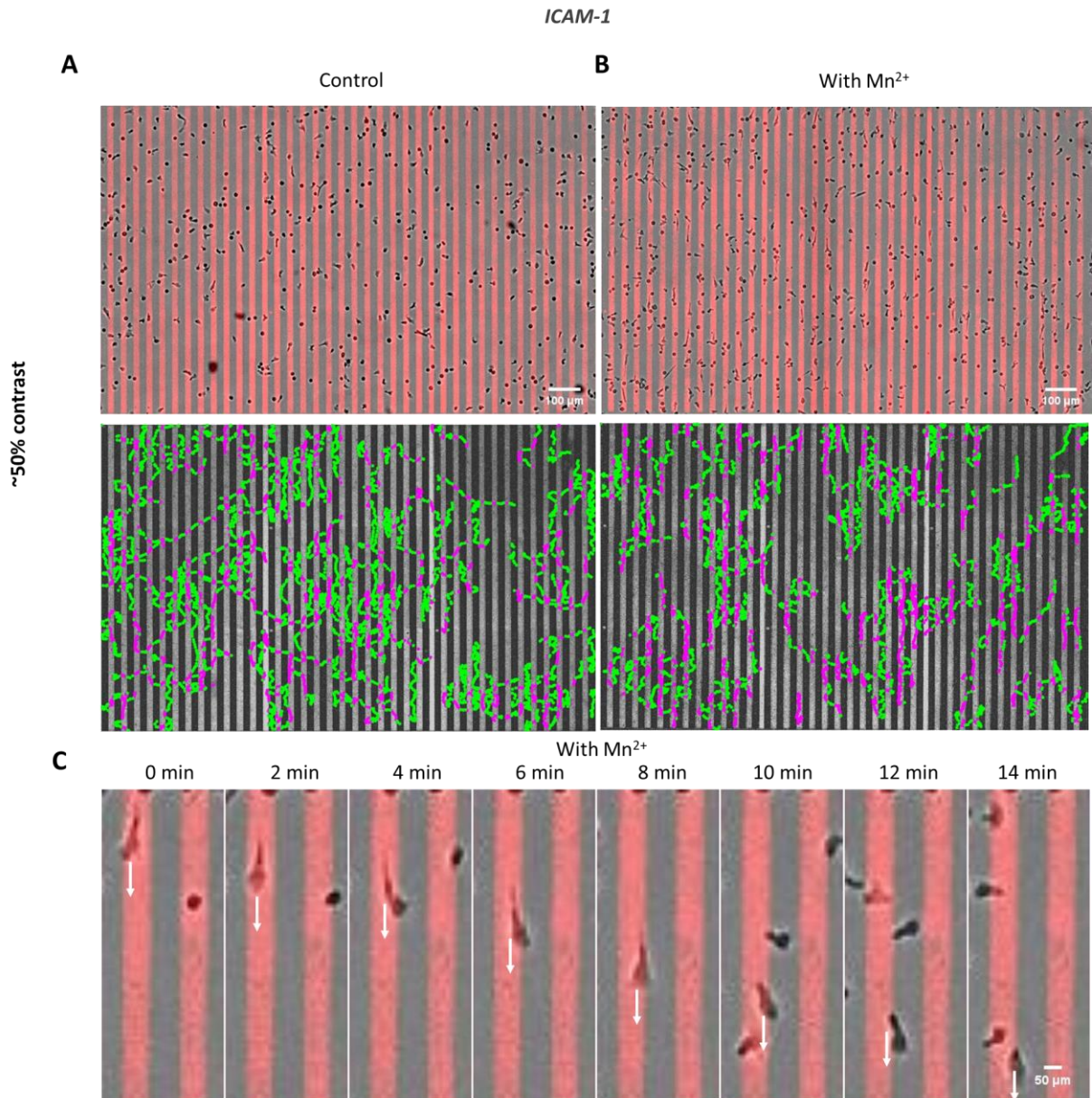


Figure 5-4 Cells favor high adhesion zones upon LFA-1 activation by Mn²⁺ on patterned stripes. (A) Control (left) and Mn²⁺ treated cells (right) adhering on patterned stripes. In grey: brightfield image showing cell body; In red: fluorescent image of patterned stripes. Scale bar=100 μ m. (B) Trajectories of tracked control (left) and Mn²⁺ treated cells (right) shown on the background of patterned stripes. In green: cell tracks on low adhesion zones; In magenta: cell tracks on high adhesion zones. (C) Example of one cell with “persistent” phenotype migration on high adhesion zone with attached uropod. White arrows indicate the direction of the cell. In grey: brightfield image showing cell body; In red: fluorescent image of patterned stripes. Scale bar = 50 μ m

	Control cells	Treated cells
Adherent cells post-rinsing	422	597
Tracked cells	29%	22%
Anisotropy Index	0.2	0.6
% cells on high adhesion zones	43%	62%
Average speed ($\mu\text{m}/\text{min}$)	14	12

Table 5-1 Summary of different migration parameters for control and Mn^{2+} treated cells.

5.2.2 LFA-1 activation by Mn^{2+} with Calcium depletion

Considering the inhibition effect on integrin activation due to the presence of Ca^{2+} in the culture media (Dransfield, 1992), we used a second method to ensure cation removal before exposing cells to Mn^{2+} . With this method, the RPMI media was firstly depleted of divalent cations by rotary mixing with 5 % w/v Chelex 100 microspheres (Biorad, Hercules, California, USA) for 4 h at 4°C and filtered using $0.2 \mu\text{m}$ filters (Millipore by Merck, Darmstadt, Germany). Cells were centrifuged at 200g for 5 min at room temperature and resuspended in 5mM EDTA (Invitrogen, Waltham, Massachusetts, USA) and incubated for 15 min at 37°C to ensure cation removal. After incubation, cells were centrifuged again at 200g for 5 min and resuspended in Calcium-depleted RPMI media containing 0.1mM MnCl_2 (Sigma-Aldrich, St. Louis, MO, USA) for 5 min at 37°C . Then, $50 \mu\text{L}$ of cell suspension at 1.5 million cells/mL were injected into the patterned flow chamber and incubated for 10 min at 37°C to allow cell adhesion. The flow chamber was then plugged to the Ibidi pump and cell adhesion and migration assays

Upon LFA-1 activation with this method, cells again presented elongated and attached uropod on more adhesive stripes (Figure 5-5-B-top) in comparison to untreated cells (Figure 5-5-A-top). The effect of immobilization is clearly shown in cell tracking analysis: while untreated control cells exhibited normal adhesive haptotaxis on less adhesive ICAM-1 pattern with typical predominant “zig-zag” phenotype (Figure 5-5-A-bottom), cells activated by Mn^{2+} had much shorter trajectories (Figure 5-5-B-bottom). Cell motility reduced drastically in presence of Mn^{2+} where only 8% of cells were mobile enough to be tracked compared to 30% in control cells and can also be confirmed by reduced speed of Mn^{2+} treated cells (Table 5-2). Figure 5-5 shows the close-up of one cell exhibiting “persistent” phenotype while advancing on high adhesion stripe with attached uropod (see also Movie 13). The anisotropy index in this case is inevitably higher since cells were attached on the stripes and therefore guided in the vertical direction (Table 5-2). The migration thus occurred also largely on areas with higher adhesion (Table 5-2).

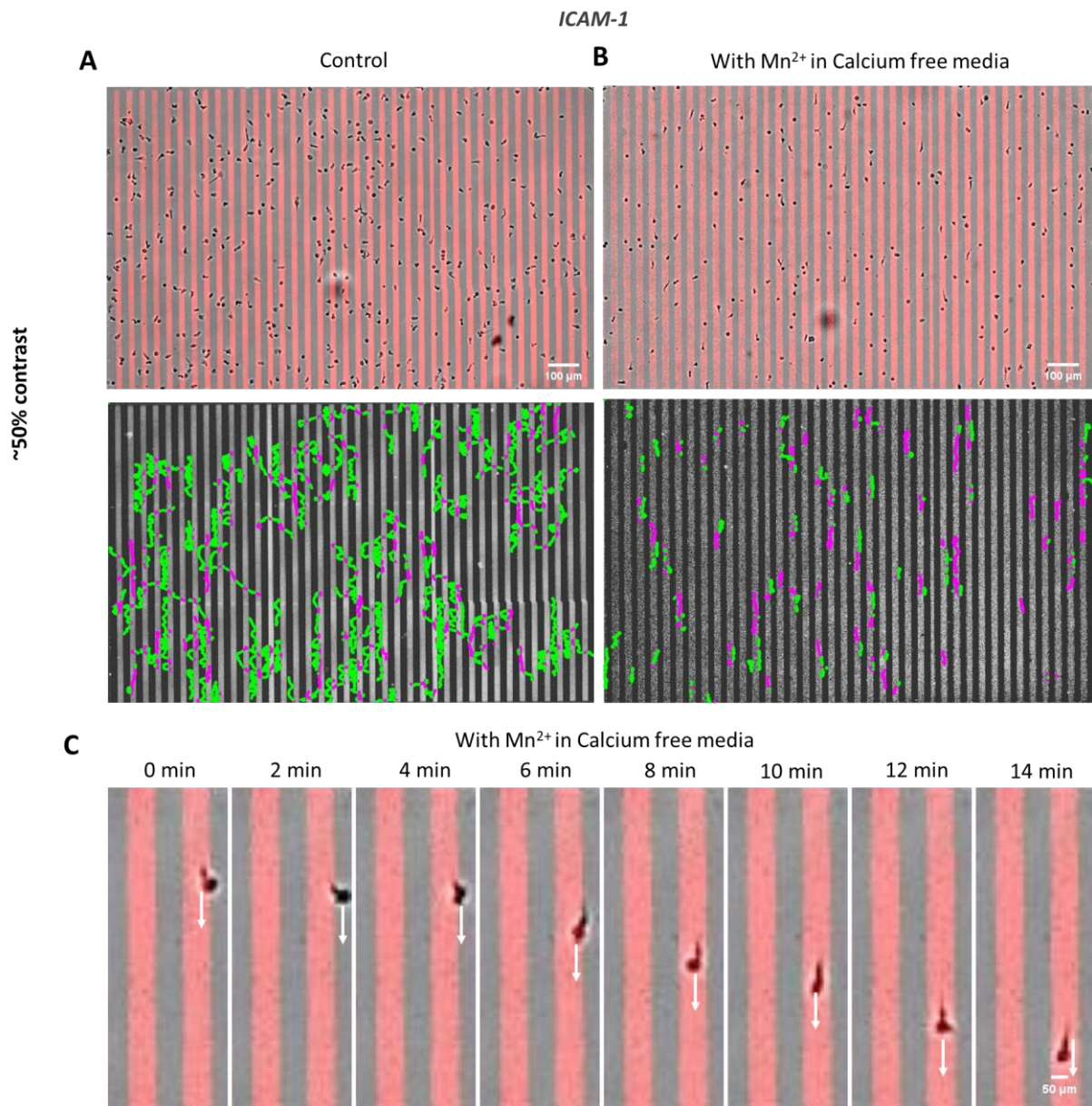


Figure 5-5 Cells become immobilized on high adhesion zones upon LFA-1 activation by Mn²⁺ in Calcium free media on patterned stripes. (A) Control (left) and Mn²⁺ treated cells (right) adhering on patterned stripes. In grey: brightfield image showing cell body; In red: fluorescent image of patterned stripes. Scale bar=100 μm. (B) Trajectories of tracked control (left) and Mn²⁺ treated cells (right) shown on the background of patterned stripes. In green: cell tracks on low adhesion zones; In magenta: cell tracks on high adhesion zones. (C) Example of one cell with “persistent” phenotype migration on high adhesion zone with attached uropod. White arrows indicate the direction of the cell. In grey: brightfield image showing cell body; In red: fluorescent image of patterned stripes. Scale bar = 50 μm

	Control cells	Treated cells
Adherent cells post-rinsing	402	338
Tracked cells	30%	8%
Anisotropy Index	0.6	0.9
% cells on high adhesion zones	35%	64%
Average speed ($\mu\text{m}/\text{min}$)	22	12

Table 5-2 Summary of different migration parameters for control and Mn^{2+} treated cells.

The LFA-1 activation in absence of Calcium was more efficient, which concurs previous findings in the literature (Dransfield, 1992), as the effect of Mn^{2+} occurred at 0.1mM instead of 3mM with the method without Calcium depletion. However, the integrin activation in calcium-free condition severely perturbed cell migration as cells became immobilized on the surface. This defective migration will bias our effort to perturbate the preexisting phenotypes. The perturbation results on phenotype modulation using this method are therefore inconclusive. From this point of view, the Mn^{2+} activation without Calcium depletion seems to better preserve cell motility as no drastic cell immobilization was observed even though some cells had attached uropod.

5.3 Anti-LFA-1 monoclonal antibody treatment leads to “persistent” phenotype

Previous perturbation experiments focused mainly on activating LFA-1 integrin. However, the unique presence of “zig-zag” phenotype during adhesive haptotaxis could be due to a reduced integrin affinity. To test this new hypothesis, we will use monoclonal antibodies targeting the α -subunit of the LFA-1 integrin as well as the drug lovastatin to inhibit LFA-1. Both control and treated cell will be subject to migration assay and cell tracking analysis to analyze haptotactic phenotypes.

Two monoclonal antibodies were used in this part of the study: the anti-LFA-1 (clone TS1/22) targeting the α -subunit of LFA-1 and thus prohibiting ligand binding as well as anti-LFA-1 (clone Hi1/11) that binds to the edge of the top face of the α_L subunit, in or near the ligand binding site (Ma et al., 2002, p. 1) (Figure 5-6).

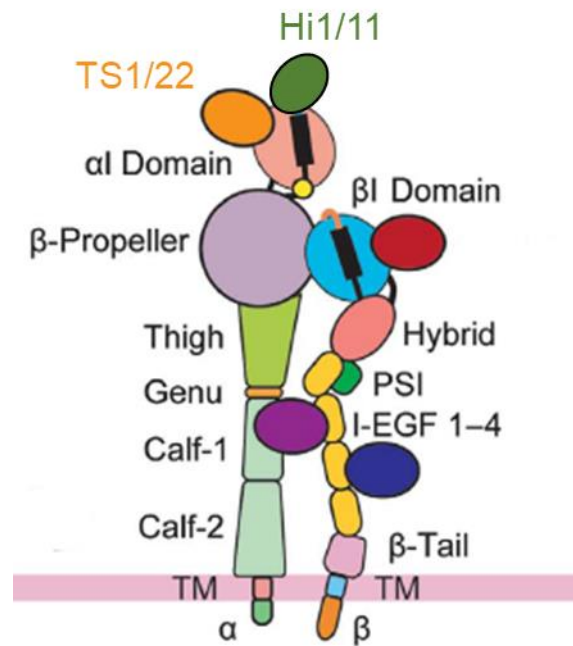


Figure 5-6 Illustration of the binding of monoclonal anti-LFA-1 antibodies (from [Schü & Springer, 2011])

5.3.1 TS1/22 treatment leads to cell immobilization and subsequent “persistent” phenotype

They were incubated directly with the integrin LFA-1 blocking antibody TS1/22 (Biolegend, San Diego, CA, USA) at 4 $\mu\text{g}/\text{mL}$ for 10 min at 37°C. Antibody treated cells (50 μL of cell suspension) were injected at 1.5 million cells/mL into the patterned flow chamber. The flow chamber was then plugged to the Ibidi pump and cell adhesion and migration assays. Surprisingly, antibody blocking almost doubled the number of adherent cells after rinsing compared to control cells (Figure 5-7-top and Table 5-3). Cell tracking confirms that only 9% of treated cells were mobile enough to be tracked versus 30% among control cells (Table 5-3), even though the speed of tracked cells for both groups remained close. The directional bias of treated cells remained in the orientation of the stripes and cell migration favored areas with higher adhesion in comparison to control cells (Table 5-3). However, significantly shortened cell tracks compared to those of control confirm that cell mobility upon antibody blocking was hindered (Figure 5-7-A and -B bottom). Figure 5-7-C shows a close-up of cells on the stripes upon antibody treatment: many unpolarized cells remained adherent on the surface whereas such cells were washed away without antibody treatment. Meanwhile, among polarized cells, the majority had attached uropod on stripes with higher adhesion (in red) with impaired mobility (see also Movie 15). These results reveal unexpected effect of cell immobilization upon TS1/22 antibody treatment, since previous findings report reduced cell adhesion with TS1/22 antibody on Jurkat cells (J. R. Chan, Hyduk, & Cybulsky, 2000), monocytes (Chuang, 2004) and CD4⁺ T lymphocytes (Watabe et al., 2007). Given that the surface contained an intermediate Protein A layer which has a high affinity for the Fc fragment, this phenomenon

could be due to the link between the antibody (which bound on the cells) via Protein A and the surface, resulting in cell immobilization (especially the adherent unpolarized cells) This defective motility hinders our investigation on the migratory phenotype using perturbation experiment. It is therefore necessary to test another anti-LFA-1 antibody that can block integrin without influencing overall cell motility.

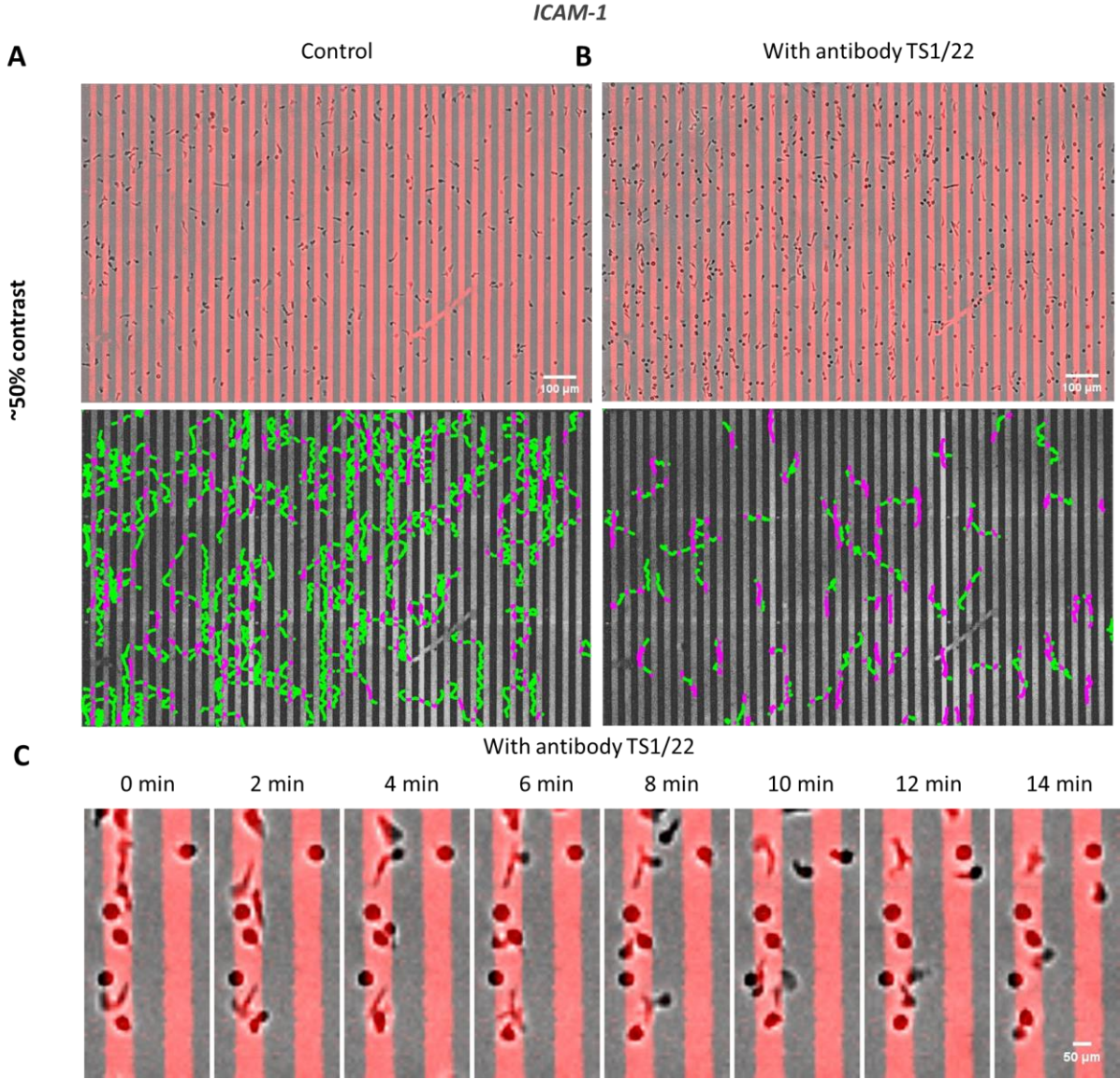


Figure 5-7 Anti-LFA-1 monoclonal antibody (clone TS1/22) leads to cell immobilization and subsequent “persistent” phenotype on patterned stripes. (A) Control (left) and antibody treated cells (right) adhering on patterned stripes. In grey: brightfield image showing cell body; In red: fluorescent image of patterned stripes. Scale bar=100 μm. (B) Trajectories of tracked control (left) and treated cells (right) shown on the background of patterned stripes. In green: cell tracks on low adhesion zones; In magenta: cell tracks on high adhesion zones. (C) Example of unpolarized cells adhering on high adhesion zones and polarized cells advancing with attached uropod; In red: fluorescent image of patterned stripes. Scale bar = 50 μm

	Control cells	Treated cells
Adherent cells post-rinsing	346	647
Tracked cells	40%	9%
Anisotropy Index	0.2	0,5
% cells on high adhesion zones	41%	68%
Average speed ($\mu\text{m}/\text{min}$)	18	15

Table 5-3 Summary of different migration parameters for control and treated cells.

5.3.2 Hi1/11 enriches “persistent” phenotype on areas with higher adhesion

Given that cell motility was severely impaired upon TS1/22 blocking, cells were treated with another monoclonal antibody Hi1/11. After LFA-1 blocking, cells were adherent and polarized on the surface without the appearance of unpolarized adherent cell population in the case of TS1/22 blocking (Figure 5-8-B-top). There was no drastic perturbation of cell motility indicated by the percentage of tracked cells of treated (12%) and control cells (18%), though the speed of tracked cell upon Hi/11 treatment was slower (Table 5-4). Cells in both cases were guided in the direction of the stripes. Cell tracking reveals cells favoring areas with higher adhesion with more persistent phenotype upon LFA-1 blocking compared to what was observed in control cells (Figure 5-8-B-bottom). Among treated cells; 83% of cells migrated on more adhesive stripes versus 41% among control cells (Table 5-4). Nevertheless, Figure 5-8-C shows that cells still advanced with attached uropod on more adhesive stripes, which means that motility was still impaired and could explain the reduced speed (see also Movie 16).

These data show once again that antibody blocking can come with unexpected effects that impair cell motility resulting in an additional phenotype of cells with attached uropod. Therefore, our attempt to disturb to preexisting cell populations is biased by the emergence of this additional phenotype. It is thus important to find another perturbation method that can reduce ligand-binding to LFA-1 without hindering cell migration.

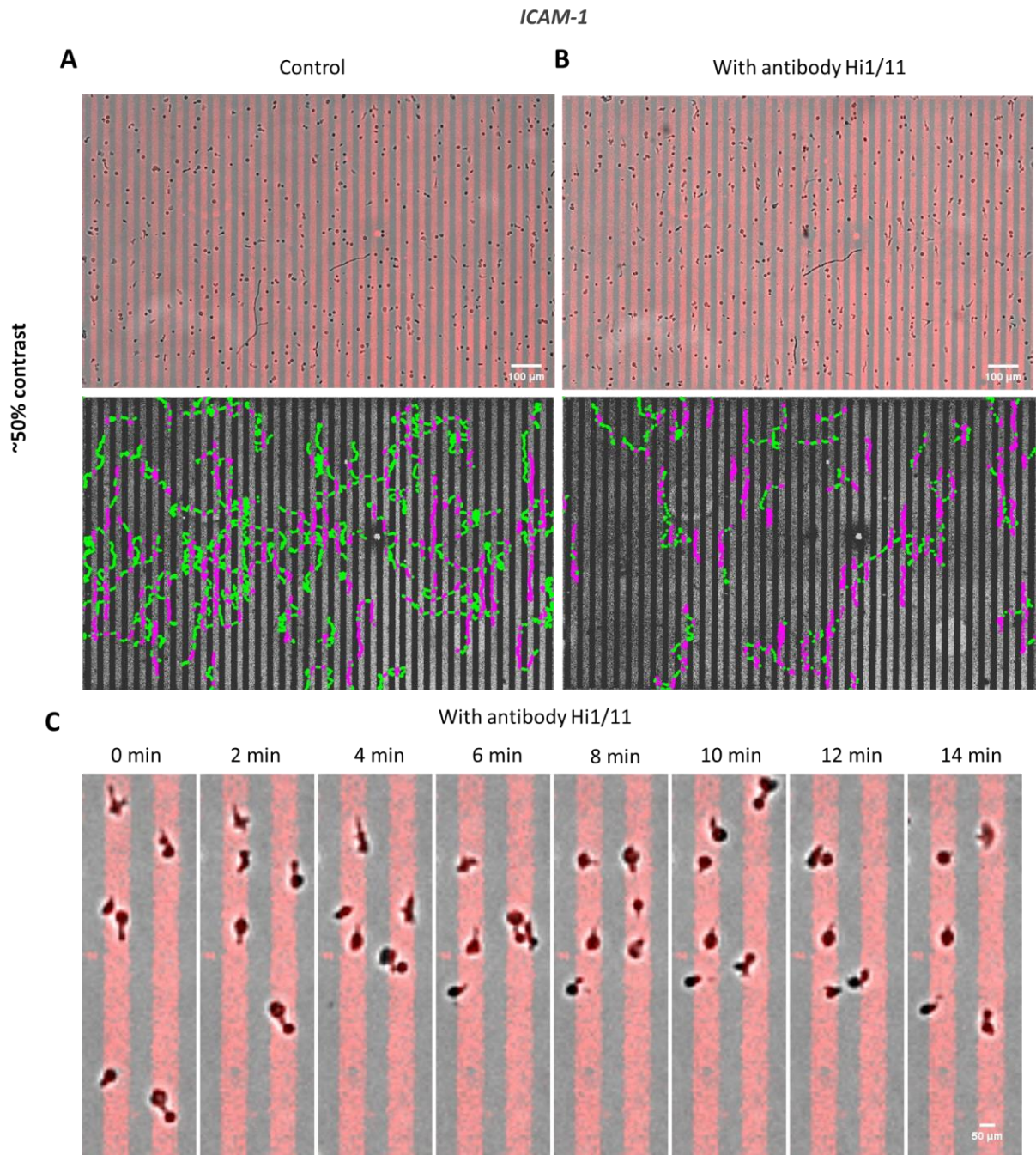


Figure 5-8 Anti-LFA-1 monoclonal antibody (clone Hi1/11) enriches “persistent” phenotype on patterned stripes. (A) Control (left) and antibody treated cells (right) adhering on patterned stripes. In grey: brightfield image showing cell body; In red: fluorescent image of patterned stripes. Scale bar=100 μ m. (B) Trajectories of tracked control (left) and treated cells (right) shown on the background of patterned stripes. In green: cell tracks on low adhesion zones; In magenta: cell tracks on high adhesion zones. (C) Example of polarized cells advancing with attached uropod on high adhesion stripes; In red: fluorescent image of patterned stripes. Scale bar = 50 μ m

	Control cells	Treated cells
Adherent cells post-rinsing	477	456
Tracked cells	19%	12%
Anisotropy Index	0.3	0.6
% cells on high adhesion zones	41%	83%
Average speed ($\mu\text{m}/\text{min}$)	12	7

Table 5-4 Summary of different migration parameters for control and treated cells.

5.4 “Zig-zag” phenotype remains dominant following Lovastatin treatment

To achieve integrin inhibition without altering overall cell mobility, we then treated cells with Lovastatin, a therapeutic LFA-1 antagonist that blocks the integrin in low-affinity state (Y. Wang et al., 2009). Compared to control cells, cell adhesion decreased nearly 4 times after rinsing (Figure 5-9-top and Table 5-5), which is consistent with the function of lovastatin. Cell tracking shows that adherent cells in both cases remained mobile (Table 5-5, see also Movie 17). Anisotropy Index confirmed that cells were guided in the direction of the stripes (Table 5-5). However, cell tracking also reveals that there was no change in the phenotypes: both “zig-zag” and “persistent” phenotypes were present with and without Lovastatin where “zig-zag” phenotype remained dominant in both cases (Figure 5-9-bottom and Table 5-5).

These results show that the lovastatin treatment has effectively reduced cell adhesion. Importantly, cell motility remained unimpaired among adherent cells. However, there was no phenotypic change among treated and control cells at population level: the “zig-zag” phenotype remained dominant with cells favoring areas with low adhesion, which was an interesting observation. Upon lovastatin treatment, cells that detached after rinsing were probably those with weaker adhesion initially and cells remaining adherent were probably those with stronger adhesion before treatment. However, the distribution of the two major haptotactic phenotypes remained the same upon lovastatin treatment. This indicates two possibilities: 1) the two phenotypes are not at all related to adhesion level of each migrating cell, which would be highly unlikely for adhesive haptotaxis. 2) The existence of the two haptotactic phenotypes is indeed related to adhesion level of each migrating cell. Different adhesion levels of individual cells may have resulted in the initial distribution of the two phenotypes where the “zig-zag” is dominant. Lovastatin reduces adhesion globally of all cells and only those with strong initial adhesion can remain. This global adhesion “shift” for each adherent cell leads again to the new distribution of the two haptotactic phenotypes, which appears to be the same as that without lovastatin. In line with this hypothesis, cells with the dominant “zig-zag” phenotype could therefore come from those with either stronger or weaker adhesion of the entire population of adherent and migrating cells. The second hypothesis (“zig-zag” phenotype correspond to cells with weaker adhesion) seems more

plausible since there was no cell immobilization observed and cell motility remained unimpaired. Future investigation is necessary to assess whether the second hypothesis is valid. Experiments at single cell level which allows observation of phenotypes of individual cells after global decrease in adhesion may be of interest.

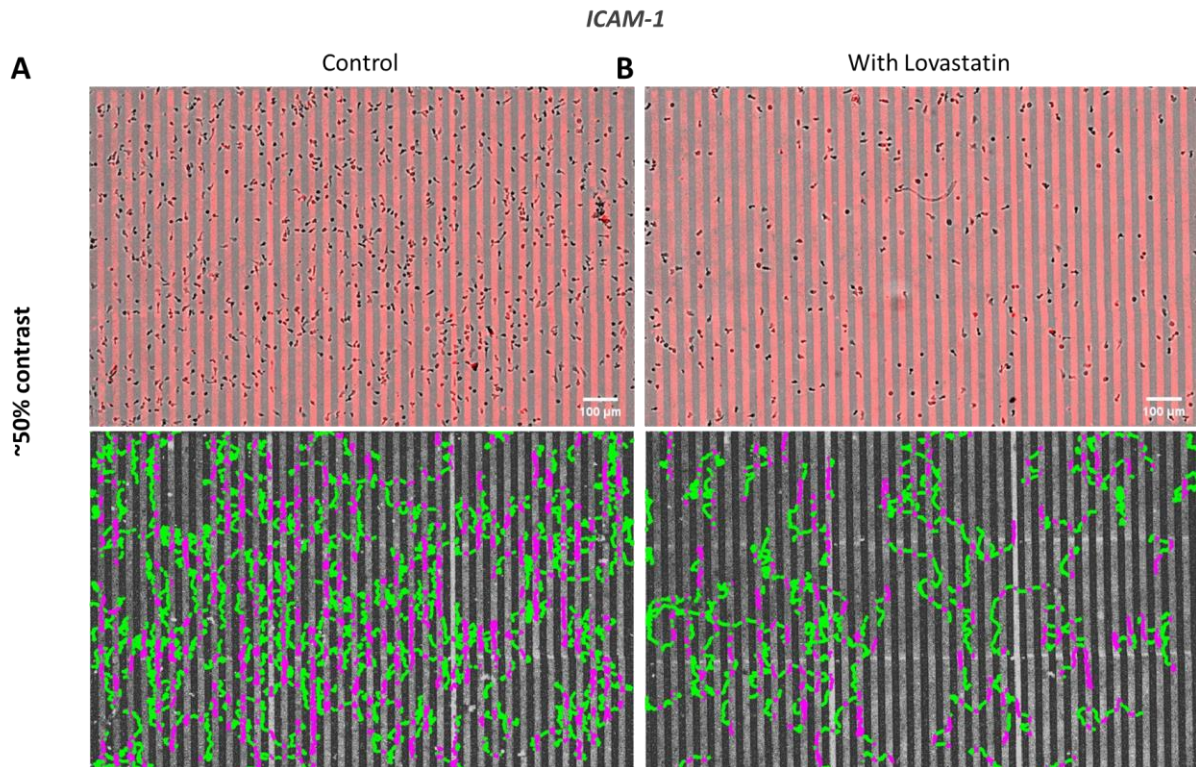


Figure 5-9 “Zig-zag” phenotype remains dominant following Lovastatin treatment. (A) Control (left) and Lovastatin treated cells (right) adhering on patterned stripes. In grey: brightfield image showing cell body; In red: fluorescent image of patterned stripes. Scale bar=100μm. (B) Trajectories of tracked control (left) and treated cells (right) shown on the background of patterned stripes. In green: cell tracks on low adhesion zones; In magenta: cell tracks on high adhesion zones.

	Control cells	Treated cells
Adherent cells post-rinsing	842	271
Tracked cells	25%	35%
Anisotropy Index	0.4	0.4
% cells on high adhesion zones	47%	41%
Average speed (μm/min)	19	15

Table 5-5 Summary of different migration parameters for control and treated cells.

5.5 Attempt to locally deplete LFA-1 enriches “persistent” phenotype favoring higher adhesion zones

The unique cell preference on less adhesive zone may also result from the spatial distribution and concentration of integrins. We therefore planned to attach ICAM coated beads on migrating cells to perturb the pool of LFA-1 molecules available to interact with the substrate.

To test this hypothesis, we prepared ICAM coated beads (Dynabeads™ M-280 Streptavidin, Invitrogen, 11205D) at a concentration of 200µg/mL and added 50µL coated beads into the flow chamber. To make sure that the beads stay attached on the cell surface, the experiment was carried out in presence of Mn²⁺ (without Calcium depletion to avoid cell immobilization) at 3mM. Upon injection of the beads, most of adherent cells have taken up multiple beads (Figure 5-10-B-top). Such perturbation did not significantly alter cell adhesion and mobility as the percentage of adherent and tracked cells remained stable between control cells and treated cells. The directional preference of cells remains in the direction of the stripes in both cases as confirmed by their corresponding anisotropy index (Table 5-6). Cell tracks show that the attempt to deplete integrin enriched again the “persistent” phenotypes (trajectories in magenta in Figure 5-10-B-bottom). Cells migrated long distance on stripes with higher adhesion as compared to control cells where the “zig-zag” phenotype was dominant (Figure 5-10-bottom and Table 5-6). A close-up of one migrating cell with persistent phenotype shows that cell advanced on the stripe with a package of beads attached at its rear (shown by black arrows), a part of which detached at the end (Figure 5-10-C, see also Movie 14).

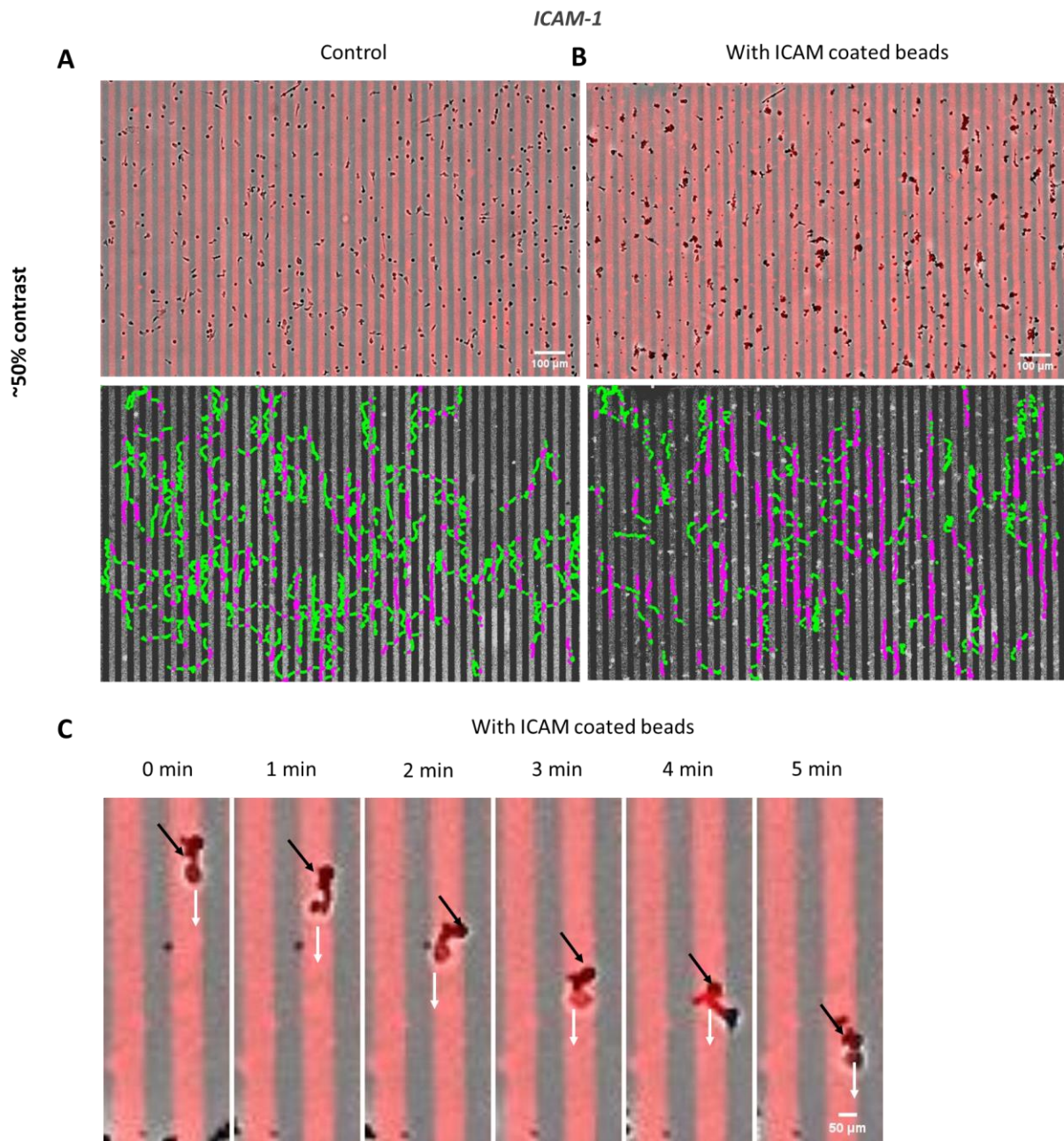


Figure 5-10 Local depletion of LFA-1 enriches “persistent” phenotype favoring higher adhesion zones on patterned stripes. (A) Control (left) and cells with ICAM coated beads (right) adhering on patterned stripes. In grey: brightfield image showing cell body; In red: fluorescent image of patterned stripes. Scale bar=100 μm. (B) Trajectories of tracked control (left) and treated cells (right) shown on the background of patterned stripes. In green: cell tracks on low adhesion zones; In magenta: cell tracks on high adhesion zones. (C) Example of one cell with beads attached at rear with “persistent” phenotype migration on high adhesion zone with attached rear. White arrows indicate the direction of the cell. Black arrows indicated the position of attached beads. In grey: brightfield image showing cell body; In red: fluorescent image of patterned stripes. Scale bar = 50 μm

	Control cells	Treated cells
Adherent cells post-rinsing	440	446
Tracked cells	25%	23%
Anisotropy Index	0.5	0.6
% cells on high adhesion zones	46%	72%
Average speed ($\mu\text{m}/\text{min}$)	12	10

Table 5-6 Summary of different migration parameters for control and treated cells.

These results represent our first attempt to deplete locally integrins on cell surface in order to modulate the preexisting phenotypes. Even though this perturbation resulted in cells favoring more the high adhesion zones with “persistent” phenotype, the results are not straightforward to interpret for the following reasons: first, the exact integrin depletion rate by ICAM-1 coated beads was not known; second, the presence of Mn^{2+} was indeed efficient in helping the beads stay attached on the cell surface, but it also activated integrin into high-affinity conformation. Given that the number of adherent cells was the same between control cells and treated cells, it was possible that the depletion was not very effective due to activation by Mn^{2+} at the same time. Further investigation on determining the depletion rate would be necessary before a more definitive conclusion can be drawn regarding its effect on modulation of the haptotactic phenotypes and further investigation can be planned.

5.6 LFA-1 staining reveals no significant difference in integrin expression between “zig-zag” and “persistent” phenotype

Neither LFA-1 activation nor inhibition appears to enrich the “zig-zag” phenotype during adhesive haptotaxis. The counterintuitive preference of low adhesion zone thus cannot be clearly linked to the change in LFA-1 affinity. We then asked whether this unique preference could be linked to the overall expression level of LFA-1 of each migrating cell. Given that the perturbation experiments often alter cell motility and bias migration analysis, we chose to analyze the integrin expression level of each migrating cell according to their phenotype by staining directly migrating cells with anti-LFA-1 antibody.

In this more approach to analyze LFA-1 expression of each migrating cell, T lymphocytes were incubated into the flow chamber on patterned ICAM-1 surfaces with around 50% adhesion contrast. The direct staining assay was carried out using the following method: Cells were subject to the migration assay at the end of which cells migrating in the patterned flow chamber were instantly fixed by quick injection of PFA 4% (ThermoScientific, Rockford, IL, USA) into the device (Figure 5-11-A). Free Fc-binding sites on the Protein A layer were blocked using human serum IgG at 100 $\mu\text{g}/\text{mL}$ solution for 20 min. The sample was further blocked with 4% BSA for another 20 min. After rinsing with PBS, the primary antibody was injected into the flow chamber and incubated for 30 min. After the incubation, the sample

was rinsed with PBS. Immediately after the PBS wash, the sample was re-fixed with PFA 2% for prevent the primary antibody from detaching. The sample was again rinsed with copious amount of PBS. Then, the secondary antibody was injected and incubated for 30 min. In the end, the surface was rinsed again for imaging: fluorescent images of the patterns were also taken besides the images from the antibody staining. The antibodies used were the following: mouse anti-human CD11a, clone name TS1/22 at 4 $\mu\text{g}/\text{mL}$; goat anti-mouse IgG, AF488 conjugated (ThermoScientific, Rockford, IL, USA) at 4 $\mu\text{g}/\text{mL}$.

Fixed cells were stained with the anti-LFA-1 antibody at 4 $\mu\text{g}/\text{mL}$ (clone TS1/22, Biolegend, San Diego, CA, USA) that binds to all conformations of LFA-1, which was later revealed by a AF488 conjugated secondary antibody at 4 $\mu\text{g}/\text{mL}$ (goat anti-mouse IgG, ThermoScientific, Rockford, IL, USA) (Figure 5-11-B). The migration phenotype of each fixed cell, which represents the last image of the migration assay, were identified and sorted into two categories (“zig-zag” and “persistent”) based on tracking of migration movies. The fluorescent intensity of each stained cell was measured with the ImageJ software and matched to their corresponding phenotypes to analyze the relation with the integrin expression level. After analysis, Figure 5-11-C shows that there is no significant difference in LFA-1 expression between two phenotypes. The results obtained with lovastatin treatments led to one hypothesis that the “zig-zag” phenotype may result from the population of cells with lower adhesion, which in turn could have lower overall integrin expression. However, the results of direct integrin staining could not confirm directly this hypothesis.

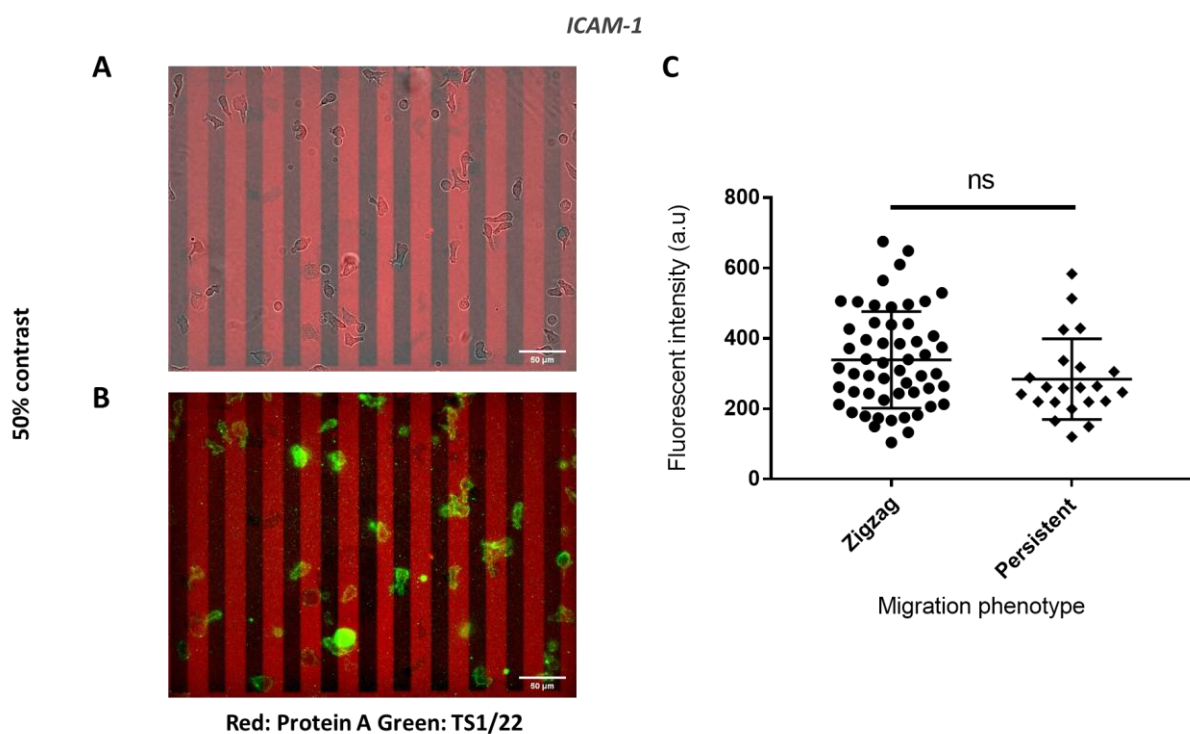


Figure 5-11 LFA-1 staining reveals no significant difference in integrin expression between “zig-zag” and “persistent” phenotype. (A) Fixed migrating cells on patterned stripes with 50% adhesion contrast. In grey: bright-field image showing the cell body. In red: fluorescent image of patterned stripes. Scale bar = 50 μm . (B)

Fixed cells stained by anti-LFA-1 (clone TS1/22) antibody on the pattern. In green: TS1/22 signal; In red: fluorescent image of the pattern indicating the density of the ligand. Scale bar = 50 μm . (C) Analysis of fluorescent intensity of the antibody showing no significant difference between the two phenotypes. The statistical difference between two groups was compared using unpaired t test.

5.7 Geometrical perturbation induces orientation shift on ICAM-1 but not VCAM-1 substrates

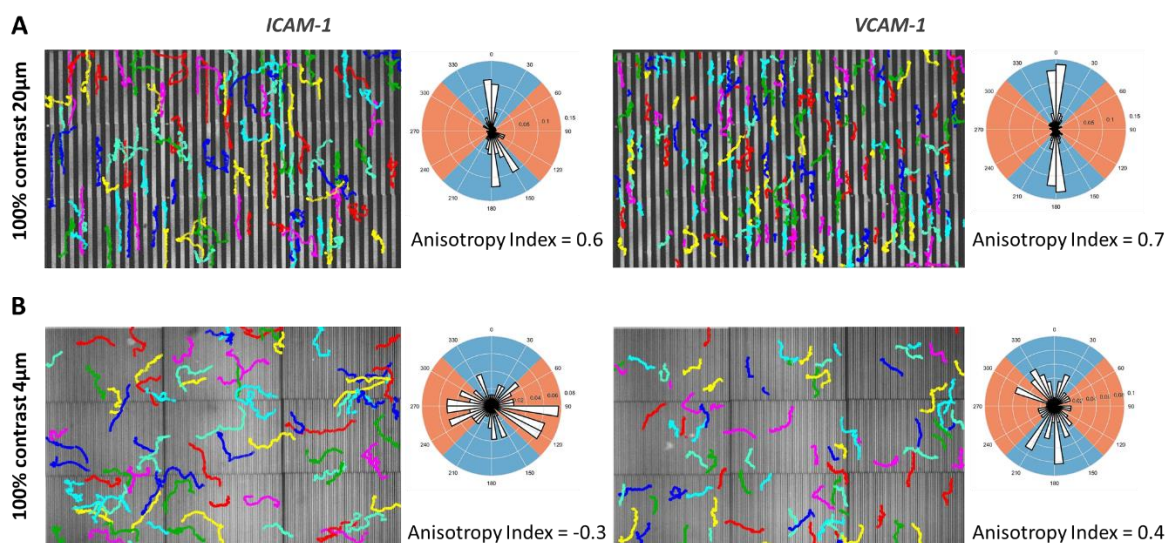
A variety of perturbation experiments and LFA-1 staining have indicated that the characteristic phenotypes may not be directly linked to integrin affinity and expression level and there may be other parameters involved. So far, the width of the patterned stripes has been fixed at 20 μm to maximal stripe detection by migrating T cells. To assess whether the geometry of the pattern could induce changes in the distribution of the phenotypes, we then tested T cell migration on patterns with different widths on both ICAM-1 and VCAM-1 substrates. Cells were subject to migration assay and then tracked for 16 min. The orientation of each individual cell was assessed from the orientation between first and final positions. Distribution of orientations were displayed on rose wind plots, and directional bias of migrating cells was determined by Anisotropy Index.

On substrates with 100% adhesion contrast patterned with 20 μm -wide stripes, while some cells were able to swim across the stripes, most cell trajectories appeared to have a steady orientation in the direction of the stripes and this directional bias was clearly revealed on the rose wind plot with an Anisotropy Index of 0.6 for ICAM-1 substrates and 0.7 for VCAM-1 substrates (Figure 5-12-A; see also Movie 18). However, when the width of the stripes was reduced to 4 μm , trajectories of migrating cells on ICAM-1 substrates exhibited complete orientation shift by 90 degrees— most of migrating cells had a steady orientation in the direction perpendicular to the stripes. This was confirmed by the rose wind plot with an Anisotropy Index of -0.3 (Figure 5-12-B left panel, see also Movie 19). On the other hand, cells continued to migrate preferentially in the direction of the stripe on VCAM-1 substrates with an Anisotropy Index of 0.4, which was also confirmed by the rose wind plot (Figure 5-12-B right panel, see also Movie 19).

In this study, we mainly focused on globally adhesive substrates for adhesive haptotaxis study. Therefore, we investigated afterwards the potential orientation shift on substrates with modulated adhesion (adhesion contrast $\sim 50\%$). On substrates patterned with 20 μm -wide stripes, migrating cells followed preferentially the direction of the stripes that was further confirmed by the rose-wind plot. The Anisotropy Index are 0.3 and 0.4 for ICAM-1 and VCAM-1 surfaces, respectively (Figure 5-12-C, see also Movie 20). When the width of patterned stripe was reduced to 4 μm , the orientation shift occurred again for cells migrating on ICAM-1 substrates. Cell trajectories showed clearly a steady orientation in the direction perpendicular to the stripes. Rose wind plot confirmed the orientation shift with an Anisotropy Index of -0.2 (Figure 5-12-D left panel, see also Movie 21). Nevertheless, this orientation shift was not

observed for cells migrating on VCAM-1 substrates. Although some cells appeared to cross the stripes, most of cells still migrated preferentially in the direction of the stripes with an Anisotropy Index of 0.15, as confirmed by the rose wind plot (Figure 5-12-D right panel, see also Movie 21). Stripes of different widths ranging from 2 to 20 μm were then patterned on ICAM-1 and VCAM-1 for both 100% and 50% adhesion contrast. The relation between Anisotropy Index and the width of the stripes was obtained. Same trend was observed regardless of the adhesion contrast: for VCAM-1 substrates, when the stripes became narrower, the Anisotropy Index decreased until zero, indicating a random migration; on the contrary, for ICAM-1 substrates, the Anisotropy Index decreased below zero and the perpendicular orientation shift started to occur when the width of the stripes was reduced to 5 μm . This shift reaches its maximum with a width of 4 μm before increasing back to zero - cells were no longer able to sense the difference in geometry so the migration became random (Figure 5-12-E, F).

These results show that the migration phenotypes depend on the pattern geometry: firstly, the two haptotactic phenotypes observed during LFA-1 mediated haptotaxis on 20 μm -wide stripes can turn into one completely different phenotype with change in pattern width. Secondly, the relation between anisotropy index and the pattern width shows that the scale of the pattern leads to this phenotypic change since the new phenotype only occurs when the width is smaller than that of a cell. Once again, this phenomenon is unique for the LFA-1 integrins. Previous studies have reported that the local anisotropy in geometry can lead to migratory bias in fibroblasts on fibronectin pattern due to local asymmetry in cell protrusions (Caballero, Comelles, Piel, Voituriez, & Riveline, 2015a; Caballero, Voituriez, & Riveline, 2014; Caballero et al., 2014). Together with our findings, these results indicate that the geometrical changes at sub-cellular scale may be involved in the LFA-1 mediated adhesive haptotaxis due to the anisotropy of cell protrusions. Observations at single cell-level to analyze the protrusion dynamic is therefore necessary to assess this hypothesis.



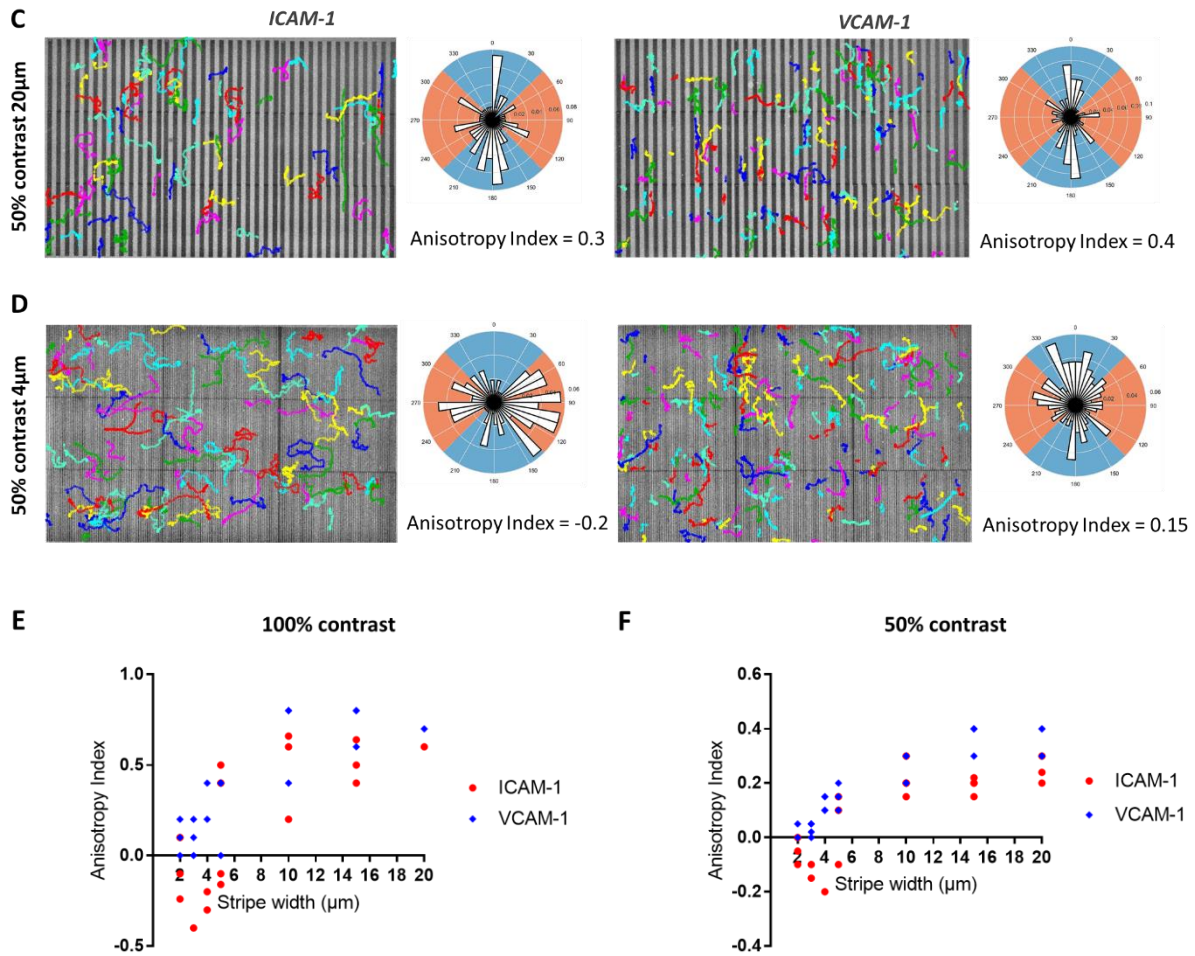


Figure 5-12 Geometrical perturbation induces orientation shift on ICAM-1 but not VCAM-1 substrates. Cell tracking results on ICAM-1 (left panel) and VCAM-1 (right panel) substrates with 100% and 50% adhesion and patterned with 20 μ m- or 4 μ m- wide patterns. (A) Positive control substrates with 100% adhesion contrast and patterned with 20 μ m-wide stripes where cells exhibited preferential haptotactic migration in the vertical quadrants (blue). (B) Positive control substrates with 100% adhesion contrast and patterned with 4 μ m-wide stripes where cells exhibited preferential haptotactic migration in the horizontal quadrants (crusta) on ICAM-1 but not on VCAM-1. (C) Substrates with 50% adhesion contrast and patterned with 20 μ m-wide stripes where cells exhibited preferential haptotactic migration in the vertical quadrants (blue). (D) Substrates with 50% adhesion contrast and patterned with 4 μ m-wide stripes where cells exhibited preferential haptotactic migration in the horizontal quadrants (crusta) on ICAM-1 and in the vertical quadrants (blue) on VCAM-1. Each color represents the trajectory of migrating cell. (E, F) Anisotropy Index versus the width of the stripes on substrates with 100% and 50% adhesion contrast, respectively.

5.8 Discussion

In this part of the work, we aimed to better understand why cells exhibit unique preference of low adhesion areas on ICAM-1 surface during adhesive haptotaxis. The initial hypothesis was that this could be linked to LFA-1 affinity and spatial distribution. To test this hypothesis, we carried out different experiments at cell population level targeting the LFA-1 integrin to modulate the preexisting phenotypes. Some of the integrin perturbation experiments are inconclusive because the cell mobility was often altered in these cases. Cells

became immobilized on the high adhesion zones by their rear and were no longer able to test different areas with modulated adhesion. Therefore, their haptotactic preference could no longer be determined. The perturbation experiment with Mn^{2+} reveals cell favoring high adhesion areas with "persistent" phenotype when their rear is partially adherent. Also, cell mobility was retained with the LFA-1 inhibition with lovastatin, which has yielded interesting observations. Even though the results were not entirely conclusive, they suggest that the phenotypes observed during LFA-1 mediated adhesive haptotaxis could still be associated with the adhesion level of each individual cell as cells again exhibited same phenotype distribution even when adhesion was globally decreased. Further investigation aiming at observing phenotypes of individual cells before and after perturbation may be of interest. On the other hand, the direct staining of LFA-1 integrin did not reveal apparent link between the phenotypes and the overall integrin expression level. Overall, the existence of haptotactic phenotypes cannot be simply be linked to LFA-1 integrin affinity and expression level based on our results.

Next, we also tried to understand whether the distribution of distinct haptotactic phenotypes could be related to pattern geometry. Indeed, the modification of the width of the pattern induced a new phenotype with complete orientation shift from parallel to perpendicular to the stripes on ICAM-1 coated substrates. This orientation shift occurred when the width of the stripe reached sub-cellular level ($4\mu m$) and only on ICAM-1 coated substrates. This astonishing change shows that geometrical parameters at sub-cellular scale could be involved in the mechanism behind the orientation shift of T lymphocytes given that similar mechanism has been reported for migration fibroblasts on patterned fibronectin (Caballero et al., 2015a, 2014, 2014).

While experiments at population level carried out in this part of the work have yielded useful information regarding parameters of cell migration and haptotaxis by tracking a large number of cells, they do not have enough resolution to observe the dynamic of the protrusion of individual cells, nor the possibility to investigate how individual cell responds to cues at sub-cellular level. It is therefore necessary to carry out experiments at single-cell level to obtain ampler information.

6 Adhesive haptotaxis at single-cell level

In this section, we plan to study the protrusion dynamic of T cell lamellipodia on patterned substrates using microscopic techniques. This part of the project is still on-going, and the upcoming subsection will present our initial findings of our assays at single-cell level.

6.1 Single-cell assay confirms different phenotypes present during adhesive haptotaxis

The first step of our investigation at single-cell level was to observe the migratory phenotypes that were present at cell population level on substrates with modulated adhesion (adhesion contrast around 50%). With the help of RICM and fluorescent microscopy, we were able to observe both the dynamic of cell lamellipodia and adhesion while locating them on the pattern. Figure 6-1-A (see also Movie 22) clearly demonstrates the typical “zig-zag” phenotype observed during LFA-1 mediated adhesive haptotaxis on ICAM-1 substrates and we were able to observe directly the lamellipodial dynamic. The “zig-zag” phenotype (cell on the right) resulted from the constant bouncing of the lamellipodia between two stripes with high adhesion while cell uropod remained detached, leading to the zig-zag trajectory of the cell on stripe with low adhesion. Our results at population level have also shown that cells exhibit preference towards high adhesion zones during VLA-4 mediated adhesive haptotaxis. Observation at single-cell level also revealed the dynamic of cell protrusion in this situation: Figure 6-1-B (see also Movie 23) shows that cell on VCAM-1 substrates had attached cell rear (shown by the RICM signal in green) and detached lamellipodia, which has been previously reported (Alexander Hornung et al., 2018). During cell migration, the attached rear limited its ability to advance and the detached lamellipodia was inefficient in detecting the adhesion of different zones. As a result, cell remained largely on high adhesion zone.

These results highlight that lamellipodia (protrusion at cell front) may indeed have crucial functions during the adhesive haptotaxis that has led to the characteristic phenotypes. Meanwhile, the cell rear appears to be a limiting factor that can regulate cell motility during adhesive haptotaxis. It is necessary to introduce sub-cellular adhesion modulation to assess how lamellipodial would response to such change in local adhesion to better understand its role in adhesive haptotaxis.

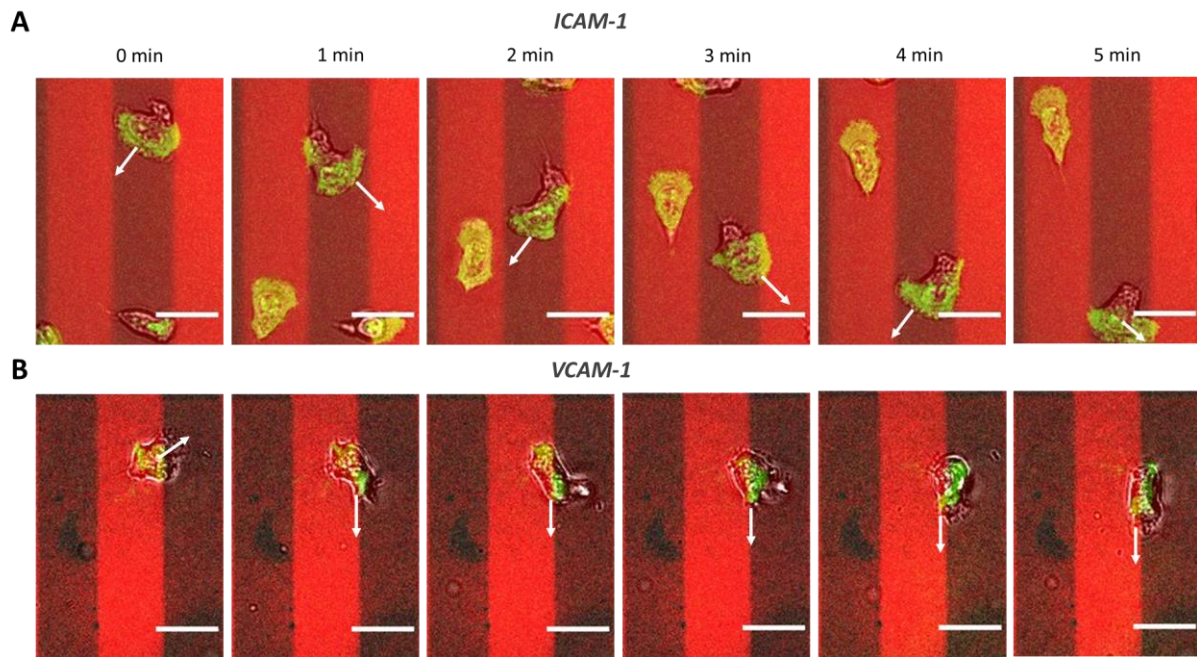


Figure 6-1 Single-cell assay confirms different phenotypes present during adhesive haptotaxis. (A) “Zig-zag” cell bouncing between two high adhesion stripes with adherent lamellipodia and detached uropod on ICAM-1 substrate. (B) Cell advancing on high adhesion stripe with detached lamellipodia and attached rear on VCAM-1 substrate. In red: fluorescent signal corresponding to integrin ligand concentration; In grey: bright-field image; In green: RICM adhesion footprint imaging. Scale bar= 20 μm

6.2 Subcellular level adhesion modulation reveals lamellipodia as adhesion sensor favoring the least adhesion zone

The first part of observation was still performed on patterns of 20 μm -wide stripes. To monitor lamellipodial response to adhesion modulation at subcellular level, Stripe-like patterns were generated using the same surface construction and patterning protocols but the geometry was modified (Figure 6-2): first, the width of the stripe was reduced to 10 μm and the adhesion between adjacent stripes was reduced to zero to confine cells on the adhesive stripe; second, each adhesive strip was divided into different sectors – a homogenous sector with maximal adhesion followed by a mixed sector where half of the stripe (5 μm in width) is of maximal adhesion and the other half of 50% adhesion. The adhesion contrast of the mixed sector is thus fixed at 50%. This pattern design would allow the lamellipodia of the cell to test two different areas of adhesion at subcellular scale.

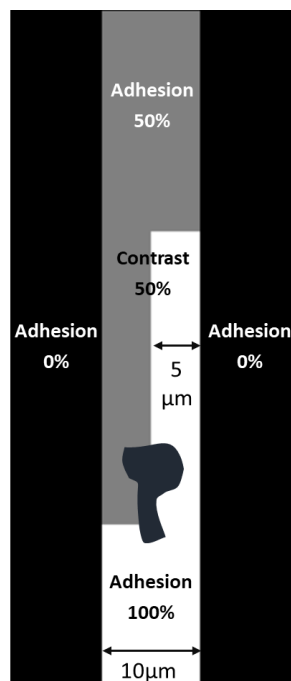


Figure 6-2 Illustration of pattern with adhesion modulation at subcellular level

Using phase-contrast microscopy combined with RICM and fluorescent microscopy, we looked at cell protrusion dynamics on both ICAM-1 and VCAM-1 substrates, especially when they crossed frontiers of homogenous and mixed sectors and migrated along the mixed sector of 50% contrast. Figure 6-3 shows sharp difference in how cell protrusion advanced on ICAM-1 and VCAM-1 surfaces. On ICAM-1 (Figure 6-3-A), cell had fully spread lamellipodia at the front with detached uropod. When cell was advancing along the patterned stripe, its lamellipodia constantly protruded at cell front as a detector towards non-adhesive area between adjacent stripe - the area with the lowest adhesion on the pattern - while the adherent patch indicated by RICM signal (color-coded in green) remained on area with higher adhesion (see also Movie 24). The lamellipodia protruded towards non adhesive area regardless of the respective adhesion level of each section of the pattern since cell tip protruded towards the non-adhesive area when migrating both over the homogenous and mixed sector (Figure 6-3-A, see also Movie 24). The situation on VCAM-1 was very different (Figure 6-3-B): cells on VCAM-1 had attached uropod and detached lamellipodia, as previously reported (Alexander Hornung et al., 2018). When the cell was unable to detach its rear, it became immobilized and remained adhered on areas with higher adhesion (such as the cell on the left in Figure 6-3-B). When cell was able to detach most of its rear, it regained some of its mobility and was able to advance on the pattern (such as the cell on the right in Figure 6-3-B). When advancing on patterned VCAM-1 stripes, cell moved forward with attached rear and elevated front. There was no flat lamellipodia at front enabling cell to probe local adhesion zones when migrating over the mixed sector. Phase contrast images shows that cell steadily advanced on area with higher adhesion with adhesion patch situated in the middle of the cell (Figure 6-3-B, see also Movie 25).

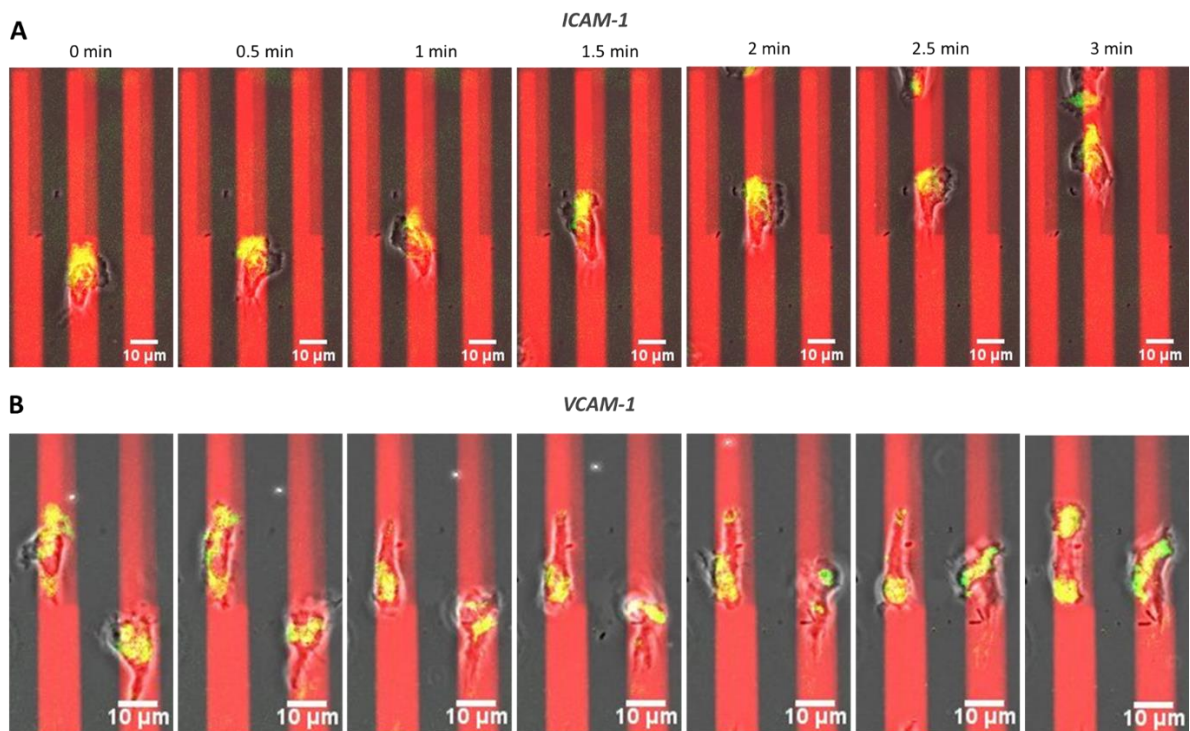


Figure 6-3 Subcellular adhesion modulation leads to different lamellipodial dynamic on ICAM-1 and VCAM-1. (A) Migrating cell with lamellipodia protruding towards area with the least adhesion. (B) Cell immobilized by its rear (left) and cell advancing with attached rear and detached lamellipodia (right). In red: fluorescent signal corresponding to integrin ligand concentration; In grey: bright-field image; In green: RICM adhesion footprint imaging. Scale bar=10 μm

6.3 Discussion

In this part of preliminary investigation at single-cell level, we were able to observe directly the lamellipodial dynamics mediated by LFA-1 and VLA-4 integrins with both cellular and subcellular level adhesion modulation, which cannot be achieved by analysis at cell population level with or without perturbation.

With adhesion modulation at cellular level, direct observation of cell lamellipodia has confirmed different migratory phenotypes mediated by LFA-1 and VLA-4 integrins and indicated the crucial function of lamellipodia in adhesion sensing during T cell adhesive haptotaxis. Bouncing of lamellipodia between high adhesion zones has resulted in the predominant “zig-zag” phenotype on ICAM-1; attached rear and detached lamellipodia has led to the preference towards high adhesion on VCAM-1.

With adhesion modulation at sub-cellular level, observation of cell protrusion has confirmed the important role of lamellipodia as adhesion sensor. On ICAM-1 substrates, lamellipodia sense different adhesion level of the local substrate and constantly protrude towards the area with the least adhesion. This sensing function is abolished on VCAM-1 substrate due to detached lamellipodia and the attached rear becomes dominant in keeping cell on high adhesion zone.

These observations are consistent with our tracking results at cell population level. Previous studies on mesenchymal adhesive haptotaxis have reported lamellipodia as indispensable haptotactic sensor and protrude toward the gradient on fibronectin substrates with fibroblasts (King et al., 2016; Wu et al., 2012). Depletion of certain actin regulators, especially the upstream regulators of Arp2/3 such as Rac1, Rac GEF Tiam1 and WAVE regulatory complex, perturbs differential lamellipodial dynamics and abrogates haptotaxis. (King et al., 2016). Together with our findings, it may be interesting to assess the effect of lamellipodial perturbation on T cell adhesive haptotaxis by targeting relevant actin regulators.

7 Adhesive haptotaxis at population level with perturbation of lamellipodial dynamic

In this chapter, we will investigate the role of lamellipodial dynamic in T cell adhesive haptotaxis at cell population level by perturbing regulatory proteins of the lamellipodia. This part of the work is still ongoing, and we will present our preliminary findings on the perturbation of two actin regulators.

7.1 WASP-deficient T cells exhibit unimpaired adhesive haptotaxis with dominant “zig-zag” phenotype

WASP is a key member of a family of proteins that play an important role in transferring signals from cell surface receptors to the actin cytoskeleton by activating Arp2/3-mediated actin polymerization (Ochs & Thrasher, 2006; Thrasher, 2002). Lack of WASP expression results in a wide range of cellular defects including impaired immune cell migration (Notarangelo, Notarangelo, & Ochs, 2005; Thrasher, 2002). Migration of multiple immune cells lineages including lymphocytes has been shown to be defective in both human and murine models of WASP deficiency (Gallego et al., 2006; Noronha et al., 2005; Snapper et al., 2005; Westerberg et al., 2005). These abnormalities have been variously ascribed to processes of chemotaxis, adhesion and migration under physiological shear flow. Based on these findings, we suspected that WASP deficiency may lead to changes in T cell adhesive haptotaxis by altering lamellipodial dynamics. To test this hypothesis, both T cells from healthy donor and WAS patients, which were a generous gift from Dr. Loïc Dupré (Inserm, Toulouse, France) were incubated on patterned ICAM-1 surfaces and subject to migration assay. Bright-field images show that cells from healthy donor and patient polarized and adhered on the substrates (Figure 7-1-top, see also Movie 26). Cell tracking revealed that WASP deficient cells adhered slightly less than control cells; in terms of motility, the percentage of tracked cells was also slightly lower in WASP-deficient cells but the speed remained constant for remaining cells in both groups (Table 7-1). On the other hand, the adhesive haptotaxis remained unimpaired for cells lacking WASP in comparison to control cells: the Anisotropy Index was 0.4 for both cell types and cell trajectories revealed the dominant “zig-zag” phenotype favoring areas with low adhesion (Figure 7-1-bottom and Table 7-1). These results show that the perturbation of WASP alone was not enough to alter the adhesive haptotaxis. This may be because WASP is one of the upstream proteins regulating the activity of lamellipodia via Arp2/3 and the presence of other upstream regulators may compensate the perturbation (Thrasher, 2002). Moreover, as an upstream regulator, WASP may not have direct link to integrin and therefore be inefficient in regulating integrin mediated adhesive haptotaxis.

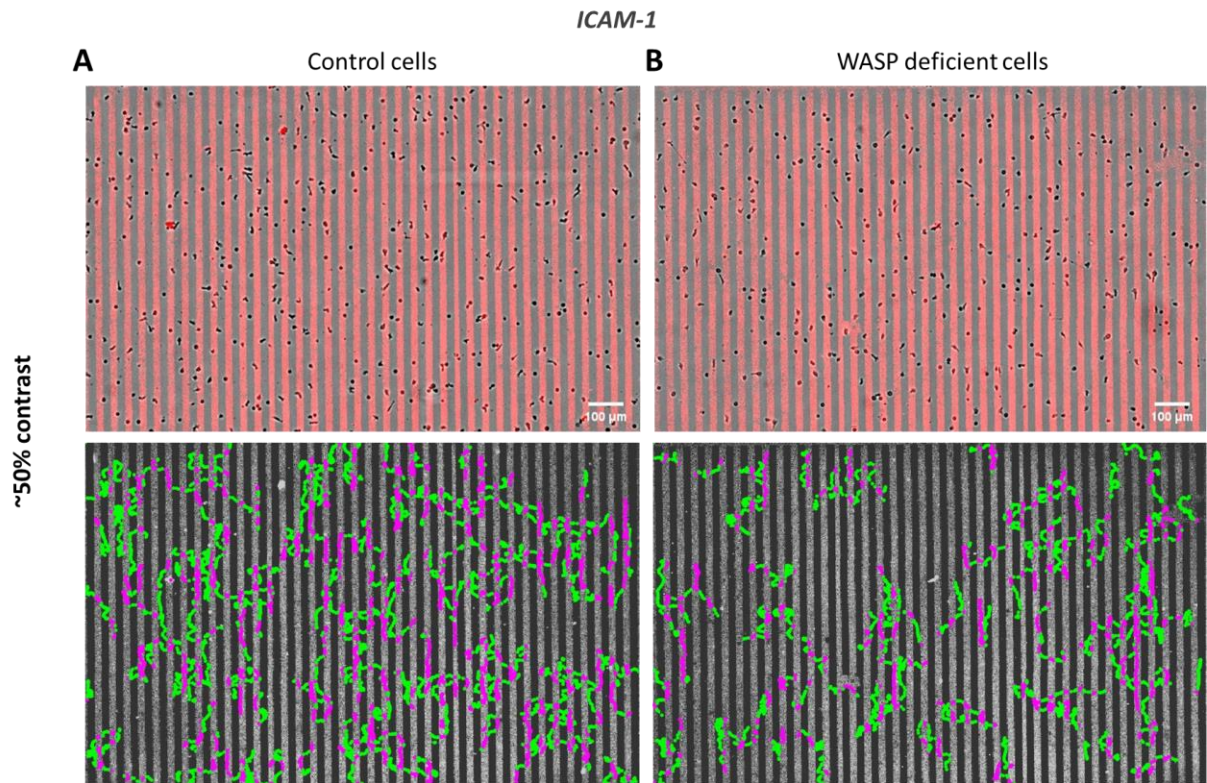


Figure 7-1 WASP depletion leads to no direct change in adhesive haptotaxis. (A) Control (left) and WASP deficient cells (right) adhering on patterned stripes. In grey: brightfield image showing cell body; In red: fluorescent image of patterned stripes. Scale bar=100 μm . (B) Trajectories of tracked control (left) and treated cells (right) shown on the background of patterned stripes. In green: cell tracks on low adhesion zones; In magenta: cell tracks on high adhesion zones.

	Control cells	WASP deficient cells
Adherent cells post-rinsing	514	448
Tracked cells	25%	18%
Anisotropy Index	0.4	0.4
% cells on high adhesion zones	46%	47%
Average speed ($\mu\text{m}/\text{min}$)	11	10

Table 7-1 Summary of different migration parameters for control and WASP deficient cells.

7.2 VASP knock-out cells exhibit unimpaired adhesive haptotaxis with slightly reduced “zig-zag” phenotype

We then targeted another key actin regulator protein VASP (vasodilator-stimulated phosphoprotein). VASP promotes actin filament elongation. It protects the barbed end of growing actin filaments against capping and increases the rate of actin polymerization in the presence of capping protein. VASP stimulates actin filament elongation by promoting the transfer of profilin-bound actin monomers onto the barbed end of growing actin filaments. In the cellular protrusion, VASP is enriched at the tip of the lamellipodia and thus participates actively in the regulation of lamellipodial dynamics. Antagonism between VASP and capping proteins regulate lamellipodial protrusion: elevated VASP activity at the leading edge antagonizes actin capping protein activity, which results in longer and less branched filaments and increases lamellipodial protrusion speed but with less persistence (Krause, Bear, Loureiro, & Gertler, 2002). On the contrary, decreased VASP activity at the leading edge results in shorter, more branched actin networks and leads to higher lamellipodial persistence and lower whole cell speed (Krause et al., 2002). VASP has also been shown to form complex with Rap1-GTP–interacting adaptor molecule (RIAM) and subsequently increased binding of talin to β_1 integrin (Worth et al., 2010). Barnhart et al. have shown in their study on fish keratocytes that VASP localizes both in the adhesion complex and the leading edge (Barnhart, Allard, Lou, Theriot, & Mogilner, 2017). Interestingly, they have shown that VASP regulates the protrusion of keratocytes in an adhesion-dependent manner where protrusion waves are due to fluctuations in actin polymerization rates and overexpression of VASP switches highly adherent keratocyte from waving to persistent protrusion (Barnhart et al., 2017). The authors have proposed that local depletion of VASP from the leading edge by high substrate adhesion – along with lateral propagation of protrusion due to the branched actin network – results in regular protrusion wave (Barnhart et al., 2017).

These findings in the literature have shown that VASP regulates lamellipodial dynamics with direct link to integrin in an adhesion-dependent manner. The VASP activity could thus influence the cell protrusion dynamics on patterned substrates with modulated adhesion and alter cell phenotypes during T cell adhesive haptotaxis. To test this hypothesis, VASP deficient effector T cells were generated by LAI engineer Martine Pélicot with the CRISPR-Cas9 method. Briefly, crRNA and tracrRNA were mixed at 200 μ M and heated at 95°C for 5min. After cooling down to room temperature, the RNA duplex was incubated with pre-diluted Cas9 enzyme at 36 μ M for 10-20min at room temperature to form the RNP complex. PBMCs were activated with CD3/CD28 beads as described in 2.1. Two days after the activation, the beads were removed, and cells were used for transfection by electroporation (1500V, 1 pulse 20ms) to introduce the RNP complex into the cells. Transfected cells were cultured as described in 2.1. Transfection efficiency was assessed either by flow cytometry or by western blot 5 days post-

transfection and determined at 80%. Cells were ready to be used for migration assay 5 days post-transfection.

Human effector T cells deficient in VASP, together with control cells, were subject to migration assay. Bright-field images show that both control and VASP deficient cells polarized and adhered (Figure 7-2-A-top). Cell tracking analysis reveals that cell adhesion and mobility remained unimpaired despite the VASP deficiency (Table 7-2, see also Movies 27). Adhesive haptotaxis remained present for both cell groups as indicated by the anisotropy index (Table 7-2). Cell trajectories indicated again the preference for the less adhesive patterns (Figure 7-2-A-bottom and Table 7-2). Nevertheless, a slight change in migratory phenotype can be noticed from VASP deficient cells (Figure 7-2-A-bottom): while control cells exhibited drastic “zig-zag” trajectories (in green) resulting from cell bouncing on less adhesive patterns, this phenomenon appears to be reduced among VASP deficient cells (see also Movie 27). VASP deficient cells appear to bounce less between the patterned stripes and become more prone to continue migrating in their original direction, which can be shown by the repetitive horizontal trajectories crossing the stripes. These results indicate that even though the overall preference at cell population level is still towards the less adhesive areas, the VASP deficiency may have perturbed the leading-edge protrusion dynamics, which is worth being further explored.

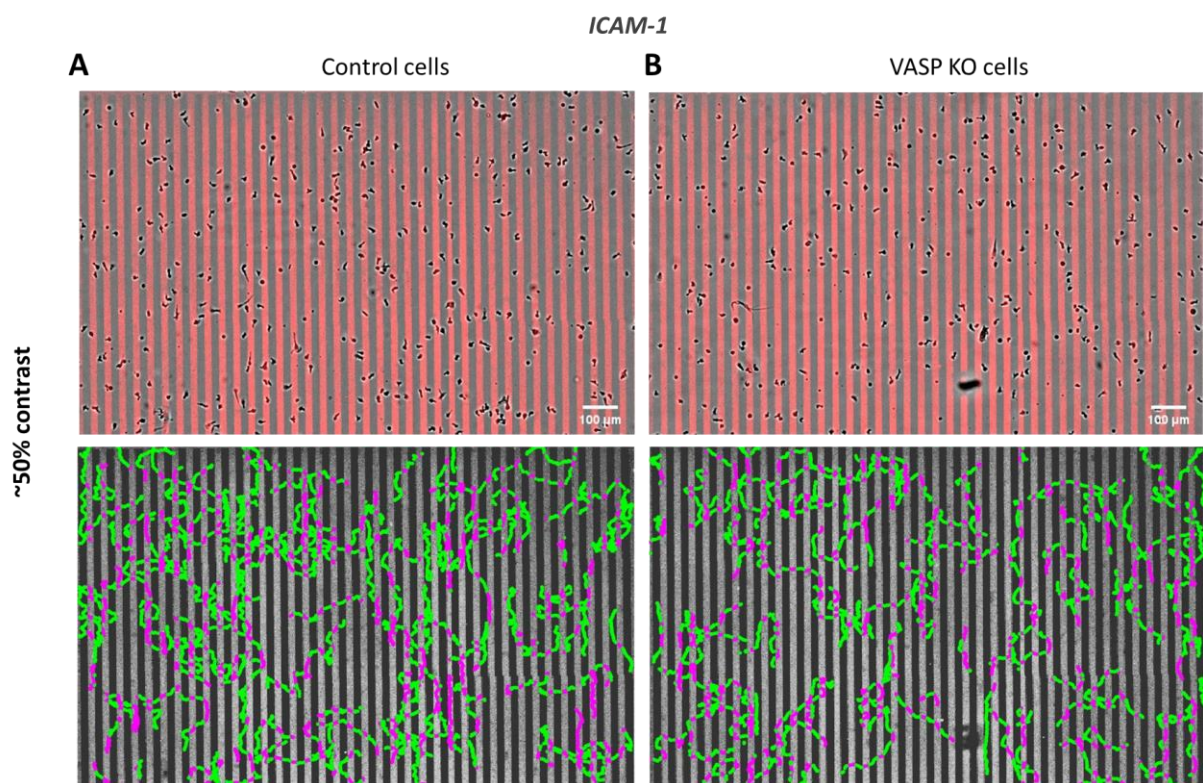


Figure 7-2 VASP knock-out cells exhibit unimpaired adhesive haptotaxis with slightly reduced “zig-zag” phenotype. (A) Control (left) and VASP deficient cells (right) adhering on patterned stripes. In grey: brightfield image showing cell body; In red: fluorescent image of patterned stripes. Scale bar=100μm. (B) Trajectories of

tracked control (left) and treated cells (right) shown on the background of patterned stripes. In green: cell tracks on low adhesion zones; In magenta: cell tracks on high adhesion zones.

	Control cells	VASP KO cells
Adherent cells post-rinsing	388	344
Tracked cells	38%	35%
Anisotropy Index	0.2	0.2
% cells on high adhesion zones	46%	45%
Average speed ($\mu\text{m}/\text{min}$)	17	16

Table 7-2 Summary of different migration parameters for control and WASP deficient cells.

7.3 Discussion

In this part of the ongoing work, we continued to probe what has mediated the presence of the unique “zig-zag” phenotype preferring the less adhesive patterns on ICAM-1 during T cell adhesive haptotaxis by targeting two key actin regulators in lamellipodia formation: WASP and VASP. we aimed to target these two regulatory proteins to disrupt the lamellipodial dynamic and to observe whether this could lead to phenotypic shift at the cell population level between the two “persistent” and “zig-zag” phenotypes.

With WAS depleted cells, even though previous studies have reported deficient T cell adhesion, chemotaxis and migration under flow (Snapper et al., 2005), the adhesive haptotaxis remains unimpaired with the dominant “zig-zag” phenotype and the preference towards the less adherent areas. Our experiments have shown that the deficiency in WASP does not appear to disrupt the adhesive haptotaxis. The fact that disruption of WASP alone has little effect on adhesive haptotaxis and corresponding phenotypes could be due to the abundance of different proteins that participate in the regulation of Arp2/3 complex and the lamellipodial dynamics (Swaney & Li, 2016) that cells use to finetune their actin network dynamic to adapt to internal perturbations or extracellular environments. As a result, disruption of one of these regulators may not be enough to induce a global change during adhesive haptotaxis. Another reason may be that the targeted protein is known to bind other upstream regulatory proteins but not directly to integrin receptors (Thrasher, 2002). Since the adhesive haptotaxis is mediated by the integrins through modulated substrate adhesiveness, such lack of direct connection between these actin regulators and the integrin may have resulted in the lack of direct disruption of adhesive haptotaxis, as the indirect disruption could also have been compensated by other abundantly present regulator proteins.

Therefore, VASP was chosen as a second target. As an important anti-capping protein, VASP is also known to form complex with RIAM which leads to talin binding the $\beta 1$ tail of the integrin – thus forming a direct link between VASP and the integrin adhesion complex (Worth

et al., 2010). Recently study has indeed demonstrated in fish keratocytes that on highly adhesive and homogenous substrates, local depletion of VASP due to strong substrate adhesion can result in keratocyte waving- asymmetrical lateral lamellipodial protrusion (Barnhart et al., 2017). These findings have encouraged us to analyze the potential effect of VASP deficiency on T cell adhesive haptotaxis. Our migration assays with VASP depleted cells have revealed that cell adhesion and migration remain unimpaired and the adhesive haptotaxis is still present. However, some cells have appeared to become indifferent to the patterns and thus continue to migrate in their original direction by crossing the stripes instead of bouncing between adjacent stripes. Other cells that remained guided in the vertical direction also seem to exhibit reduced “zig-zag” trajectories by bouncing less between stripes. This slight phenotypic shift occurred at the population level suggests that even though VASP may not alter completely the adhesive haptotaxis, it may still have changed the lamellipodial dynamic to some extent, which may not have been fully reflected by analysis at cell population level. Future investigations with VASP depleted cells at single cell level to monitor lamellipodial dynamic of individual cells would be necessary.

8 Conclusion and perspective

T lymphocytes are at the center of the adaptive immune system and their directional migration is crucial for their proper functions. Although different components and guidance cues involved in T cell migration have been studied in the past, many questions, especially ones regarding the potential guidance by adhesion, remain open. This is partially due to the limits of *in vivo* experimental systems and models as well as the lack of robust and quantifiable *in vitro* assays. During this PhD project, we aim to develop an *in vitro* quantitative assay to study the adhesive haptotaxis of human effector T cells. Within the framework of this project, we have achieved the following objectives:

Firstly, we have successfully implemented the optical patterning system to our study on T cell migration through extensive troubleshooting and technical optimization during the first part of the project. As a result, we have created functional substrates with integrin ligands for T cell migration study that can be further implemented into a quantitative assay in a microfluidic system. The adhesion of the substrates can be modulated with optical patterning with any designed pattern profile. More importantly, each parameter of the assay can be quantified for each experiment: the adhesion rate of the substrate was quantified by cell adhesion assay under flow; cell migration was quantified with different migration parameters thanks to the cell tracking program; the ligand density was also quantified using fluorescent antibody quantification method. This assay allows us to study substrate adhesiveness induced haptotaxis in highly controlled environment where all the parameters can be quantified. Moreover, the first part of technical optimization has also allowed us to better understand different aspects of this novel patterning technique and its applications to leukocyte-related assays. During this process, we have standardized various protocols regarding substrate preparation and the optical patterning designed for different applications. Not only has this ensured the reproducibility of our assay in this project, this extensive optimization phase has also paved the way for future projects using this technique: two independent PhD projects are in progress, one related to the T cell homing and intranodal trafficking and the other related to antibody micropatterning. This newly developed technique will open doors and help us better answer the remaining questions regarding leukocyte motility and guidance.

Secondly, after the initial technical optimization, we have set out to study the T cell adhesive haptotaxis. The existence of adhesive haptotaxis is not conceptually straightforward for amoeboid cells as they, unlike their mesenchymal counterparts, can migrate with minimal interaction with the underlying substrate. To the best of our knowledge, adhesive haptotaxis has never been evidenced for amoeboid cells in the past. In this project, with our single parameter haptotaxis assay where cells were subject to an adhesion gradient with infinite slope and various concentration ranges, we have shown that T cells exhibit robust adhesive haptotaxis on both ICAM-1 and VCAM-1 substrates, demonstrated by their directional

anisotropy on patterned surfaces with modulated adhesion. Moreover, we have also shown that different integrins mediate different haptotactic phenotypes: T cells prefer migrating on VCAM-1 substrate towards higher adhesion areas, whereas on ICAM-1 substrates, they counterintuitively prefer migrating on areas with lower adhesion. With our modified single parameter assay where we fixed concentration range and varied the slope to create a gradient roller-coaster, we further confirmed this unique phenomenon, which suggest that T cells may adopt an alternative mechanism other than the “tug-of-war” employed by mesenchymal cells during their adhesive haptotaxis. Meanwhile, calcium flux monitoring showed that the mechanotransduction was not involved, suggesting that an intermediate mechanism between active mechanotransduction and passive leading-edge competition mediated by integrins may be involved.

Thirdly, after confirming the existence of T cell adhesive haptotaxis and unique migratory phenotypes during LFA-1 mediated adhesive haptotaxis, we have proceeded to decipher the underlying mechanisms behind this interesting phenomenon. Several lines of investigation were pursued both at cell population and single cell level. A series of integrin perturbation experiences was first performed: LFA-1 activation has reduced the “zig-zag” phenotype and led to more cells on high adhesion zones. On the contrary, inhibition of LFA-1 has resulted in dominant “zig-zag” phenotype with more cells favoring low adhesion zones. These perturbation experiments have also revealed that the “persistent” phenotype resulted from cells migrating with attached rear and the “zig-zag” phenotype from cells migrating with detached rear and attached lamellipodia. Lamellipodial dynamic study at single-cell level has further confirmed that cells used lamellipodia as an adhesion sensor and constantly protruded towards the least adhesive areas when cell had attached lamellipodia and detached rear. This adhesion sensing was lost due to detached lamellipodia and attached uropod. On the other hand, the overall expression integrin level does not appear to be correlated with the presence of different phenotypes. Though further investigation is necessary to reach final confirmation, the mechanism behind the integrin-mediated adhesive haptotaxis appears to be highly related to the sensing ability of the lamellipodia which can be limited by the cell rear.

In the near future, the challenge would be to fully unveil the mechanism that is responsible for the LFA-1 mediated T cell adhesive haptotaxis and the unique “zig-zag” phenotype that prefers areas with lower adhesion. Several lines of investigation can be followed: The effect of local anisotropy has been reported in fibroblast directional migration (Caballero, Comelles, Piel, Voituriez, & Riveline, 2015b). However, the reported effect still stems from the “tug-of-war” mechanism used by mesenchymal cells resulting in preference of high adhesion zone, which is not the case during LFA-1 mediated T cell adhesive haptotaxis. The effect of subcellular geometrical cue on T cells (or ameboid cells in general) may be worthy of further exploration both at population and single-cell level. In our case, it would be interesting to further modify the geometry of the patterns (for instance, by varying the stripe width, distance or both) to introduce a new level of local anisotropy in adhesion at subcellular

level and to assess how T cells would respond to these anisotropic cues. Moreover, given the role of VASP in regulating lamellipodia directly through integrin, it would also be interesting to check, both at population and single-cell level, the response on patterns with subcellular geometrical cues on both VASP depleted and wildtype cells.

The present work has shed light on the guiding effect of integrins during T cell planar migration. In the longer term, it would be interesting to complexify the *in vitro* system to better mimic the *in vivo* microenvironment and decipher the role of different guidance cues involved during T cell migration. For instance, although in homeostatic conditions, leukocyte interstitial migration is integrin-independent, it becomes integrin-dependent under inflammatory conditions (Overstreet et al., 2013) and may regulate T cell interstitial crawling (C. H. Kim, 2014). It would first be interesting to analyze the potential guiding role of integrin in 3D migration under inflammatory conditions. Moreover, several chemical cues are known to be surface-bound and may be potentially haptotactic for T cell migration (Okada et al., 2002). Another logic development of the current work would then be implementing the current system to create patterns of one or multiple surface-bound molecules to decipher T cell haptotaxis induced by one or multiple chemical cues. Moreover, these patterns can also be coupled with gradients of integrin-ligands to study the potential combinatory effect of the chemokines and integrins

9 Bibliography

- Abadier, M., Haghayegh Jahromi, N., Cardoso Alves, L., Boscacci, R., Vestweber, D., Barnum, S., ... Lyck, R. (2015). Cell surface levels of endothelial ICAM-1 influence the transcellular or paracellular T-cell diapedesis across the blood-brain barrier. *European Journal of Immunology*, *45*(4), 1043–1058. <https://doi.org/10.1002/eji.201445125>
- Aizel, K., Clark, A. G., Simon, A., Geraldo, S., Funfak, A., Vargas, P., ... Bremond, N. (2017). A tuneable microfluidic system for long duration chemotaxis experiments in a 3D collagen matrix. *Lab Chip*, *17*, 3851–3861. <https://doi.org/10.1039/C7LC00649G>
- Akira, S., Uematsu, S., & Takeuchi, O. (2006). Pathogen Recognition and Innate Immunity. *Cell*, *124*(4), 783–801. <https://doi.org/10.1016/j.cell.2006.02.015>
- Alberts, B., Johnson, A., Lewis, J., Raff, M., Roberts, K., & Walter, P. (2002). *Molecular Biology of the Cell* (4th ed.). Garland Science.
- Alon, R., Hammer, D. A., & Springer, T. A. (1995). Lifetime of the P-selectin-carbohydrate bond and its response to tensile force in hydrodynamic flow. *Nature*, *374*(6522), 539–542. <https://doi.org/10.1038/374539a0>
- Alon, Ronen, & Dustin, M. L. (2007). Force as a Facilitator of Integrin Conformational Changes during Leukocyte Arrest on Blood Vessels and Antigen-Presenting Cells. *Immunity*, *26*(1), 17–27. <https://doi.org/10.1016/j.immuni.2007.01.002>
- Alon, Ronen, & Feigelson, S. W. (2009). Chemokine Signaling to Lymphocyte Integrins Under Shear Flow. *Microcirculation*, *16*(1), 3–16. <https://doi.org/10.1080/10739680802026076>
- Ambravaneswaran, V., Wong, I. Y., Aranyosi, A. J., Toner, M., & Irimia, D. (2010). Directional decisions during neutrophil chemotaxis inside bifurcating channels. *Integrative*

Biology: Quantitative Biosciences from Nano to Macro, 2(11–12), 639–647.

<https://doi.org/10.1039/c0ib00011f>

Andrew, N., & Insall, R. H. (2007). Chemotaxis in shallow gradients is mediated independently of PtdIns 3-kinase by biased choices between random protrusions.

Nature Cell Biology, 9(2), 193–200. <https://doi.org/10.1038/ncb1536>

Aoun, L., Negre, P., Farutin, A., Garcia-Seyda, N., Rivzi, M. S., Galland, R., ... Theodoly, O. (2019). Mammalian Amoeboid Swimming is propelled by molecular and not protrusion-based paddling in Lymphocytes. *BioRxiv*, 509182.

<https://doi.org/10.1101/509182>

Auffray, C., Fogg, D., Garfa, M., Elain, G., Join-Lambert, O., Kayal, S., ... Geissmann, F. (2007). Monitoring of Blood Vessels and Tissues by a Population of Monocytes with Patrolling Behavior. *Science*, 317(5838), 666–670.

<https://doi.org/10.1126/science.1142883>

Azioune, A., Carpi, N., Tseng, Q., Th, M., & Piel, M. (2010). Chapter 8 - Protein Micropatterns: A Direct Printing Protocol Using Deep UVs. *Methods in Cell Biology - Volume 97*, 97, 133–146. [https://doi.org/10.1016/S0091-679X\(10\)97008-8](https://doi.org/10.1016/S0091-679X(10)97008-8)

Azioune, A., Storch, M., Bornens, M., Théry, M., & Piel, M. (2009). Simple and rapid process for single cell micro-patterning. *Lab on a Chip*, 9(11), 1640–1642.

<https://doi.org/10.1039/B821581M>

Aznavoorian, S., Stracke, M. L., Krutzsch, H., Schiffmann, E., & Liotta, L. A. (1990). *Signal Transduction for Chemotaxis and Haptotaxis by Matrix Molecules in Tumor Cells*. 110, 1427–1438. <https://doi.org/10.1083/jcb.110.4.1427>

Bajénoff, M., Egen, J. G., Koo, L. Y., Laugier, J. P., Brau, F., Glaichenhaus, N., & Germain, R. N. (2006). Stromal Cell Networks Regulate Lymphocyte Entry, Migration, and

- Territoriality in Lymph Nodes. *Immunity*, 25(6), 989–1001.
<https://doi.org/10.1016/j.immuni.2006.10.011>
- Bajénoff, M., Egen, J. G., Qi, H., Huang, A. Y. C., Castellino, F., & Germain, R. N. (2007).
Highways, byways and breadcrumbs: directing lymphocyte traffic in the lymph node.
Trends in Immunology, 28(8), 346–352. <https://doi.org/10.1016/j.it.2007.06.005>
- Barnhart, E. L., Allard, J., Lou, S. S., Theriot, J. A., & Mogilner, A. (2017). Adhesion-dependent
wave generation in crawling cells. *Current Biology : CB*, 27(1), 27–38.
<https://doi.org/10.1016/j.cub.2016.11.011>
- Bartholomäus, I., Kawakami, N., Odoardi, F., Schläger, C., Miljkovic, D., Ellwart, J. W., ...
Flügel, A. (2009). Effector T cell interactions with meningeal vascular structures in
nascent autoimmune CNS lesions. *Nature*, 462(7269), 94–98.
<https://doi.org/10.1038/nature08478>
- Bear, J. E., & Haugh, J. M. (2014). Directed migration of mesenchymal cells: Where signaling
and the cytoskeleton meet. *Current Opinion in Cell Biology*, 30(1), 74–82.
<https://doi.org/10.1016/j.ceb.2014.06.005>
- Bear, J. E., Svitkina, T. M., Krause, M., Schafer, D. A., Loureiro, J. J., Strasser, G. A., ... Gertler,
F. B. (2002). Antagonism between Ena/VASP proteins and actin filament capping
regulates fibroblast motility. *Cell*, 109(4), 509–521.
- Bélisle, J. M., Correia, J. P., Wiseman, P. W., Kennedy, T. E., & Costantino, S. (2008).
Patterning protein concentration using laser-assisted adsorption by photobleaching,
LAPAP. *Lab on a Chip*, 8(12), 2164–2167. <https://doi.org/10.1039/B813897D>
- Bélisle, J. M., Kunik, D., & Costantino, S. (2009). Rapid multicomponent optical protein
patterning. *Lab on a Chip*, 9(24), 3580–3585. <https://doi.org/10.1039/B911967A>

- Beningo, K. A., Dembo, M., Kaverina, I., Small, J. V., & Wang, Y. L. (2001). Nascent focal adhesions are responsible for the generation of strong propulsive forces in migrating fibroblasts. *The Journal of Cell Biology*, *153*(4), 881–888.
- Benvenuti, F., Hugues, S., Walmsley, M., Ruf, S., Fetler, L., Popoff, M., ... Amigorena, S. (2004). Requirement of Rac1 and Rac2 Expression by Mature Dendritic Cells for T Cell Priming. *Science*, *305*(5687), 1150–1153. <https://doi.org/10.1126/science.1099159>
- Berlin, C., Bargatze, R. F., Campbell, J. J., von Andrian, U. H., Szabo, M. C., Hasslen, S. R., ... Butcher, E. C. (1995). $\alpha 4$ integrins mediate lymphocyte attachment and rolling under physiologic flow. *Cell*, *80*(3), 413–422. [https://doi.org/10.1016/0092-8674\(95\)90491-3](https://doi.org/10.1016/0092-8674(95)90491-3)
- Berthier, E., Surfus, J., Verbsky, J., Huttenlocher, A., & Beebe, D. (2010). An arrayed high-content chemotaxis assay for patient diagnosis. *Integrative Biology*, *2*(11–12), 630–638. <https://doi.org/10.1039/c0ib00030b>
- Bonilla, F. A., & Oettgen, H. C. (2010). Adaptive immunity. *Journal of Allergy and Clinical Immunology*, *125*(2), S33–S40. <https://doi.org/10.1016/j.jaci.2009.09.017>
- Boscacci, R. T., Pfeiffer, F., Gollmer, K., Sevilla, A. I. C., Martin, A. M., Soriano, S. F., ... Stein, J. V. (2010). Comprehensive analysis of lymph node stroma-expressed Ig superfamily members reveals redundant and nonredundant roles for ICAM-1, ICAM-2, and VCAM-1 in lymphocyte homing. *Blood*, *116*(6), 915–925. <https://doi.org/10.1182/blood-2009-11-254334>
- Böttcher, R. T., Veelders, M., Rombaut, P., Faix, J., Theodosiou, M., Stradal, T. E., ... Fässler, R. (2017). Kindlin-2 recruits paxillin and Arp2/3 to promote membrane protrusions during initial cell spreading. *J Cell Biol*, *216*(11), 3785–3798. <https://doi.org/10.1083/jcb.201701176>

- Bouma, G., Burns, S. O., & Thrasher, A. J. (2009). Wiskott–Aldrich Syndrome: Immunodeficiency resulting from defective cell migration and impaired immunostimulatory activation. *Immunobiology*, *214*(9–10), 778–790. <https://doi.org/10.1016/j.imbio.2009.06.009>
- Boyton, R. J., & Openshaw, P. J. (2002). Pulmonary defences to acute respiratory infection. *British Medical Bulletin*, *61*(1), 1–12. <https://doi.org/10.1093/bmb/61.1.1>
- Brandley, B. K., & Schnaar, R. L. (1989). Tumor cell haptotaxis on covalently immobilized linear and exponential gradients of a cell adhesion peptide. *Developmental Biology*, *135*(1), 74–86. [https://doi.org/10.1016/0012-1606\(89\)90159-0](https://doi.org/10.1016/0012-1606(89)90159-0)
- Breitsprecher, D., Koestler, S. A., Chizhov, I., Nemethova, M., Mueller, J., Goode, B. L., ... Faix, J. (2011). Cofilin cooperates with fascin to disassemble filopodial actin filaments. *Journal of Cell Science*, *124*(19), 3305–3318. <https://doi.org/10.1242/jcs.086934>
- Bromley, S. K., Mempel, T. R., & Luster, A. D. (2008). Orchestrating the orchestrators: chemokines in control of T cell traffic. *Nature Immunology*, *9*(9), 970–980. <https://doi.org/10.1038/ni.f.213>
- Buffone, A., Anderson, N. R., & Hammer, D. A. (2018). Migration against the direction of flow is LFA-1-dependent in human hematopoietic stem and progenitor cells. *J Cell Sci*, *131*(1), jcs205575. <https://doi.org/10.1242/jcs.205575>
- Butler, K. L., Ambravaneswaran, V., Agrawal, N., Bilodeau, M., Toner, M., Tompkins, R. G., ... Irimia, D. (2010). Burn injury reduces neutrophil directional migration speed in microfluidic devices. *PloS One*, *5*(7), e11921. <https://doi.org/10.1371/journal.pone.0011921>

- Caballero, D., Comelles, J., Piel, M., Voituriez, R., & Riveline, D. (2015a). Ratchetaxis: Long-Range Directed Cell Migration by Local Cues. *Trends in Cell Biology*, 25(12), 815–827. <https://doi.org/10.1016/j.tcb.2015.10.009>
- Caballero, D., Comelles, J., Piel, M., Voituriez, R., & Riveline, D. (2015b). Special Issue: Quantitative Cell Biology Ratchetaxis: Long-Range Directed Cell Migration by Local Cues. *Trends in Cell Biology*, 25, 815–827. <https://doi.org/10.1016/j.tcb.2015.10.009>
- Caballero, D., Voituriez, R., & Riveline, D. (2014). Protrusion Fluctuations Direct Cell Motion. *Biophysical Journal*, 107(1), 34–42. <https://doi.org/10.1016/j.bpj.2014.05.002>
- Campbell, I. D., & Humphries, M. J. (2011). Integrin Structure, Activation, and Interactions. *Cold Spring Harbor Perspectives in Biology*, 3(3), a004994. <https://doi.org/10.1101/cshperspect.a004994>
- Carman, C. V., Sage, P. T., Sciuto, T. E., de la Fuente, M. A., Geha, R. S., Ochs, H. D., ... Springer, T. A. (2007). Transcellular Diapedesis Is Initiated by Invasive Podosomes. *Immunity*, 26(6), 784–797. <https://doi.org/10.1016/j.immuni.2007.04.015>
- Carman, C. V., & Springer, T. A. (2003). Integrin avidity regulation: are changes in affinity and conformation underemphasized? *Current Opinion in Cell Biology*, 15(5), 547–556. <https://doi.org/10.1016/j.ceb.2003.08.003>
- Carman, C. V., & Springer, T. A. (2004). A transmigratory cup in leukocyte diapedesis both through individual vascular endothelial cells and between them. *The Journal of Cell Biology*, 167(2), 377–388. <https://doi.org/10.1083/jcb.200404129>
- Carman, C. V., & Springer, T. A. (2008). Trans-cellular migration: cell-cell contacts get intimate. *Current Opinion in Cell Biology*, 20(5), 533–540. <https://doi.org/10.1016/j.ceb.2008.05.007>

- Carpi, N., Piel, M., Azioune, A., Cuvelier, D., & Fink, J. (2011). *Micropatterning on silicon elastomer (PDMS) with deep UVs*. Retrieved from <http://www.nature.com/protocolexchange/protocols/2131#/procedure>
- Carpi, N., Piel, M., Azioune, A., & Fink, J. (2011). *Micropatterning on glass with deep UV*. Retrieved from <http://www.nature.com/protocolexchange/protocols/2129>
- Carter, S. (1965). Principles of cell motility: the direction of cell movement and cancer invasion. *Nature*, *208*(5016), 1183. <https://doi.org/10.1038/2081183a0>
- Carter, S. B. (1967). Haptotaxis and the Mechanism of Cell Motility. *Nature*, *213*(5073), 256–260. <https://doi.org/10.1038/213256a0>
- Chabaud, M., Heuzé, M. L., Bretou, M., Vargas, P., Maiuri, P., Solanes, P., ... Lennon-Duménil, A.-M. (2015). Cell migration and antigen capture are antagonistic processes coupled by myosin II in dendritic cells. *Nature Communications*, *6*, 7526. <https://doi.org/10.1038/ncomms8526>
- Chan, C., Beltzner, C. C., & Pollard, T. D. (2009). Cofilin dissociates Arp2/3 complex and branches from actin filaments. *Current Biology: CB*, *19*(7), 537–545. <https://doi.org/10.1016/j.cub.2009.02.060>
- Chan, J. R., Hyduk, S. J., & Cybulsky, M. I. (2000). 4 1 Integrin/VCAM-1 Interaction Activates L 2 Integrin-Mediated Adhesion to ICAM-1 in Human T Cells. *The Journal of Immunology*, *164*(2), 746–753. <https://doi.org/10.4049/jimmunol.164.2.746>
- Chan, Jason R., Hyduk, S. J., & Cybulsky, M. I. (2001). Chemoattractants Induce a Rapid and Transient Upregulation of Monocyte $\alpha 4$ Integrin Affinity for Vascular Cell Adhesion Molecule 1 Which Mediates Arrest. *The Journal of Experimental Medicine*, *193*(10), 1149–1158.

- Chen, J., Salas, A., & Springer, T. A. (2003). Bistable regulation of integrin adhesiveness by a bipolar metal ion cluster. *Nature Structural Biology*, *10*(12), 995–1001.
<https://doi.org/10.1038/nsb1011>
- Cho, H., Hashimoto, T., Wong, E., Hori, Y., Wood, L. B., Zhao, L., ... Irimia, D. (2013). Microfluidic Chemotaxis Platform for Differentiating the Roles of Soluble and Bound Amyloid- β on Microglial Accumulation. *Scientific Reports*, *3*, 1823.
<https://doi.org/10.1038/srep01823>
- Chuang, K.-P. (2004). Ligation of lymphocyte function-associated antigen-1 on monocytes decreases very late antigen-4-mediated adhesion through a reactive oxygen species-dependent pathway. *Blood*, *104*(13), 4046–4053. <https://doi.org/10.1182/blood-2004-05-1822>
- Cinamon, G., Shinder, V., & Alon, R. (2001). Shear forces promote lymphocyte migration across vascular endothelium bearing apical chemokines. *Nature Immunology*, *2*(6), 515–522. <https://doi.org/10.1038/88710>
- Clark, K., Langeslag, M., Figdor, C. G., & van Leeuwen, F. N. (2007). Myosin II and mechanotransduction: a balancing act. *Trends in Cell Biology*, *17*(4), 178–186.
<https://doi.org/10.1016/j.tcb.2007.02.002>
- Coughlin, M. F., & Schmid-Schönbein, G. W. (2004). Pseudopod Projection and Cell Spreading of Passive Leukocytes in Response to Fluid Shear Stress. *Biophysical Journal*, *87*(3), 2035–2042. <https://doi.org/10.1529/biophysj.104.042192>
- D'Andrea, L. D., Iaccarino, G., Fattorusso, R., Sorriento, D., Carannante, C., Capasso, D., ... Pedone, C. (2005). Targeting angiogenesis: structural characterization and biological properties of a de novo engineered VEGF mimicking peptide. *Proceedings of the*

- National Academy of Sciences of the United States of America*, 102(40), 14215–14220. <https://doi.org/10.1073/pnas.0505047102>
- Davies, J. A. (2013a). Chapter 9 - Guidance by Chemotaxis. In J. A. Davies (Ed.), *Mechanisms of Morphogenesis (Second Edition)* (pp. 99–115). <https://doi.org/10.1016/B978-0-12-391062-2.00009-7>
- Davies, J. A. (2013b). Chapter 11 - Guidance by Contact. In J. A. Davies (Ed.), *Mechanisms of Morphogenesis (Second Edition)* (pp. 129–145). <https://doi.org/10.1016/B978-0-12-391062-2.00011-5>
- Decock, J., Schlenk, M., & Salmon, J.-B. (2018). In situ photo-patterning of pressure-resistant hydrogel membranes with controlled permeabilities in PEGDA microfluidic channels. *Lab on a Chip*, 18(7), 1075–1083. <https://doi.org/10.1039/C7LC01342F>
- del Rio, A., Perez-Jimenez, R., Liu, R., Roca-Cusachs, P., Fernandez, J. M., & Sheetz, M. P. (2009). Stretching single talin rod molecules activates vinculin binding. *Science (New York, N.Y.)*, 323(5914), 638–641. <https://doi.org/10.1126/science.1162912>
- Dertinger, S. K. W., Chiu, D. T., Jeon, N. L., & Whitesides, G. M. (2001). Generation of Gradients Having Complex Shapes Using Microfluidic Networks Generation of Gradients Having Complex Shapes Using Microfluidic Networks. *Analytical Chemistry*, 73(February), 1240–1246. <https://doi.org/10.1021/ac001132d>
- Discher, D. E., Janmey, P., & Wang, Y.-L. (2005). Tissue cells feel and respond to the stiffness of their substrate. *Science (New York, N.Y.)*, 310(5751), 1139–1143. <https://doi.org/10.1126/science.1116995>
- Dixit, N., & Simon, S. I. (2012). Chemokines, selectins and intracellular calcium flux: temporal and spatial cues for leukocyte arrest. *Frontiers in Immunology*, 3, 188. <https://doi.org/10.3389/fimmu.2012.00188>

- Diz-Muñoz, A., Krieg, M., Bergert, M., Ibarlucea-Benitez, I., Muller, D. J., Paluch, E., & Heisenberg, C.-P. (2010). Control of directed cell migration in vivo by membrane-to-cortex attachment. *PLoS Biology*, *8*(11), e1000544.
<https://doi.org/10.1371/journal.pbio.1000544>
- Dominguez, G. A., Anderson, N. R., & Hammer, D. A. (2015). The direction of migration of T-lymphocytes under flow depends upon which adhesion receptors are engaged. *Integr. Biol.*, *7*(3), 345–355. <https://doi.org/10.1039/C4IB00201F>
- Doyle, A. D., Wang, F. W., Matsumoto, K., & Yamada, K. M. (2009). One-dimensional topography underlies three-dimensional fibrillar cell migration. *The Journal of Cell Biology*, *184*(4), 481–490. <https://doi.org/10.1083/jcb.200810041>
- Dransfield, I. (1992). Divalent cation regulation of the function of the leukocyte integrin LFA-1. *The Journal of Cell Biology*, *116*(1), 219–226. <https://doi.org/10.1083/jcb.116.1.219>
- Ducret, A., Valignat, M.-P., Mouhamar, F., Mignot, T., & Theodoly, O. (2012). Wet-surface-enhanced ellipsometric contrast microscopy identifies slime as a major adhesion factor during bacterial surface motility. *Proceedings of the National Academy of Sciences*, *109*(25), 10036–10041. <https://doi.org/10.1073/pnas.1120979109>
- Dupré, L., Houmadi, R., Tang, C., & Rey-Barroso, J. (2015). T Lymphocyte Migration: An Action Movie Starring the Actin and Associated Actors. *Frontiers in Immunology*, *6*.
<https://doi.org/10.3389/fimmu.2015.00586>
- Dustin, M. L., & Springer, T. A. (1988). Lymphocyte function-associated antigen-1 (LFA-1) interaction with intercellular adhesion molecule-1 (ICAM-1) is one of at least three mechanisms for lymphocyte adhesion to cultured endothelial cells. *The Journal of Cell Biology*, *107*(1), 321 LP – 331.

- Eddy, R. J., Pierini, L. M., Matsumura, F., & Maxfield, F. R. (2000). Ca²⁺-dependent myosin II activation is required for uropod retraction during neutrophil migration. *Journal of Cell Science*, *113* (Pt 7), 1287–1298.
- Edelstein, A., Amodaj, N., Hoover, K., Vale, R., & Stuurman, N. (2010). Computer Control of Microscopes Using μ Manager. In *Current Protocols in Molecular Biology* (Vol. 92, pp. 14.20.1-14.20.17). <https://doi.org/10.1002/0471142727.mb1420s92>
- Eichinger, C. D., Hsiao, T. W., & Hlady, V. (2012). Multiprotein Microcontact Printing with Micrometer Resolution. *Langmuir*, *28*(4), 2238–2243.
<https://doi.org/10.1021/la2039202>
- Eriksson, E. E., Xie, X., Werr, J., Thoren, P., & Lindbom, L. (2001). Importance of Primary Capture and L-Selectin–Dependent Secondary Capture in Leukocyte Accumulation in Inflammation and Atherosclerosis in Vivo. *The Journal of Experimental Medicine*, *194*(2), 205–218.
- Even-Ram, S., Doyle, A. D., Conti, M. A., Matsumoto, K., Adelstein, R. S., & Yamada, K. M. (2007). Myosin IIA regulates cell motility and actomyosin-microtubule crosstalk. *Nature Cell Biology*, *9*(3), 299–309. <https://doi.org/10.1038/ncb1540>
- Faroudi, M., Hons, M., Zachacz, A., Dumont, C., Lyck, R., Stein, J. V., & Tybulewicz, V. L. J. (2010). Critical roles for Rac GTPases in T-cell migration to and within lymph nodes. *Blood*, *116*(25), 5536–5547. <https://doi.org/10.1182/blood-2010-08-299438>
- Faveeuw, C., Mauro, D., E, M., Price, A. A., & Ager, A. (2000). Roles of α 4 integrins/VCAM-1 and LFA-1/ICAM-1 in the binding and transendothelial migration of T lymphocytes and T lymphoblasts across high endothelial venules. *International Immunology*, *12*(3), 241–251. <https://doi.org/10.1093/intimm/12.3.241>

- Finger, E. B., Purl, K. D., Alon, R., Lawrence, M. B., von Andrian, U. H., & Springer, T. A. (1996). Adhesion through L-selectin requires a threshold hydrodynamic shear. *Nature*, *379*(6562), 266–269. <https://doi.org/10.1038/379266a0>
- Förster, R., Davalos-Missslitz, A. C., & Rot, A. (2008). CCR7 and its ligands: balancing immunity and tolerance. *Nature Reviews Immunology*, *8*(5), 362–371. <https://doi.org/10.1038/nri2297>
- Friedl, P., Entschladen, F., Conrad, C., Niggemann, B., & Zänker, K. S. (1998). CD4+ T lymphocytes migrating in three-dimensional collagen lattices lack focal adhesions and utilize β 1 integrin-independent strategies for polarization, interaction with collagen fibers and locomotion. *European Journal of Immunology*, *28*(8), 2331–2343. [https://doi.org/10.1002/\(SICI\)1521-4141\(199808\)28:08<2331::AID-IMMU2331>3.0.CO;2-C](https://doi.org/10.1002/(SICI)1521-4141(199808)28:08<2331::AID-IMMU2331>3.0.CO;2-C)
- Friedl, P., & Weigelin, B. (2008). Interstitial leukocyte migration and immune function. *Nature Immunology*, *9*(9), 960–969. <https://doi.org/10.1038/ni.f.212>
- Fukuda, K., Bledzka, K., Yang, J., Perera, H. D., Plow, E. F., & Qin, J. (2014). Molecular Basis of Kindlin-2 Binding to Integrin-linked Kinase Pseudokinase for Regulating Cell Adhesion. *The Journal of Biological Chemistry*, *289*(41), 28363–28375. <https://doi.org/10.1074/jbc.M114.596692>
- Gallego, M. D., de la Fuente, M. A., Anton, I. M., Snapper, S., Fuhlbrigge, R., & Geha, R. S. (2006). WIP and WASP play complementary roles in T cell homing and chemotaxis to SDF-1 α . *International Immunology*, *18*(2), 221–232. <https://doi.org/10.1093/intimm/dxh310>
- Ghosh, M., Song, X., Mouneimne, G., Sidani, M., Lawrence, D. S., & Condeelis, J. S. (2004). Cofilin promotes actin polymerization and defines the direction of cell motility.

Science (New York, N.Y.), 304(5671), 743–746.

<https://doi.org/10.1126/science.1094561>

Goethem, E. V., Poincloux, R., Gauffre, F., Maridonneau-Parini, I., & Cabec, V. L. (2010).

Matrix Architecture Dictates Three-Dimensional Migration Modes of Human Macrophages: Differential Involvement of Proteases and Podosome-Like Structures.

The Journal of Immunology, 184(2), 1049–1061.

<https://doi.org/10.4049/jimmunol.0902223>

Granger, D. N., & Kubes, P. (1994). The microcirculation and inflammation: modulation of

leukocyte-endothelial cell adhesion. *Journal of Leukocyte Biology*, 55(5), 662–675.

Haessler, U., Kalinin, Y., Swartz, M. A., & Wu, M. (2009). An agarose-based microfluidic

platform with a gradient buffer for 3D chemotaxis studies. *Biomedical Microdevices*,

11(4), 827–835. <https://doi.org/10.1007/s10544-009-9299-3>

Haessler, U., Pisano, M., Wu, M., & Swartz, M. A. (2011). Dendritic cell chemotaxis in 3D

under defined chemokine gradients reveals differential response to ligands CCL21

and CCL19. *Proceedings of the National Academy of Sciences of the United States of*

America, 108(14), 5614–5619. <https://doi.org/10.1073/pnas.1014920108>

Harada, Y., Tanaka, Y., Terasawa, M., Pieczyk, M., Habiro, K., Katakai, T., ... Fukui, Y. (2012).

DOCK8 is a Cdc42 activator critical for interstitial dendritic cell migration during

immune responses. *Blood*, 119(19), 4451–4461. [https://doi.org/10.1182/blood-2012-](https://doi.org/10.1182/blood-2012-01-407098)

01-407098

Heissler, S. M., & Manstein, D. J. (2013). Nonmuscle myosin-2: mix and match. *Cellular and*

Molecular Life Sciences: CMLS, 70(1), 1–21. [https://doi.org/10.1007/s00018-012-](https://doi.org/10.1007/s00018-012-1002-9)

1002-9

- Heuzé, M. L., Vargas, P., Chabaud, M., Berre, M. L., Liu, Y.-J., Collin, O., ... Lennon-Duménil, A.-M. (2013). Migration of dendritic cells: physical principles, molecular mechanisms, and functional implications. *Immunological Reviews*, 256(1), 240–254.
<https://doi.org/10.1111/imr.12108>
- Hoffman, B. D., Grashoff, C., & Schwartz, M. A. (2011). Dynamic molecular processes mediate cellular mechanotransduction. *Nature*, 475(7356), 316–323.
<https://doi.org/10.1038/nature10316>
- Hogg, N., Patzak, I., & Willenbrock, F. (2011). The insider's guide to leukocyte integrin signalling and function. *Nature Publishing Group*, 11.
<https://doi.org/10.1038/nri2986>
- Homem, C. C. F., & Peifer, M. (2009). Exploring the Roles of Diaphanous and Enabled Activity in Shaping the Balance between Filopodia and Lamellipodia. *Molecular Biology of the Cell*, 20(24), 5138–5155. <https://doi.org/10.1091/mbc.e09-02-0144>
- Hons, M., Kopf, A., Hauschild, R., Leithner, A., Gaertner, F., Abe, J., ... Sixt, M. (2018). Chemokines and integrins independently tune actin flow and substrate friction during intranodal migration of T cells. *Nature Immunology*, 19(6), 606–616.
<https://doi.org/10.1038/s41590-018-0109-z>
- Hornung, Alexander, Sbarrato, T., Garcia-Seyda, N., Aoun, L., Luo, X., Biarnes-Pelicot, M., ... Valignat, M.-P. (2018). A Bistable Mechanism Mediated by Integrins Controls Mechanotaxis of Leukocytes. *BioRxiv*, 509091. <https://doi.org/10.1101/509091>
- Hornung, Alexander. (2016). *Two-dimensional migration of human effector T-cells : Integrin-dependent motility studies under shear stress*. Aix-Marseille University.
- Hou, S., Feng, X. Z., Wang, L. K., & Chan, Q. L. (2007). Microcontact Printing of Multiproteins on the GA Modified Glass Substrate and Its Applications in the Research of

- Immunoassays. *Solid State Phenomena*, 121–123, 721–724.
<https://doi.org/10.4028/www.scientific.net/SSP.121-123.721>
- Hu, P., & Luo, B.-H. (2013). Integrin bi-directional signaling across the plasma membrane. *Journal of Cellular Physiology*, 228(2), 306–312. <https://doi.org/10.1002/jcp.24154>
- Hu, S., Chen, T.-H., Zhao, Y., Wang, Z., & Lam, R. H. W. (2018). Protein–Substrate Adhesion in Microcontact Printing Regulates Cell Behavior. *Langmuir*, 34(4), 1750–1759.
<https://doi.org/10.1021/acs.langmuir.7b02935>
- Huerre, A., Jullien, M.-C., Theodoly, O., & Valignat, M.-P. (2016). Absolute 3D reconstruction of thin films topography in microfluidic channels by interference reflection microscopy. *Lab on a Chip*, 16(5), 911–916. <https://doi.org/10.1039/C5LC01417D>
- Huo, Y., Hafezi-Moghadam, A., & Ley, K. (2000). Role of vascular cell adhesion molecule-1 and fibronectin connecting segment-1 in monocyte rolling and adhesion on early atherosclerotic lesions. *Circulation Research*, 87(2), 153–159.
- Hyun, Y.-M., Sumagin, R., Sarangi, P. P., Lomakina, E., Overstreet, M. G., Baker, C. M., ... Kim, M. (2012). Uropod elongation is a common final step in leukocyte extravasation through inflamed vessels. *Journal of Experimental Medicine*, 209(7), 1349–1362.
<https://doi.org/10.1084/jem.20111426>
- Irimia, D., Balázsi, G., Agrawal, N., & Toner, M. (2009). Adaptive-Control Model for Neutrophil Orientation in the Direction of Chemical Gradients. *Biophysical Journal*, 96(10), 3897–3916. <https://doi.org/10.1016/j.bpj.2008.12.3967>
- Irimia, D., Charras, G., Agrawal, N., Mitchison, T., & Toner, M. (2007). Polar stimulation and constrained cell migration in microfluidic channels. *Lab on a Chip*, 7(12), 1783–1790.
<https://doi.org/10.1039/b710524j>

- Jacobelli, J., Friedman, R. S., Conti, M. A., Lennon-Dumenil, A.-M., Piel, M., Sorensen, C. M., ... Krummel, M. F. (2010). Confinement-optimized three-dimensional T cell amoeboid motility is modulated via myosin IIA-regulated adhesions. *Nature Immunology*, *11*(10), 953–961. <https://doi.org/10.1038/ni.1936>
- Janeway, C. A., Travers, P., Walport, M., Shlomchik, M. J., Jr, C. A. J., Travers, P., ... Shlomchik, M. J. (2016). *Immunobiology* (9th ed.). Garland Science.
- Jeon, N. L., Dertinger, S. K. W., Chiu, D. T., Choi, I. S., Stroock, A. D., & Whitesides, G. M. (2000). Generation of Gradients Having Complex Shapes Using Microfluidic Networks. *Langmuir*, *16*(22), 8311–8316. <https://doi.org/10.1039/b610011b>
- Jiang, X., Xu, Q., Dertinger, S. K. W., Stroock, A. D., Fu, T., & Whitesides, G. M. (2005). A General Method for Patterning Gradients of Biomolecules on Surfaces Using Microfluidic Networks. *Analytical Chemistry*, *77*(8), 2338–2347. <https://doi.org/10.1021/ac048440m>
- Kerber, M. L., & Cheney, R. E. (2011). Myosin-X: a MyTH-FERM myosin at the tips of filopodia. *Journal of Cell Science*, *124*(22), 3733–3741. <https://doi.org/10.1242/jcs.023549>
- Kilian, K. A., Bugarija, B., Lahn, B. T., & Mrksich, M. (2010). Geometric cues for directing the differentiation of mesenchymal stem cells. *Proceedings of the National Academy of Sciences*, *107*(11), 4872–4877. <https://doi.org/10.1073/pnas.0903269107>
- Kim, C. H. (2014). Crawling of effector T cells on extracellular matrix: role of integrins in interstitial migration in inflamed tissues. *Cellular and Molecular Immunology*, *11*(1), 1–4. <https://doi.org/10.1038/cmi.2013.47>

- Kim, S., Kim, H. J., & Jeon, N. L. (2010). Biological applications of microfluidic gradient devices. *Integrative Biology*, 2(11–12), 584. <https://doi.org/10.1039/c0ib00055h>
- King, S. J., Asokan, S. B., Haynes, E. M., Zimmerman, S. P., Rotty, J. D., Alb, J. G., ... Bear, J. E. (2016). Lamellipodia are crucial for haptotactic sensing and response. *J Cell Sci*, 129(12), 2329–2342. <https://doi.org/10.1242/jcs.184507>
- Klominek, J., Robert, K.-H., & Sundqvist, K.-C. (1993). *Chemotaxis and Haptotaxis of Human Malignant Mesothelioma Cells: Effects of Fibronectin, Laminin, Type IV Collagen, and an Autocrine Motility Factor-like Substance*. 53, 4376–4382.
- Koelink, P. J., Overbeek, S. A., Braber, S., de Kruijf, P., Folkerts, G., Smit, M. J., & Kraneveld, A. D. (2012). Targeting chemokine receptors in chronic inflammatory diseases: An extensive review. *Pharmacology & Therapeutics*, 133(1), 1–18. <https://doi.org/10.1016/j.pharmthera.2011.06.008>
- Koutsiaris, A. G., Tachmitzi, S. V., Batis, N., Kotoula, M. G., Karabatsas, C. H., Tsironi, E., & Chatzoulis, D. Z. (2007). Volume flow and wall shear stress quantification in the human conjunctival capillaries and post-capillary venules in vivo. *Biorheology*, 44(5–6), 375–386.
- Kovar, D. R., & Pollard, T. D. (2004). Insertional assembly of actin filament barbed ends in association with formins produces piconewton forces. *Proceedings of the National Academy of Sciences*, 101(41), 14725–14730. <https://doi.org/10.1073/pnas.0405902101>
- Krause, M., Bear, J. E., Loureiro, J. J., & Gertler, F. B. (2002). The Ena/VASP enigma. *Journal of Cell Science*, 115(24), 4721–4726. <https://doi.org/10.1242/jcs.00218>

- Kumar, A., Biebuyck, H. A., & Whitesides, G. M. (1994). Patterning Self-Assembled Monolayers: Applications in Materials Science. *Langmuir*, *10*(5), 1498–1511.
<https://doi.org/10.1021/la00017a030>
- Kumar, H., Kawai, T., & Akira, S. (2011). Pathogen Recognition by the Innate Immune System. *International Reviews of Immunology*, *30*(1), 16–34.
<https://doi.org/10.3109/08830185.2010.529976>
- Kunkel, E. J., & Ley, K. (1996). Distinct phenotype of E-selectin-deficient mice. E-selectin is required for slow leukocyte rolling *in vivo*. *Circulation Research*, *79*(6), 1196–1204.
- Lagarrigue, F., Kim, C., & Ginsberg, M. H. (2016). The Rap1-RIAM-talin axis of integrin activation and blood cell function. *Blood*, *128*(4), 479–487.
<https://doi.org/10.1182/blood-2015-12-638700>
- Lämmermann, T., Afonso, P. V., Angermann, B. R., Wang, J. M., Kastenmüller, W., Parent, C. A., & Germain, R. N. (2013). Neutrophil swarms require LTB4 and integrins at sites of cell death *in vivo*. *Nature*, *498*(7454), 371–375.
<https://doi.org/10.1038/nature12175>
- Lämmermann, T., Bader, B. L., Monkley, S. J., Worbs, T., Wedlich-Söldner, R., Hirsch, K., ... Sixt, M. (2008). Rapid leukocyte migration by integrin-independent flowing and squeezing. *Nature*, *453*(7191), 51–55. <https://doi.org/10.1038/nature06887>
- Lämmermann, T., & Germain, R. N. (2014). The multiple faces of leukocyte interstitial migration. *Seminars in Immunopathology*, *36*(2), 227–251.
<https://doi.org/10.1007/s00281-014-0418-8>
- Lämmermann, T., Renkawitz, J., Wu, X., Hirsch, K., Brakebusch, C., & Sixt, M. (2009). Cdc42-dependent leading edge coordination is essential for interstitial dendritic cell

- migration. *Blood*, 113(23), 5703–5710. <https://doi.org/10.1182/blood-2008-11-191882>
- Lämmermann, T., & Sixt, M. (2009). Mechanical modes of ‘amoeboid’ cell migration. *Current Opinion in Cell Biology*, 21(5), 636–644. <https://doi.org/10.1016/j.ceb.2009.05.003>
- Lang, S., von Philipsborn, A. C., Bernard, A., Bonhoeffer, F., & Bastmeyer, M. (2008). Growth cone response to ephrin gradients produced by microfluidic networks. *Analytical and Bioanalytical Chemistry*, 390(3), 809–816. <https://doi.org/10.1007/s00216-007-1363-3>
- Lavi, I., Piel, M., Lennon-Duménil, A.-M., Voituriez, R., & Gov, N. S. (2016). Deterministic patterns in cell motility. *Nature Physics*, 12(12), 1146–1152. <https://doi.org/10.1038/nphys3836>
- Lawrence, M. B., Kansas, G. S., Kunkel, E. J., & Ley, K. (1997). Threshold Levels of Fluid Shear Promote Leukocyte Adhesion through Selectins (CD62L,P,E). *The Journal of Cell Biology*, 136(3), 717–727.
- Le Berre, M., Aubertin, J., & Piel, M. (2012). Fine control of nuclear confinement identifies a threshold deformation leading to lamina rupture and induction of specific genes. *Integrative Biology*, 4(11), 1406–1414. <https://doi.org/10.1039/c2ib20056b>
- Lebrand, C., Dent, E. W., Strasser, G. A., Lanier, L. M., Krause, M., Svitkina, T. M., ... Gertler, F. B. (2004). Critical Role of Ena/VASP Proteins for Filopodia Formation in Neurons and in Function Downstream of Netrin-1. *Neuron*, 42(1), 37–49. [https://doi.org/10.1016/S0896-6273\(04\)00108-4](https://doi.org/10.1016/S0896-6273(04)00108-4)
- Lee, Y. B., Kim, S., Kim, E. M., Byun, H., Chang, H., Park, J., ... Shin, H. (2017). Microcontact printing of polydopamine on thermally expandable hydrogels for controlled cell

- adhesion and delivery of geometrically defined microtissues. *Acta Biomaterialia*, *61*, 75–87. <https://doi.org/10.1016/j.actbio.2017.07.040>
- Leithner, A., Eichner, A., Müller, J., Reversat, A., Brown, M., Schwarz, J., ... Sixt, M. (2016). Diversified actin protrusions promote environmental exploration but are dispensable for locomotion of leukocytes. *Nature Cell Biology*, *18*(11), 1253–1259. <https://doi.org/10.1038/ncb3426>
- Ley, K., Laudanna, C., Cybulsky, M. I., & Nourshargh, S. (2007). Getting to the site of inflammation: the leukocyte adhesion cascade updated. *Nature Reviews. Immunology*, *7*(9), 678–689. <https://doi.org/10.1038/nri2156>
- Li, Q., Wayman, A., Lin, J., Fang, Y., Zhu, C., & Wu, J. (2016). Flow-Enhanced Stability of Rolling Adhesion through E-Selectin. *Biophysical Journal*, *111*(4), 686–699. <https://doi.org/10.1016/j.bpj.2016.07.014>
- Lim, K., Hyun, Y. M., Lambert-Emo, K., Capece, T., Bae, S., Miller, R., ... Kim, M. (2015). Neutrophil trails guide influenza-specific CD8(+) T cells in the airways. *Science*, *349*(6252), aaa4352. <https://doi.org/10.1126/science.aaa4352>
- Limozin, L., & Sengupta, K. (2009). Quantitative reflection interference contrast microscopy (RICM) in soft matter and cell adhesion. *Chemphyschem: A European Journal of Chemical Physics and Physical Chemistry*, *10*(16), 2752–2768. <https://doi.org/10.1002/cphc.200900601>
- Lin, F., & Butcher, E. C. (2006). T cell chemotaxis in a simple microfluidic device. *Lab on a Chip*, *6*(11), 1462–1469. <https://doi.org/10.1039/B607071J>
- Lipowsky, H. H., Kovalcheck, S., & Zweifach, B. W. (1978). The distribution of blood rheological parameters in the microvasculature of cat mesentery. *Circulation Research*, *43*(5), 738–749.

- Liu, Z., Xiao, L., Xu, B., Zhang, Yu, Ft Mak, A., Li, Y., ... Yang, Mo. (2012). Covalently immobilized biomolecule gradient on hydrogel surface using a gradient generating microfluidic device for a quantitative mesenchymal stem cell study. *Biomicrofluidics*, 6, 241111–2411112. <https://doi.org/10.1063/1.4704522>
- Luckashenak, N., Wähe, A., Breit, K., Brakebusch, C., & Brocker, T. (2013). Rho-Family GTPase Cdc42 Controls Migration of Langerhans Cells In Vivo. *The Journal of Immunology*, 190(1), 27–35. <https://doi.org/10.4049/jimmunol.1201082>
- Luo, B.-H., Carman, C. V., & Springer, T. A. (2007). Structural basis of integrin regulation and signaling. *Annual Review of Immunology*, 25, 619–647. <https://doi.org/10.1146/annurev.immunol.25.022106.141618>
- Ma, Q., Shimaoka, M., Lu, C., Jing, H., Carman, C. V., & Springer, T. A. (2002). Activation-induced Conformational Changes in the I Domain Region of Lymphocyte Function-associated Antigen 1. *Journal of Biological Chemistry*, 277(12), 10638–10641. <https://doi.org/10.1074/jbc.M112417200>
- Machacek, M., Hodgson, L., Welch, C., Elliott, H., Pertz, O., Nalbant, P., ... Danuser, G. (2009). Coordination of Rho GTPase activities during cell protrusion. *Nature*, 461(7260), 99–103. <https://doi.org/10.1038/nature08242>
- Makgoba, M. W., Sanders, M. E., & Shaw, S. (1989). The CD2-LFA-3 and LFA-1-ICAM pathways: relevance to T-cell recognition. *Immunology Today*, 10(12), 417–422. [https://doi.org/10.1016/0167-5699\(89\)90039-X](https://doi.org/10.1016/0167-5699(89)90039-X)
- Malawista, S. E., & Chevance, A. de B. (1997). Random locomotion and chemotaxis of human blood polymorphonuclear leukocytes (PMN) in the presence of EDTA: PMN in close quarters require neither leukocyte integrins nor external divalent cations.

- Proceedings of the National Academy of Sciences*, 94(21), 11577–11582.
<https://doi.org/10.1073/pnas.94.21.11577>
- Mallavarapu, A., & Mitchison, T. (1999). Regulated Actin Cytoskeleton Assembly at Filopodium Tips Controls Their Extension and Retraction. *The Journal of Cell Biology*, 146(5), 1097–1106. <https://doi.org/10.1083/jcb.146.5.1097>
- Massena, S., & Phillipso, M. (2012). Intravascular Leukocyte Chemotaxis: The Rules of Attraction. In C. Lawrie (Ed.), *Hematology - Science and Practice*.
<https://doi.org/10.5772/35840>
- McBeath, R., Pirone, D. M., Nelson, C. M., Bhadriraju, K., & Chen, C. S. (2004). Cell Shape, Cytoskeletal Tension, and RhoA Regulate Stem Cell Lineage Commitment. *Developmental Cell*, 6(4), 483–495. [https://doi.org/10.1016/S1534-5807\(04\)00075-9](https://doi.org/10.1016/S1534-5807(04)00075-9)
- Mccarthy, J. B., & Furcht, L. T. (1984). *Laminin and Fibronectin Promote the Haptotactic Migration of B16 Mouse Melanoma Cells In Vitro*. 98, 1474–1480.
- Medeiros, N. A., Burnette, D. T., & Forscher, P. (2006). Myosin II functions in actin-bundle turnover in neuronal growth cones. *Nature Cell Biology*, 8(3), 216–226.
<https://doi.org/10.1038/ncb1367>
- Millet, L. J., Stewart, M. E., Nuzzo, R. G., & Gillette, M. U. (2010). Guiding neuron development with planar surface gradients of substrate cues deposited using microfluidic devices. *Lab on a Chip*, 10(12), 1525–1535.
<https://doi.org/10.1039/C001552K>
- Moazzam, F., DeLano, F. A., Zweifach, B. W., & Schmid-Schönbein, G. W. (1997). The leukocyte response to fluid stress. *Proceedings of the National Academy of Sciences*, 94(10), 5338–5343. <https://doi.org/10.1073/pnas.94.10.5338>

- Morel, M., Shynkar, V., Galas, J. C., Dupin, I., Bouzigues, C., Studer, V., & Dahan, M. (2012). Amplification and temporal filtering during gradient sensing by nerve growth cones probed with a microfluidic assay. *Biophysical Journal*, *103*(8), 1648–1656. <https://doi.org/10.1016/j.bpj.2012.08.040>
- Morin, N. A., Oakes, P. W., Hyun, Y.-M., Lee, D., Chin, Y. E., Chin, E. Y., ... Kim, M. (2008). Nonmuscle myosin heavy chain IIA mediates integrin LFA-1 de-adhesion during T lymphocyte migration. *The Journal of Experimental Medicine*, *205*(1), 195–205. <https://doi.org/10.1084/jem.20071543>
- Mould, A. P., Barton, S. J., Askari, J. A., Craig, S. E., & Humphries, M. J. (2003). Role of ADMIDAS cation-binding site in ligand recognition by integrin alpha 5 beta 1. *The Journal of Biological Chemistry*, *278*(51), 51622–51629. <https://doi.org/10.1074/jbc.M306655200>
- Mrksich, M., & Whitesides, G. M. (1996). Using self-assembled monolayers to understand the interactions of man-made surfaces with proteins and cells. *Annual Review of Biophysics and Biomolecular Structure*, *25*, 55–78. <https://doi.org/10.1146/annurev.bb.25.060196.000415>
- Mullins, R. D., Heuser, J. A., & Pollard, T. D. (1998). The interaction of Arp2/3 complex with actin: nucleation, high affinity pointed end capping, and formation of branching networks of filaments. *Proceedings of the National Academy of Sciences of the United States of America*, *95*(11), 6181–6186.
- Murphy, P. M. (2008). 11 - Chemokines and chemokine receptors. In R. R. Rich, T. A. Fleisher, W. T. Shearer, H. W. Schroeder, A. J. Frew, & C. M. Weyand (Eds.), *Clinical Immunology (Third Edition)* (pp. 173–196). <https://doi.org/10.1016/B978-0-323-04404-2.10011-9>

- Niggli, V., & Rossy, J. (2008). Ezrin/radixin/moesin: Versatile controllers of signaling molecules and of the cortical cytoskeleton. *The International Journal of Biochemistry & Cell Biology*, 40(3), 344–349. <https://doi.org/10.1016/j.biocel.2007.02.012>
- Nombela-Arrieta, C., Mempel, T. R., Soriano, S. F., Mazo, I., Wymann, M. P., Hirsch, E., ... Stein, J. V. (2007). A central role for DOCK2 during interstitial lymphocyte motility and sphingosine-1-phosphate-mediated egress. *Journal of Experimental Medicine*, 204(3), 497–510. <https://doi.org/10.1084/jem.20061780>
- Nordenfelt, P., Moore, T. I., Mehta, S. B., Kalappurakkal, J. M., Swaminathan, V., Koga, N., ... Springer, T. A. (2017). Direction of actin flow dictates integrin LFA-1 orientation during leukocyte migration. *Nature Communications*, 8(1), 2047. <https://doi.org/10.1038/s41467-017-01848-y>
- Noronha, S. de, Hardy, S., Sinclair, J., Blundell, M. P., Strid, J., Schulz, O., ... Thrasher, A. J. (2005). Impaired dendritic-cell homing in vivo in the absence of Wiskott-Aldrich syndrome protein. *Blood*, 105(4), 1590–1597. <https://doi.org/10.1182/blood-2004-06-2332>
- Notarangelo, L. D., Notarangelo, L. D., & Ochs, H. D. (2005). WASP and the phenotypic range associated with deficiency. *Current Opinion in Allergy and Clinical Immunology*, 5(6), 485. <https://doi.org/10.1097/01.all.0000191243.25757.ce>
- Nourshargh, S., & Alon, R. (2014). *Leukocyte Migration into Inflamed Tissues*. <https://doi.org/10.1016/j.immuni.2014.10.008>
- Oakes, P. W., Patel, D. C., Morin, N. A., Zitterbart, D. P., Fabry, B., Reichner, J. S., & Tang, J. X. (2009). Neutrophil morphology and migration are affected by substrate elasticity. *Blood*, 114(7), 1387–1395. <https://doi.org/10.1182/blood-2008-11-191445>

- Ochs, H. D., & Thrasher, A. J. (2006). The Wiskott-Aldrich syndrome. *The Journal of Allergy and Clinical Immunology*, *117*(4), 725–738; quiz 739.
<https://doi.org/10.1016/j.jaci.2006.02.005>
- O'Connor, T. P., Duerr, J. S., & Bentley, D. (1990a). Pioneer growth cone steering decisions mediated by single filopodial contacts in situ. *Journal of Neuroscience*, *10*(12), 3935–3946.
- O'Connor, T. P., Duerr, J. S., & Bentley, D. (1990b). Pioneer growth cone steering decisions mediated by single filopodial contacts in situ. *Journal of Neuroscience*, *10*(12), 3935–3946.
- Okada, T., Ngo, V. N., Ekland, E. H., Förster, R., Lipp, M., Littman, D. R., & Cyster, J. G. (2002). Chemokine requirements for B cell entry to lymph nodes and Peyer's patches. *The Journal of Experimental Medicine*, *196*(1), 65–75.
- Overstreet, M. G., Gaylo, A., Angermann, B. R., Hughson, A., Hyun, Y.-M., Lambert, K., ... Fowell, D. J. (2013). Inflammation-induced interstitial migration of effector CD4⁺ T cells is dependent on integrin α V. *Nature Immunology*, *14*(9), 949–958.
<https://doi.org/10.1038/ni.2682>
- Park, E. J., Peixoto, A., Imai, Y., Goodarzi, A., Cheng, G., Carman, C. V., ... Shimaoka, M. (2010). Distinct roles for LFA-1 affinity regulation during T-cell adhesion, diapedesis, and interstitial migration in lymph nodes. *Blood*, *115*(8), 1572–1581.
<https://doi.org/10.1182/blood-2009-08-237917>
- Pasapera, A. M., Plotnikov, S. V., Fischer, R. S., Case, L. B., Egelhoff, T. T., & Waterman, C. M. (2015). Rac1-Dependent Phosphorylation and Focal Adhesion Recruitment of Myosin IIA Regulates Migration and Mechanosensing. *Current Biology*, *25*(2), 175–186.
<https://doi.org/10.1016/j.cub.2014.11.043>

- Pasturel, A., Strale, P.-O., & Studer, V. (2018). A generic widefield topographical and chemical photopatterning method for hydrogels. *BioRxiv*.
<https://doi.org/10.1101/370882>
- Peng, J., Wallar, B. J., Flanders, A., Swiatek, P. J., & Alberts, A. S. (2003). Disruption of the Diaphanous-related formin Drf1 gene encoding mDia1 reveals a role for Drf3 as an effector for Cdc42. *Current Biology: CB*, *13*(7), 534–545.
- Perry, M. A., & Granger, D. N. (1991). Role of CD11/CD18 in shear rate-dependent leukocyte-endothelial cell interactions in cat mesenteric venules. *Journal of Clinical Investigation*, *87*(5), 1798–1804.
- Petri, B., Phillipson, M., & Kubes, P. (2008). The Physiology of Leukocyte Recruitment: An In Vivo Perspective. *The Journal of Immunology*, *180*(10), 6439–6446.
<https://doi.org/10.4049/jimmunol.180.10.6439>
- Petrie, R. J., Doyle, A. D., & Yamada, K. M. (2009). Random versus directionally persistent cell migration. *Nature Reviews Molecular Cell Biology*, *10*(8), 538–549.
<https://doi.org/10.1038/nrm2729>
- Phillipson, M., Heit, B., Colarusso, P., Liu, L., Ballantyne, C. M., & Kubes, P. (2006). Intraluminal crawling of neutrophils to emigration sites: a molecularly distinct process from adhesion in the recruitment cascade. *The Journal of Experimental Medicine*, *203*(12), 2569–2575. <https://doi.org/10.1084/jem.20060925>
- Phillipson, M., Heit, B., Parsons, S. A., Petri, B., Mullaly, S. C., Colarusso, P., ... Kubes, P. (2009). Vav1 is essential for mechanotactic crawling and migration of neutrophils out of the inflamed microvasculature. *Journal of Immunology (Baltimore, Md.: 1950)*, *182*(11), 6870–6878. <https://doi.org/10.4049/jimmunol.0803414>

- Pollard, T. D. (2016). Actin and Actin-Binding Proteins. *Cold Spring Harbor Perspectives in Biology*, 8(8), a018226. <https://doi.org/10.1101/cshperspect.a018226>
- R Lagraff, J., Zhao, Y.-P., Graber, D., Rainville, D., Wang, G.-C., Lu, T.-M., ... N Turner, J. (2011). Fabrication and Imaging of Protein Crossover Structures. *MRS Proceedings*, 735. <https://doi.org/10.1557/PROC-735-C3.6>
- Rainger, G. E., Buckley, C. D., Simmons, D. L., & Nash, G. B. (1999). Neutrophils sense flow-generated stress and direct their migration through $\alpha V\beta 3$ -integrin. *American Journal of Physiology-Heart and Circulatory Physiology*, 276(3), H858–H864. <https://doi.org/10.1152/ajpheart.1999.276.3.H858>
- Randolph, G. J., Angeli, V., & Swartz, M. A. (2005). Dendritic-cell trafficking to lymph nodes through lymphatic vessels. *Nature Reviews. Immunology*, 5(8), 617–628. <https://doi.org/10.1038/nri1670>
- Reichardt, P., Patzak, I., Jones, K., Etemire, E., Gunzer, M., & Hogg, N. (2013). A role for LFA-1 in delaying T-lymphocyte egress from lymph nodes. *The EMBO Journal*, 32(6), 829–843. <https://doi.org/10.1038/emboj.2013.33>
- Reinhard, M., Jouvenal, K., Tripier, D., & Walter, U. (1995). Identification, purification, and characterization of a zyxin-related protein that binds the focal adhesion and microfilament protein VASP (vasodilator-stimulated phosphoprotein). *Proceedings of the National Academy of Sciences of the United States of America*, 92(17), 7956–7960.
- Ricart, B. G., John, B., Lee, D., Hunter, C. A., & Hammer, D. A. (2011). Dendritic cells distinguish individual chemokine signals through CCR7 and CXCR4. *Journal of Immunology (Baltimore, Md.: 1950)*, 186(1), 53–61. <https://doi.org/10.4049/jimmunol.1002358>

- Ricoult, S. G., Pla-Roca, M., Safavieh, R., Lopez-Ayon, G. M., Grütter, P., Kennedy, T. E., & Juncker, D. (2013). Large Dynamic Range Digital Nanodot Gradients of Biomolecules Made by Low-Cost Nanocontact Printing for Cell Haptotaxis. *Small*, *9*(19), 3308–3313. <https://doi.org/10.1002/sml.201202915>
- Ridley, A. J. (2011). Life at the Leading Edge. *Cell*, *145*(7), 1012–1022. <https://doi.org/10.1016/j.cell.2011.06.010>
- Ridley, A. J., Schwartz, M. A., Burridge, K., Firtel, R. A., Ginsberg, M. H., Borisy, G., ... Horwitz, A. R. (2003). Cell Migration: Integrating Signals from Front to Back. *Science*, *302*(5651), 1704–1709. <https://doi.org/10.1126/science.1092053>
- Roca-Cusachs, P., Rio, A. del, Puklin-Faucher, E., Gauthier, N. C., Biais, N., & Sheetz, M. P. (2013). Integrin-dependent force transmission to the extracellular matrix by α -actinin triggers adhesion maturation. *Proceedings of the National Academy of Sciences*, *110*(15), E1361–E1370. <https://doi.org/10.1073/pnas.1220723110>
- Rognoni, E., Ruppert, R., & Fässler, R. (2016). The kindlin family: functions, signaling properties and implications for human disease. *J Cell Sci*, *129*(1), 17–27. <https://doi.org/10.1242/jcs.161190>
- Rohatgi, R., Ma, L., Miki, H., Lopez, M., Kirchhausen, T., Takenawa, T., & Kirschner, M. W. (1999). The interaction between N-WASP and the Arp2/3 complex links Cdc42-dependent signals to actin assembly. *Cell*, *97*(2), 221–231.
- Romero, S., Grompone, G., Carayol, N., Mounier, J., Guadagnini, S., Prevost, M.-C., ... Tran Van Nhieu, G. (2011). ATP-Mediated Erk1/2 Activation Stimulates Bacterial Capture by Filopodia, which Precedes Shigella Invasion of Epithelial Cells. *Cell Host & Microbe*, *9*(6), 508–519. <https://doi.org/10.1016/j.chom.2011.05.005>

- Rose, D. M., Alon, R., & Ginsberg, M. H. (2007). Integrin modulation and signaling in leukocyte adhesion and migration. *Immunological Reviews*, 218(1), 126–134. <https://doi.org/10.1111/j.1600-065X.2007.00536.x>
- Saadi, W., Rhee, S. W., Lin, F., Vahidi, B., Chung, B. G., & Jeon, N. L. (2007). Generation of stable concentration gradients in 2D and 3D environments using a microfluidic ladder chamber. *Biomedical Microdevices*, 9(5), 627–635. <https://doi.org/10.1007/s10544-007-9051-9>
- Sadoun, A. (2018). *Adhésion et mécanique standardisées de lymphocytes T : rôles dans l'activation par anticorps et cellules présentatrices d'antigène, sous force*. Aix-Marseille University.
- Salbreux, G., Charras, G., & Paluch, E. (2012). Actin cortex mechanics and cellular morphogenesis. *Trends in Cell Biology*, 22(10), 536–545. <https://doi.org/10.1016/j.tcb.2012.07.001>
- Sasaki, A. T., Chun, C., Takeda, K., & Firtel, R. A. (2004). Localized Ras signaling at the leading edge regulates PI3K, cell polarity, and directional cell movement. *The Journal of Cell Biology*, 167(3), 505–518. <https://doi.org/10.1083/jcb.200406177>
- Sato, M., Nagayama, K., Kataoka, N., Sasaki, M., & Hane, K. (2000). Local mechanical properties measured by atomic force microscopy for cultured bovine endothelial cells exposed to shear stress. *Journal of Biomechanics*, 33(1), 127–135. [https://doi.org/10.1016/S0021-9290\(99\)00178-5](https://doi.org/10.1016/S0021-9290(99)00178-5)
- Sawada, Y., Tamada, M., Dubin-Thaler, B. J., Cherniavskaya, O., Sakai, R., Tanaka, S., & Sheetz, M. P. (2006). Force sensing by mechanical extension of the Src family kinase substrate p130Cas. *Cell*, 127(5), 1015–1026. <https://doi.org/10.1016/j.cell.2006.09.044>

- Schaefer, A., Te Riet, J., Ritz, K., Hoogenboezem, M., Anthony, E. C., Mul, F. P. J., ... Hordijk, P. L. (2014). Actin-binding proteins differentially regulate endothelial cell stiffness, ICAM-1 function and neutrophil transmigration. *J. Cell Sci. Journal of Cell Science*, *127*(000), 4470–4482. <https://doi.org/10.1242/jcs.164814>
- Schimmel, L., Heemskerk, N., & Van Buul, J. D. (2017). *Small GTPases Leukocyte transendothelial migration: A local affair*. *Leukocyte transendothelial migration: A local affair*. <https://doi.org/10.1080/21541248.2016.1197872>
72
- Schoen, I., Pruitt, B. L., & Vogel, V. (2013). The Yin-Yang of Rigidity Sensing: How Forces and Mechanical Properties Regulate the Cellular Response to Materials. *Annual Review of Materials Research*, *43*(1), 589–618. <https://doi.org/10.1146/annurev-matsci-062910-100407>
- Schreiber, T. H., Shinder, V., Cain, D. W., Alon, R., & Sackstein, R. (2007). Shear flow-dependent integration of apical and subendothelial chemokines in T-cell transmigration: implications for locomotion and the multistep paradigm. *Blood*, *109*(4), 1381–1386. <https://doi.org/10.1182/blood-2006-07-032995>
- Schü, T., & Springer, T. A. (2011). Regulation of integrin affinity on cell surfaces. *The EMBO Journal*, *30*, 4712–4727. <https://doi.org/10.1038/emboj.2011.333>
- Schumann, K., L??mmermann, T., Bruckner, M., Legler, D. F., Polleux, J., Spatz, J. P., ... Sixt, M. (2010). Immobilized Chemokine Fields and Soluble Chemokine Gradients Cooperatively Shape Migration Patterns of Dendritic Cells. *Immunity*, *32*(5), 703–713. <https://doi.org/10.1016/j.immuni.2010.04.017>

- Schwarz, J., Bierbaum, V., Merrin, J., Frank, T., Hauschild, R., Bollenbach, T., ... Mehling, M. (2016). A microfluidic device for measuring cell migration towards substrate-bound and soluble chemokine gradients OPEN. *Nature Publishing Group*.
<https://doi.org/10.1038/srep36440>
- Schwarz, J., Bierbaum, V., Vaahtomeri, K., Hauschild, R., Brown, M., de Vries, I., ... Sixt, M. (2017). Dendritic Cells Interpret Haptotactic Chemokine Gradients in a Manner Governed by Signal-to-Noise Ratio and Dependent on GRK6. *Current Biology*, 27(9), 1314–1325. <https://doi.org/10.1016/j.cub.2017.04.004>
- Schwarz, J., & Sixt, M. (2016). Chapter Twenty-Four - Quantitative Analysis of Dendritic Cell Haptotaxis. In T. M. Handel (Ed.), *Methods in Enzymology* (pp. 567–581).
<https://doi.org/10.1016/bs.mie.2015.11.004>
- Scott, M. A., Wissner-Gross, Z. D., & Yanik, M. F. (2012). Ultra-rapid laser protein micropatterning: screening for directed polarization of single neurons. *Lab on a Chip*, 12(12), 2265–2276. <https://doi.org/10.1039/c2lc21105j>
- Shamri, R., Grabovsky, V., Gauguier, J.-M., Feigelson, S., Manevich, E., Kolanus, W., ... Alon, R. (2005). Lymphocyte arrest requires instantaneous induction of an extended LFA-1 conformation mediated by endothelium-bound chemokines. *Nature Immunology*, 6(5), 497–506. <https://doi.org/10.1038/ni1194>
- Shi, X., Ostrovidov, S., Shu, Y., Liang, X., Nakajima, K., Wu, H., & Khademhosseini, A. (2014). Microfluidic Generation of Polydopamine Gradients on Hydrophobic Surfaces. *Langmuir*, 30(3), 832–838. <https://doi.org/10.1021/la4041216>
- Shimaoka, M., Xiao, T., Liu, J.-H., Yang, Y., Dong, Y., Jun, C.-D., ... Springer, T. A. (2003). Structures of the α L I Domain and Its Complex with ICAM-1 Reveal a Shape-Shifting Pathway for Integrin Regulation. *Cell*, 112(1), 99–111.

- Shulman, Z., Shinder, V., Klein, E., Grabovsky, V., Yeger, O., Geron, E., ... Alon, R. (2009). Lymphocyte Crawling and Transendothelial Migration Require Chemokine Triggering of High-Affinity LFA-1 Integrin. *Immunity*, *30*, 384–396. <https://doi.org/10.1016/j.immuni.2008.12.020>
- Simon, S. I., & Goldsmith, H. L. (2002). Leukocyte Adhesion Dynamics in Shear Flow. *Annals of Biomedical Engineering*, *30*(3), 315–332. <https://doi.org/10.1114/1.1467677>
- Singbartl, K., Thatte, J., Smith, M. L., Wethmar, K., Day, K., & Ley, K. (2001). A CD2-Green Fluorescence Protein-Transgenic Mouse Reveals Very Late Antigen-4-Dependent CD8+ Lymphocyte Rolling in Inflamed Venules. *The Journal of Immunology*, *166*(12), 7520–7526. <https://doi.org/10.4049/jimmunol.166.12.7520>
- Small, J., Isenberg, G., & Celis, J. (1978). *Polarity of actin at the leading edge of cultured cells*. *272*, 638–639.
- Smith, A., Bracke, M., Leitinger, B., Porter, J. C., & Hogg, N. (2003). LFA-1-induced T cell migration on ICAM-1 involves regulation of MLCK-mediated attachment and ROCK-dependent detachment. *Journal of Cell Science*, *116*(Pt 15), 3123–3133. <https://doi.org/10.1242/jcs.00606>
- Smith, J. T., Tomfohr, J. K., Wells, M. C., Beebe, T. P., Kepler, T. B., & Reichert, W. M. (2004). Measurement of Cell Migration on Surface-Bound Fibronectin Gradients. *Langmuir*, *20*(19), 8279–8286. <https://doi.org/10.1021/la0489763>
- Smith, L. A., Aranda-Espinoza, H., Haun, J. B., & Hammer, D. A. (2007). Interplay between shear stress and adhesion on neutrophil locomotion. *Biophysical Journal*, *92*(2), 632–640. <https://doi.org/10.1529/biophysj.105.079418>

- Smith, M. A., Blankman, E., Gardel, M. L., Luettjohann, L., Waterman, C. M., & Beckerle, M. C. (2010). A zyxin-mediated mechanism for actin stress fiber maintenance and repair. *Developmental Cell*, *19*(3), 365–376. <https://doi.org/10.1016/j.devcel.2010.08.008>
- Snapper, S. B., Meelu, P., Nguyen, D., Stockton, B. M., Bozza, P., Alt, F. W., ... Klein, C. (2005). WASP deficiency leads to global defects of directed leukocyte migration in vitro and in vivo. *Journal of Leukocyte Biology*, *77*(6), 993–998. <https://doi.org/10.1189/jlb.0804444>
- Solanes, P., Heuzé, M. L., Maurin, M., Bretou, M., Lautenschlaeger, F., Maiuri, P., ... Lennon-Duménil, A.-M. (2015). Space exploration by dendritic cells requires maintenance of myosin II activity by IP3 receptor 1. *The EMBO Journal*, *34*(6), 798–810. <https://doi.org/10.15252/emj.201489056>
- Soriano, S. F., Hons, M., Schumann, K., Kumar, V., Dennier, T. J., Lyck, R., ... Stein, J. V. (2011). In Vivo Analysis of Uropod Function during Physiological T Cell Trafficking. *The Journal of Immunology*, *187*(5), 2356–2364. <https://doi.org/10.4049/jimmunol.1100935>
- Squires, T. M., Messinger, R. J., & Manalis, S. R. (2008). Making it stick: convection, reaction and diffusion in surface-based biosensors. *Nature Biotechnology*, *26*(4), 417–426. <https://doi.org/10.1038/nbt1388>
- Steiner, O., Coisne, C., Cecchelli, R., Boscacci, R., Deutsch, U., Engelhardt, B., & Lyck, R. (2010). Differential roles for endothelial ICAM-1, ICAM-2, and VCAM-1 in shear-resistant T cell arrest, polarization, and directed crawling on blood-brain barrier endothelium. *Journal of Immunology (Baltimore, Md.: 1950)*, *185*(8), 4846–4855. <https://doi.org/10.4049/jimmunol.0903732>
- Stoecklin, C., Yue, Z., Chen, W. W., de Mets, R., Fong, E., Studer, V., & Viasnoff, V. (2018). A New Approach to Design Artificial 3D Microniches with Combined Chemical,

- Topographical, and Rheological Cues. *Advanced Biosystems*, 2(7), 1700237.
<https://doi.org/10.1002/adbi.201700237>
- Strale, P. O., Azioune, A., Bugnicourt, G., Lecomte, Y., Chahid, M., & Studer, V. (2015).
Multiprotein Printing by Light-Induced Molecular Adsorption. *Advanced Materials*.
<https://doi.org/10.1002/adma.201504154>
- Strale, P.-O., Azioune, A., Bugnicourt, G., Lecomte, Y., Chahid, M., & Studer, V. (2016).
Multiprotein Printing by Light-Induced Molecular Adsorption. *Advanced Materials*,
28(10), 2024-+. <https://doi.org/10.1002/adma.201504154>
- Stroka, K. M., & Aranda-Espinoza, H. (2009). Neutrophils display biphasic relationship
between migration and substrate stiffness. *Cell Motility*, 66(6), 328–341.
<https://doi.org/10.1002/cm.20363>
- Stroka, K. M., & Aranda-Espinoza, H. (2011). Endothelial cell substrate stiffness influences
neutrophil transmigration via myosin light chain kinase-dependent cell contraction.
Blood, 118(6), 1632–1640. <https://doi.org/10.1182/blood-2010-11-321125>
- Sumagin, R., Prizant, H., Lomakina, E., Waugh, R. E., & Sarelius, I. H. (2010). LFA-1 and Mac-1
Define Characteristically Different Intraluminal Crawling and Emigration Patterns for
Monocytes and Neutrophils In Situ. *The Journal of Immunology*, 185(11), 7057–7066.
<https://doi.org/10.4049/jimmunol.1001638>
- Sumagin, Ronen, & Sarelius, I. H. (2010). Intercellular Adhesion Molecule-1 Enrichment near
Tricellular Endothelial Junctions Is Preferentially Associated with Leukocyte
Transmigration and Signals for Reorganization of These Junctions To Accommodate
Leukocyte Passage. *The Journal of Immunology*, 184(9), 5242–5252.
<https://doi.org/10.4049/jimmunol.0903319>

- Sun, Z., Costell, M., & Fässler, R. (2019). Integrin activation by talin, kindlin and mechanical forces. *Nature Cell Biology*, 21(1), 25. <https://doi.org/10.1038/s41556-018-0234-9>
- Sun, Z., Guo, S. S., & Fässler, R. (2016). Integrin-mediated mechanotransduction. *J Cell Biol*, 215(4), 445–456. <https://doi.org/10.1083/jcb.201609037>
- Svitkina, T. (2018). The Actin Cytoskeleton and Actin-Based Motility. *Cold Spring Harbor Perspectives in Biology*, 10(1). <https://doi.org/10.1101/cshperspect.a018267>
- Svitkina, T. M., Bulanova, E. A., Chaga, O. Y., Vignjevic, D. M., Kojima, S., Vasiliev, J. M., & Borisy, G. G. (2003). Mechanism of filopodia initiation by reorganization of a dendritic network. *The Journal of Cell Biology*, 160(3), 409–421. <https://doi.org/10.1083/jcb.200210174>
- Swaney, K. F., & Li, R. (2016). Function and regulation of the Arp2/3 complex during cell migration in diverse environments. *Current Opinion in Cell Biology*, 42, 63–72. <https://doi.org/10.1016/j.ceb.2016.04.005>
- Sweeney, H. L., & Holzbaur, E. L. F. (2018). Motor Proteins. *Cold Spring Harbor Perspectives in Biology*, 10(5), a021931. <https://doi.org/10.1101/cshperspect.a021931>
- Tanizaki, H., Egawa, G., Inaba, K., Honda, T., Nakajima, S., Moniaga, C. S., ... Kabashima, K. (2010). Rho-mDia1 pathway is required for adhesion, migration, and T-cell stimulation in dendritic cells. *Blood*, 116(26), 5875–5884. <https://doi.org/10.1182/blood-2010-01-264150>
- Theodoly, O., Huang, Z.-H., & Valignat, M.-P. (2010). New Modeling of Reflection Interference Contrast Microscopy Including Polarization and Numerical Aperture Effects: Application to Nanometric Distance Measurements and Object Profile Reconstruction. *Langmuir*, 26(3), 1940–1948. <https://doi.org/10.1021/la902504y>

- Theodoly, Olivier, Garcia-Seyda, N., Bedu, F., Luo, X., Gabriele, S., Mignot, T., ... Valignat, M.-P. (2018). Live nanoscopic to mesoscopic topography reconstruction with an optical microscope for chemical and biological samples. *PLOS ONE*, *13*(12), e0207881. <https://doi.org/10.1371/journal.pone.0207881>
- Theodosiou, M., Widmaier, M., Böttcher, R. T., Rognoni, E., Veelders, M., Bharadwaj, M., ... Fässler, R. (2016). Kindlin-2 cooperates with talin to activate integrins and induces cell spreading by directly binding paxillin. *ELife*, *5*, e10130. <https://doi.org/10.7554/eLife.10130>
- They, M. (2010). Micropatterning as a tool to decipher cell morphogenesis and functions. *Journal of Cell Science*, *123*(24), 4201–4213. <https://doi.org/10.1242/jcs.075150>
- Théry, M., Jiménez-Dalmaroni, A., Racine, V., Bornens, M., & Jülicher, F. (2007). Experimental and theoretical study of mitotic spindle orientation. *Nature*, *447*(7143), 493–496. <https://doi.org/10.1038/nature05786>
- Théry, M., Racine, V., Pépin, A., Piel, M., Chen, Y., Sibarita, J.-B., & Bornens, M. (2005). The extracellular matrix guides the orientation of the cell division axis. *Nature Cell Biology*, *7*(10), 947–953. <https://doi.org/10.1038/ncb1307>
- Thibault, M. M., Hoemann, C. D., & Buschmann, M. D. (2007). Fibronectin, Vitronectin, and Collagen I Induce Chemotaxis and Haptotaxis of Human and Rabbit Mesenchymal Stem Cells in a Standardized Transmembrane Assay. *Stem Cells and Development*, *16*(3), 489–502. <https://doi.org/10.1089/scd.2006.0100>
- Thrasher, A. J. (2002). Wasp in immune-system organization and function. *Nature Reviews Immunology*, *2*(9), 635–646. <https://doi.org/10.1038/nri884>
- Trichet, L., Digabel, J. L., Hawkins, R. J., Vedula, S. R. K., Gupta, M., Ribault, C., ... Ladoux, B. (2012). Evidence of a large-scale mechanosensing mechanism for cellular adaptation

- to substrate stiffness. *Proceedings of the National Academy of Sciences*, 109(18), 6933–6938. <https://doi.org/10.1073/pnas.1117810109>
- Tybulewicz, V. L. J., & Henderson, R. B. (2009). Rho family GTPases and their regulators in lymphocytes. *Nature Reviews. Immunology*, 9(9), 630–644. <https://doi.org/10.1038/nri2606>
- Urbich, C., Dernbach, E., Reissner, A., Vasa, M., Zeiher, A. M., & Dimmeler, S. (2002). Shear stress-induced endothelial cell migration involves integrin signaling via the fibronectin receptor subunits alpha(5) and beta(1). *Arteriosclerosis, Thrombosis, and Vascular Biology*, 22(1), 69–75.
- Valignat, M. P., Theodoly, O., Gucciardi, A., Hogg, N., & Lellouch, A. C. (2013). T lymphocytes orient against the direction of fluid flow during LFA-1-mediated migration. *Biophysical Journal*, 104(2), 322–331. <https://doi.org/10.1016/j.bpj.2012.12.007>
- Valignat, M.-P., Nègre, P., Cadra, S., Lellouch, A. C., Gallet, F., Hénon, S., & Theodoly, O. (2014). Lymphocytes can self-steer passively with wind vane uropods. *Nature Communications*, 5, 5213. <https://doi.org/10.1038/ncomms6213>
- Vargas, P., Maiuri, P., Bretou, M., Saéz, P. J., Pierobon, P., Maurin, M., ... Lennon-Duménil, A. M. (2016). Innate control of actin nucleation determines two distinct migration behaviours in dendritic cells. *Nature Cell Biology*, 18(1), 43–53. <https://doi.org/10.1038/ncb3284>
- Vicente-Manzanares, M., Koach, M. A., Whitmore, L., Lamers, M. L., & Horwitz, A. F. (2008). Segregation and activation of myosin IIB creates a rear in migrating cells. *The Journal of Cell Biology*, 183(3), 543–554. <https://doi.org/10.1083/jcb.200806030>

- Vicente-Manzanares, M., Ma, X., Adelstein, R. S., & Horwitz, A. R. (2009). Non-muscle myosin II takes centre stage in cell adhesion and migration. *Nature Reviews. Molecular Cell Biology*, 10(11), 778–790. <https://doi.org/10.1038/nrm2786>
- Vicente-Manzanares, M., Zareno, J., Whitmore, L., Choi, C. K., & Horwitz, A. F. (2007). Regulation of protrusion, adhesion dynamics, and polarity by myosins IIA and IIB in migrating cells. *The Journal of Cell Biology*, 176(5), 573–580. <https://doi.org/10.1083/jcb.200612043>
- Vignjevic, D., Kojima, S., Aratyn, Y., Danciu, O., Svitkina, T., & Borisy, G. G. (2006). Role of fascin in filopodial protrusion. *The Journal of Cell Biology*, 174(6), 863–875. <https://doi.org/10.1083/jcb.200603013>
- Von Philipsborn, A. C., Lang, S., Jiang, Z., Bonhoeffer, F., & Bastmeyer, M. (2007). Substrate-Bound Protein Gradients for Cell Culture Fabricated by Microfluidic Networks and Microcontact Printing. *Science Signaling*, 2007(414), p16–p16. <https://doi.org/10.1126/stke.4142007p16>
- Von Philipsborn, A. C., Lang, S., Loeschinger, J., Bernard, A., David, C., Lehnert, D., ... Bastmeyer, M. (2006). Growth cone navigation in substrate-bound ephrin gradients. *Development*, 133(13), 2487–2495. <https://doi.org/10.1242/dev.02412>
- Waldbaur, A., Waterkotte, B., Schmitz, K., & Rapp, B. E. (2012). Maskless Projection Lithography for the Fast and Flexible Generation of Grayscale Protein Patterns. *Small*, 8(10), 1570–1578. <https://doi.org/10.1002/sml.201102163>
- Walling, B. L., & Kim, M. (2018). LFA-1 in T Cell Migration and Differentiation. *Frontiers in Immunology*, 9. <https://doi.org/10.3389/fimmu.2018.00952>
- Wang, C. J., Li, X., Lin, B., Shim, S., Ming, G., & Levchenko, A. (2008). A microfluidics-based turning assay reveals complex growth cone responses to integrated gradients of

- substrate-bound ECM molecules and diffusible guidance cues. *Lab on a Chip*, 8(2), 227–237. <https://doi.org/10.1039/B713945D>
- Wang, Y. L. (1985). Exchange of actin subunits at the leading edge of living fibroblasts: possible role of treadmilling. *The Journal of Cell Biology*, 101(2), 597–602. <https://doi.org/10.1083/jcb.101.2.597>
- Wang, Y., Li, D., Jones, D., Bassett, R., Sale, G. E., Khalili, J., ... Ma, Q. (2009). Blocking LFA-1 Activation with Lovastatin Prevents Graft-versus-Host Disease in Mouse Bone Marrow Transplantation. *Biology of Blood and Marrow Transplantation*, 15(12), 1513–1522. <https://doi.org/10.1016/j.bbmt.2009.08.013>
- Watabe, D., Kanno, H., Yoshida, A., Kurose, A., Akasaka, T., & Sawai, T. (2007). Adhesion of peripheral blood mononuclear cells and CD4+ T cells from patients with psoriasis to cultured endothelial cells via the interaction between lymphocyte function-associated antigen type 1 and intercellular adhesion molecule 1. *British Journal of Dermatology*, 157(2), 259–265. <https://doi.org/10.1111/j.1365-2133.2007.08039.x>
- Weaver, A. M., Karginov, A. V., Kinley, A. W., Weed, S. A., Li, Y., Parsons, J. T., & Cooper, J. A. (2001). Cortactin promotes and stabilizes Arp2/3-induced actin filament network formation. *Current Biology: CB*, 11(5), 370–374.
- Weber, M., Hauschild, R., Schwarz, J., Moussion, C., de Vries, I., Legler, D. F., ... Sixt, M. (2013). Interstitial Dendritic Cell Guidance by Haptotactic Chemokine Gradients. *Science*, 339(6117), 328–332. <https://doi.org/10.1126/science.1228456>
- Wehrle-Haller, B. (2012). Structure and function of focal adhesions. *Current Opinion in Cell Biology*, 24(1), 116–124. <https://doi.org/10.1016/j.ceb.2011.11.001>

- Weninger, W., Biro, M., & Jain, R. (2014). Leukocyte migration in the interstitial space of non-lymphoid organs. *Nature Reviews Immunology*, *14*(4).
<https://doi.org/10.1038/nri3641>
- Westerberg, L., Larsson, M., Hardy, S. J., Fernández, C., Thrasher, A. J., & Severinson, E. (2005). Wiskott-Aldrich syndrome protein deficiency leads to reduced B-cell adhesion, migration, and homing, and a delayed humoral immune response. *Blood*, *105*(3), 1144–1152. <https://doi.org/10.1182/blood-2004-03-1003>
- Whitesides, G. M. (2006). The origins and the future of microfluidics. *Nature*, *442*(7101), 368–373. <https://doi.org/10.1038/nature05058>
- Wilkinson, P. C. (1998). Chemotaxis. In P. J. Delves (Ed.), *Encyclopedia of Immunology (Second Edition)* (pp. 533–537). <https://doi.org/10.1006/rwei.1999.0140>
- Wolf, K., Lindert, M. te, Krause, M., Alexander, S., Riet, J. te, Willis, A. L., ... Friedl, P. (2013). Physical limits of cell migration: Control by ECM space and nuclear deformation and tuning by proteolysis and traction force. *J Cell Biol*, *201*(7), 1069–1084.
<https://doi.org/10.1083/jcb.201210152>
- Wolf, K., Müller, R., Borgmann, S., Bröcker, E.-B., & Friedl, P. (2003). Amoeboid shape change and contact guidance: T-lymphocyte crawling through fibrillar collagen is independent of matrix remodeling by MMPs and other proteases. *Blood*, *102*(9), 3262–3269. <https://doi.org/10.1182/blood-2002-12-3791>
- Wolfenson, H., Bershadsky, A., Henis, Y. I., & Geiger, B. (2011). Actomyosin-generated tension controls the molecular kinetics of focal adhesions. *Journal of Cell Science*, *124*(Pt 9), 1425–1432. <https://doi.org/10.1242/jcs.077388>

- Woodrum, D. T. (1975). Evidence for biased bidirectional polymerization of actin filaments using heavy meromyosin prepared by an improved method. *The Journal of Cell Biology*, 67(1), 231–237. <https://doi.org/10.1083/jcb.67.1.231>
- Woolf, E., Grigorova, I., Sagiv, A., Grabovsky, V., Feigelson, S. W., Shulman, Z., ... Alon, R. (2007). Lymph node chemokines promote sustained T lymphocyte motility without triggering stable integrin adhesiveness in the absence of shear forces. *Nature Immunology*, 8(10), 1076–1085. <https://doi.org/10.1038/ni1499>
- Worth, D. C., Hovalala-Dilke, K., Robinson, S. D., King, S. J., Morton, P. E., Gertler, F. B., ... Parsons, M. (2010). $\alpha\beta 3$ integrin spatially regulates VASP and RIAM to control adhesion dynamics and migration. *The Journal of Cell Biology*, 189(2), 369–383. <https://doi.org/10.1083/jcb.200912014>
- Wu, C., Asokan, S. B., Berginski, M. E., Haynes, E. M., Sharpless, N. E., Griffith, J. D., ... Bear, J. E. (2012). Arp2/3 Is Critical for Lamellipodia and Response to Extracellular Matrix Cues but Is Dispensable for Chemotaxis. *Cell*, 148(5), 973–987. <https://doi.org/10.1016/j.cell.2011.12.034>
- Xiao, T., Takagi, J., Collier, B. S., Wang, J.-H., & Springer, T. A. (2004). Structural basis for allostery in integrins and binding to fibrinogen-mimetic therapeutics. *Nature*, 432(7013), 59–67. <https://doi.org/10.1038/nature02976>
- Xiong, J.-P., Stehle, T., Diefenbach, B., Zhang, R., Dunker, R., Scott, D. L., ... Arnaout, M. A. (2001). Crystal Structure of the Extracellular Segment of Integrin $\alpha\beta 3$. *Science (New York, N.Y.)*, 294(5541), 339–345. <https://doi.org/10.1126/science.1064535>
- Xu, H., Manivannan, A., Goatman, K. A., Jiang, H.-R., Liversidge, J., Sharp, P. F., ... Crane, I. J. (2004). Reduction in shear stress, activation of the endothelium, and leukocyte

- priming are all required for leukocyte passage across the blood--retina barrier. *Journal of Leukocyte Biology*, 75(2), 224–232. <https://doi.org/10.1189/jlb.1002479>
- Yago, T., Wu, J., Wey, C. D., Klopocki, A. G., Zhu, C., & McEver, R. P. (2004). Catch bonds govern adhesion through L-selectin at threshold shear. *The Journal of Cell Biology*, 166(6), 913–923. <https://doi.org/10.1083/jcb.200403144>
- Yang, C., Czech, L., Gerboth, S., Kojima, S., Scita, G., & Svitkina, T. (2007). Novel Roles of Formin mDia2 in Lamellipodia and Filopodia Formation in Motile Cells. *PLoS Biology*, 5(11), e317. <https://doi.org/10.1371/journal.pbio.0050317>
- Yang, H. W., Collins, S. R., & Meyer, T. (2016). Locally excitable Cdc42 signals steer cells during chemotaxis. *Nature Cell Biology*, 18(2), 191–201. <https://doi.org/10.1038/ncb3292>
- Yang, L., Froio, R. M., Sciuto, T. E., Dvorak, A. M., Alon, R., & Luscinskas, F. W. (2005). ICAM-1 regulates neutrophil adhesion and transcellular migration of TNF-alpha-activated vascular endothelium under flow. *Blood*, 106(2), 584–592. <https://doi.org/10.1182/blood-2004-12-4942>
- Ye, F., Hu, G., Taylor, D., Ratnikov, B., Bobkov, A. A., McLean, M. A., ... Ginsberg, M. H. (2010). Recreation of the terminal events in physiological integrin activation. *The Journal of Cell Biology*, 188(1), 157–173. <https://doi.org/10.1083/jcb.200908045>
- Zaidel-Bar, R., Kam, Z., & Geiger, B. (2005). Polarized downregulation of the paxillin-p130CAS-Rac1 pathway induced by shear flow. *Journal of Cell Science*, 118(Pt 17), 3997–4007. <https://doi.org/10.1242/jcs.02523>
- Zhang, K., Sugawara, A., & Tirrell, D. A. (2009). Generation of surface-bound multicomponent protein gradients. *Chembiochem : A European Journal of Chemical Biology*, 10(16), 2617–2619. <https://doi.org/10.1002/cbic.200900542>

Zhang, X., Jiang, G., Cai, Y., Monkley, S. J., Critchley, D. R., & Sheetz, M. P. (2008). Talin depletion reveals independence of initial cell spreading from integrin activation and traction. *Nature Cell Biology*, *10*(9), 1062–1068. <https://doi.org/10.1038/ncb1765>

Zhu, J., Luo, B.-H., Xiao, T., Zhang, C., Nishida, N., & Springer, T. A. (2008). Structure of a complete integrin ectodomain in a physiologic resting state and activation and deactivation by applied forces. *Molecular Cell*, *32*(6), 849–861.

<https://doi.org/10.1016/j.molcel.2008.11.018>

Appendice

Appendix 1 T cell culture protocol

To prepare:

- Frozen PBMC vial and IL2 (in the -80°C freezer of the cell culture platform)
- Culture media without antibiotics: RPMI + 10% FCS + Glutamax
- MACS buffer: PBS 0.5% BSA 2mM EDTA
- Washing buffer: PBS 0.1% BSA 2mM EDTA
- Miltenyi isolation kit (ref 130-096-535), LS column and miltenyi magnet
- Dynabeads CD3/CD28 (ref 11131D) and stemcell magnet

D0 (Tuesday): Isolation Pan T cell from frozen PBMC (kit Miltenyi 130-096-535)

1. Thaw one tube of PBMC (20 million of cells) in 10 mL RPMI 10%SVF + glutamax
2. Transfer the cells into a T75 flask and let them rest for 3h at 37°C
3. Centrifuge for 5 min at 1000 rpm
4. Resuspend the pellet in 80µl of « MACS » buffer (PBS 0.5% BSA 2mM EDTA)
5. Add 20µL of Pan T cell biotin antibody cocktail
6. Vortex a few seconds and incubate for 5 min in the fridge
7. Add 60µL of « MACS » buffer
8. Add 40µL of Pan T cell microbeads cocktail
9. Vortex few sec and incubate 10 min in the fridge
 - During incubation: Load the LS column on the Miltenyi magnet and rinse it with 3 ml of « MACS » buffer
10. Add 300 µL of « MACS » buffer in the cell suspension
11. Place a new flacon tube above the column to collect the enriched T cells
12. Apply all the suspension on the column and collect flow-trough
13. Wash column with 3mL of « MACS » buffer and collect in the same tube
14. Homogenize the suspension and determine cell number
15. Centrifuge for 5 min at 1000rpm
16. Determine the volume of dynabeads: 25µl par million de T cell
17. Vortex dynabeads 30 sec
18. Transfer the desired volume in a 5ml sterile tube (BD #352058)
19. Add 1ml of « washing buffer » (PBS 0.1% BSA 2mM EDTA)
20. Vortex few sec and incubate 1min on stemcell magnet
21. Discard the supernatant
22. Remove the tube from the magnet
23. Resuspend cell pellet + dynabeads in a final volume of RPMI 10%SVF + glutamax to get 1million of cell/ml
24. Incubate the flask at 37°C with 5% CO₂ for 48h

D1 (Wednesday): check the cell culture and homogenize the suspension by pipetting up and down 2 or 3 times

D2 (Thursday): Removing dynabeads from cell culture (it's best to do it early in the day)

1. Homogenize suspension to break binding between beads and cells
2. Put 2mL of this suspension in a 5mL sterile tube (BD #352058)
3. Place the tube (without lid) into the stemcell magnet and incubate for 1min
4. Pick up the magnet, and in one continuous motion, invert the magnet and tube, pouring the cell suspension into a new tube (falcon 15mL)
5. Repeat the above steps until all the suspension has been passed
6. Rinse the tube with 1 mL of RPMI 10%SVF + glutamax media
7. Incubation for 1min on the magnet and add it to the cell suspension
8. Note the final volume of the suspension and determine cell number
9. Centrifuge for 5 min at 1000 rpm
10. Resuspend the cell pellet in RPMI 10%SVF + glutamax at 1 million cells/mL
11. Add I12 at 1/1000

D3 (Friday): Subculture (it's best to do it late in the afternoon)

1. Determine cell number
2. Centrifuge for 5min at 1000 rpm
3. Resuspend the cell pellet in RPMI 10%SVF + glutamax at 1 million /mL
4. Add I12 at 1/1000

D5 (Monday): Subculture

1. Determine cell number
2. Centrifuge for 5min at 1000 rpm
3. Resuspend the cell pellet in RPMI 10%SVF + glutamax at **1.5 million/mL**
4. Add I12 at 1/1000
5. Split the volume in 2 culture flasks: A and B

Subcultures (same protocole as J5):

1. Tuesday and Thursday for B culture
2. Wednesday for A culture

Cells are used for experiments from Monday J5.

And except on Monday, experiments are done with cells sub-cultured the day before.

3. Monday, Tuesday and Thursday with A culture
4. Wednesday and Friday with B culture

Appendix 2 PDMS microwell preparation protocol

Part one: surface silanization with APTES (gas phase)

1. Activate glass coverslip (Schott coverslip ultraclean) with air plasma (5min, level high)
2. Take out the activated plasma and put them onto the lid of a petri-dish (medium size)

Note: put a small piece of tissue wipe on the lid beforehand to avoid binding between the activated coverslip and the plastic

3. Put 80 μ l of APTS stock solution into the cap of the 1.5mL Eppendorf tube and put the cap also onto the lid of the petri-dish

Note: bottle in the cold room, shelf Théo; it is highly recommended to take a smaller volume for future use and to stock both the aliquot and original bottle in the dark and in N₂ at 4°C

4. Stick the PDMS microwell (precut, 4 wells per sticker) onto the glass coverslip
5. Put everything in 3 in to the silanization chamber (plastic pipette box with drying grains on the bottom), close the box and **wrapped it up carefully with parafilm!!!**
6. Incubate at RT for an hour
7. Take out the treated glass coverslip and heat it at 95°C for 15min
8. The coverslip is then ready for future use

Part two: Grafting PEG-SVA onto APTES coated surface

1. Weigh 0.126g Sodium Bicarbonate and dissolve it in 15mL distilled water (100mM solution)
2. Prepare 70 μ L 10mM Bicarbonate solution from the 100mM mother solution

Note: the solution must be freshly prepared before the experiment

3. Weigh 0.016g mPEG-SVA (Note: let the reagent return to room temperature before opening the bottle)
4. Before dissolving mPEG-SVA, glue the coverslip onto the bottom of a precut small petri-dish with the epoxy glue and wait for it to dry
5. Dissolve the mPEG-SVA in 70 μ L 10M Sodium Bicarbonate

Note: the solution is only active for 10 minutes so only do step 5 in the very end

6. Add 4 μ L mPEG-SVA solution into each microwell already treated with APTES
7. Incubate the glass coverslip at room temperature in humidified box for 1h

8. Rinse the microwells with copious amount of PBS (use the pump at the Alevole workstation)
9. Preserve the coverslip in humidified containers. The sample can be kept for the experiments of the same week Note: evaporation must be avoided!!!

Appendix 3 Glass-bottom Ibidi channel preparation protocol

1. Take out gently one piece of ultraclean Schott coverslip (25mm x 75mm) from its box
2. Activate the glass coverslip with air plasma (5min at high)
3. Put 80 μ l of APTS stock solution into the cap of the 1.5mL Eppendorf tube

Note: the bottle is in the cold room, shelf Théo; it is highly recommended to take a smaller volume for future use and to stock both the aliquot and original bottle in the dark and in N₂ at 4°C

4. Put both the APTS solution and the glass coverslip into the silanization chamber (plastic pipette box with BLUE drying grains on the bottom), close the box and **wrapped it up carefully with parafilm!!!**
5. Incubate at RT for an hour
6. Heat the silanized glass coverslip for 15min at 95°C on a heating plate
7. The silanized glass coverslip is ready for mounting
8. Take out one piece of Ibidi Sticky slide V0.4 (400 μ m in height) with 6 empty channels ready to be mounted and peel off the protection sticker
9. Take out the silanized the glass coverslip and stick the treated side onto the sticky slide
10. Carefully remove all the air trapped between the coverslip and the slide by firmly pressing the coverslip against the slide
11. The glass-bottom Ibidi slide is ready for future coating
 - a. For Peg coating: Incubate Peg-SVA solution (5mg powder in 100 μ L Sodium Bicarbonate solution at 1mM) for 1h at RT.
 - b. For ICAM coating: following the steps below
 - 1) Incubate fluorescently-labeled Protein A (AlexaFluo 647) at 50 μ g/mL for 1h at RT in the dark to avoid photobleaching (approximately 50 μ L per channel)
 - 2) Rinse extensively with PBS (approximately 2-3mL per channel)
 - 3) Incubate 4% (w/v) BSA solution for 15min to avoid unspecific binding (approximately 50 μ L per channel)
 - 4) Rinse extensively with PBS (approximately 2-3mL per channel)
 - 5) Incubate Fc-ICAM solution at 10 μ g/mL for 1h at RT or overnight at 4°C (the stock concentration is 500 μ g/mL and is aliquoted in 3 μ L)

- 6) Rinse extensively with PBS (approximately 2-3mL per channel)

Appendix 4 Optical protein printing protocol

Part 1 Switch-on order

General guideline: First the peripheral accessories then the microscope and at last the computer

Personal order:

1. Switch on the fluorescent lamp (in the most left corner)
2. Switch on the transmission light lamp (next to the fluorescent lamp)
3. Switch on the motorized stage (the power adapter is under the transmission lamp)
4. Transmission shutter (behind the microscope)
5. Power adapter of Primo (protein printer): press the black button to "on" at the back of the power adapter
6. Switch on the laser by turning the key to the right side
7. Switch on the camera which is installed at the left side of the microscope
8. Switch on the microscope (the power button is in the back of the microscope and on the right side)
9. Switch on the computer

Part 2 NIS software pre-printing configuration

1. Double click the icon NIS to launch the software
2. Select the camera by clicking on OK of the prompt window (after this you will enter the main interface of the NIS software)
3. Select the optical configuration "Primo" for printing
4. Go to the right part of the software and select the Primo plug-in named "Alvéole Primo" - now you are in the panel for protein printing

Part 3 Protein printing- calibration

1. Reduce the size of the window – do not work on full-screen mode!
2. Click on the first sub-panel "Device"
3. Switch on the DMD by clicking on "Open"
4. Click on the next sub-panel to go to "Calibration"
5. Prepare a glass cover-slide for calibration: take a glass cover-slide, draw a cross in the middle and coat the surface with a stabilo highlighter which will be auto-fluorescent under UV light
6. Put the coated cover-slide on the sample holder
7. Click on "Live", adjust the transmission light intensity and find the cross by moving the stage with the joystick which is on the right side of the microscope

8. Adjust the focus to see the cross clearly and once it's done, activate the PFS by pressing the button on in the front of the microscope
9. Move slightly away from the cross and turn off the transmission light
10. In the "Calibration" sub-panel, click on "Dots" and note that the size should be 10px
11. Turn on the laser manually by clicking on "ON" which is above the "Calibration" sub-panel
12. Adjust the camera exposure time (inside the panel Flash 4.0 settings) and/or the contrast (using the panel LUT) to see the 4 small rectangles projected onto the surface
13. Adjust the off-set to see the rectangles clearly
14. Go back to the sub-panel "Calibration", click on the button "calibrate"

Possible error messages and solutions:

- Too much light: decrease camera exposure time
 - Too little light: increase camera exposure time
 - More than 4 dots: increase the threshold (inside the calibration sub-panel)
 - Less than 4 dots: decrease the threshold (inside the calibration sub-panel)
15. Once the calibration is completed, the calculation results will be automatically filled
 16. Please turn off manually the laser by clicking on "ON" again
 17. Please erase manually the dots from the DMD by clicking on "Dots" again

Part 3bis Protein printing- PLPP injection and fluidic mixing set up for flow chamber

1. Fill both reservoirs with PBS to avoid air bubbles
2. Plug the shorter tubing onto one of the reservoirs
3. Aspire 80µL PLPP into the longer tubing with the micro-syringe and remove all air bubbles in the tubing
4. Slightly push the syringe so that there is a drop of PLPP at the end of the tubing to avoid the entry of air bubbles
5. Plug the tubing onto the other reservoir and inject 50µL of PLPP
6. Mix the solution in the channel with the syringe

Part 4 Protein printing- patterning

Please note that evaporation and surface drying must be avoided!

1. Set the UV intensity at 5V (normally this value is not to be changed)
2. Set the UV insolation time (63s for positive printing from Peg surface and 31s for negative printing from a functional protein surface)
3. Click on "pattern" to go to the corresponding sub-panel for protein patterning

4. Click on "Browse" to find the desired pattern and click on "Initialize" to load the pattern onto the DMD (Please note that this step must be repeated after each UV insolation)
5. If necessary, define the number of rows and columns to be patterned and the interval in X and Y direction
6. Add 10 μ L of PLPP (photo-initiators) into the microwell by replacing the PBS (Please adjust the volume according to the size of the microwell)
7. Verify the focus (to ensure optimal pattern quality, please use reflected light and focus on the shadow of the diaphragm)
8. Move to the area to be patterned using the joystick after verifying the focus
9. Turn on the carbogene flow and adjust the valve to obtain a gentle and continuous flow
10. Put the carbogene cap onto the sample
11. Click on "Set reference" in the "Pattern" sub-panel to mark the starting point of patterning
12. Once everything is ready, click on "Run" and then on "OK" of the prompt window to start the patterning
13. If necessary, it's possible to pattern again at another position of the same surface without refilling the PLPP and with the carbogene cap left on, repeat simply 4,5,7,8,11,12
14. At the end of patterning, rinse extensively the surface with PBS using the syringe pump with suction
15. If necessary, it's possible to pattern first multiple surfaces and rinse everything in the end
16. Incubate the protein of interest
17. Rinse extensively with PBS at the end of incubation

Appendix 5 Cell adhesion and migration assay protocol

Part 1 Ibidi pump set-up

1. Plug the power supply of the Ibidi pump and verify the connection cable, the air entry and the filters
2. Launch the software: choose the corresponding tubing (white) and the channel size (VI0.4) and click on the "apply" button to initialize all the parameters
3. Fill the pump with 5.5mL culture media in each syringe
4. Set the shear stress at 8dyn/cm^2 and start pumping for at least 10min to remove the air bubbles trapped in the tubing and the syringes
5. Stop the pump when it's equilibrated: the liquid on both syringes should be at the same level and clamp the tubing

Part 2 Channel plugging and cell seeding

1. Replace the PBS in the patterned channel with culture media and incubate for 5min at 37°C
2. After incubation, inject $50\mu\text{L}$ cell suspension at a concentration of 1.5M cells/mL and incubate for 10mins
3. Check the cells at microscope before plugging the pump
4. Before plugging, fill both reservoirs with culture media to avoid air bubbles
5. Separate the tubing, remove the air bubbles trapped at the connection and plug the tube with blue marker into the top reservoir (so that the flow comes from the top)
6. Plug the second tubing into the bottom reservoir

Part 3 Cell adhesion and migration assay on patterned surface under flow

1. Find the first pattern with the help of fluorescent label, move the sample so that the pattern appears in the right orientation on camera
2. Immobilize the sample by taping the Ibidi slide to the microscope stage and place the sample clip on top (The sample must not move during the entire acquisition)
3. For each pattern, switch to the Cy5 filter cube, take a snapshot of the fluorescent pattern and record the X and Y position
4. Then, switch to transmitted light, for each pattern, choose the best focal plane to visualize cells and update the position list by recording the Z position using the DefiniteFocus system
5. Make a first movie for every position in absence of flow and rinsing: one image is to be taken every 10s for 20 images
6. Release the clamp and make a second movie with a shear stress of 1dyn/cm^2 to rinse non-adherent cells on the surface: one image is to be taken every 10s for 20 images

7. Make a third movie after rinsing in absence of the flow: one image is to be taken every 10s for 100 images
8. Only on homogenous patterns (large rectangular patterns), make a fourth movie with a shear stress of 4dyn/cm², one image is to be taken every 10s for 100 images
9. Only on homogenous patterns (large rectangular patterns), make a fourth movie with a shear stress of 8dyn/cm², one image is to be taken every 10s for 50 images
10. At the end of the acquisition, remove the sample and take a snapshot of the background
11. Carefully unplug the tubing and rinse the channel extensively with PBS (approximately 3mL)
12. The surface can be used to test another experimental condition and/or to be stained with corresponding antibody and the user can also test separate conditions in separate channels
13. In case of antiICAM and/or antiVCAM staining, inject 50μL antibody solution at 10μg/mL (Stock solution at 50μg/mL) and incubate overnight at 4°C

Part 4a Cell adhesion and migration assay on patterned surface under flow with Mn²⁺

To prepare:

- Culture media without Ca²⁺ and Mg²⁺: RPMI + 10% FCS + Glutamax treated with Chelax100 resin
 - Weigh 25g resin for 500mL media
 - Under the hood, add the resin directly into the media
 - Rotate mix at 4°C for 4h
 - Filter the media with filtration kit and store at 4°C
- RPMI media treated with Chelax resin complemented with 0.1mM Mn²⁺
 1. Put the previously rinsed channel at 4°C for 15min
 2. Rinse extensively with COLD PBS to remove adherent cells without damaging the surface (or start with a new channel)
 3. Take 100μL cell suspension at 1.5M cells/mL and centrifuge them for 5min at 200g
 4. Centrifuge at 200g for 5 min then resuspend the cells in 5mM EDTA the incubate at 37°C for 15 min
 5. Centrifuge again at 200g for 5 min the resuspend the cells in the RPMI media containing 0.1mM Mn²⁺
 6. Replace the PBS inside the channel with warm culture media containing 0.1mM MnCl₂ and incubate for 5min at 37°C
 7. Inject 50μL of Mn²⁺ treated cell suspension and incubate the cells for 10min at 37°C
 8. Plug the pump according to Part 2 and repeat Part 3

Part 4b Cell adhesion and migration assay on patterned surface under flow with Hi111

1. Put the previously rinsed channel at 4°C for 15min
2. Rinse extensively with COLD PBS to remove adherent cells without damaging the surface (or start with a new channel)
3. Replace the PBS inside the channel with warm culture media and incubate for 5min at 37°C
4. Incubate the integrin blocking antibody Hi111 with the cells at 50µg/mL at 37°C for 10 min in the dark
5. Incubate the cells at 1.5M cells/mL for 10min at 37°C
6. Plug the pump according to Part 2 and repeat Part 3

Part 4c Cell adhesion and migration assay on patterned surface under flow with TS1/22

1. Put the previously rinsed channel at 4°C for 15min
2. Rinse extensively with COLD PBS to remove adherent cells without damaging the surface (or start with a new channel)
3. Replace the PBS inside the channel with warm culture media and incubate for 5min at 37°C
4. Incubate the integrin blocking antibody TS1/22 with the cells at 4µg/mL (2µL stock solution into 150µL cell suspension) at 37°C for 10 min in the dark
5. Incubate the cells at 1.5M cells/mL for 10 min at 37°C
6. Plug the pump according to Part 2 and repeat Part 3

Part 4d Cell adhesion and migration assay on patterned surface under flow with Lovastatin

To prepare:

- Lovastatin solution at 50mM (stock concentration at 10mg/mL, molar mass: 404.54 g/mol)
 - To reach the target concentration, dilute 25µL stock solution into 12mL RPMI media (calculate the volume to have enough for the pump and other manipulation)
1. Put the previously rinsed channel at 4°C for 15min
 2. Rinse extensively with COLD PBS to remove adherent cells without damaging the surface (or start with a new channel)
 3. Replace the PBS inside the channel with warm culture media and incubate for 5min at 37°C
 4. Homogenize the cell suspension and take 100µL
 5. Centrifuge at 1500rpm for 5min and resuspend the cells into Lovastatin containing media
 6. Inject 50µL into the channel and incubate for 10min at 37°C
 7. Plug the pump according to Part 2 and repeat Part 3

Appendix 6 Fluorescent quantification protocol

To prepare:

- PDMS microchannels (Height=48 μ m) treated with Pluronic F127
- PE-labeled antiICAM solution of different concentrations: 7, 5, 3, 1.5, 0 μ g/mL (Note: choose the range of dilution according to the working concentration, which is 10 μ g/mL in this case)

Fluorescent calibration with antibody solution in standardized channels:

1. Incubate antibody solution of different concentrations into separate microchannels
2. Take 5 fluorescent images of each channel (Optical settings: 20X objective lens with the 0.5X camera adaptive lens, LED lamp: 3GR at 50%, F/A max) and calculate the average fluorescent intensity of each channel (Mean)
3. Wash each channel three times with PBS and repeat 2 and calculate the fluorescent intensity of each channel after rinsing (Background)
4. Subtract the Background from the Mean, plot the new average fluorescent intensity against the antibody concentrations and calculate the slope (Mean-Background=slope*concentration)
5. The obtained relation in 4 will be used as the fluorescent calibration information that allow us to convert a volume concentration into surface concentration for a channel height of 48 μ m. The molar weight of an antibody being 150kDa, then 1 μ g/mL of antibody corresponds to 4 molecules/ μ m². This value will allow us to further convert the obtained surface concentration μ g/ μ m² to the molecular surface density (molecules/ μ m²)

Fluorescent quantification of stained samples:

1. Prepare the ICAM surface or rinse the ICAM surface extensively with cold PBS to remove attached cells after an experiment
2. Stain the surface with fluorescent antibody (10 μ g/mL). Be careful to inject enough antibody solution and mix well
3. Incubate the surface overnight at 4°C (it can also be done at room temperature for at least 40 min if the measurement is time-sensitive).
4. Rinse extensively the sample after incubation with PBS.
5. Take fluorescent measurements of the sample using the same optical parameters as the ones used for the calibration (5 images per sample) and take one image for the background
6. Calculate the fluorescent intensity of the images, calculate the average intensity and normalized it by the exposure time
7. With the help of the calibration curve, calculate the surface density of the molecule:

I_{norm} : normalized fluorescent intensity

Surface density = $((I_{norm} - \text{background}) / \text{slope}) * \text{Height} * 4$

Appendix 7 ICAM beads protocol

Part 1 ICAM beads coating

To prepare

- PBS+ 4% BSA solution and +0.1% BSA solution
 - Streptavidin coated magnetic beads (Dynabeads™ M-280 Streptavidin, Invitrogen, 11205D). Stock concentration: 10 mg/mL
 - Magnet
 - 1 mL Eppendorf tube
 - Biotinylate Protein A solution (1 mg/mL)
 - ICAM solution at 500µg/mL
 - Complemented RPMI culture media
1. Take one eppendorf tube (1 mL) and passivated the inner surface of the tube with 500 µL of 4% BSA solution for 15 min at room temperature
 2. Rinse the tube twice with 1 mL PBS with agitation
 3. Centrifuge the tube with the PBS inside for 5 min at 1500 rpm
 4. Add 5 µL microbeads (stock concentration at 10 mg/mL) into the tube
 5. Place the tube onto the magnet for 1 min
 6. Aspirate the liquid and add 500 µL PBS+0.1% BSA solution. Repeat three times
 7. After the washing step, leave the microbeads in 500 µL PBS+0.1% BSA and add 2 µL biotinylated protein A solution.
 8. Incubated the microbeads with the Protein A for 1h30 with agitation at room temperature
 9. Wash the microbeads three times with PBS+0.1% BSA as described in 7
 10. Leave the microbeads in 500 µL PBS+0.1% BSA
 11. Add 3.8 µL ICAM solution into the microbeads
 12. Incubate with agitation at room temperature for 2h at room temperature or overnight at 4°C
 13. Wash the microbeads three time as described in 7 and leave the washed microbeads in 250 µL PBS+0.1% BSA

Part 2 Migration assay with ICAM coated beads and Mn^{2+}

1. Resuspend 75 µL ICAM coated microbeads into 100 µL complemented RPMI media
2. Treat cells with Mn^{2+} (see protocol regarding perturbation experiment with Mn^{2+})
3. Incubate treated cells into patterned flow chamber for 10 min at 37°C
4. Inject 50µL microbeads into the flow chamber and incubated for 10 min at 37°C

5. Launch the migration assay according to the adhesion and migration assay protocol

Appendix 8 Calcium influx detection experimental protocol

To prepare:

- HBSS (with CaCl₂ and MgCl₂) + 1% BSA and filter the media
- HBSS (with CaCl₂ and MgCl₂) + 10% FCS and filter the media
- DMSO + 20% F127 (gentle warming at ~40°C to accelerate the dissolution)
- Calcium probe working stock: Oregon Green 488 BAPTA-1 50µg in powder to be dissolved into 8µL of DMSO containing 20% F127. This stock is to be aliquoted into 8 working samples of 1µL (in a 1.5mL Eppendorf tube) and to be stocked at -20°C

Part 1 Cell loading with Calcium probe Oregon Green 488 BAPTA-1

1. Seed the cells (cultured in RPMI with 10% FCS) into the channel and incubate for 10 min at 37°C in the dark to allow cell adhesion
2. Gently rinse the channel with warm HBSS + 1% BSA (twice with 100µL) to remove non-adherent cells
3. Dilute the Oregon Green 488 BAPTA-1 to reach a working concentration of 5µM: 1µL aliquot + 1mL HBSS + 1% BSA
4. Inject 50µL of diluted Oregon Green 488 BAPTA-1 into the channel and incubated for 10min at 37°C in the dark
5. Gently rinse the channel with warm HBSS + 1% BSA (three times with 100µL)
6. Replace the medium with warm HBSS + 10% FCS
7. Plug the channel to the Ibidi pump system according the "cell migration assay protocol"

Part 2 Imaging

1. Optical set-up:
 - a. LED fluorescent light-source: channel blue at 10% intensity
 - b. Objectif: 20x with the 0.5x camera adapter with maximal numeric aperture
 - c. µManager configuration: RICM 3couleurs
 - d. Filter set: GFP with recommended illumination time at 100ms
2. Once everything is set-up, launch the movie to record the fluorescent signal of migrating cells: 100 images with 1 image captured every 10s
3. At the end of the movie, take a background photo either without the sample or in an empty channel
4. Positive control with ionomycin
 - a. Dilute the ionomycin stock solution (30µL at 1mg/mL) to 1µg/mL

- b. Set everything up according to Part 1 and Part2 step1 and 2 (do not plug the pump)
- c. Wait for 3 images to be captured and inject quickly the ionomycin into the channel and normally we should see a peak of the signal on the next image
- d. Let the movie finish

Appendix 9 Cell fixation and integrin staining protocol

To prepare:

- PBS (for all rinsing and dilution)
- PFA 4% (1.5mL) (Note: it should be trashed to specific PFA recipient)
- Human serum IgG at 100µg/mL (1mL)
- Mouse antihuman TS1/22 antibody (1/50 dilution, 400µL)
- Mouse antihuman Mb24 antibody (1/50 dilution, 400µL)
- Goat anti-mouse IgG₁ AF488 conjugate antibody (1/500 dilution, 1mL)
- BSA 4% (3mL)
- Trash liquid recipient
- Three-way valve (Note: principal port=the one connects directly the syringe and the flow chamber, lateral port=the one next to the principal port that is reserved for PFA!)
- Connecting tubes, several 1mL syringes and one 5 mL syringe

Part 1: Migration assay

1. Incubate cells into the patterned flow chamber for 10 min at 37°C
2. Plug the exit reservoir without adding any bubble (the exit goes to the trash recipient)
3. Plug the three-way valve onto the syringe and connect the tubing
4. Before plugging onto the flow chamber, fill the syringe and tubing by aspirating directly PBS solution until all the tubings and the valve are filled (there may be resistance due to the length of the tubing, but patience is required to avoid bubbles. One may first use the 5mL syringe to fill the tubing and the valve. Once the liquid arrives in the syringe, change to the 1 mL syringe and continue to fill it with PBS). By the end of the filling, there should be no bubble between the syringe, two ports on which the tubing and the syringe are connected and the tubing. At this point, turn the valve to open the lateral port (which is not yet plugged), push gently the syringe to have some PBS present in the port so avoid future bubble upon syringe connection.
5. Plug the mounted system in 4 to the entry reservoir of the flow chamber without any bubbles
6. Put the flow chamber to the microscope

7. Find the patterns with x10 objective with x0.5 camera adapter
8. Tape the flow chamber firmly to the stage to avoid any future movement
9. Change to the x40 objective
10. Record positions to cover the entire patterned area
11. Put the valves to 45 degree to close both ports
12. Perform cell migration assay and record images (do not forget the images of the patterns). Record more than 100 images to capture the fixation.

Part 2 Fixation and staining

1. Towards the end of the recording, plug the PFA 4% syringe to the lateral port. Turn the valve to open the lateral port and close the other to avoid PFA back flowing into the syringe and the principle tubing
2. By the end of the recording, inject quickly but gently the PFA 4% into the flow chamber while observing the movie to see if the fixation is successful (the cells should be fixed instantly without bubbles) (To avoid bubbles, fill the port manually with PBS the connect the syringe by ensuring liquid-liquid contact)
3. Incubate for 10 min
4. Close lateral port, connect the syringe with PBS, open principal port and rinse the channel with 1 mL PBS (Pay close attention not to allow bubble into the system when changing syringe: to do so, first put the valve into the 45 degree position to close all access; then disconnect gently the syringe; fill the port manually with PBS and remove any microbubbles; finally, connect new syringe by ensuing liquid-liquid contact)
5. Connect hIgG syringe, open principal port and close lateral port, inject 400 μ L and incubate for 20min
6. Change to BSA4% syringe, inject 400 μ L and incubate for another 20min
7. Change to PBS syringe and inject 1mL to rinse the flow chamber
8. Change to TS1/22 syringe, inject 400mL and incubate for 30min
9. Prepare PBS syringe for rinsing and PFA2% syringe for refixation and plug the PFA syringe to the lateral port
10. By the end of the incubation, change to PBS syringe and inject 1mL to quickly rinse the flow chamber
11. Close principle port, open lateral port, inject quickly PFA 2% and incubate for 10min
12. Close lateral port, open principle port, change to the PBS syringe, inject 1mL to rinse
13. Change to the secondary antibody syringe, inject 400 μ L and incubate for 30min in the dark
14. Change to PBS syringe, inject 1mL to rinse
15. Take fluorescent images for each position
16. To stain with another antibody, move to another channel and repeat the above steps.

Appendix 10 Cell tracking and analysis protocol

Important:

- For analysis of the bright-field images, please take photo of the background before or after the experiment.
- Please make sure that all matlab scripts (main scripts and home-made functions) are in the same file directory (in the folder " Migration 2bin x20x05 -zeiss-2")
- Please make sure that the background image is inside each folder containing experimental image sequences

Part 1 Image quality enhancement and threshold selection

1. Open the first program: "DiviseFond_bis.m". This program performs background treatments and intensity normalization on each image and automatically rename the images in format of LTfondXXX (in case of image sequence with 100 images: LTfond001-LTfond100)
2. Inside the program, some parameters need to be modified manually
 - enter the file directory at line 4 after command "fileloc"
 - enter the file image format indicator at line 5 with variable fileimg (enter 1 if the file name starts with img_000000, 0 if the file name starts with LT)
3. Click on the "Run" icon and launch the program (you may need to change file directory or add the current directory on the matlab path)
4. On the prompt window, draw a rectangle to define the background and then double-click inside the rectangle to confirm the selection
5. Wait for the program to finish
6. Open each image sequence in the ImageJ (or Fiji) either by drag-and-drop or with File/Import/Image Sequence command
7. Find the appropriate threshold for each image sequence using Image/Adjust/Threshold command and take note of the value. Please note that the cells should appear in white on a black background with very tiny white pixels

Note: if the analysis will not be performed on the entire field of view, you should crop the image according to the position of the pattern. To crop, please use the ROI manager under the Analyze/Tools/ROI Manager to register the position the pattern: select the pattern, click add inside the ROI manager. Then, please go back to the image sequence, select the recorded ROI and crop the image using Image/Crop command. Finally, save the cropped images as image sequence under the name LTcropXXX (starting from 1 and with 3 digits)

Part 2 Image analysis

1. Open the second program: "analysis_cell_migration_obj20_TO2.m". This program detects and numbers cells in the first image and track them in the following images. It then saves the spatial and temporal coordinates of the cells for further analysis
2. Inside the program, some parameters need to be modified manually:
 - Fileloc indicating the file directory where the images are stored
 - Filename corresponding to the name of the images
 - Filedata corresponding to the name of the file containing the coordinates of each cells that will be saved in the end
 - First and Last corresponding to the first and last images to be analyzed
 - Thold corresponding to the threshold value to detect cells (obtained previously in ImageJ)
 - Minsize and maxsize corresponding to the minimal and maximal size of object on the surface. Note that this value should be changed if a different objective is used during experiments. The default values are set for x10 x0.5 magnification (minsize=3 and maxsize=200)
3. Once all the parameters are set, click the "Run" icon to launch the program

Part 3 Analysis of migration parameters

Note: the third program contains different variations designed to calculate different migration parameters according to the objectives of the analysis. The name of the script of all the variations starts with statistic_cell_migration

- **To quantify cell adhesion**
 1. Open program: statistic_cell_migration_drapeau_adhesion.m.
 2. Inside the program, modify the following parameters:
 - Fileloc corresponding to the file directory where the images are stored
 - Filename corresponding to the name of the images
 - File data corresponding to the file containing the coordinates of the cells
 - Pixel corresponding to the ratio between the size and the pixel. This value varies with the magnification used 1 pixel = 2.5 μm for x10 x0.5 magnification
 3. Once all the parameters are set, click the "Run" icon to launch the program
- **To quantify migration on patterned stripes**
 1. Open the fluorescent photo of the pattern in Image J
 2. Perform background subtraction and image flattening
 - First possibility: Process/Subtract Background
 - Image/Duplicate to make a copy of the image
 - On the copied image, Process/Filter/Gaussian Blur to make a blurred image

- Process/Image Calculator (Image 1=Original Image, Image 2 = Blurred image and Result=Image 1 – Image 2)
 - On the previously treated image, Image/Adjust/Threshold, find the right threshold to binarize the image and note the value
3. Open program statistic_cell_migration_Xua_patternCorrelation_V5.m
 4. Inside the program, modify the following parameters
 - Fileloc corresponding to the file directory where the images are stored
 - Filename corresponding to the name of the images
 - Filenamepattern corresponding to the name of the fluorescent image of the pattern inside the same folder of the image sequence
 - File data corresponding to the file containing the coordinates of the cells
 - tholdp corresponding to threshold value binarize the pattern
 - Pixel corresponding to the ratio between the size and the pixel. This value varies with the magnification used 1 pixel = 2.5 μm for x10 x0.5 magnification
 - time corresponding to the time between the recording of two images
 - Line 100: disactivate the command by putting it into comment
 - Line 101: for ICAM surfaces enter: `fr=find(nbpasCell<40|EuclSpeedCell<4)`; for VCAM surfaces enter: `fr=find(nbpasCell<10|EuclSpeedCell<4)`. This ensures that only cells having migrated for a certain distance will be considered in the analysis
 5. Once all the parameters are set, click the “Run” icon to launch the program
 - **To quantify migration on adhesion roller-coasters**

Note: The analysis of the cell migration on adhesion roller-coasters is divided into two parts and two programs. The first will create a mask (simulated binary pattern) according to the fluorescent experimental pattern) and the second will analyze the cell migration on the pattern in the same way as the “statistic_cell_migration_Xua_patternCorrelation”

1. Open the image sequence as well as the fluorescent pattern in the same stack in ImageJ
2. Given the fact that the experimental image of the pattern is often a bit tilted, the first step is to rotate the images into a horizontal position. To do so, calculate the angle between the bottom border of the fluorescent pattern and the horizontal line then go to Image/Transform/Rotate and enter the angle (positive angle for clockwise rotation)
3. Crop the patterned area (please note to leave a little white area on both lateral sides, before the first black stripe and after the last black stripe); save the image sequence of cells and the fluorescent image separately
4. Open the program: Mask_pattern_rolleravecplateau.m that will create an artificial pattern from the fluorescent experimental image

5. Inside the program, the following parameters need to be modified
 - Fileloc and filename as previously described
 - Largeur: the width corresponding to half of the stripe in pixel (12 in the case of roller-coaster)
6. Once all parameters are set, click on the “Run” button and launch the program. In the end, the binary artificial pattern will be saved in the same directory
7. Run the program in Part 1 and Part 2 to perform image processing and calculate cell coordinates
8. Open the program: Statistic_cell_migration_Xuan_rollerCoaster.m. This program will use the artificial pattern created by the previous program as mask to analyze cell migration, especially their preference of the areas with higher or lower adhesion.
9. Inside the program, the following parameters need to be modified:
 - Fileloc, filename, filedata as previously described
 - Filenamepattern corresponding to the filename of the artificial pattern.
10. Once all parameters are set, click on the “Run” and launch the program